Source reconstruction of the neural correlates of ongoing pain using magnetoencephalography

Thomas Graeme-Drury

A thesis submitted in partial fulfilment of the requirements of Birmingham City University for the degree of Doctor of Philosophy

Birmingham City University

July 2022

Faculty of Health, Education and Life Science, in collaboration with the Institute of Health and Neurodevelopment

Source reconstruction of the neural correlates of ongoing pain using magnetoencephalography

Thomas Graeme-Drury

Birmingham City University

2022

Thesis summary

Pain is a pervasive, complex, and subjective phenomenon that can be described by many features and researched using many paradigms; chronic pain has a significant impact on the quality of life of patients experiencing it and constitutes a large burden on the National Health Service. Discovering neural biomarkers for ongoing pain and pain sensitivity has the potential to elucidate underlying mechanisms, evaluate therapy effectiveness, and identify regions of interest within the brain for further study or intervention; something that is possible with functional imaging of brain activity. Magnetoencephalography (MEG) is a non-invasive technique that records brain activity through magnetic fields unobstructed by tissue of the head. This thesis utilises modern source reconstruction of MEG data to explore brain activity that characterises tonic pain conditions, and explores the future of tonic pain research by evaluating the utility of the PATHWAY Contact Heat Evoked Potentials Stimulator (CHEPS) – a tool used both as an experimental pain stimulus, and a clinical evaluation method in chronic pain – in current and future MEG research.

A systematic review of studies exploring the CHEPS and MEG, which highlights the paucity of the literature combining the two despite the potential benefits of each, is presented within.

Study one investigates the brain activity changes resulting from paraesthesia-based Spinal Cord Stimulation for chronic pain: significant enhancements in synchrony for theta and delta frequency bands during SCS-on resting-state are demonstrated, and a significant reduction in Somatosensory Evoked Potential (SSEP) power spectra in the SCS-on condition – providing evidence that conventional SCS influences resting and ascending processing in the brain, but does not necessarily suppress the field strength of SSEPs. Study two compared the neural activity of participants with high and low pain sensitivity during the Cold Pressor Test, and identifies regions of interest for future study. Study three is a methodological chapter which attempts to mitigate the methodological challenges involved in utilising the PATHWAY CHEPS in MEG research: The thorough exploration of independent component analysis, signal space separation and beamforming parameters demonstrates that it is possible to suppress the artefacts generated by the non-fMRI compatible CHEPS' thermode with the application of signal attenuation techniques, but only in an empty room dataset; the implications of this for future research are discussed.

Key words:

Pain, magnetoencephalography, beamforming, cold pressor test, spinal cord stimulation, contact heat evoked potential stimulator

Acknowledgements:

I would like to acknowledge the supervision of Dr Salim Khan, Dr Martin Vreugdenhil, Dr Rui Duarte and Dr Jon Raphael, whose faith and ongoing support facilitated the completion of this thesis even in the face of a global pandemic.

I owe my sincere gratitude to both Professor Paul Furlong and Dr Siân Worthen at the Aston Brain Centre for training me in MEG analysis, for patiently enduring my long strings of questions about FieldTrip and MEG data analysis, and for allowing me access to previously acquired datasets when the COVID-19 pandemic brought my project to a halt.

I would like to acknowledge Alex Hunt and Lisa Bentley for the aforementioned datasets – without their data, this thesis would not be possible.

I would additionally like to thank Dr Ashok Patel for the support and encouragement to pursue a lectureship when my PhD funding had run its course – and Dr Andy Powell for the employment that followed.

-

Thank you to the academic Twitter community members who encouraged me to stick it out when I felt like my PhD journey had come to an abrupt end due to the pandemic. I hope to pay it forward one day.

Thank you to my family, whose support made this thesis possible – and whose reassurances in the later stages of my journey kept me from floundering.

I extend my love and gratitude to all my friends that kept me together throughout. Thank you to Juliette for listening to me complain, and for our canal walks in the snow. Thank you to everyone in the Sleep Squad discord server that encouraged me when I had to vent. Thank you to Adam and Jess for giving me international doctoral encouragement. A special thanks to Jack and James, who supported me when I had to dip my toes into physics, scripting, and mathematics.

My final acknowledgement is reserved for my partner, Jenni. Thank you for your faith in me, your unfaltering encouragement, and your boundless patience. Thank you for the work clubs and the distractions. Thank you for your love and support.

Publication:

Since the original thesis submission, the systematic review presented in subchapter 2.3 has been published:

Graeme-Drury, T. J., Worthen, S.F., Maden, M., Raphael, J.H., Khan, S., Vreugdenhil, M., & Duarte, R. V. (2023). Contact Heat in Magnetoencephalography: A Systematic Review, *Canadian Journal of Neurological Sciences,* pp. 1-8. doi: 10.1017/cjn.2023.25

Abbreviations:

5HT – Serotonin

AAL – Automatic Anatomical Labelling

ACC = Anterior Cingulate Cortex,

Ach – Acetylcholine

AMY = Amygdala

ANOVA - Analysis of Variance

BG = Basal Ganglia

BOLD – Blood Oxygen Level Dependent

CPT – Cold Pressor Test

CRPS – Chronic Regional Pain Syndrome

DAS – descending antinociceptive system

DBS – Deep Brain Stimulator

DFT – Discrete Fourier Transform

DICS – Dynamic Imaging of Coherent Sources

DSM – Damped Sinusoid Modelling

EEG - Electroencephalography

ERD – Event-related Desynchronisation

ERF – Event-Related Field

ERS – Event-related Synchronisation

fMRI – Functional Magnetic Resonance Imaging

GABA - γ-aminobutyric acid

HPI - Head position indicator

ICA – Independent Component Analysis

IQR – Inter-quartile range

ISI – Inter-Stimulus Interval

LCMV – Linearly Constrained Minimum Variance

LEP – Laser Evoked Potential

MATLAB = MATrix LABoratory, a programming language and software

MCC – Mid-Cingulate Cortex

MEG – Magnetoencephalography

MNI – Montreal Neurological Institute

MSR – Magnetically shielded room

NAI – Neural Activity Index

NE – norepinephrine

NMDA - N-methyl-D-aspartate

NPS – No Pain Stimuli

NRS – Numerical Rating Scale

NS – Nociceptive specific

PAF – Peak Alpha Frequency

PAG = Periaqueductal Grey

PB = Parabrachial Nucleus

PCC – Posterior Cingulate Cortex

PET – Positron Emission Tomography

PFC = Prefrontal Cortex

PRISMA – Preferred Reporting Items for Systematic Reviews and Meta-Analyses

PS – Pain Stimuli

PSPS – Persistent Spine Pain Syndrome or Post-Stroke Pain Syndrome (Chapter six only)

ROI = Region(s) of Interest

RVM – Rostroventral medulla

SAM – Synthetic Aperture Magnetometry

SCS – Spinal Cord Stimulation

SCS-off – Spinal Cord Stimulator disabled

SCS-on – Spinal Cord Stimulator enabled

SD – Standard deviation

SI = Primary somatosensory cortex

SII = Secondary somatosensory cortex

SPECT – Single Photon Emission Computed Tomography

SQUID – Superconducting Quantum Interference Device

SSEP (SEP) – Somatosensory Evoked Potential

SSP – Signal Space Projection

SSS – Signal Space Separation

TFR – Time-frequency Representation

tSSS – temporal Signal Space Separation

VAS – Verbal or Visual Analogue Scale

VAS = Verbal Analogue Scale

VEF – Visually Evoked Field

VRS – Verbal Rating Scale

VTA – Ventral tegmental area

WDR – Wide Dynamic Range

Contents

Figure summary

Table summary

Thesis outline and background context

This research initially involved a source localisation exploration of pain sensitivity using the Contact Heat Evoked Potential Stimulator (CHEPS; Medoc Ltd., Ramat-Yoshai, Israel) in magnetoencephalography (MEG), but – despite best efforts – this was indefinitely postponed by the COVID-19 global pandemic at the point of data collection. Consequently, previously acquired datasets obtained at Institute of Health and Neurodevelopment were identified for additional analysis. Original analyses of those datasets are presented in this thesis, aligned with the narrative of the previous project – the exploration of pain using MEG beamforming. An outline of the thesis narrative is presented below (Figure 1.1).

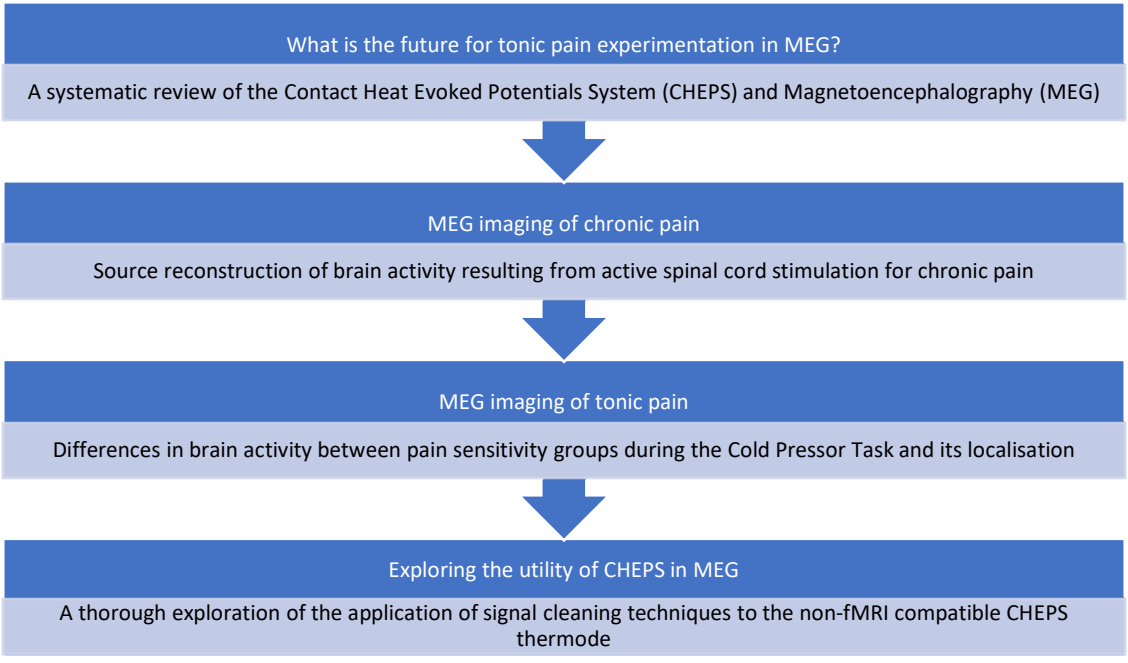

Figure 1.1: A diagram outlining the narrative of this thesis.

This thesis aims to determine whether MEG beamforming can reconstruct the neural correlates of ongoing pain. Primarily this was achieved by using beamforming source reconstruction analysis of MEG data in two datasets:

- Healthy control participants undergoing a tonic pain task
- Chronic pain patients with a Spinal Cord Stimulator implant experimentally turned on or off

Prior to the experimental chapters, brief introductory summaries and literature reviews are presented to describe pain physiology, the proposed anti-nociceptive mechanisms of Spinal Cord Stimulation, the research surrounding the brain imaging of the Cold Pressor Test to date, and the acquisition and analysis of MEG data.

Following the initial literature reviews, a systematic review is presented which synthesises the literature that combines magnetoencephalography and a promising experimental pain stimulator – the PATHWAY CHEPS (Medoc Ltd., Ramat-Yoshai, Israel). Pursual of publishing options for this review was ongoing at the time of writing.

In the first study, patients with spinal cord stimulators were observed in the MEG with their stimulators turned on and off. During these conditions, they were stimulated by electrodes to acquire somatosensory evoked potentials. The effects of spinal cord stimulation on evoked fields and oscillatory activity in the resting state were evaluated using beamforming source localisation and virtual sensors: The purpose of this experiment was to use modern MEG techniques to observe the effect that spinal cord stimulation has on ascending somatosensory

signals using a novel stimulation paradigm, to determine what frequency effects spinal cord stimulation might have on the brain, and to localise those effects.

In the second study, an ice-pack alternative of the Cold Pressor Test was used to induce pain during MEG acquisition – after which participants were grouped into 'high' or 'low' pain sensitivity based on their maximum pain score. These data are then evaluated for differences in the localisation of brain activity. The purpose of this experiment was to identify biological markers for pain sensitivity as measured by a tonic pain stimulus.

The final chapter contributing to this thesis follows the conclusions of the systematic review, and is a thorough exploration of available signal cleaning methods and their effectiveness in removing the electromagnetic artefacts produced by the PATHWAY CHEPS. This methodological chapter aims to determine whether or not it is possible to use modern signal cleaning techniques to facilitate the combination of magnetoencephalography and the CHEPS without a functional Magnetic Resonance Imaging-compatible thermode. This technical analysis was achieved using Independent Component Analysis (RUNICA; Bell and Sejnowski, 1995), Signal Space Separation (SSS; Taulu et al., 2004), temporal Signal Space Separation (tSSS, Taulu and Hari, 2009) and beamforming.

1. An introduction to pain

This chapter provides a brief overview of pain physiology. It includes a description of the neural pathways that transduce, transmit and process pain, factors that influence the perception of pain, and how what experimental techniques are used to observe brain activity resulting from pain.

1.1 Pain physiology

Pain, as described by the International Association for the Study of Pain, is an unpleasant experience with sensory and emotional components that resemble or are associated with actual or potential tissue damage (IASP, n.d.). Pain is a protective mechanism that encourages self-preservation when functioning normally (e.g., signalling to remove one's finger from a hot stove, or avoiding touching a wound), but pathological chronic pain conditions can have a devastating impact on the functioning and quality of life of those it affects (Fitzcharles et al., 2021). Chronic pain has a prevalence between 35-51% in the UK and constitutes a significant societal burden that is expected to increase further (Fayaz et al., 2016). Whilst the physiological mechanisms of pain signalling are well understood, the brain activity associated with its experience, including characteristics that describe it and interindividual differences in its perception, has not been fully elucidated: objective biomarkers for pain and pain sensitivity, for example, have been elusive; though their identification could provide targets for therapies, or means by which the effectiveness of therapies could be evaluated.

Though pain itself is widely regarded to be a complex phenomenon that extends beyond the simple sensing of noxious stimuli, the primary component of pain perception is nociception: The signalling of real or potential damage to physical tissues. Nociception is described by five

physiological processes: transduction of noxious stimuli into action potentials at nociceptors (unencapsulated nerve endings); conduction of the action potential along thin nerve fibres; transmission through the central nervous system by second-order neurons (the transference of action potentials from primary nerves to the spine and the brain); conscious perception of the experience of pain by processing in the brain, and modulation of ascending signals by activation of descending inhibitory systems. Primarily, different members of the Transient Receptor Potential (TRP) channel family are responsible for the sensation of thermal, chemical, and mechanical nociception (Hudspith, 2016; Jardín et al., 2017), the expression of which dictates the type of stimuli that activate nociceptors (Dubin and Patapoutian, 2010). Nociceptors are high-threshold mechanoreceptors or polymodal sensory nerves – each of which responds to mechanical pressure and deformation, changes in temperature, or extracellular agents liberated during real or potential tissue damage and inflammation (Hudspith, 2016; Steeds, 2016). Specific molecules (such as protein kinases, prostaglandins, histamine, nerve growth factor, substance P and calcitonin gene-related peptide) can act on membrane proteins to change the membrane potential of the nociceptor directly or indirectly. This modulation lowers the threshold for aversive painful signals, thereby deterring further manipulation.

Sensory nerve fibres (bundles of sensory afferent axons) are divided into four main subtypes: Aα, Aβ, Aδ and C. These are responsible for the transmission of sensory signals through the peripheral nervous system and are characterised by their varying thickness, conductance velocities, degrees of myelination, and where they terminate in the spinal cord. Conveniently, these divisions also generally separate the nerve fibres by the information they carry. Aα and Aβ fibres have the fastest conductance velocities, greatest myelination, and are referred to as

“thick” fibres; they carry sensory neuron information used in proprioception and low-threshold (i.e., innocuous) mechanoreception. Aδ fibres are thin and myelinated; they are the fastest of the nociceptive fibres, and carry “first” pain: the term used to define pain that is often described as immediate and well localised. C fibres are thin, unmyelinated, and are characterised by slow conductance velocities; alongside innocuous temperature stimuli, they carry “secondary” pain, slower velocity and poorly localised signals that have large receptive fields (Ploner et al., 2002). Nerve fibres can also be divided into peptidergic and non-peptidergic based on neurotransmitters they carry, peptidergic nerve ablation has shown abolition of noxious heat responsiveness and non-peptidergic ablation has demonstrated reduced responsiveness to noxious mechanical stimulation (Hudspith, 2016; Zhang et al., 2013); though the majority of nociceptors are recognised to be polymodal, and the differences between peptidergic and non-peptidergic nerves have been challenged in human models in recent years (Shiers et al., 2021).

As nociceptors fire on the same ‘all-or-nothing’ principle as all neurons, they cannot fire with varying intensity depending on the stimulus: The frequency of their activation codes stimulus intensity. Repeated activation of nociceptors can increase pain perception by lowering the threshold of post-synaptic central nervous system projections (second-order neurons) through the recruitment of N-methyl-D-aspartate (NMDA) receptors, which consequentially permits greater frequency of depolarisation (Mendell, 2022). This is referred to as wind-up or temporal summation (achieved in experimental pain models by presenting stimuli with between 1-6 seconds inter-stimulus intervals; Sarlani and Greenspan, 2002). Conversely, repetitive activation can also cause fatigue of pain intensity, possibly through neurotransmitter supply exhaustion

and desensitisation of attentional systems, with a more pronounced effect and slower normalisation in C-fibres (McMahon et al., 2013; Mouraux et al., 2013).

Nociceptors synapse at second-order neurons in the ipsilateral dorsal horn of the spine. The signal from nerve fibres is transferred to second-order neurons before crossing to the contralateral spine and ascending to the brain. First-order neurons (primary afferents) terminate in different layers of the spine (Laminae I, II and V; Figure 1.2). Second-order neurons are nociceptor-specific, wide dynamic range or low-threshold; these receive input from pain signalling, mixed, or innocuous sensory neurons respectively (Steeds et al., 2016). Many of the neurons in the dorsal horn are inter-neurons that branch locally and allow for excitatory (glutamatergic) or inhibitory (GABA-ergic or Glycinergic) interaction between inputs (Todd, 2010). The complex suppressive and facilitative interactions of primary afferents and second-order neurons was originally described in the Gate Control Theory of pain, first proposed by Melzack and Wall (Melzack and Wall, 1965), whereby incoming signals of nociceptive and innocuous origin were integrated by a control centre before projecting to the brain. Though this theory failed to accurately describe the complex network of segmental spinal neurons and descending antinociceptive paths, it helpfully illuminates the complicated nature of nociceptive signalling at the spine, and has informed the development of therapies targeting the suppressive components of this network (see SCS, chapter 2.1).

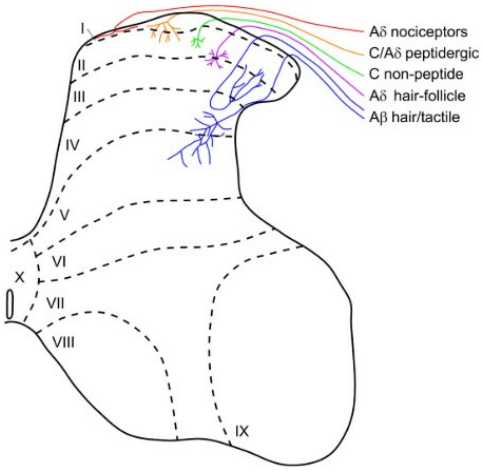

Figure 1.2: Lamina terminations of first-order neurons (Todd, 2010)

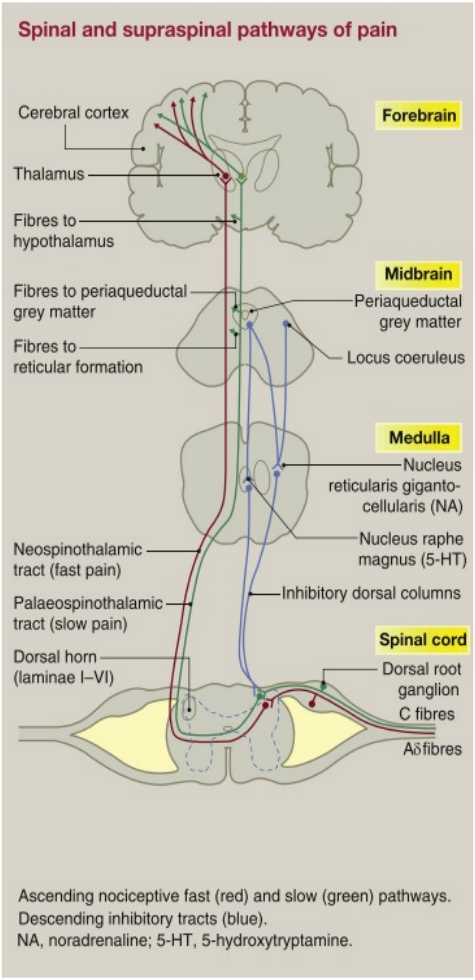

Figure 1.3: The spinothalamic and descending pain pathways (From Steeds, 2016)

Second-order neurons ascend through various tracts, eventually terminating in the brainstem and the brain. Though there are many subdivisions of these ascending paths depending on where they terminate, they are commonly referred to as either spinothalamic or spinoreticular tracts. The spinothalamic tract has medial (paleospinothalamic) and lateral (neospinothalamic) pathways that project to the cerebrum; the paleospinothalamic tract is responsible for projections through the medial nucleus of the thalamus, and the neospinothalamic tract is responsible for projections through the ventral posterior lateral nucleus of the thalamus (Figure 1.3; Steeds, 2016). Spinoreticular tracts project to the reticular formation of the brainstem, and from there modulate incoming pain signals. Both carry wide-dynamic range and nociceptor-specific signals.

Once sensory information reaches the supraspinal areas of the central nervous system, pain perception begins (Dubin & Patapoutian, 2010). The network of brain areas responsible for the processing of pain is often referred to as the 'neuromatrix', as coined by Melzack (1990), and necessitates the inclusion of areas responsible for the processing of cognitive and affective components of the pain experience as well as the somatosensory components; it is commonly proposed to include the primary and secondary somatosensory cortices, the anterior cingulate cortices, the amygdala, insula and prefrontal cortex (Figure 1.4), though many other brain areas have been implicated (Bushnell, Lucie and Low, 2013). No singular brain area is thought to process all characteristics of nociception or pain specifically, and the search for brain areas that are selectively activated during pain is ongoing.

Excited by ascending spinothalamic signals and modulated by descending cortical projections, endogenous antinociceptive systems are innate mechanisms by which the central nervous

system interacts with incoming nociceptive signals. Descending neurons terminate at interneurons or synaptic terminals in the dorsal horn, inhibiting their activation and resulting in a reduced output of nociceptive signal in ascending fibres (Figure 1.3; Steeds, 2016); these neurons originate in the periaqueductal grey and the nucleus raphe magnus of the brain stem, and can release inhibitory or facilitatory neurotransmitters (e.g., opioids, serotonin). Studies have demonstrated that the activity of the descending pathway can be influenced by the action of dopaminergic brain areas associated with reward: directly descending projections from the hippocampus have inhibitory effects on trigeminal nerves, and ventral tegmental area projections to the nucleus accumbens have antinociceptive effects moderated by dopamine receptors (Mitsi and Zachariou, 2016; Li et al., 2019). Spinal cord stimulation (See section 2.1; Tazawa et al., 2015), age (Edwards, Fillingim and Ness, 2003; Riley III et al., 2010), expression of opioid gene polymorphism A118G (Peciña et al., 2015) and sex have also been associated with moderating descending pathways (Bulls et al., 2015). Dysfunction of endogenous antinociceptive systems has been proposed to be involved in the maintenance or development of chronic pain conditions, such as Complex Regional Pain Syndrome (CRPS; Ossipov, Morimura and Porreca, 2014), and could explain some differences between how individuals experience ongoing pain.

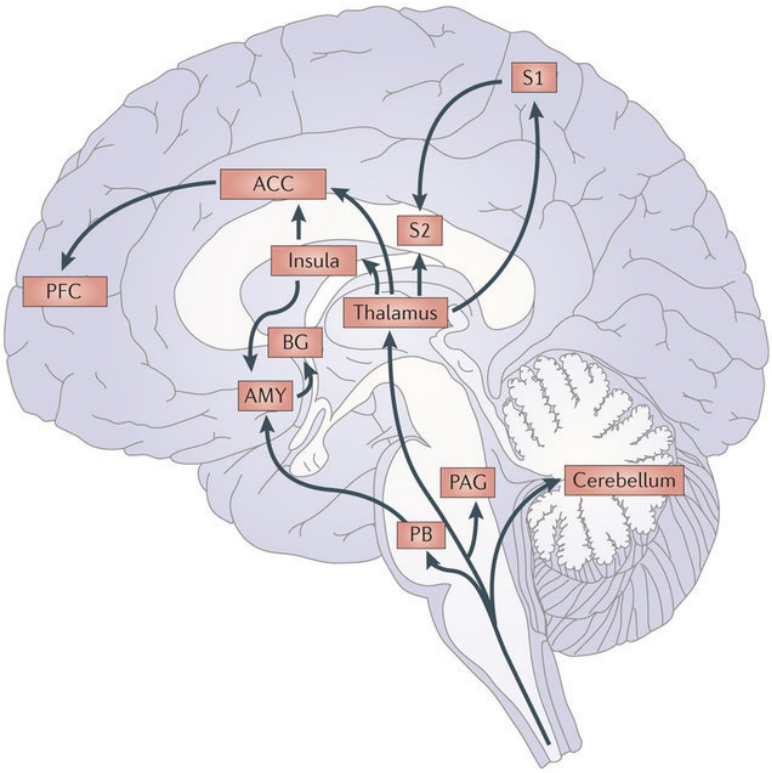

Figure 1.4: Brain areas implicated in the processing of pain. Figure from Bushnell, Čeko and Low (2013).

AMY = Amygdala, ACC = Anterior Cingulate Cortex, BG = Basal Ganglia, PFC = Prefrontal Cortex, PB = Parabrachial Nucleus, PAG = Periaqueductal Grey, SI = Primary somatosensory cortex, SII = Secondary somatosensory cortex

1.2 Pain sensitivity

Pain is a complex phenomenon, and as such, there are several facets to its experience. The extent to which an individual is considered resilient to the experience of pain is referred to as pain sensitivity, and can be observed via multiple other pain metrics: endurance of ongoing (tonic) noxious stimuli, the threshold at which a stimulus becomes painful, and maximal intensity an individual can comfortably endure are all examples of operationalisations of the pain experience. Pain intensity is readily available, and can be measured simply by the subjective magnitude of the noxious stimuli as reported by an individual on a discrete or continuous visual or verbal rating scale between the values of 1-10 (Hjermstad et al., 2011).

Enhancement of pain sensitivity can be attributed to gain control mechanisms in pain pathways, and can be identified by the location of its sensitisation in the peripheral or central nerves. Peripheral sensitisation is marked by increased signalling in response to lower threshold stimuli, and is often associated with localised tissue or nerve damage. Central sensitisation is an increase in the signalling of central nervous system neurons in the spine or brain, often as a result of dysfunction or disease, and can be a result of neuronal plasticity enhanced by peripheral stimulation (IASP, n.d.; Mendell, 2022).

Individual differences in pain sensitivity have been correlated with sex (Bulls et al., 2015; Esterlis et al., 2013; Ravn et al., 2012), age (El Tumi et al., 2017; Yezierski, 2012), gender role-conformity (Alabas et al., 2012), menstrual cycle phase (Iacovides et al., 2015), ethnic identity (Ostrom et al., 2017; Rahim-Williams et al., 2007), handedness (Pud et al., 2009), cortical density (Emerson et al., 2014; Erpelding et al., 2012), genes (Afari et al., 2011; Nielsen et al., 2008), and neurotransmitter levels (Zunhammer et al., 2016), as well as stress levels (Timmers

et al., 2018; Vachon-Presseau et al., 2013), depression (Schwier et al., 2010), anxiety and anxiety sensitivity (Dodo and Hashimoto, 2017), fear of pain (Timmers et al., 2018), pain catastrophising (Banozic et al., 2018) and attention (Miron et al., 1989).

Whilst pain sensitivity can also be enhanced in pathological pain states like CRPS, fibromyalgia, chronic headache syndromes and post-surgical pain syndrome (PSPS), and has been tied to long-term opioid usage (Borsook and Becerra, 2011; Buchgreitz et al., 2008; Zahari et al., 2016), increased pain sensitivity is also occasionally reported in conditions where pain is not a primary feature (Bouin et al., 2002; Bromm and Treede, 1991; Lautenbacher et al., 1999; Sung et al., 2018). Though its effectiveness as a predictor of treatment outcome is occasionally contested (Ruscheweyh et al., 2015), enhanced pain sensitivity has been identified as a marker for post-surgical acute pain, post-surgical recovery and the chronification of pain (Abrishami et al., 2011; Coronado et al., 2015; Kim et al., 2015; Nim et al., 2020). Experimentally measuring pain sensitivity can be achieved using subjective reporting of upper and lower pain thresholds across any number of modalities, and can be observed using evoked or tonic stimuli whilst recording brain activity to evaluate its neural correlates (see chapter 5). Identifying neural biomarkers associated with pain sensitivity could have far-reaching implications across many fields, and assist in treatment selection, evaluation of treatment effectiveness and responsiveness, and evaluation of risk, stage, and progression in disease (Lleó, 2021; Mouraux and Iannetti, 2018).

1.3 Pain in the brain

Evaluating the contribution of specific brain areas to the experience of pain is achieved with imaging and reconstruction of brain activity using several methods. Most commonly, electroencephalography (EEG) and functional magnetic resonance imaging (fMRI) studies record surrogates of brain activity (i.e., electrical potential on the scalp originating from electrical currents in the brain and blood oxygenation) in pain populations or during experimental pain conditions. Imaging methods with low temporal resolution (such as fMRI, SPECT, and PET) give poor estimations of activity over time but have high spatial resolution, they provide good candidates for brain areas that are involved in the processing of pain, but are limited to activity oscillating at a frequencies far below 1 Hz. EEG and magnetoencephalography (MEG) techniques often record 1000-2000 data-points a second, enabling the analysis of real-time time series, and high-frequency oscillatory components. EEG and MEG are commonly combined with 3D models generated using MRIs to facilitate the reconstruction of currents and fields associated with specific tasks or conditions. Whilst EEG and MEG methods acquire similar measurements, they have key differences in their implications and interpretations: EEG records electrical currents as they appear on the scalp, which is influenced by the skin, skull and brain's conductance of electricity; MEG records magnetic fields generated by neural currents in the brain that are unaffected by the conductance of the volume, but are invisible when radial to the sensors (MEG acquisition and analysis described in more detail in chapter 3). For these reasons, MEG is capable of achieving greater spatial resolution than EEG, but is thought to be insensitive

to activity limited to gyri of the cortex; and neither have the spatial resolution or accuracy in deep brain regions that fMRI can achieve.

In EEG and MEG literature, brain signal analysis is often performed in the time, frequency, or time-frequency domains. In the time domain, signals are often observed as they are at the channel (EEG) or sensor (MEG), which appears as a wave that represents ongoing electrical or magnetic activity in the brain under the electrode or flux transformer. This time series can be time-locked to when a stimulus was applied, and averaged across many trials and sensors to observe an "evoked" waveform. The energy attributable to different frequency bands within measured brain signals can be estimated using Fourier transformation (a method used to deconstruct signals and estimate the power of the underlying frequency components). Analysing brain signals acquired using MEG or EEG enables the observation of a broad range of frequency bands, most often divided into delta (0-4 Hz), theta (4-8 Hz), alpha (8-14 Hz), beta (14-30 Hz) and gamma (30+ Hz), though their boundaries are rarely consistent (Figure 1.5). Synchrony in these bands has been associated with different behavioural, perceptual, and processing functions in the brain, and are changes or differences in the frequency characteristics of brain signals are thought to reflect underlying differences in brain activity. Whilst the functions of frequency bands may be specific to an observed brain area, some commonality has been prescribed to them: the delta frequency band has been linked to memory and motivation; the theta frequency band has been associated with episodic memory and pain; alpha frequency enhancements reflect attention and has been identified as a marker of pain sensitivity; the beta frequency band is often associated with movement initiation and anticipation, and the gamma band is thought to represent localised processing and cognitive

function (Kim and Davis, 2021). Analysis of underlying frequency power in signal data is achieved by the use of a Fourier transformation. A Fourier transform decomposes signal data, such as M/EEG timeseries, and estimates the contributions of each specified frequency to that signal (E.g., How much of the observed signal is 1 Hz, 2 Hz, 100 Hz), and can be achieved using most M/EEG analysis software. Repeating a Fourier transform over short segments of timeseries data can enable the analysis of changes in the power of frequency bands over time (more detail on MEG acquisition and analysis in chapter 3).

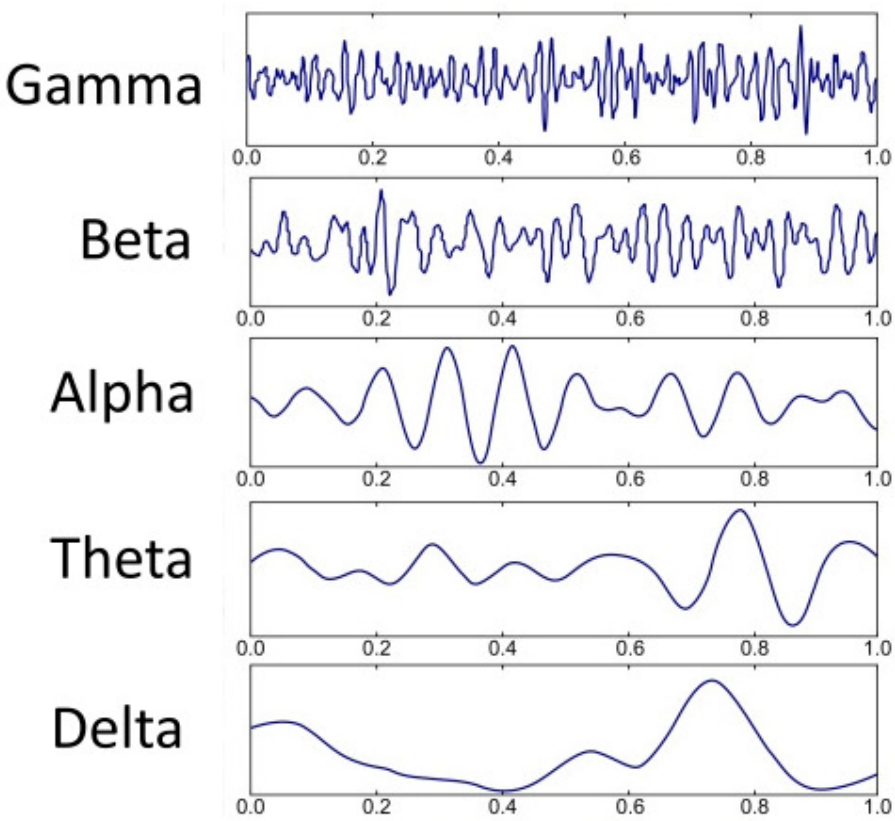

Figure 1.5: Frequency bands observed in EEG and MEG (Adapted from Abhang et al., 2016).

Observing somatosensory activity in the human brain is most often achieved by evoking activity with an acute or tonic stimulus, or analysing the brain at rest in individuals with chronic pain

conditions. Evoked methodologies often reflect different nociceptive modalities (including heat, cold and mechanical), but can also utilise electrodes to recruit nociceptive or sensory nerves directly and selectively. Components of various latencies can reflect the processing of acute pain transmitted by nociceptive fibres with different conductance velocities (i.e., Aδ and C fibres), though their amplitudes and latencies are modulated by the characteristics of the stimuli also (Frahm et al., 2020).

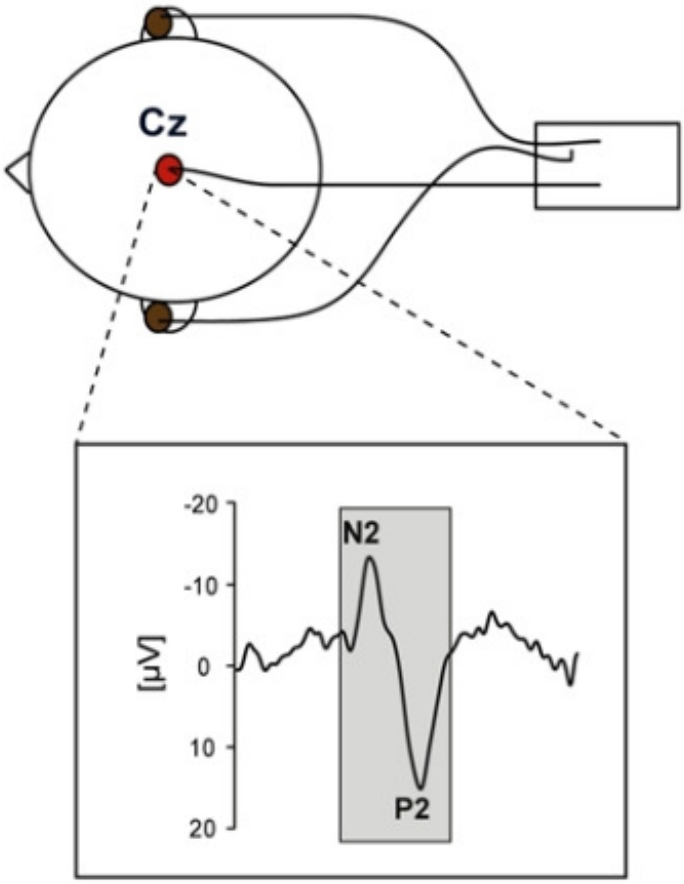

Figure 1.6: The N2P2 component of an evoked waveform, as measured by EEG at the Cz channel. Adapted from Rosner et al., (2018a).

The waveform component most commonly associated with the processing of evoked Aδ pain in EEG and MEG is N2P2 (Figure 1.6). N2P2 is a waveform consisting of a clear negative deflection followed by a positive deflection, and it is the source of some contention in pain literature. Initially, the waveform was thought to represent nociception in the cortex, but comparisons with non-noxious stimuli of similar novelty and salience have cast doubt on its specificity, instead suggesting that the N2P2 reflects attention: Mouraux & Plaghki (2006) first hypothesised that laser-evoked potentials (LEPs) were not fully representative of nociception, evidenced by the fact that C-fibre activation does not consistently provoke late or ultra-late LEP activity and that N2P2 components can be evoked by many sensory stimulation modalities, and that involuntary attentional capture was more likely responsible for the N2P2 waveform. Their subsequent research investigated the specificity of the N2P2 waveform and demonstrated a significantly reduced magnitude for N1, N2-P2 and event-related synchronisation (ERS) when making the stimulus timings predictable, and that randomising or batching trios of stimuli and their intensities had no influence on pain perception despite this (Iannetti et al., 2008). They concluded that the N2P2 component was reflective of stimulus saliency rather than pain processing, though they conceded that evoked waveforms and the synchronisation of frequency bands in the time-frequency domain remain useful in exploring nociception. Mouraux & Iannetti (2009) further demonstrated this exact phenomenon with a study that showed the entire LEP waveform could be explained by the variance introduced by auditory, visual or non-nociceptive specific somatosensory stimuli, and Wang et al (2010) reported that the inter-stimulus-interval suppression of LEP amplitude was highly dependent on the predictability of the stimulus. Regardless of its selectivity, the N2P2 remains an effective marker

of stimulus intensity on its merit as a reflection of salience, and is still used to evaluate pain in clinical populations (Hüllemann et al., 2019).

The gold standard for evoking N2P2 waveforms from pain stimuli is an infrared neodymium yttrium aluminium perovskite (Nd:YAP) laser: a heat stimulus applied to the skin via radiation through superficial layers of the skin. Laser stimuli are highly localised and do not have a long ramp-up time, which results in a well synchronised evoked response, providing clearer signal-to-noise ratio in M/EEG data, and thereby greater amplitudes (Arendt-Nielsen and Chen, 2003). However, the equipment is expensive, the stimulus is influenced by skin reflectivity, the heat can stimulate only a very small area, and studies require extensive safety protocols to avoid injuring the participant or operator (Frahm et al., 2020). An alternative to LEPs are Somatosensory Evoked Potentials (SSEPs), which are achieved through electrical stimulation of sensory nerves. Carefully controlling the stimulus qualities and utilising selective electrodes, it is possible to evoke highly synchronous and selective activity by selectively stimulating only nociceptors; though it is well recognised that these techniques circumvent the transduction of pain, a key component to nociception, and this limits their ecological validity: they do not fully reflect the typical pain experience of a participant. A notable alternative to these is the Contact Heat Evoked Potentials Stimulator (CHEPS; Medoc Ltd., Ramat-Yoshai, Israel), a Peltier thermode capable of heating at a rate of 70˚C/s (discussed in more depth in chapter 6). The CHEPS is capable of achieving noxious temperatures quickly enough to evoke time-locked brain activity, but at reduced risk of injury, and with a contact area that better reflects the pain that participants might experience in everyday life.

Observations of brain activity in pain studies have given rise to a 'pain neuromatrix', as described by Melzack & Wall (1965; Melzack, 1990, 1999). Despite many brain areas being implicated in the processing of pain, few areas of the pain matrix have entirely consistent evidence supporting their addition (Apkarian et al., 2005; Peyron et al., 2000; Peyron and Fauchon, 2019; Tracey and Mantyh, 2007). Most commonly, the pain neuromatrix is identified as the anterior cingulate cortex, primary and secondary somatosensory cortices, the thalamus, the insular cortex, prefrontal cortex, and cerebellum (Figure 1.4).

1.3.1 Thalamus

Almost all ascending nociceptive neurons from the spine, through the spinothalamic, spinoreticular, spinomesencephalic, spinotectal and spinohypothalamic fibres, arrive in the thalamus directly (15%) or indirectly (85%, Patestas and Gartner, 2006). Intracortical recordings have demonstrated activity in the thalamus in response to experimental stimuli (Pralong et al., 2004), and Gauriau & Bernard (2004) demonstrated that 41% of posterior thalamic neurons responded to cutaneous stimulation, with 45% of those being nociceptive-specific and 19% nociceptive non-specific. Though this suggests an association with pain processing, the thalamus is a diverse neuronal structure that corresponds with activity in many networks, including the default mode, attention, executive, motor, auditory, visual and salience networks (Yuan et al., 2016), and is purported to primarily function as a thoroughfare for projections to other brain centres. Stimulation of specific nuclei in the thalamus has been shown to reduce pain scores in neuropathic pain conditions up to and beyond 50% a reduction even at 4 years follow-up, though its efficacy was not equal across all neuropathic conditions (Abdallat et al., 2021). A recent review has proposed that specific thalamic nuclei act as ascending promoters of

pain modulation via descending pathways with nociceptive selectivity, suggesting that it is not simply a relay for pain signals, but also involved in both facilitation and suppression of pain by controlling which signals are projected to the insular and cingulate cortices (You et al., 2022).

1.3.2 Primary and secondary somatosensory cortices

Early lesion studies hypothesised that the primary somatosensory cortex (SI) was not necessary for pain perception: Head (1920) identified that individuals with parietal lobe lesions still experienced pain. This was explored by Ploner et al. (1999) who identified stroke patients with damage of SI and SII who reported they were able to experience pain, but not localise the sensation, or the modality of nociceptive stimuli – instead simply reporting a negative affective experience. More recently, the functional heterogeneity between SI and SII has been highlighted (Worthen et al., 2011), casting doubt over lesion studies that do not differentiate between the two.

In modern literature, SI's contribution to sensation is recognised ubiquitously; it has been consistently validated with several event-related potential electrophysiological imaging studies using a variety of stimuli modes (Iwamoto et al., 2021; Okada et al., 2021; Patestas and Gartner, 2006; Ploner et al., 1999; Tarkka and Treede, 1993; Vierck et al., 2013). Inui et al. (2003) demonstrated SI activity as the earliest component in neural activity in response to intra-epidermal stimulation, a method that avoids Aβ fibre activation, clarifying that SI is capable of responding to ascending signals in a pain-specific manner; it is recognised as the primary area for processing of Aδ nociceptive inputs and discriminative characteristics of sensation (Panchuelo et al., 2020). Studies using painful stimuli have shown painful stimulation recruits significant gamma-band oscillatory activity in SI when compared to non-painful stimulation

intensities and this power increases with intensity (Gross et al., 2007; Kropf et al., 2018; Rossiter et al., 2013; Tiemann et al., 2010). Recent research has also highlighted SI's influence on descending antinociception (Tan et al., 2019), and forward projections to areas that contribute to pain anxiety (Jin et al., 2020).

Unlike SI, SII has been shown to elicit the sensation of pain when stimulated with intracerebral electrodes alongside the insula (Mazzola et al., 2006), and its disruption with transcranial magnetic stimulation can interfere with the processing of intensity (Lindholm et al., 2015; Lockwood et al., 2013). It is suggested that SII is activated primarily during pain, where SI activity ramps with stimulus intensity regardless of its innocuous or nociceptive nature (Bornhövd et al., 2002; Timmermann et al., 2001). SII has been linked with pain sensitivity by studies that have identified reduced mechanical and thermal pain thresholds as a result of its disruption (Liu et al., 2018; Valmunen et al., 2009).

1.3.3 Insular cortex

Gogolla's (2017) review of the literature surrounding the insular cortex summarises its function as a convergence gateway for bodily sensations, autonomic control, afferents associated with emotional processing, and highlights its membership of a network responsible for fear association, possibly reflecting its integration of information to influence decision making. Gogolla notes that stimulus recognition and valence appear to be a core aspect of the insular cortex's function; it is consistently activated regardless of the mode of salience, whether the stimulus is painful or not, and whether the pain is acute or chronic (Uddin, 2015). Lesions of the insula cortices show patients and rats experiencing inappropriate emotional responses, especially in response to pain (pain asymbolia; Klein, 2015).

Garcia-Larrea's review (2012) suggests the posterior granular insular and the adjacent medial operculum are the strongest contenders for a primary pain cortex. This is due to it being the brain area that suits pain-specificity criteria to the greatest extent: i.e. a) there is evidence for anatomical projections terminating here from the spinothalamic tract (Dum et al., 2009), b) there is consistent activation in response to noxious stimuli presentation (Apkarian et al., 2005; Garcia-Larrea et al., 2000), c) there is pain experienced by stimulation of the brain area (Mazzola et al., 2012, 2006) and d) lesions to the area produce alterations to nociception (Garcia-Larrea, 2012). Their evaluation of the research, however, concluded that it has pain-preferential activation, not pain-specific: Gamma-band oscillatory activity in the insula appears to show a preference for nociception, since it is not present in the processing of equally salient non-nociceptive stimuli (Liberati et al., 2018, 2019; Peyron and Fauchon, 2019). Many studies have associated the insula cortices with the salience of a stimulus and the salience network itself (Frot et al., 2008; Iannetti et al., 2005; Seeley et al., 2007; Villemure and Bushnell, 2009; Wiech et al., 2010).

1.3.4 Cingulate cortex

The mid-cingulate cortex (MCC) receives 24% of spino-thalamocortical projections, projects to the periaqueductal grey and has been identified as a candidate for the pain neuromatrix by several reviews of experimental research (Apkarian et al., 2005; Dum et al., 2009; Peyron et al., 2000). The MCC appears to be responsible for the cognitive-evaluative stages of pain processing, as well as the affective dimension of the pain experience, and a contributor to later brain evoked brain signal activity, and the anticipation of noxious stimuli, though its selectivity

for pain is not clear (Gopalakrishnan et al., 2015; Ploghaus et al., 1999). Early research reported finding single neurons in the anterior cingulate cortex (ACC) of 4 out of 11 patients that respond selectively to contralateral painful thermal and mechanical stimuli, though these were also active in the anticipation or observation of painful stimuli and did not elicit pain upon stimulation (Hutchison et al., 1999). Other anatomical studies of the cingulate cortex have demonstrated an inverse relationship between grey matter density in the posterior cingulate cortex (PCC) and pain sensitivity (Emerson et al., 2014), an activation of the ACC in response to pain-evoked stimuli using intracerebral electrodes (Lenz et al., 1998) and effectiveness of cingulotomies in treating chronic pain (Boccard et al., 2014a). However, ACC lesions do not appear to stop the pain response altogether, and do not influence pain sensitivity (Fuchs et al., 2014).

Though the cingulate cortices are separated into other areas that can each be associated with many different functions (such as motor and cognitive aspects of pain; Kwan *et al.*, 2000), the most commonly cited function of the CC is its contribution to pain affect. Vogt et al. (2005) posited that the four-region neurobiological model of the CC were effective subdivisions for emotion, and that their overlap with pain responses were accurate reflections of their contribution to the pain experience: anterior MCC & fear-avoidance; posterior ACC & unpleasantness; posterior MCC and dorsal PCC & skeletomotor orientation in response. Manipulation of pain unpleasantness by hypnosis by Rainville et al (2002) has increased activation in the ACC, and increased unpleasantness associated with repetition of a pain stimulus is also associated with this increase (Price, 2000). It is unsurprising, then, that this greater activation is also found in chronic pain patients, since pain is defined as an unpleasant

experience (Bliss et al., 2016; Gungor and Johansen, 2019; Meda et al., 2019), and targeting the ACC with deep brain stimulation has found some success in reducing its unpleasantness and intensity in certain neuropathic pain disorders (Boccard et al., 2014b; Levi et al., 2019).

2. Literature review

In pathological cases, pain can become dysfunctional and no longer provide a protective benefit. Individuals are diagnosed with chronic pain after enduring it for a minimum of three months, with a number of underlying aetiologies; most commonly damage to, or disease and dysfunction of, neurons involved in signalling pain in the peripheral or central nervous system. The prevalence of chronic pain has been reported as high as 35-51% in the UK (Brown et al., 2021; Fayaz et al., 2016), and is associated with negative impact on the individual beyond the scope of injury, including depression, anxiety, lower quality of life, lower job satisfaction, reduced sleep, higher levels of opioid consumption, social withdrawal, and suicide risk (Fitzcharles et al., 2021). Individuals with chronic pain often find mixed therapeutic relief from pharmaceutical methods, and despite broad applications and many potential therapeutic targets, many have to live with unacceptable levels of ongoing pain (Majedi et al., 2019). Research continues to explore avenues for improving pain relief in chronic pain patients, with some promising nervous system stimulation interventions available to those with otherwise intractable pain, but much experimental research is difficult to generalise to chronic pain. Many studies hoping to identify the neural correlates of pain use stimuli and methods which do not reflect the enduring characteristics of chronic pain (i.e., laser and electrical stimuli). Lasting (tonic) pain stimuli are the closest experimental analogues, but do not always lend themselves to brain imaging due to ferrous metal components, electromagnetic signal generation and practical size constraints.

Identifying the neural correlates of pain could provide insights into disease, targets for therapy, or metrics by which to evaluate them – but few biomarker candidates exist (Lleó, 2021; Mouraux and Iannetti, 2018). MEG beamforming (an analysis technique that utilises MEG data to produce an image of brain activity in a 3D model of the brain) can be used to reconstruct activity using whole-brain analysis and virtual sensors, enabling the analysis of frequency power and magnetic field strength whilst suppressing external magnetic fields by using spatial weights: filters that selectively reconstruct signals that only originate from each point of interest within the brain. Beamforming MEG data can be used to identify differences in brain activity between pain conditions, and groups of individuals or patients that experience pain differently without suffering from volume conduction distortion or contributions from external noise generators such as spinal cord stimulators. Though MEG beamforming has clear advantages, several areas of tonic pain research are yet to be explored with it. The research question for this thesis follows this narrative: can MEG beamforming reconstruct the neural correlates of ongoing pain?

In chapter four chronic pain states in patients with therapeutic Spinal Cord Stimulation (SCS) are observed by comparing brain activity with their generators enabled and disabled. The neural activity recorded during these timeframes reflect different levels of pain relief, as reported by the participants, but also the supraspinal mechanisms of SCS.

In chapter five, healthy control participants enduring a Cold Pressor Test (CPT) analogue have their neural correlates of pain sensitivity evaluated; self-reported ongoing pain values were used to form high-sensitivity and low-sensitivity participant groups, and their brain activity during the CPT is compared to a baseline to evaluate their experience of pain.

The following subchapters describe SCS and CPT research in M/EEG to date. Subchapter 2.1 illuminates the literature surrounding conventional SCS, relevant brain imaging studies, and how they are informed by theories for its mechanism of action. Subchapter 2.2 describes the literature surrounding the CPT and relevant brain imaging findings.

2.1 Spinal cord stimulation and its mechanisms

Spinal cord stimulation (SCS) is an invasive neuromodulation technique used for the management of chronic neuropathic pain. It is achieved by percutaneously implanting electrodes in the epidural space adjacent to the dorsal column of the spinal cord (Lundeland et al., 2021) (Figure 2.1); those electrodes, powered by an implanted generator, then stimulate between 4-60 Hz, with pulse width between 150-500 ms and an amplitude strong enough to generate a sense of paraesthesia (an abnormal sensation that usually presents as a tingling in the skin; (De Groote et al., 2018; Linderoth and Foreman, 2017). Its concept was initially founded on the Gate Control Theory (Melzack and Wall, 1965) on the premise that stimulation of Aβ fibres could 'close the gate' on the ascending pain projections via inhibitory synapses, and was first introduced in 1967 (more on the Gate Control Theory in Chapter 1.1; Shealy et al., 1967). Primarily this therapy is reserved for intractable chronic pain patients that have had limited or no success with alternative therapies; it is most often used to treat chronic pain conditions such as PSPS type 2, CRPS, neuropathic pain, visceral abdominal pain, diabetic neuropathy, and angina pectoris (Caylor et al., 2019), but has also shown promise in ameliorating movement disorders such as Parkinson's disease, multiple sclerosis and dystonia (Sivanesan et al., 2019). The electrodes are implanted in pairs on either side of the spine or

individually, located based on anatomy or intraoperative stimulation/collision assessments (De Groote et al., 2018; Shils and Arle, 2018). Traditional SCS is often referred to as 'conventional', 'tonic' or 'paraesthetic' SCS because many patients experience paraesthesia as an intended result of the high-charge delivery stimulation of the dorsal column's Aβ tracts (as opposed to burst or high-frequency alternatives; Miller et al., 2016). In this thesis, unless otherwise specified, 'SCS' will refer to the conventional tonic method.

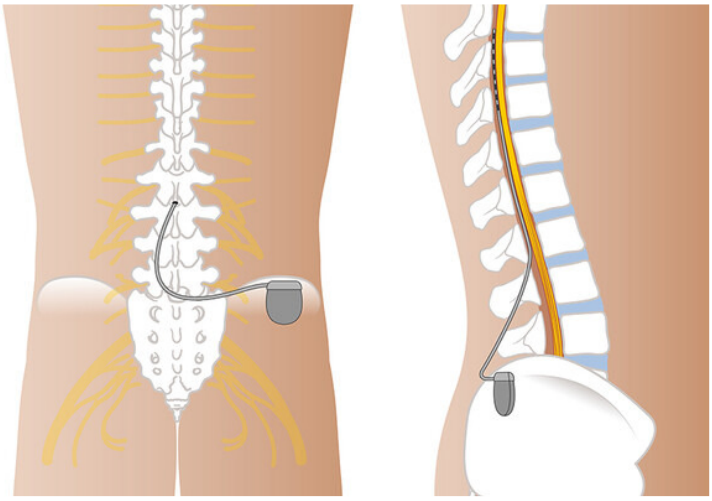

Figure 2.1: Spinal cord stimulator with an epidural electrode and subcutaneous pulse generator, from Lundeland et al., 2021.

SCS has been shown to improve quality of life, pain, disability index scores, treatment costs, opioid dosage, employment and satisfaction, with some studies demonstrating up to 54% of patients experience over 50% pain reduction after 24 months (Deer et al., 2014; Harat et al., 2012; Kay et al., 2001; Kumar et al., 2008; McClure et al., 2021; Meyerson et al., 2006; Visnjevac et al., 2017). A recent meta-analysis of randomised control trials confirmed the efficacy is greater than that of placebo (Duarte et al., 2020b), though the quality of current SCS randomised control trials has been called into question due to the difficulty of blinding

participants when stimulations can be sensed in certain stimulation paradigms and calibration settings (Duarte et al., 2020a). The most commonly recognised mechanisms of action in SCS are supraspinal and segmental, and reflect the orthodromic, antidromic and localised effects of stimulation and action potentials elicited by currents generated in the epidural electrode.

2.1.1 Orthodromic action of SCS

2.1.1.1 Supraspinal activity during SCS

Current theories of supraspinal SCS mechanisms rely on the recruitment of the descending antinociceptive system (DAS; Figure 2.2b), as elicited by orthodromic action potentials initiating Aβ dorsal column signalling. Ascending dorsal column fibres carry Aβ myelinated thick-fibre sensory information and decussate in the medulla before projecting through the thalamus to the sensory cortices. Ascending dorsal column fibres have excitatory terminals in the periaqueductal grey (PAG), which in turn projects to the rostroventral medulla (RVM), an area responsible for descending inhibition of pain; this feedback is the mechanism by which ascending signals can reduce painful inputs. Dorsal column fibres carry axons of second-order neurons that enable our perception of touch, and can additionally modulate ascending pain integration with inhibitory synapses at wide dynamic range (WDR) neurons in the spinal cord (discussed more in chapter 1). WDR neurons ascend via the anterior spinothalamic tract, and have numerous terminals in the RVM, reticular formation and PAG (Irvine and Clark, 2018). In this way, both innocuous and noxious sensory pathways can activate the DAS (Caylor et al., 2019). After terminating in the thalamus, projections from the anterior spinothalamic pathway are sent to many brain structures associated with sensory, affective, and motivational processing of pain, such as the primary and secondary somatosensory cortices (SI & SII),

Anterior Cingulate Cortex (ACC), prefrontal cortex (PFC), amygdala, ventral tegmental area (VTA) and the nucleus accumbens (NAc). These cortical areas can additionally facilitate antinociception at the dorsal horn by directly or indirectly exciting a locus coeruleus-PAG-RVM loop that inhibits second-order projection neurons at the spine, suppressing ascending nociceptive signals (Song et al., 2013; Todd, 2010).

Descending antinociceptive projections release serotonin (5HT), norepinephrine (NE), acetylcholine (Ach), γ-aminobutyric acid (GABA) and opioids into synapses in the dorsal horn to reduce excitability, inevitably reducing the frequency at which pain signals ascend to the cortex for processing. The contribution of descending serotonergic neurons has been documented (Song et al., 2011), showing that selectively antagonising 5HT receptor subtypes can attenuate SCS effectiveness. Dorsal horn 5HT levels has been shown to increase after SCS, and increased presentation of spinal 5HT and 5HT-like receptors have been observed in rats that responded to SCS (Song et al., 2009). Similarly, a potential role for GABA with SCS has been observed, with antagonists reducing its effectiveness (Rees and Roberts, 1989), reduction in GABA levels after SCS (Stiller et al., 1995) and antinociceptive effects observed with the introduction of GABA antagonists (McMahon et al., 2013). It is possible the descending fibres themselves are directly and orthodromically recruited by SCS, though the columns carrying these fibres are separate and distant (i.e., the ventrolateral, dorsal and dorsolateral funiculi), so the effect of stimulation would be greatly reduced; indeed, stimulations of the magnitude of SCS's recruitment of dorsal columns themselves have estimated as few as 1% of the fibres being recruited (Holsheimer, 1998), so recruitment of orthodromic descending signals seems unlikely in conventional SCS.

Other studies have evaluated the contribution of orthodromic and antidromic signalling of SCS leads by observing antinociception relative to lead placement and cord transection. In Rees & Robert's study (1989) the spine was stimulated above and below a transection of the dorsal column to evaluate whether the orthodromic dorsal column pathway was necessary for pain relief, and showed that stimulation caudal (inferior) to the lesion only produced very short-term suppression in comparison to long-term inhibition from rostral (superior) stimulation of the dorsal column; El-Khoury et al. (2002) replicated these findings, demonstrating a reduction of allodynia in rats (measured with paw withdrawals) with neuropathic pain when stimulating rostral to a transection at the spine. Barchini et al. (2012) elucidated this relationship further, showing that transection of the dorsal column does not absolutely halt antinociception provided by caudal stimulation of the spinal cord, implicating some localised segmental mechanisms – perhaps including recruitment of DAS or local glia. The evidence reviewed here strongly implies that descending inhibition as activated by the orthodromic dorsal column pathway is a significant component of SCS antinociception, but also demonstrates that it is not able to explain its entire mechanism.

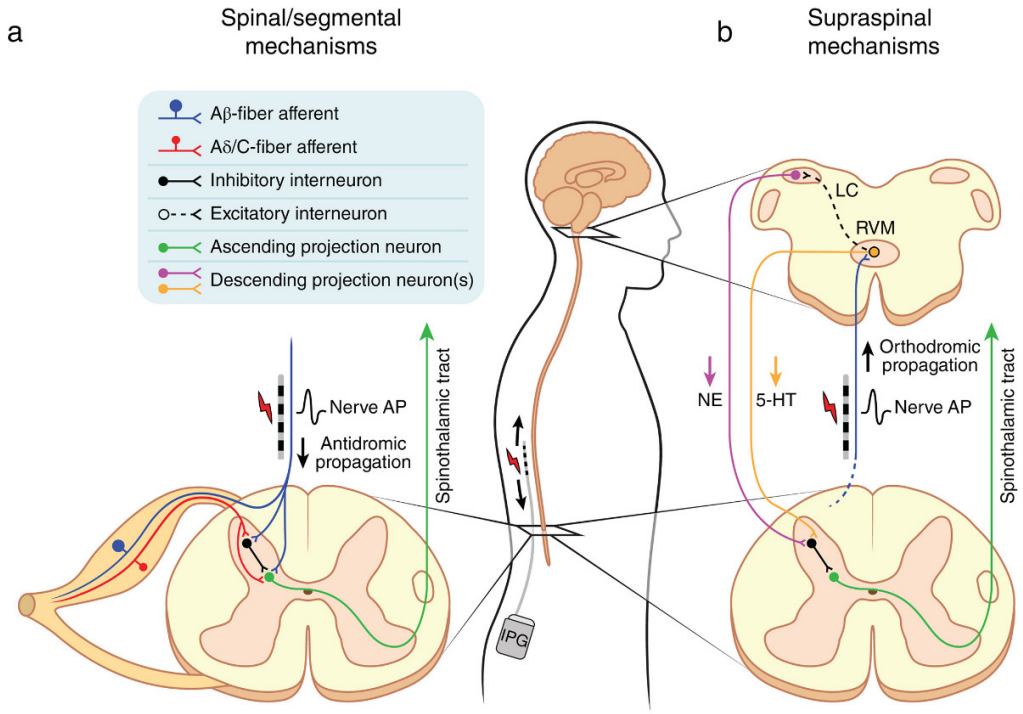

Figure 2.2: Proposed mechanisms of SCS. A. Spinal and segmental mechanisms: antidromic signalling caused by the SCS leads activate inhibitory interneurons and innervate wide dynamic range neurons, whilst localised stimulation of microglia may also influence local circuitry. B. Supraspinal mechanisms: orthodromic signalling of dorsal column fibres activate brainstem centres that are associated with descending antinociception at the second-order neurons in the spine, resulting in a suppression of pain signals along the spinothalamic tract. AP: Action potential. IPG: Implantable Pulse Generator. LC: Locus Coeruleus. RVM: Rostroventral Medulla. NE: Norepinephrine. 5-HT: Serotonin (5-hydroxytryptamine). Adapted from Sankarasubramanian et al. (2019).

2.1.1.2 Cortical activity during SCS

With modulation of ascending fibres, it follows that there may be some resulting pattern of activity in the cortex. This has been explored across multiple modalities, with convincing evidence for the recruitment or suppression of brain areas associated with the processing of pain. PET and SPECT imaging studies have identified increased activity in the thalamus,

orbitofrontal cortex, parietal cortex, anterior cingulate cortices, cerebellum, and dorsolateral prefrontal cortex; these studies also observed decreased activity in the anterior cingulate gyri, subcallosal gyri, superior temporal gyri and anterior cingulate gyri as a result of active SCS (Kishima et al., 2010; Nagamachi et al., 2006). Rat fMRI studies have demonstrated that SCS increases blood oxygen level-dependent signal in the primary somatosensory cortex, premotor cortex, anterior cingulate cortex, amygdala, and insula (Meuwissen et al., 2020). Human studies have shown activation in the primary somatosensory cortices and insula (Stančák et al., 2008), the cingulate gyri, thalamus, and prefrontal cortices (Rasche et al., 2005) and deactivations of the parahippocampus, posterior cingulate gyrus, precuneus, secondary somatosensory cortices, caudate putamen and superior temporal gyrus (De Groote et al., 2018; Saber et al., 2022). These findings show activation of brain areas that are commonly associated with the processing of nociceptive aspects of pain and sensation, and suppression of brain areas linked with the affective characteristics of the pain experience – but elucidate very little about the nature of these changes in anything other than magnitude and location.

2.1.2 Antidromic action of SCS

2.1.2.1 Segmental action of SCS

Action potentials generated by SCS electrodes can travel caudally against the usual propagation tract of the dorsal columns, and antidromically stimulate terminals at inhibitory and projecting neurons (Figure 2.2a). The inhibitory activity of these local connections is a result of glycine and GABAergic synapses, though they can be influenced by the descending mechanisms mentioned in the previous section (Todd, 2010). In contrast to the reduction of GABA in the brainstem,

studies have demonstrated that SCS induces an increase in GABA and GABA receptors in the spinal cord (Barchini et al., 2012; Cui et al., 1997, 1996; Song et al., 2011, 2009; Stiller et al., 1995); these mechanisms are associated with a concurrent reduction in glutamate and decreased WDR excitability, as measured by the reduced amplitude of evoked potentials and less frequent spontaneous firing (Cui et al., 1997; Yakhnitsa et al., 1999).

At the spinal level, local microglia and astrocytes are also involved in the moderation of circuitry, and SCS has been demonstrated to decrease activation in both (McCarthy et al., 2013; Sato et al., 2013). Reduction of inflammatory responses and facilitatory gliosis have been proposed as mechanisms of SCS' antinociceptive effect, though changes in glial mediators throughout the central and peripheral nervous system as a result of SCS are not uniform, and some of them are pro-nociceptive (Caylor et al., 2019; Kim et al., 2013; Tilley et al., 2015). The inactivation of microglia and the resulting antinociceptive effect have been linked to their cannabinoid CB1 receptors, which have been thought to mediate SCS-induced reduction in mechanical hypersensitivity resulting from the use of CB1 antagonists (Sdrulla et al., 2015). With simulations of lead current dispersion estimating that as few as 1% of Aβ fibres are effectively stimulated, it is not a surprise that other local structures may be influenced and contribute to its antinociceptive effect (Holsheimer, 1998).

2.1.2.2 Antidromic stimulation and collision of SSEPs

Ascending somatosensory signals propagate along the dorsal columns towards the cortex, but have synapses along this pathway that inhibit WDR neurons at the spinal cord. These fibres are those targeted by SCS, and are capable of carrying SCS signals antidromically, inhibiting

ascending pain signals at the WDR neurons, as naturally ascending somatosensory signals might. In an attempt to demonstrate this, research has focused on the collision of somatosensory evoked potentials (SSEPs) – action potentials generated by a sensory stimulus – with antidromic stimulations originating from the stimulating leads along the dorsal columns. In theory, somatosensory signals that ascend the dorsal columns will be extinguished by out-of-phase collision with antidromic stimulation, and the smaller amplitude orthodromic currents generated by the SCS are responsible for the sense of paraesthesia (Fig 2.3) (Caylor et al., 2019).

This concept has been thoroughly researched, with the majority of electro- and magneto-physiological recordings studying SCS focusing on this topic. Reduced SSEPs recorded by single-cell electrodes and EEG during SCS are well documented in rat and human experiments (Buonocore et al., 2012; Buonocore and Demartini, 2016; Lang et al., 1989; Larson et al., 1974; Poláček et al., 2007; Urasaki et al., 2014; Wolter et al., 2013); though it does not appear to be entirely consistent (Doerr et al., 1978; Mazzonea et al., 1994; Weigel et al., 2015).

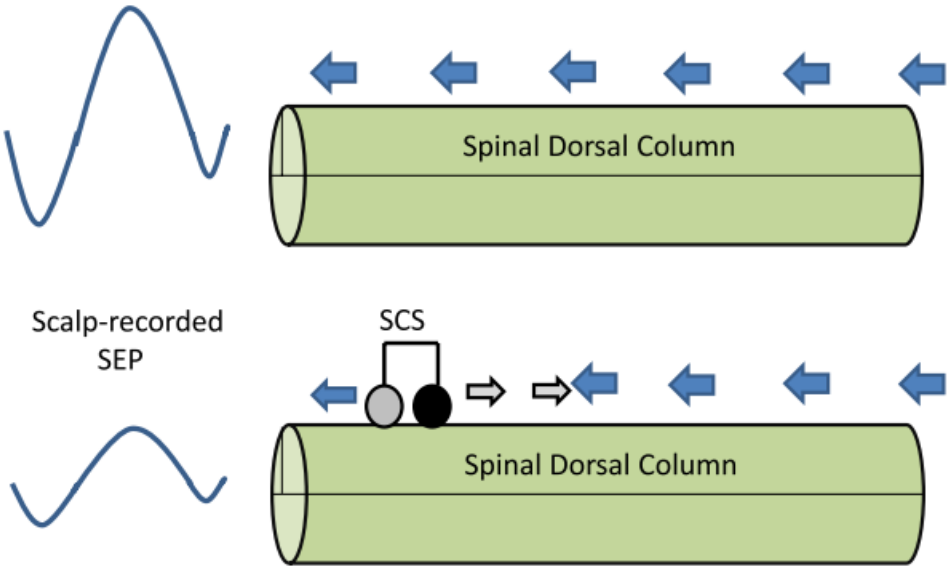

Figure 2.3: The proposed collision of somatosensory evoked potentials (SSEP, or SEP) as a result of antidromic SCS signals. Adapted from Urasaki et al. (2014).

The collision of SSEPs has been thought to be a marker for SCS effectiveness (Sindou et al., 2003), whilst others have remarked that SSEP response could be parameter-specific (Poláček et al., 2007). Dorsal horn nuclei have been shown to have reduced excitability during SCS (Yakhnitsa et al., 1999), and nociceptive stimuli have also been found to be suppressed by SCS patients undergoing stimulation (Bocci et al., 2018; Hylands-White et al., 2016; Pluijms et al., 2015a; Stančák et al., 2008), though it is not possible that this is the result of collisions in the dorsal column as nociceptive stimuli ascend the spine laterally: instead, it has been suggested to be the result of the antidromic inhibition of WDRs by Aβ fibres. Investigating this, Testani et al. (2015) used laser stimulation on the arm in conjunction with delayed electrical stimulation of Aβ fibres of the second and third fingers of the same limb: They demonstrated that N2P2 components were only significantly reduced when the Aβ stimulation was between 150-200ms

after the laser stimulation, and concluded that the conductance velocities demonstrated that the anti-nociceptive mechanism of Aβ stimulation took place in the cortex, perhaps in a 'first-come-first-served' manner. Further support for this comes from the observation that SCS suppression of dorsal horn excitability lasts beyond SCS stimulation (Yakhnitsa et al., 1999). Though these findings do not rule out simultaneous spinal-level inhibition, it does imply that there are additional components contributing to the antinociceptive effect of SCS.

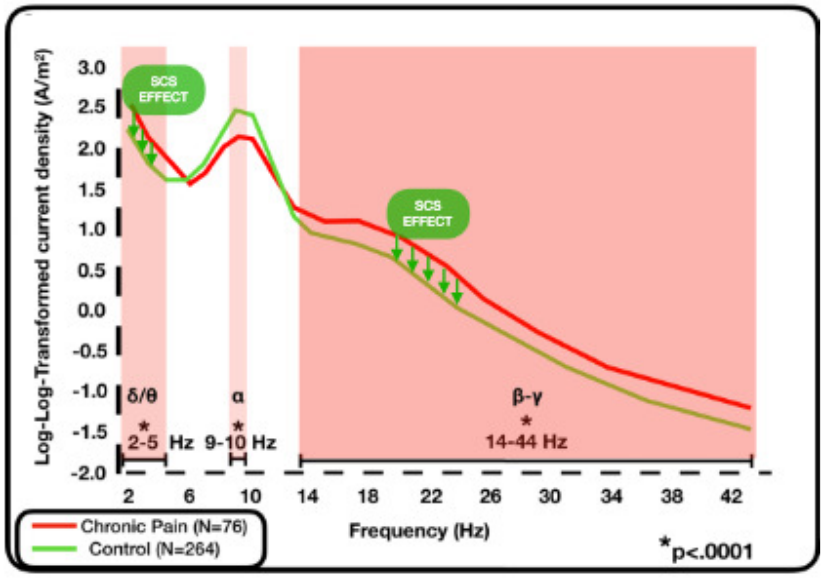

Figure 2.4: An example of the normalisation of thalamocortical dysrhythmia as presented in Caylor et al., (2019), originally adapted from Vanneste, Song & De Ridder (2018). The pink boxes show areas of significant differences between healthy controls and chronic pain patients, the green arrows added by Caylor et al. demonstrate the suppression of delta, theta, beta, and gamma frequency power to 'normal' levels by SCS.

Somatosensory and pain-evoked potential findings, electro- and magneto-physiological studies have identified SCS alterations of oscillatory and networking behaviour in the brain as a result of ongoing SCS. The normalisation of thalamocortical dysrhythmia has been observed in CRPS and PSPS patients (Schulman et al., 2005; Pahapill and Zhang, 2014; Sufianov et al., 2014)

(Figure 2.4), and resting-state analyses have elucidated some underlying oscillatory components in patients undergoing SCS in active and baseline states (Goudman et al., 2019; De Ridder and Vanneste, 2016). Though most of this research has analysed only sensor-level data in small patient groups, one EEG study has used source-level data to explore oscillatory power in the range of 1-44 Hz, and identified suppression of beta and low gamma in the posterior cingulate gyrus and parahippocampus in SCS conditions (De Ridder & Vanneste, 2016).

It is clear that the effects of SCS are not isolated to one mechanism, and that extracting them is not a simple feat; there is evidence for mechanisms at segmental, supraspinal and cortical levels. Attenuation of evoked activity seems to reflect the modulation of innocuous and nociceptive sensory input, with some areas of the pain matrix being identified as regions of interest by indirect blood-flow measurements of neural activity. Evoked waveforms elicited by sensory and nociceptive stimuli do appear to be attenuated or abolished, but not in a consistent way. This is likely due to the heterogeneous nature of the patients, therapeutic coverage of SCS-generated paraesthesia, stimulation parameters and low dispersion of charge to spinal cord fibres. Little research has been conducted that explores the localisation of brain activity in source-space outside of PET, SPECT, and fMRI – which are only able to follow slow changes in brain activity, despite clear evidence of oscillatory power changes as a result of SCS in EEG and MEG. These changes likely reflect the orthodromic supraspinal effects of SCS, and delineating them could elucidate their antinociceptive mechanisms, and identify therapeutic targets, especially for deep brain and transcranial stimulation.

2.2. The Cold Pressor Test

The cold pressor test (CPT) is an experimental tool to induce pain or elicit a physiological stress response. It is a cooling water bath that is kept at a consistently cold temperature (most commonly 1°, 3°, 5° or 7° Celsius according to a review by Mitchell et al., 2004), that participants or patients submerge their hand in. The CPT was originally designed and validated by Hines & Brown (1932) as a tool for testing vascular reactivity with the premise that blood pressure changes caused by the CPT would screen for high blood pressure. Upon being subjected to the stimulus of the CPT, a sympathetic nervous system activation constricts capillaries in the skin as a homeostatic mechanism to reduce body temperature loss. This reaction to the stimulus can be used to observe blood pressure changes in clinical conditions such as hypertension. Though the stimulus is initially non-painful, participants submerging their hand will quickly find the cold water painful due to temporal summation, and the cold temperatures penetrating the skin and activating more nociceptors (Dubin and Patapoutian, 2010).

The CPT is a valid and consistent measure of pain tolerance and pain threshold at different time points and temperatures (two weeks apart, 4°C-6°C; Koenig et al., 2014); however, using different equipment and laboratory settings can have a significant influence on pain outcomes (Vigil et al., 2014)– and very few studies have homogenous parameters (Mitchell, MacDonald and Brodie, 2004). This is compounded by differences in equipment, older (and even some contemporary studies) use iced buckets of water, whilst the gold standard is a circulating cooling water bath: Traditional methods that do not circulate water allow a pocket of warmer water to form around the hand and will passively warm up over time.

CPT studies have contributed mostly to our understanding of pain tolerance, with the primary outcome metric being the duration a participant can endure hand submersion: studies have shown that CPT endurance can be influenced by sex (Hellström and Lundberg, 2000; Jasrotia et al., 2018; Kowalczyk et al., 2006; Lighthall et al., 2012; Stening et al., 2007), gender (Martin, 2019), investigator gender (Vigil et al., 2014), menstrual cycle phase and oral contraceptive use (Eichhorn et al., 2018; Hellström and Lundberg, 2000; Jasrotia et al., 2018; Stening et al., 2007), and ethnicity (Weisse et al., 2005). High scores on psychological variables like pain-related fear (George et al., 2006; Hirsh et al., 2008; Patanwala et al., 2019; Sullivan et al., 1995), pain anxiety (Jones et al., 2002; Roebuck et al., 2018), anxiety sensitivity (Schmidt and Cook, 1999) are associated with lessened CPT endurance and higher pain scores. Lower CPT pain sensitivity has been observed in males (Vigil et al., 2014), stress-induced analgesia (Al'absi et al., 2021), those listening to music or otherwise distracted (Choi et al., 2018), individuals who exercise (Petkova and Nikolov, 2018), those with higher hopefulness and optimism traits (Berg et al., 2008; Hanssen et al., 2014; Snyder et al., 2005) and controls in distraction and priming paradigms (Dahlquist et al., 2009; Damme et al., 2008; Stephens et al., 2009). The CPT's utility in clinical applications has also been explored, with studies showing validating its effectiveness at delineating treatment outcomes in opioid-induced hyperalgesia and fibromyalgia (Compton et al., 2022; Oaks et al., 2018), demonstrating increased pain sensitivity in chronic pain patients (Butler et al., 2020), identifying opioid responders (Gram et al., 2015), recovery from whiplash (Kasch et al., 2005) and predicting postoperative pain (Werner et al., 2010).

Alternatives to the traditional CPT technique have been validated to varying extents, with cooling thermodes (Peckerman et al., 1991; Ruscheweyh et al., 2010), cooling wraps (Porcelli,

2014) and gel packs (Lapotka et al., 2017) being shown to replicate the pain and cardiovascular effects of the traditional CPT method; these advancements are vital for brain imaging methods such as fMRI and MEG, where large buckets of stationary water may be impossible to manoeuvre practically, and circulating cool water baths may introduce electromagnetic artefacts. Despite these compatible techniques, studies combining them are limited. Using alternative fMRI-compatible CPT methods, researchers have observed enhanced BOLD in several brain areas including the periaqueductal grey, frontal gyrus, anterior cingulate cortex, thalamus, insula, temporal gyrus posterior parietal cortex (La Cesa et al., 2014; Frankenstein et al., 2001; Kakeda et al., 2010; Lighthall et al., 2012).

Much of neuroimaging research in CPT uses electroencephalography (EEG) recording, thanks to fewer practical limitations with the equipment. Studies exploring the time course of EEG recordings during CPT consistently identified consistent alpha desynchronisation, with evidence for increased synchronisation of beta, delta, and theta oscillations across contralateral parietal sensors (Backonja et al., 1991; Chang et al., 2002; Chen et al., 1989; Dowman et al., 2008; Ferracuti et al., 1994; M. Gram et al., 2015; Shao et al., 2012; Wang et al., 2020). Explorations of underlying sources by Shao et al. (2012) and Hansen et al. (2017) identified alpha suppression in the central gyri, with increases in prefrontal cortices, insula, temporal, and cingulate regions across beta and gamma bands.

To date, no published studies have combined CPT analogues and magnetoencephalography in an exploration of neural dynamics of pain. Few studies have utilised CPT to explore the brain biomarkers of pain sensitivity, but none have used modern source reconstruction techniques to elucidate their underlying neural generators. Such a study could provide valuable insight into

markers of pain sensitivity, and could assist in treatment selection, effectiveness and responsiveness or diagnosis, risk, stage, or progression of disease (Lleó, 2021; Mouraux and Iannetti, 2018).

2.3. The Contact Heat Evoked Potential Stimulator and MEG, a systematic review

2.3.1 Introduction

The PATHWAY Contact Heat Evoked Potential Stimulator (CHEPS) (hereby referred to simply as the CHEPS; Medoc Ltd., Ramat-Yoshai, Israel) is a method for evoking and assessing somatosensory functioning in clinical settings and has been used as a stimulus in somatosensory brain imaging research. The CHEPS is a commercially available thermode with an external heating foil that is surrounded by an electrically isolated plastic layer to protect the skin. It has a standard temperature range of 20-51°C, a rising temperature rate of 70°C/s, and a cooling rate of 40°C/s. The CHEPS can ramp and hold targeted temperatures for extended durations, but also produce brief pulses of thermal stimuli, which facilitate the recording and analysis of event-locked waveform data.

Pain is a sensory and psychological experience that is cortically processed; methods that evoke pain in combination with functional neuroimaging methods that have a high temporal resolution, can provide valuable insights into how pain is represented temporally, spectrally, and spatially in the brain. Separating nociception from innocuous sensory input can be problematic, as often stimuli activate Aβ fibres alongside Aδ and C fibres. Additionally, it is important to consider how well a stimulus emulates pain that might be experienced outside of a laboratory or in clinical cases. In contrast to some electrical and mechanical techniques, the CHEPS does not activate Aβ fibres. It also generates a more ecologically valid pain experience via transduction, as opposed to direct electrical stimulation. As an alternative to laser stimuli, the CHEPS is more accessible and affordable, does not require special safety precautions for

experimenters or participants, poses a significantly reduced burn risk, and is not impacted by skin reflectance (Frahm et al., 2020).

There is a sizeable body of research exploring CHEPS with EEG, but the use of CHEPS in conjunction with magnetoencephalography (MEG) has been less explored. MEG and EEG brain recordings share similarities in temporal resolution and, it is assumed, their underlying sources, but their data are not identical, and have different characteristics due to the way they obtain their signal; EEG recordings acquire information about the electrical currents generated by neural tissue, which can be distorted by tissue conductivity, resulting in lower spatial resolution and smaller signal-to-noise ratios than MEG recordings (Singh, 2014). MEG is more capable of accurately localising brain activity, as the magnetic fields it records are less distorted by volume conductance; MEG systems also have much-reduced preparation time and up to 320 sensors in some models, which is of benefit for high-density recordings. Though the hardware specifications of the CHEPS are proprietary, researchers have suggested that thermode feedback components likely contribute to significant electromagnetic signal interference that MEG sensors are sensitive to (Gopalakrishnan et al., 2013). Advances in temporal signal space separation (tSSS; Taulu and Hari, 2009; Taulu and Simola, 2006) and research exploring beamforming techniques have demonstrated the ability to reduce this artefact (Adjamian et al., 2009); despite the potential advantages for the identification of electromagnetic components in thermal somatosensory research, studies combining the methods appear sparse.

This systematic review aims to identify and critically appraise current literature that explores the use of CHEPS in combination with MEG, highlighting findings and methodological implications for the study of pain and sensation.

2.3.2 Methodology

This systematic review is reported following Preferred Reporting Items for Systematic Reviews and Meta-Analyses (PRISMA) guidelines, to elucidate the literature combining MEG and CHEPS methodologies with a focus on pain research (Page et al., 2021). The protocol for this review is registered on PROSPERO as CRD42020178324.

2.3.2.1 Search strategy

Electronic databases searched included MEDLINE, The Cochrane Library (CENTRAL), Embase, CINAHL, PsycINFO, SportDISCUS, Scopus, and Google Scholar, searched from inception until 1st March 2020 (Appendix B.1). An experienced information specialist (Michelle Maden; MM) conducted the searches. The search strategy included a combination of free-text and indexing terms and was restricted to the English language. Reference lists and literature that cited included studies, were hand-searched for additional relevant items. Force-directed graphs based on co-citation and bibliographic coupling were then created for all included studies via ConnectedPapers (www.connectedpapers.com), and these graphs were scrutinised for possible inclusions.

2.3.2.2 Study selection

Two reviewers (Thomas Graeme-Drury and Rui Duarte; TGD and RD) independently screened all titles and abstracts to identify potentially relevant studies. Any papers with methods that were unclear in their abstract were included for assessment of the full text. Full texts of potentially relevant studies were retrieved, and the same reviewers evaluated their eligibility, using the criteria outlined in Table 2.1. Disagreements at each stage were resolved through discussion, with a third author available to consult on any disagreements (Siân Worthen; SW).

Table 2.1: Eligibility criteria

Inclusion (if all criteria met)	Exclusion (if any criteria met)
Adults (18 years+)	Participants under 18 years of age
MEG used as part of the study	Participants unable to communicate pain outcomes
CHEPS used as part of the study	Conference proceedings, case reports, qualitative studies and studies that do not present original data (i.e., reviews, letters, or editorials)
	Non-English language

2.3.2.3 Data extraction

One reviewer (TGD) extracted data using a piloted data extraction form. A second reviewer checked for accuracy (RD), with a third reviewer available to consult where necessary (SW). Due to the predicted heterogeneity across studies, a broad style of data extraction was implemented. The extraction of data from the included studies focused on any significant event-related fields (ERF), time-frequency, and source localisation characteristics in response to sensory stimulation; the expected outcomes for which were direct findings or implications for pain processing or methodology in clinical or experimental settings. Additional data regarding the parameters of CHEPS stimulation, titration, participant sample, study designs, MEG acquisition, and analysis were collected and presented to evaluate their consistency and any missing information.

2.3.2.4 Risk of bias assessment

The risk of bias was evaluated by one reviewer (TGD) and checked by a second (RD). The risk of bias was assessed using a version of the National Heart, Lung and Blood Institute Study Quality Assessment Tools for Case Series studies that were altered to reflect the studies identified

(National Heart, Blood and Lungs Institute, 2019)(see Appendix B.2). The alterations refocused the questions on experimental procedures and randomisation. A third reviewer was available to consult on any disagreements if necessary (SW).

2.3.2.5 Data synthesis

Due to heterogeneity across the included studies, a narrative synthesis was conducted. A meta-analysis was not considered appropriate given the aim for this review and the numerical data presented within the studies being inadequate for pooling. The included studies are aligned with the type of research (i.e., somatosensory or pain anticipation research) and methods of analysis (i.e., ERF or time-frequency analysis). The data has been synthesised by presenting expected outcomes for which there were direct findings or implications for pain processing or methodology in clinical or experimental settings.

2.3.3 Results

2.3.3.1 Study selection

The database searches produced 646 results. Six additional papers were identified through other sources. After the removal of duplicates, 275 abstracts were screened, and 58 studies were identified as requiring full-text evaluation. Of these, eight were identified as meeting the eligibility criteria (Adjamian et al., 2009; Gopalakrishnan et al., 2013, 2015, 2016a, 2016b, 2018; Machado et al., 2014; Fardo et al., 2017). Fifty studies were excluded because they did not use MEG in their design. The PRISMA flow chart outlining the process is shown in Figure 2.5.

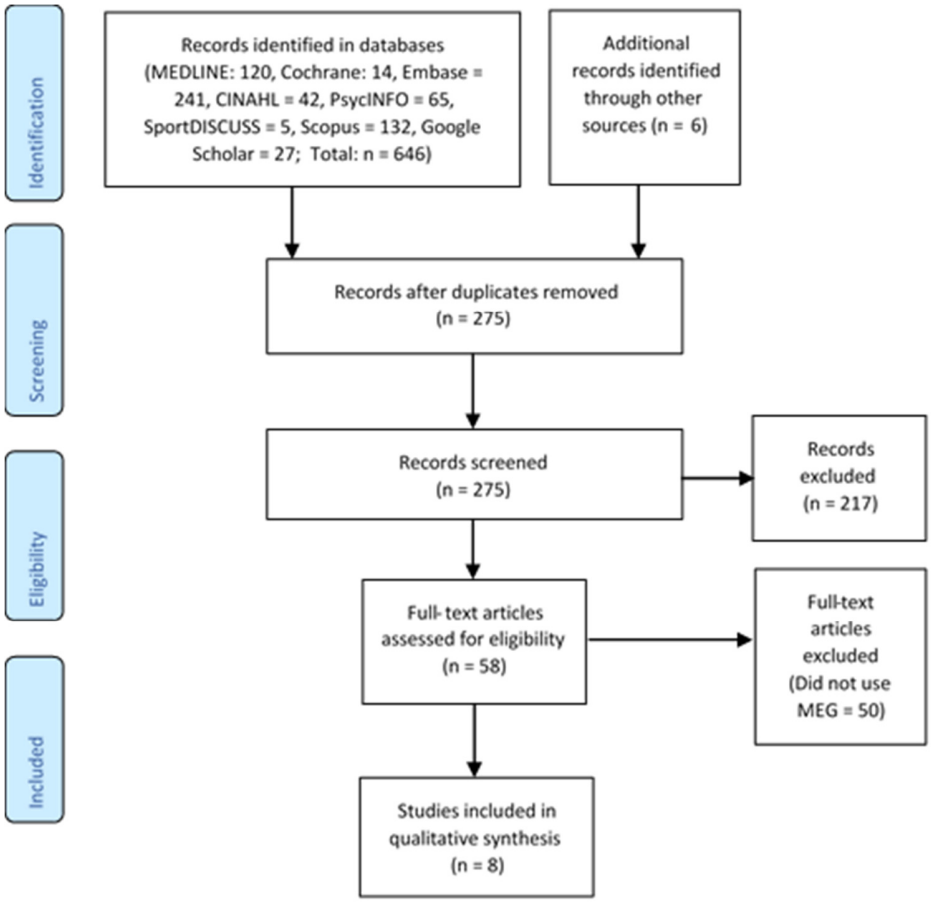

Figure 2.5: PRISMA flow chart for studies identified throughout the review process.

2.3.3.2 Study characteristics

Table 2.2 outlines the included study characteristics. Included studies were experimental and primarily recruited healthy controls. Two of the eight studies investigated Post-Stroke Pain Syndrome (PSPS; or "Central Post-Stroke Pain") (Gopalakrishnan et al., 2016b, 2018), five used the CHEPS as a noxious stimulus to elicit pain anticipation (Machado et al., 2014; Gopalakrishnan et al., 2015, 2016a, 2016b, 2018), two papers outlined artefact rejection methods to combat the electromagnetic noise generator by the CHEPS (Adjamian et al., 2009;

Gopalakrishnan et al., 2013) and one used the CHEPS to induce cold innocuous sensation (Fardo et al., 2017).

CHEPS equipment, stimulation, titration, and trial parameters are outlined in Table 2.3. All studies used the Pathway model Contact Heat-Evoked Potential Stimulator (Medoc, Ramat-Yoshai, Israel). All but one study recorded data using an Elekta Neuromag TRIUX MEG system with 204 planar gradiometers and 102 magnetometers; the other used a CTF 275-channel axial gradiometer MEG (VSM Medtech, Canada) (Adjamian et al., 2009). Of the seven studies that used the systems with planar gradiometers, five chose to use only planar gradiometer data in their analysis (Gopalakrishnan et al., 2013, 2015, 2016a, 2016b, 2018), one used both combined where possible (Fardo et al., 2017) and one did not report their selection (Machado et al., 2014). In six of the studies, tSSS was used in the pre-processing of the data, two did not report its use or any alternatives (e.g., Signal Space Projection, Signal Space) (Machado et al., 2014; Adjamian et al., 2009). Only one study mentioned prewhitening to reintroduce dimensionality to the data removed by tSSS (Machado et al., 2014). Results directly linked to CHEPS, somatosensory outcomes, or utility in MEG are highlighted.

Table 2.2: Characteristics of studies included in this review

Author (year)	Sample	Study design focus	Control	Outcomes	Regions of Interest (where applicable)
Adjamian (2009)	HC	CHEPS used to elicit an evoked field in response to a painful stimulation; investigate the effectiveness of SAM beamforming in reducing the noise generated by the stimulator and successfully localising the evoked field	Electrical SEF condition to confirm CHEPS accuracy. Sham condition.	Effectiveness of SAM beamformer in localising peak activation in CHEPS data; time-frequency profile of primary somatosensory cortex in response to CHEPS stimulation	S1
Gopalakrishnan (2013)	HC	CHEPS electromagnetic artefact in MEG setting, evaluation of the effectiveness of preprocessing techniques in its removal	N/A	Effectiveness of artefact removal techniques	
Machado (2014)	HC	Oscillatory characteristics in pain neuromatrix and visual cortex ROI in anticipation of CHEPS-induced pain during three countdown visual cues in HCs.	Non-painful and no-stimulation conditions	Significant differences in TF power between conditions and cues in ROI	V1, OFC, DLPFC, ACC, MCC, PCC, INS
Gopalakrishnan (2015)	HC	Oscillatory characteristics in pain neuromatrix and visual cortex ROI in anticipation of CHEPS-induced pain during two countdown cues of tactile, auditory, or visual modality	Non-painful and no-stimulation conditions	Significant differences in TF power between conditions and cues in ROI	V1, S1, A1, DLPFC, OFC, INS, ACC, MCC, PCC
Gopalakrishnan (2016a)	HC	CHEPS pain anticipation ERFs and their source location as cued by three visual cues in HCs, compared to non-pain anticipation.	Non-painful and non-stimulation conditions	Significant differences between ERFs in each condition, the sequential cues, and their underlying sources	
Gopalakrishnan (2016b)	PSPS	Pain anticipation in PSPS patients and its neural correlates following three visual countdown cues for CHEPS stimuli on affected and non-affected stimuli	Matched HCs (data from Golpalakrishnan (2016a)); Non-painful, non-stimulation and unaffected limb conditions	Significant differences between ERFs in each condition, the sequential cues, and their underlying sources; significant differences between conditions and cues in TF power in ROI.	ACC, MCC, PCC, S1, V1, PFC, PC, OIC, MTC
Fardo (2017)	HC	ERFs generated by Δ3˚C and Δ5˚C cooling sensation using the CHEPS in HCs.	Non-stimulation trials	Significant differences in ERF between conditions in left, central and right clusters; TF and localisation of frequencies of interest identified in the signal	
Gopalakrishnan (2018)	DBS-PSPS	CHEPS pain anticipation ERF characteristics and their source locations in DBS-PSPS responders and non-responders; with DBS on and off, and in affected vs non-affected extremities	Non-painful, no-stimulation conditions and pre-surgery baseline recordings	Differences in ERF and their underlying sources between all conditions; CHEPS pain threshold and pain rating between on/off, baseline and control conditions	

ROI = Region(s) of Interest; TF = Time-frequency; PSPS = Post-stroke Pain Syndrome; HC = healthy control; SEF = Sensory Evoked Field; DBS-PSPS = Deep Brain Stimulation – Post-Stroke Pain Syndrome; ERF = Event-Related Field; V1 = Primary visual cortex; S1 = Primary sensory cortex; A1 = Primary auditory cortex; DLPFC = Dorsolateral pre-frontal cortex; ACC = Anterior cingulate cortex; MCC = Medial Temporal Cortex; PCC = Posterior Cingulate Cortex; INS = Insula; OFC = Orbitofrontal Cortex; OIC = Operculo-insular Cortex; MTC = Medial Temporal Cortex; PFC = Prefrontal Cortex

Table 2.3: CHEPS and MEG parameters of the included studies

First author (Year)	Number of participants* and age (SD)	CHEPS stimulation location	Baseline temp ˚C	Target temp C˚ (Mean +-SD)	Titration method	Stimulation duration	Number of trials (Total)	MEG data pre-processing			
								Data cleaning	Filtering	Co-register MRI	HPI coils
Adjamian (2009)	8 NR	Dorsum of non-dominant hand	32	Titrated (48.1, 1.5)	Equivalent of 7/10 on a VAS; no other details reported	500ms	30	N/A	BP 13-20, 20-30 Hz	Yes	Yes
Gopalakrishnan (2013)	1 NR	Palmar surface	30	Titrated (NR)	Ramp and hold for 2s from 40˚C to 50˚C; stopping at "tolerable yet painful", never above 50˚C.	2s	36	SSP, tSSS, DSM separately; selected gradiometers	DC offset	NR	NR
Machado (2014)[1]	10 (M =7, F = 3) 45 (15)	Volar forearm; Left vs right	NR	Titrated (48.4, 1.4)	Ramp and hold for 2s every 1˚C from 40˚C to 50˚C, stopping at VAS of 8/10	2s	240 per condition, 40% of which were no-stim controls (480)	Temporal prewhitening	DC offset; BP 8-100 Hz.	Yes	Yes
Gopalakrishnan (2015)[1]	10 (M = 7, F = 3) 45 (15)	Dominant volar forearm	30	Titrated (49.1, 0.7)	Ramp and hold for 2s every 1˚C from 40˚C to 50˚C, stopping at VAS of 8/10	2s	105 per condition (945)	tSSS; selected gradiometers	DC offset; BP 1-100 Hz	Yes	NR
Gopalakrishnan (2016a)[1]	10 (M = 7, F = 3) 45 (15)	Volar forearm; Left vs right	NR	Titrated (48.6, 1.5; 48.6, 1.3)	Ramp and hold for 2s every 1˚C from 40˚C to 50˚C, stopping at VAS of 8/10	NR	240 per condition; 40% of which were no-stim controls (480)	tSSS; selected gradiometers; head-movement compensation	DC offset; BP 1-70 Hz	Yes	Yes
Gopalakrishnan (2016b)	7 (M = 4, F = 2) 51 (6)	Volar forearm; affected extremity vs non-affected	NR	Titrated (47.5, 1.7; 47.8, 1.3)	Ramp and hold for 2s every 1˚C from 40˚C to 50˚C, stopping at VAS of 8/10	NR	240 per condition, 40% of which were no-stim controls. (480)	tSSS; selected gradiometers	DC offset; BP 1-70 Hz	Yes	Yes
Fardo (2017)	6 (M = 3, F = 3) 23 (12)	Dorsum of non-dominant left hand	35	32, 30	NA	200ms	80 per condition, plus 40 blank trials (200)	tSSS; ICA; used combined gradiometers in TFA; head-movement compensation	ERF data LP 20 Hz; TF data no filter	Yes	Yes
Gopalakrishnan (2018)	7 (M = 5, F = 2) 52 (5)	Volar forearm; affected extremity vs non-affected	NR	Titrated (48‡, CD)	Ramp and hold for 2s every 1˚C from 40˚C to 50˚C, stopping at VAS of 8/10	NR	120 of each condition on affected and non-affected extremity, 40% no-stim trials (480)	tSSS; selected gradiometers; head-movement compensation	DC offset; BP 1-70	Yes	Yes

[1]Same participants, though the dataset presented is different; *After any participant attrition; ‡ Estimated from Figures; VAS = Verbal Analogue Scale; NR = not reported; NA = not applicable; M = Male; F = Female; LP = Low pass; BP = bandpass; SSP = Signal Space Projection; tSSS = Temporal Signal Space Separation; DSM = Damped Sinusoid Model; ERF = Event-Related Field; ICA = Independent Component Analysis; DC = Direct Current; TFA = Time-frequency analysis

2.3.3.3 Risk of bias assessment

Details of the risk of bias assessment are presented in appendix B.2. All studies were judged to have a low risk of bias in the domains of clear experimental procedure, research questions, statistical methodology, and outcomes. None of the studies identified consecutive case samples, and of the experimental studies, only Fardo et al. (2017) and Gopalakrishnan et al. (2015) sufficiently counterbalanced or randomised conditions, adding a considerable risk of desensitisation of thermoreceptors to four studies, as discussed later in this review.

2.3.3.4 Findings of included studies

The included studies are divided into methodological (Gopalakrishnan et al., 2013; Adjamian et al., 2009), somatosensory (Fardo et al., 2017), and pain anticipation research (Machado et al., 2014; Gopalakrishnan et al., 2015, 2016a, 2016b, 2018). The pain anticipation findings are grouped by ERF and or time-frequency analyses.

2.3.3.4.1 Methodological research

Two studies identified by this review, specifically evaluate the utility of preprocessing and analysis techniques in combined MEG and CHEPS research. Adjamian et al. (2009) demonstrated significant attenuation of CHEPS artefact by using a 3rd order synthetic gradiometer. In addition, the effectiveness of Synthetic Aperture Magnetometry (SAM) beamforming in localising CHEPS event-related power change in the 13-20 Hz frequency band was evaluated and found to have similar accuracy and greater precision in localisation of peak activation in S1 when compared to somatosensory evoked potentials following electrical stimulation. Blocking the thermal element of the CHEPS confirmed pain processing was responsible for the recorded output. Comparison of virtual sensor time series and

beamforming output showed that applying regularisation reduced the effectiveness of the spatial filtering, as was evidenced by artefacts in the regularised dataset that were absent beforehand.

Gopalakrishnan et al. (2013) explored different artefact rejection techniques used to suppress the electromagnetic noise associated with the CHEPS' presence in magnetically-shielded chambers, and with its activation. It was demonstrated that SSP (Uusitalo and Ilmoniemi, 1997) failed to adequately remove the CHEPS artefacts using any variety of the method in any phase of the stimulus, while tSSS (Taulu & Simola, 2006) performed well in removing temporal and spectral artefact components, but reduced the dimensionality of the data significantly. The authors piloted a Damped Sinusoid Modelling (DSM) technique in which they decomposed the artefact into varying signal components that decrease over time, then subtracted the modelled waveform from the dataset; they showed similar artefact removal with a lesser reduction of data dimensionality, as well as tighter control of the sinusoids being removed; though some of the artefact did remain in all methods, the authors concluded that the artefact was sufficiently attenuated. The DSM method is not widely available, and this research group did not go on to explore post-stimulus time windows.

2.3.3.4.2 Somatosensory research

Fardo et al. (2017) is the only identified study that applied the CHEPS at a non-noxious temperature. Additionally, their mode of stimulation was that of innocuous cold as opposed to heat: a baseline temperature of 35˚C was applied to their right hand and reduced to 30˚C and 32˚C (Δ5 and Δ3°C) 80 times each in random order with 40 catch trials dispersed after a visual cue. For comparison, 64-channel EEG data were acquired simultaneously. Both MEG

and EEG analysis identified N2-P2 peaks with similar latencies; though EEG data did not show a significant difference between Δ5 and Δ3°C trials, MEG analysis identified higher field strength for N1 (100-304 ms) in Δ3°C and P2 (456-544 ms) in Δ5°C trials across left, central, and right frontal sensors. These windows were then explored by time-frequency analysis to reveal significant increases in delta (1-4 Hz) and gamma-band (30-90 Hz) activity coinciding with these peak differences that were not identified by EEG analysis. Subsequent beamforming linked Δ3°C and Δ5°C to delta power increase in bilateral operculo-insular and calcarine and dorsolateral prefrontal areas respectively; high gamma (55-90 Hz) power was significantly increased in bilateral operculo-insular cortices when comparing cold to no-stimulation conditions, and in the contralateral motor region when comparing Δ5°C to Δ3°C conditions. The findings of activity in the operculo-insular cortices contribute to previous evidence implicating their role in cold sensory processing. Their findings of activity in frontoparietal areas in MEG analysis are attributable to the superior spatial resolution; the frontal delta rhythms were linked to top-down attention required for their sensory detection task and evocation of bottom-up attention as a result of cold sensation. The authors surmised the gamma synchronisation in operculo-insular and motor cortices were responsible for the localised processing of sensory and attentional components of cold stimuli.

2.3.3.3.3 Pain anticipation research

Six studies were conducted by groups comprised of researchers across institutes at the Cleveland Clinic in Cleveland, Ohio (Gopalakrishnan et al., 2013, 2015, 2016a, 2016b, 2018); one of these explored the effectiveness of data cleaning methods (Gopalakrishnan et al., 2013), five were designed to elucidate the mechanisms of processing pain anticipation (Machado et al., 2014; Gopalakrishnan et al., 2015, 2016a, 2016b, 2018), and as such, most

analyses were focused on the time windows following anticipation cues before painful stimulation. The studies published by this group use a consistent protocol: in the first paradigm, a participant-titrated noxious CHEPS or innocuous sensory stimulus was presented following three visual cues; in the second paradigm an alternative titrated innocuous electrical stimulus was presented. Cluster permutation analyses were performed on post-cue time windows to evaluate significant between- and within-condition differences in time-locked waveform component amplitudes across all sensors. Time-frequency analysis was performed using virtual channels in regions of interest. All relevant findings below were reported as statistically significant at $P<0.05$ or $P<0.01$.

2.3.3.3.3.1 Event-Related Field (ERF) analysis

In the first of this series of CHEPS and MEG pain anticipation studies, Machado et al. (2014) observed significantly greater power for V1 ERFs time-locked to the first cue in pain stimuli (PS) compared to no-pain (NPS) or no-stimulus conditions. Using the same dataset, Gopalakrishnan et al. (2016a) performed a non-parametric cluster analysis to test for significant differences between conditions across sensors: this analysis identified central and frontal sensor groups as determinants for pain-specific between-condition differences in first cue visually evoked fields (VEF); additional analysis identified significantly greater power in components evoked by the first cue over later cues. These findings demonstrate fronto-central areas' association with pain-specific anticipation in healthy controls.

Additional studies using this study design and these analysis methods were performed on Post-Stroke Pain Syndrome (PSPS) patients, before and after undergoing Deep Brain Stimulator (DBS) surgery (Gopalakrishnan et al, 2016b, 2018). Gopalakrishnan et al. (2016b) observed cue VEFs in PSPS patients at baseline and found significant differences in frontal

and central sensors only when comparing second and third pain cues to innocuous or no stimulation cues in unaffected limbs. In limbs affected by the chronic pain condition, no significant differences were found between any cues or conditions, elucidating a lack of cue saliency as a result of the chronic pain. After circumventing DBS stimulation artefacts with a bipolar configuration, the follow-up DBS study demonstrated restoration of affected limb cue saliency in conditions with the DBS turned on and off: greater amplitude in first pain cue N1 components were observed, and their differences localised to parietal and midline sensors. Further exploration of the role of responder (n= 4) vs non-responder (n= 3), as operationalised by a change in their Montgomery Åsberg Depression Rating Scale (Montgomery and Asberg, 1979) score, showed responders had significant differences in frontal N1 components within both painful and non-painful cues that correlated with affective benefits. Non-responders also showed a difference between PS and NPS P2 that they claim is a biomarker for the maladaptive hypervigilant attentional processes that are not successfully modulated by DBS in these PSPS patients.

2.3.3.3.3.2 Time-frequency analysis

Gamma and beta VEF time-frequency representations were explored by three studies within this category of anticipatory research. Machado et al. (2014) used virtual channels in dorsolateral prefrontal (DLPFC), orbitofrontal (OFC), calcarine, cingulate (CC), and insula cortices, and observed increased gamma oscillation power throughout pain cues in the left calcarine and right DLPFC, and increased beta oscillation power in the right OFC. A follow-up study that compared visual, auditory, and somatosensory methods of cueing stimulations showed that visual cues recruited greater high beta and low gamma oscillations in the calcarine cortex than any other modality in their associated brain area; cross-modal gamma

activations in primary sensory cortices were present only in pain conditions, and to a lesser extent in A1.

The baseline assessment of PSPS patients in Gopalakrishnan et al. (2016b) demonstrated significant beta and gamma activity in the supramarginal gyrus and frontal polar region during cues two and three when comparing PS to NPS, but no significant effects in the non-affected extremity, consolidating their previous conclusions about the lack of saliency.

2.3.4 Discussion

2.3.4.1 The use of CHEPS in MEG

The results of this review highlight the scarcity of research combining CHEPS and MEG. Using broad search terms, only eight papers were identified. The paucity in this area of literature is likely due to challenges associated with the significant electromagnetic noise generated by the thermode: This review highlights two papers that specifically aim to evaluate analysis techniques that facilitate artefact removal, the results of which demonstrated adequate artefact rejection using SAM beamforming (Adjamian et al., 2009), tSSS or DSM methods (Gopalakrishnan et al., 2013). Indeed, most studies selected here use tSSS to remove external artefacts, though this method is not readily available for all MEG systems and some frequency components may remain. Though the following is only mentioned in three studies, the manufacturers have recommended the MRI-compatible thermode for MEG recording, implying there are possibly unsuccessful research projects that have failed to collect useful data because of using the alternative, less expensive MRI incompatible thermode.

Nevertheless, the findings of this review demonstrate the validity of CHEPS in hot or cold configurations when cleaned with tSSS or DSM. The success of SAM, MNE, and Bayes source

localisation methods implies the possible utility of spatial filtering in other beamformers. Source localisation techniques using MEG data are capable of localising frequency and power changes associated with CHEPS at beta and gamma frequency bands that could not be detected by EEG due to its lower spatial resolution and ability to detect deeper sources; this was demonstrated with a direct comparison by Fardo et al (2017), whose study revealed temporal characteristics of discriminative sensory processing that were not clear with EEG analysis, and beyond the scope of fMRI.

2.3.4.2 Methodological considerations

The designs of the identified CHEPS studies vary in parameters that are noteworthy in the literature and should be considered (Table 2.3). Baseline CHEPS temperature has been shown to influence the amplitude and latency of evoked responses in EEG (Kramer et al., 2012; Rosner et al., 2018b, 2018a), as have stimulation location (Granovsky et al., 2005; Rosner et al., 2018b), fixed vs variable placement (Greffrath et al., 2007), hairy vs glabrous skin (Granovsky et al., 2005, 2017) and inter-stimulus interval (Granot et al., 2006). Baseline temperature in the studies we have reported on ranged from 32-35˚C, though the alternative of 42˚C has revealed lower latency and higher amplitude responses over multiple stimulation locations (Rosner et al., 2018), and it is possible that baseline temperature maintenance could contribute to the noise floor in a MEG environment (Gopalakrishnan et al., 2013). The heat stimuli in the studies identified here were most often titrated to 8/10 on a Verbal Analogue Scale (VAS), with an average temperature of 48˚C. This variable, however, is not comparable across all studies: In at least three of the identified studies the stimulation was held for as long as two seconds, as opposed to the range of 200-500 ms for a standard

CHEPS pulse, which could significantly influence the experience of pain. In addition, no studies in this review reported or mentioned the overshoot control values that can be set within the CHEPS software, which can interfere with how the target temperature is reached at default settings. It is important to report CHEPS parameters and record pain outcomes throughout CHEPS paradigms, and reflect upon study findings with the stimulus parameters in mind. Recommendations for designing and reporting on these are found in Table 2.4.

Table 2.4: Recommendations for designing and reporting on combined CHEPS MEG studies

Report and justify CHEPS baseline temperature
Report CHEPS overshoot value and how often the CHEPS failed to reach the destination temperature
Report and justify CHEPS stimulation location
Titrate destination temperature and report titration method
Report CHEPS stimulation peak duration
Use an inter-stimulus interval of at least 8-12s unless otherwise justified
Report whether a fixed or variable stimulation was used
Report artefact rejection techniques implemented, and any attempts to reintroduce dimensionality

With each of the five studies that investigated anticipation cues, a minimum of 480 trials were collected (one study recorded 945) in one session. To avoid enduring pain effects, four of these studies presented non-painful stimuli and painful stimuli (with no-stimulation control trials) as separate experiments and did not counter-balance them. This lack of randomisation or counterbalancing leaves the data vulnerable to the effects of participant exhaustion, which are a considerable concern for the integrity of data in long recording sessions, especially in pain research (Gross et al., 2013). Of particular note is the paper by Gopalakrishnan et al. (2016a), that compares the no-stimulation control trials from

paradigms one and two, identifying a difference between the two and deducing that the control linked with the painful condition was more susceptible to vigilance; though this may be the case, the authors did not suggest that the difference between the two may be due to exhaustion or cue learning after many trials.

2.3.4.3 Pain anticipation

Most of the results presented focus on the anticipation of CHEPS pain following visual cues in healthy controls. The studies presented consistently identify increases in the relative power of gamma and beta oscillations in frontal regions such as the DLPFC and OFC in response to cues that signal pain when non-pain stimulation control data is subtracted; frontal cortices were associated with the greatest pain specificity in N1 components of ERF analyses, whilst central sensors demonstrated differences among cues. PSPS patients did not have significant differences between pain and non-pain anticipation when expecting pain to be presented to their affected limb, demonstrating a lack of saliency possibly due to chronic vigilance even for non-painful stimuli; this saliency was reintroduced by DBS, especially in those that scored better on depression scales after the intervention. Presenting the CHEPS stimuli for 2s may prove to be more effective at eliciting affective anticipatory components, achieving greater saliency in those with restored affective capability; the CHEPS' capability to maintain longer duration, ecologically valid stimulations without injury remains an advantage over laser and electrical techniques here.

2.3.4.4 Limitations

Some limitations to this review should be noted. First, most of the studies presented in this review do not assess CHEPS' use in generating evoked potentials, instead opting to analyse data in an anticipation time window. Though we identified studies discussing the

methodology of combined use of MEG and CHEPS, including one experimental study that used the cold configuration, no participant studies analysing the post-stimulus time window following heat stimulations were identified in the search. Second, though thorough searches of adjacent literature, citing papers, and reference lists were conducted, unpublished research was not explored.

The systematic literature search for this review was completed in 2020. Whilst not systematic, thorough database searches performed in January 2023 using similar search terms have not found any additional eligible journal articles appropriate for inclusion.

2.3.4.5 Future research

Though the literature is sparse, the studies identified in this review provide a good overview of some available methods of analysis when combining CHEPS and MEG. MEG analysis methods with proper preprocessing are capable of localising activity with improved spatial resolution in comparison to EEG. Future research would benefit from comparing fMRI and MEG methods, as demonstrated with EEG by Roberts et al. (2008); though simultaneous recording would not be possible, more precise virtual time series data could more accurately elucidate the contribution of cortical subregions to pain processing. The capability of the CHEPS to generate long-duration stimulations without harming the participant facilitates thermal tonic pain experimentation, which opens doors to exploring affective, summative, and sensitisation dynamics (Linde et al., 2020; Staud et al., 2020). No studies experimentally analysing post-stimulus noxious CHEPS epochs in MEG currently exist, but this avenue of research could elucidate mechanisms previously not detected by EEG (Fardo et al., 2017). Utilising this combination to explore treatment response is a promising avenue of research (Gopalakrishnan et al., 2016b; 2018), and any additional

benefits over standard or single-electrode EEG recordings for clinical diagnostic use should be properly explored by further study.

2.3.4.6 Conclusions

The CHEPS is well validated as a method to diagnose small fibre pathophysiologies with EEG, and is a more accessible and safer alternative to laser methods. Studies demonstrating the effectiveness of artefact removal and source localisation techniques in clearing electromagnetic noise generated by the CHEPS exist, and though the most effective methods are not available as standard for all MEG systems. A portfolio of research was presented in this review that demonstrates the utility of MEG in CHEPS research, including its improved spatial resolution in comparison to EEG. Though MEG can identify spectral components that are not identified by other imaging methods and CHEPS is a commonly used clinical evaluative and diagnostic tool, few published studies explore them in combination. Future MEG analysis of CHEPS data could improve our understanding of spectral correlates underpinning pathophysiological pain and sensory conditions, and contribute to contemporary discourse surrounding chronic and neuropathic pain treatment response and mechanisms.

3. Magnetoencephalography: Acquisition and analysis

The purpose of this chapter is to provide an overview of magnetoencephalography (MEG). It includes a description of the data that is acquired using this technique, that hardware that is used to observe and record the magnetic fields produced by activity in the brain, and a typical pipeline for the MEG data analysis in the chapters that follow.

3.1 Theory, hardware, and software

The objective of MEG is to measure the magnetic fields generated by the current dipoles of large populations of neuronal axons: signals that are roughly one billion times weaker than the earth's magnetic field, and orders of magnitude weaker than electromagnetic noise generated by passing cars or electronics (Cheyne and Papanicolaou, 2015). Electromagnetic fields follow Fleming's right-hand rule: they propagate anti-clockwise around a dipole, like the fingers of a clenched hand (Figure 3.1). They are also not constrained by tissue or bone, and do not disperse into nearby tissue (i.e., the problem of volume conduction of electrophysiological currents). These two phenomena mean magnetic fields generated by neuronal activity can be recorded outside of the head, but also limit the measurement of fields that can travel through MEG sensors, namely those generated by currents tangential to the surface of the brain (mostly by pyramidal cells). Fortunately, much of the surface of the cortex can be accessed by MEG sensors thanks to the sulci of the brain, and the fact that there are very few perfectly radial areas of the cortex.

The recording of magnetic fields is achieved non-invasively by a combination of super-cooled flux transformers and Superconducting Quantum Interference Devices (SQUIDs) that are arranged in a helmet ('dewar helmet') close to the head. Because of the super-cooling by liquid helium, the magnetic fields generated by neuronal dipoles (Figure 3.2) in the brain can induce an electric current in flux transformer pick-up coils. The flux transformers are

then coiled in such a way that they induce electrical currents in adjacent SQUIDs with their own magnetic fields, which in turn utilise Josephson junctions to measure voltage; this is then further amplified and recorded by the MEG system.

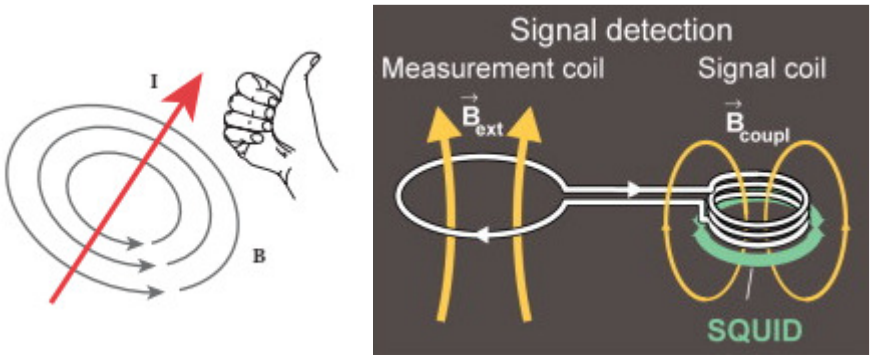

Figure 3.1: Left: The right-hand rule. I = current, B = magnetic field, from Cheyne & Papanicolau (2017). Right: Magnetic field detection in flux transformers. External magnetic fields (B_{ext}) induce an electrical current in the flux transformer; the resulting electrical current then generates its own amplified magnetic field, which is detected by the SQUID (B_{coupl}). From Hari & Salmelin (1997).

There are three types of flux transformers commonly used in MEG: magnetometers, axial gradiometers, and planar gradiometers, though other types (such as second- or third-order axial gradiometers) exist.

Magnetometers use one coil to detect magnetic flux, whereas gradiometers use two oppositely wound coils to facilitate the calculation of the magnetic field's spatial change in Teslas per meter (T/m; or fT/cm), effectively cancelling out the effect of noise common in both pick-up coils (Figure 3.3). Dual coils at different (planar or axial) positions enable the measurement of changes in field strength changes over distance, and thus nullify environmental signal; noise that is uniform across both coils will induce no fluctuation in

field strength, but magnetic fields that are different across both coils (such as brain activity) will be measured as a net change.

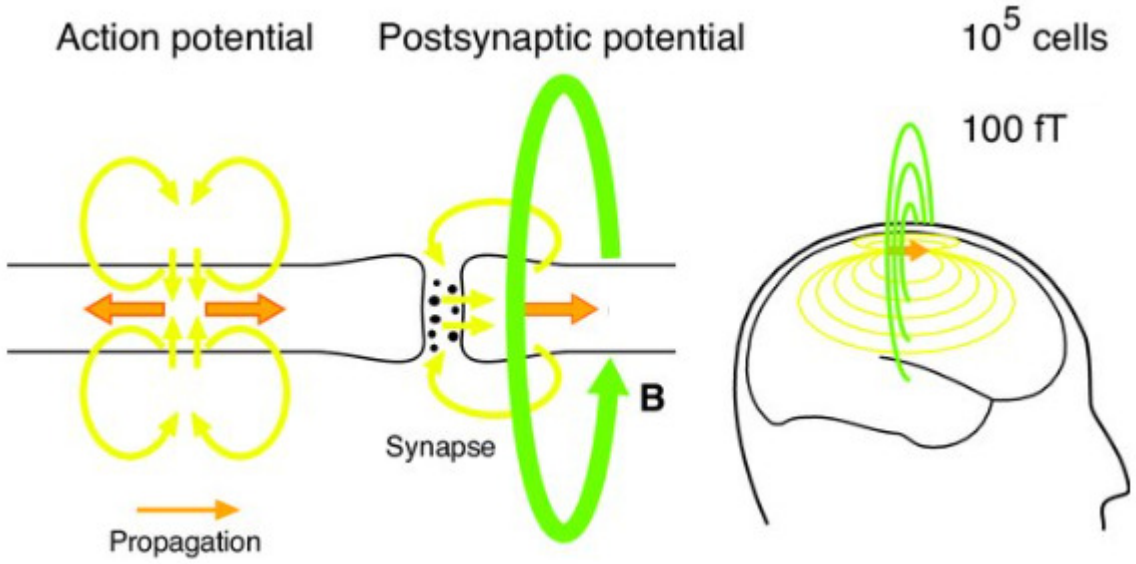

Figure 3.2: Neuronal dipoles detectable by MEG. Action potentials propagating through networks of at least 100,000 neuronal cells will generate an electromagnetic field strength of roughly 100 fT, detectable if the source is not radial to the sensors. Adapted from Taulu (2008). fT: Femtotesla. B = Magnetic field.

Different flux transformers are most sensitive to fields at different regions depending on their configuration (Figure 3.3), and as such, conceptualising this as part of a "lead field" (a matrix of sensors by points in the brain that describes the range of sensitivity for each sensor) is an important component of MEG analysis. Magnetometers have greater sensitivity to deep sources when compared to axial and planar gradiometers, and though MEG is occasionally criticised for its low-resolution reconstruction of the subcortex, research has demonstrated effective reproduction of activity in deep brain areas (Ioannides et al., 1995; Korczyn et al., 2013).

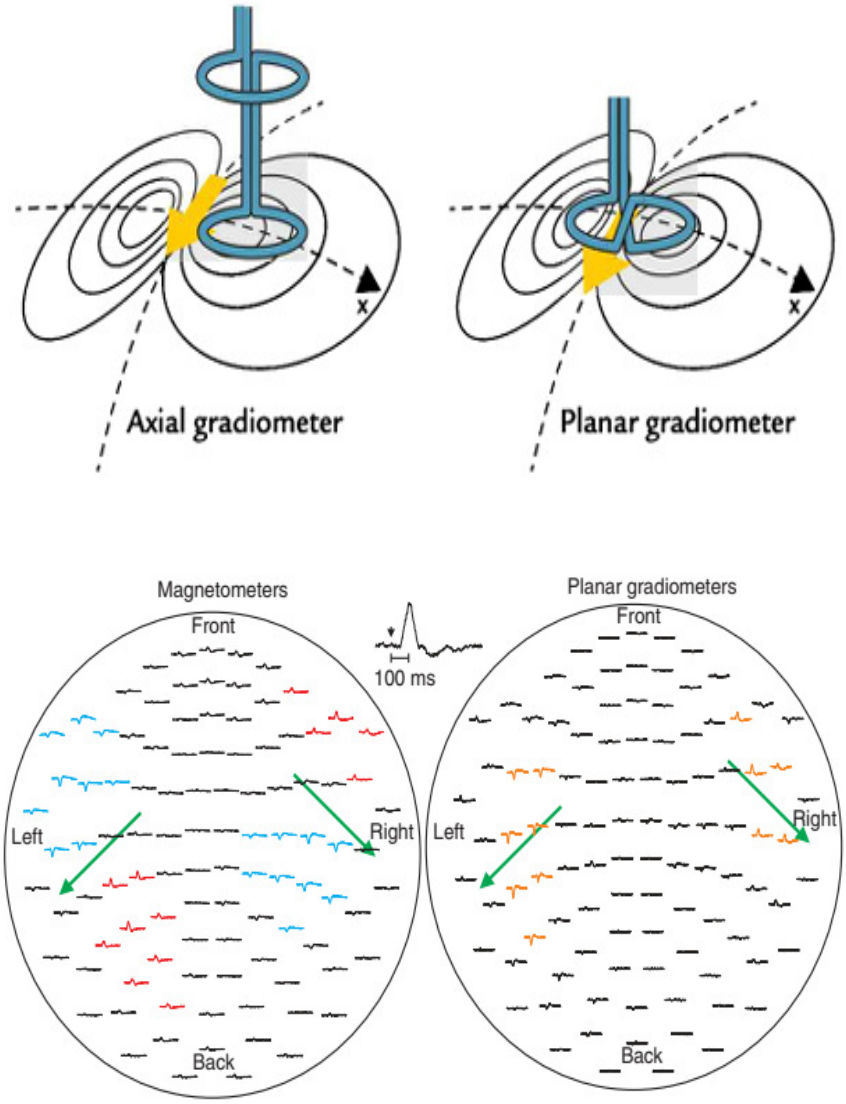

Figure 3.3: A Figure demonstrating the difference between gradiometers and magnetometers. Top: Axial and planar gradiometer configurations and their respective optimal recording zones. Bottom: The topography of auditory event-related fields as detected by magnetometers and planar gradiometers. From (Hari and Puce, 2017).

In addition to gradiometry, other hardware methods can be implemented to reduce the impact of environmental and external noise. MEG systems are typically housed in Magnetically Shielded Rooms (MSRs) – chambers that are constructed with a mixture of ferromagnetic and highly conductive metals that attenuate external noise with eddy currents and passive shielding – and this alone can be very effective (Hari and Puce, 2017).

Additional noise cancelling can be achieved by active shielding, with the generation of a compensatory opposing magnetic field outside the MSR based on real-time recordings from a reference magnetometer inside the chamber – though the active coils can produce artefacts of their own if the external noise is not large. Reference sensors inside the dewar helmet– but far from the brain – can record and subtract homogenous environmental noise, but can potentially interfere with coherence or correlation analyses.

During data acquisition, participants are fitted with Head Position Indicator (HPI) coils and the shape of their head is digitised for later head model construction. The HPI coils are used to track head movements for individuals in the scanner; this is achieved by running a small current through these coils that the MEG system can track online. Recording the position of these coils enables post hoc correction with offline interpolation techniques, though these methods are not suitable for large movements (Hari and Puce, 2017). Additional electrodes can be fitted for electrooculogram and electromyogram that can complement later data cleaning or analysis.

3.1.1 Data cleaning

Because of the sensitive nature of the acquisition hardware and the scale of the neuronal sources that are being recorded, raw MEG data is often contaminated with signals that are not of interest to investigators: The magnetic fields generated by eyeblinks, eye movements, scalp muscle contraction, heartbeats and metal tooth fillings can negatively impact the quality of the recorded data. Because of this, an essential part of MEG data analysis is the 'cleaning' of acquired data, thereby removing, or suppressing these signal artefacts. To complement hardware noise reduction, software artefact rejection methods are also effective in reducing extraneous signals. Neuromag (Elekta^{TM} Neuromag, Oy) MEG

systems have the option of using Signal Space Separation (SSS; Taulu, Simola and Kajola, 2004) or temporal SSS (tSSS; Taulu and Simola, 2006): both of these methods use Maxwell's equations of the physical properties of magnetic fields to mathematically construct subspaces that represent the inside and outside of the dewar helmet. SSS uses the estimations of internal and external components to reconstruct the data at the sensor level whilst discarding the external components; tSSS uses this information to remove any components identified inside the signal space that also correlate significantly with external signals over time. SSS and tSSS applied through MaxFilter software (Elekta Neuromag Oy) are especially effective at removing noise that originates inside the MSR, though tSSS is more effective at removing artefacts that are temporally consistent, such as magnetic fields from piercings, it could potentially influence brain data if there is a low signal-to-noise ratio. The application of SSS or tSSS through MaxFilter software can also include Maxwell Filtering, a process which identifies components of the signal that originate from the sensors themselves, and projects them out of the dataset.

Signal Space Projection (SSP; Uusitalo and Ilmoniemi, 1997) uses empty-room recordings to identify the "interference" dimensions that can be attributed to non-brain activity, separates the data into individual components, then projects the components with the greatest eigenvalues (i.e. a value that represents the magnitude of variance in a component; components with large eigenvalues in an empty room represent environmental noise) out of the participant data. Independent Component Analysis (ICA) identifies components of the data that are statistically independent of each other, and can be used to identify artefacts generated by phenomena like blinks and eye movements with no a priori information. Using any of these methods makes the data rank deficient (i.e., there are fewer unique components than there are sensors that recorded the original data), which must be

acknowledged in later source reconstruction analysis steps. Haumann et al. (2016) compared the external and internal artefact noise suppression qualities of SSS against tSSS, and SSP against ICA respectively, and demonstrated that greater noise reduction was achieved by ICA and tSSS against their respective comparators – but with the additional note that low signal-to-noise data, such as those from magnetometers, are at risk of attenuating artefacts whilst also increasing baseline noise. An essential step in data cleaning is simply removing trials with artefacts that were not successfully suppressed, and excluding sensors that were identified as 'bad' because of sensor-level artefacts.

3.1.2. MEG data

MEG data is initially represented as a time series of T/m or fT/cm over time at each sensor (Figure 3.4), in epochs around a stimulus trigger or in continuous segments. The time resolution of MEG can be very high, though often systems sample between 1000-2000 Hz. Many types of analysis are possible, and are broadly classified as sensor-level, or source-level techniques: sensor-level analyses process the data as they are recorded at the magnetometers or gradiometers, and are often performed based on select sensors or the topography of the scalp; source-level methods attempt to reconstruct activity in the brain based on models of the head and lead fields of the sensors, or reconstruct activity based on weights attributed to three-dimensional points (voxels) within a source model. This subchapter will go on to describe some of the most popular techniques within these categories, then the steps required to perform the analyses performed in this thesis.

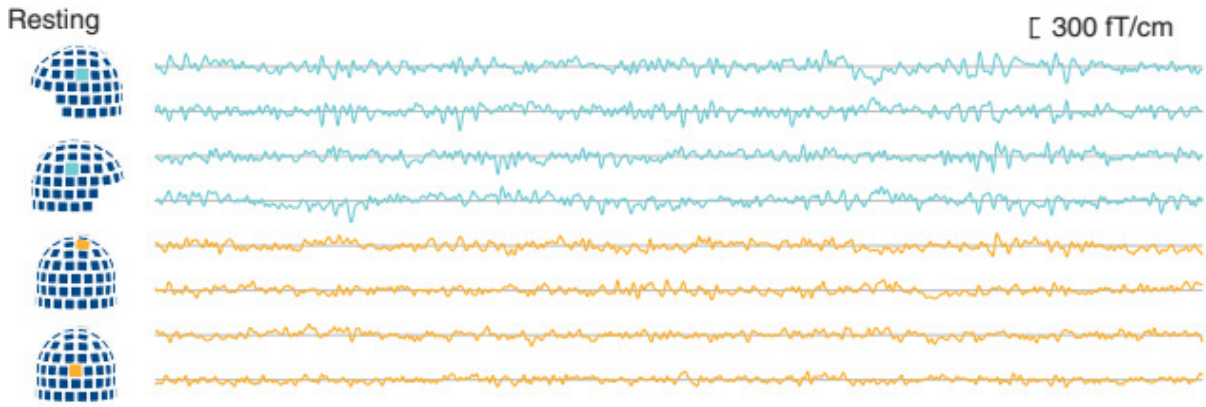

Figure 3.4: Time series data for four gradiometer pairs in locations as indicated on the dewar helmet, recording a participant at rest. From Parkkonen & Salmelin (2010).

3.1.3 Sensor-level analysis

Analyses at the sensor level are most commonly performed to observe differences between event-related field characteristics or (time-) frequency power. Averaging trials around a time-locked stimulus creates an Event-Related Field (ERF) waveform that is a summary of evoked brain activity. This averaging can be performed with select sensors to characterise a particular area of the scalp, or performed on virtual sensors extracted using source reconstruction techniques. These waveforms are attributed to the synchronous firing of large neuronal structures and have peak and trough components that are characterised by their timepoint (e.g., 20ms), positivity/negativity (i.e. N or P), position (e.g. cZ for central electrode on the Z-axis) on the scalp or number in the series (e.g. N1 is the first negative component). The location, amplitude and latency of these waveforms and their components reflect underlying phase-locked ('evoked') brain activity, as the nature of averaging removes any non-phase-locked data.

Frequency analysis involves the use of Fourier transformations (a method to decompose signal data into frequency components) to calculate the contributions of frequency bands in

a signal. This analysis is performed on an epoch or in a small, sliding time-window to interrogate frequency power changes over time, and can be achieved in most M/EEG analysis software. The result of a Fourier analysis is an estimation of the power of specified frequencies across a spectrum, often a frequency band that was selected *a priori*. When compared against a baseline window, time-frequency analysis can outline changes in synchronisation after an event, which may illuminate underlying functional activity (Figure 3.5).

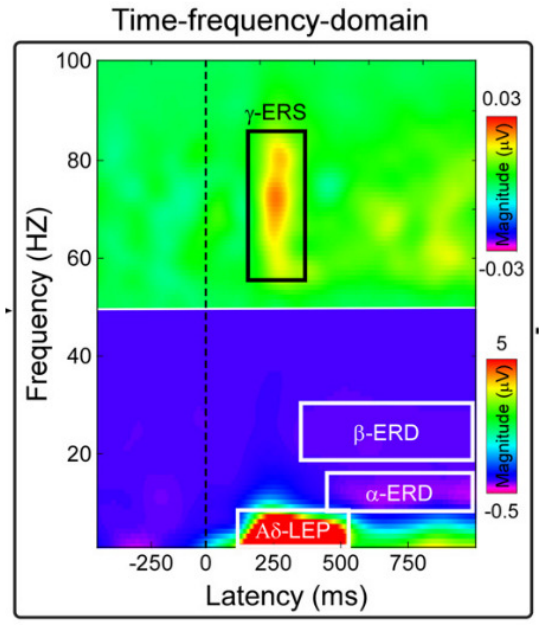

Figure 3.5: Time-frequency analysis of EEG data of a laser-evoked potential, with baseline-relative synchronisation of gamma and theta, and desynchronisation of alpha and beta frequency bands. Adapted from Peng and Tang (2016).

Sensor-level analysis is the most commonly performed type of M/EEG analysis: it is simpler to perform, and can utilise more powerful statistical methods. However, recent research has evidenced the spatial mixing of brain signals, and demonstrated that volume conduction and superposition of neural generators can significantly confound sensor-level analysis; up to 75% of the activity detected on frontal sensors was associated with central components

in simulated datasets (Schaworonkow and Nikulin, 2022). The most accurate use of sensor-level analysis is achieved using reconstruction of virtual sensors in the brain using spatial weights constructed during source analysis.

3.1.4 Source space analysis

Sensor space analyses are limited in their ability to accurately estimate underlying brain activity due to the superposition of magnetic fields – the contribution of fields from nearby brain areas, or at varying depths, which can lead to inaccurate detection of sources (Cheyne & Papanicolau, 2017). The ideal outcome of MEG imaging is to be able to accurately identify and recreate the position, field strength, and time course of brain activity in a 3d model of the brain (source space). To achieve this, one must attempt to solve the "inverse problem" – the estimation of underlying sources based on recorded magnetic fields. This is difficult, or "ill-posed," because there could be a near-infinite number of varying current generators that explain the magnetic fields measured by the MEG sensors. To solve this problem, one must create constraints to limit the estimations. This inverse solution is the creation of a source model based on the shape of the head and boundaries of the brain that put physical limitations on where the sources can reside.

Source space analyses ("inverse modelling") can be performed in the time or frequency domain to reconstruct underlying activity in the brain. A popular technique for source analysis is beamforming: a spatial filtering method that uses mathematical operators as weights for signals recorded in sensor space. Spatial weights define the contribution of each sensor to a given voxel, ensuring that sensor-level data is accurately passed or suppressed. The beamformers used throughout this thesis operate by utilising these spatial weights with a unit-gain constraint, enabling the signal at each location to be reconstructed without

attenuation, whilst suppressing the contribution of nearby points in the brain under the assumption that they are temporally uncorrelated.

Weights are calculated with the MEG lead field and a matrix that describes the relationship in field strength between pairs of sensors (a "covariance matrix") for each channel-by-channel pair, then data is multiplied by the weights for each voxel in the grid; this enables the suppression of extracranial, environmental noise and signals from spatially distant sources in the brain. Because of this, the time series for any voxel can be reconstructed, simulating a virtual sensor that can be comparable to intercranial electrodes (Korczyn et al., 2013)(Figure 3.6), which can then be analysed as described above. Common methods of beamforming include the Dynamic Imaging of Coherent Sources (DICS; Gross *et al.*, 2001) and Linearly Constrained Minimum Variance (LCMV) as techniques to analyse the power of oscillatory components or averaged waveforms respectively. These techniques can be calculated with vector or scalar metrics, facilitating measurements of field strength in three directions (vectors) simultaneously from each point of the grid or just the signal orientation with the greatest variance at that point.

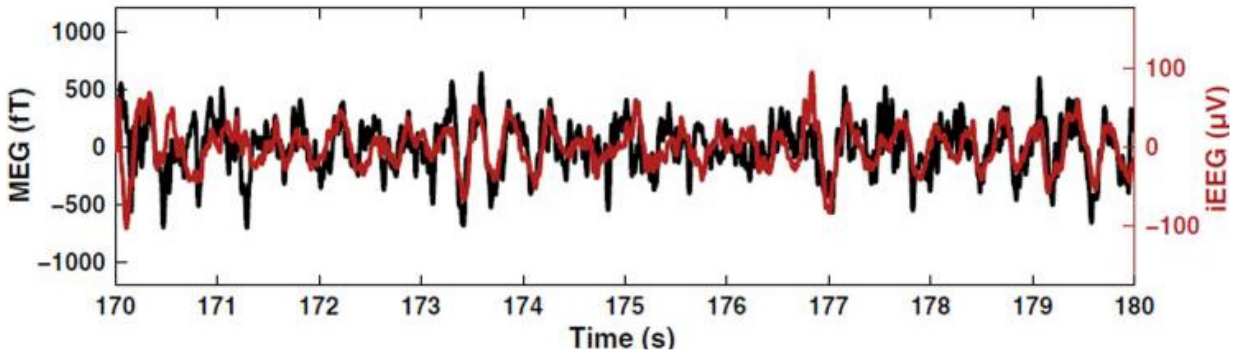

Figure 3.6: An approximate virtual sensor time series in the hippocampus estimated with beamforming weights, plotted with the same time series recorded directly by intercranial electrode (Korczyn et al., 2013).

3.2 Analysis pipeline

FieldTrip (Oostenveld et al., 2011) is an open-source toolbox for MATLAB that facilitates M/EEG data analysis with high-level functions for reading, processing, sensor and source-level mapping, and statistical inference. It forgoes a graphical user interface for scriptwriting that facilitates batching and nuanced analysis protocols. Functions are named using the format “ft_xxx” to designate their purpose, and a configuration variable structure “cfg.xxx” is used to designate parameters for specific FieldTrip functions (Figure 3.7). In figure 3.7 a configuration variable is made, filled with parameters for the “ft_definetrial” function; the output of the function is then saved in the configuration variable for the next function to use. The following subsection explains the pipeline followed for both Elekta™ Neuromag and CTF™ datasets used in this thesis, though specific parameters are described in the respective experimental chapters.

```
cfg=[];
cfg.dataset = datafile_off;
cfg.trialfun = 'ft_trialfun_general';
cfg.trialdef.eventtype = 'Trigger';
cfg.trialdef.eventvalue = 2;
cfg.trialdef.prestim = 0.25;
cfg.trialdef.poststim = 0.40;
cfg = ft_definetrial(cfg);
```

Figure 3.7: An excerpt of a FieldTrip script that demonstrates the configuration-function relationship. Here a variable containing the information for an SCS-off dataset is called into the configuration and the trial parameters are set. The output of ft_definetrial will be stored in the configuration variable to be called again later.

3.2.1 Cleaning the data

The first step in cleaning Elekta™ Neuromag data is ascertaining whether the application of SSS or tSSS is necessary by visually browsing the dataset. Artefacts in M/EEG data are similar across both methodologies and are well-documented (Burgess, 2020); SSS or tSSS should be applied to attenuate or remove noise or artefacts that originate outside of the dewar helmet, but should be used sparingly if possible due to its impact on the data's dimensionality. At this point data is checked for its quality, including identifying any bad channels to be removed due to regular artefacts introduced by the equipment, line noise, and whether movement correction is required (possible with ft_qualitycheck). Channels removed due to consistent signal artefacts can be interpolated from neighbouring sensors by using the FieldTrip function ft_channelrepair.

The next step in a FieldTrip pipeline is to filter the data; filtering is a crucial component of pre-processing that enables additional attenuation of particular frequency bands, or enhancement of waveforms for visualisation. Filtering can be high-pass, low-pass, band-stop, and band-pass – subtraction of frequencies below, above, within and outside of certain parameters, respectively. Primarily done as a way to remove DC line components, filtering can also achieve a baseline correction effect by applying a high-pass filter of from <1Hz, reducing the impact of slow drifts introduced by SQUIDs and ambient noise (Gross et al., 2013). The shape of the filters applied, as well as their phase response, stability and computational efficiency should be considered before application, and they should be applied before defining trials where possible to avoid edge-artefacts. It is advised as good practice in MEG analysis to apply an anti-aliasing low-pass filter of 1/3 or 1/4 of the sampling frequency (Gross et al., 2013). At this stage, data can also be detrended and

demeaned – correcting drifts and removing the average of the baseline from the epochs to correct for environmental effects and noise.

Following cleaning of the data using MaxFilter and preprocessing, trials are read into FieldTrip and the epochs in the time series data are defined using the function ft_definetrial, where the pre- and post-stimulus windows are set on either side of a trigger within the data. For data that does not have triggers ('continuous' data), data is split into trials of a few seconds each, with some overlap.

After pre-processing, ICA is performed to identify any components associated with internal artefacts (e.g., blinks, heartbeat, eye movements; ft_componentanalysis). This can be performed by several techniques; the default in FieldTrip is RUNICA (Bell and Sejnowski, 1995), though other algorithms exist to perform ICA, their objective is the same: the separation of linearly mixed sources, i.e., components within signal space that are unique but combined on the same scale at the sensor. The algorithm will automatically calculate the number of components within the signal after whitening, though this can be erroneous when applied to data that has been cleaned with MaxFilter; it is recommended to restrict the analysis to roughly 64 components in MaxFilter-cleaned Neuromag data to account for its rank-deficiency. It is here that downsampling the data from 1000 or 2000 Hz to 200 Hz is helpful, as performing ICA takes a long time and the components can be removed from the data in its previous state. ICA will extract component time series that can be plotted alongside their topography to assist with the appropriate rejection of artefacts (ft_rejectcomponent). After ICA, trials that still contain errors (such as muscle artefacts) are removed using the 'summary' option of ft_rejectvisual that plots trial variability.

3.2.2 Forward modelling

To create a volume and grid that can be used to model activity in a participant's brain, it is best if the prerequisite components are participant-specific – though this is not always possible. In MEG, forward modelling can be achieved with the extraction of boundaries from MRIs. The models that most precisely match an individual's brain for MEG in FieldTrip are single-shell or boundary element models that use segmented MRIs (ft_volumesegment) to generate mesh "head models" of the cortex (ft_prepare_headmodel). A standard source model is loaded and prepared for further analysis by combination with the individual's MRI (ft_prepare_sourcemodel) and warped to standardised positions defined by the Montreal Neurological Institute (MNI; Evans, Collins & Milner, 1992)(Figure 3.8) to facilitate group analysis later; this is then used in combination with the head model and sensor descriptions to compute the lead field (ft_prepare_leadfield). Where an individual's MRI is unavailable, head models are generated by using standard open-source MRIs and realigning them to the coordinate system being used during analysis. It is important to ensure the head shape (obtained from digitised head shape or other software) for the participant is aligned with the lead field and sensors after the fact, for the most accurate forward model.

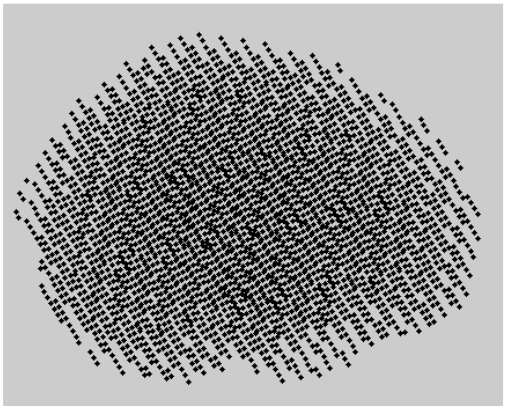

Figure 3.8: A figure produced in MATLAB demonstrating a standard 3d source model with 5mm resolution tailored to a head shape (tilted for depth perspective).

3.2.3 Inverse modelling

Once the forward model has been made, the inverse solution is computed. This is achieved using FieldTrip LCMV and DICS beamforming in this thesis (ft_sourceanalysis). LCMV and DICS use the previously generated lead field and head models, whilst the LCMV beamformer also requires a matrix that contains the covariance of each channel (obtained from ft_timelockanalysis). A covariance matrix is a sensor-by-sensor matrix that reflects signal amplitude and distribution, and a key ingredient for creating spatial beamformer weights. It is important to generate a covariance matrix that accurately reflects the data. If the signal-to-noise ratio is low, or there is little data to compare, the covariance matrix can give inaccurate beamformer reconstructions. This is often solved with regularisation. LCMV and DICS beamformer outputs can be analysed at the group level in statistical analysis.

3.2.4 Beamformer considerations

These methods can be configured with additional options, such as fixed orientation output (one direction of greatest strength, as opposed to a vector of three directions), and kappa or lambda regularisation. The latter is an injection of signal noise (Woolrich et al., 2011), which is commonly used to whiten data that is too short to provide a good estimation of covariance (Brookes et al., 2008); as regularisation can have a significantly negative effect on accurate source reconstruction, it is recommended its parameters are data-driven and avoided entirely if possible (Adjamian et al., 2009; Brookes et al., 2008; Jaiswal et al., 2020). Rank-deficient data (such as data that has been cleaned with MaxFilter) will also require its lead field matrix to be truncated based on the number of retained components (roughly 60, referred to as Kappa regularisation; Westner et al., 2022), to ensure the covariance matrices meet the component number assumptions of the beamformer equations (Jensen and Hesse,

2010). The covariance matrix can be erroneous if its dimensions do not accurately reflect the data (i.e., rank deficiency). An example of this is a matrix of 204 gradiometers that has been cleaned with tSSS: when applied to suppress external signal noise, tSSS effectively reduces dimensionality of the data from 204 to closer to 60 (Westner et al., 2022). The covariance matrix can be truncated at 60 by defining κ=60 in FieldTrip, thereby avoiding erroneous beamformer output.

Due to the equations that generate spatial weights, signal noise that is unaccounted for contributes to poor localisation in beamform analysis (Quraan, 2011) – often with a bias to the centre of the head – and distorts source estimations. It is possible to avoid this by estimating the Neural Activity Index (NAI) – average power divided by average noise – and using that to project noise from the data; most commonly, however, this is simply achieved by performing the source analysis on two contrasting time windows (such as a baseline condition or pre-stimulus window against a window of interest) and calculating the ratio of change (i.e. window of interest minus the baseline, divided by the baseline; Quraan, 2014) (Fig 3.9). Beamformers can also suffer from leakage when presented with strong signals outside of their region of interest, which can eventually dominate over weaker sources that might be of interest, and they can be biased by strong correlations across space (Quraan, 2011).

$$\text{Relative difference in frequency power} = \left(\text{Source reconstruction of frequency power in time-window of interest} - \text{Source reconstruction of frequency in baseline}\right) / \text{Source reconstruction of frequency in baseline}$$

Figure 3.9: Calculation of relative difference for source reconstructions, performed separately for CPT-max and CPT-late. The relative difference for each time window was then compared between high pain sensitivity and low pain sensitivity groups.

3.2.5 Virtual sensors

The weights generated by the beamformer inverse solution can be used to reconstruct the time course of a virtual sensor for a particular voxel, but vector beamformers reconstruct fields in 3 dimensions at each voxel, resulting in three sets of timeseries data. Singular value decomposition, a process by which the vector dimension with the greatest variability is identified, enables analysis of the single timeseries that is most likely to explain brain activity. This is achieved by performing an LCMV beamformer analysis on an appropriate dataset with fixed orientation output (using 'cfg.fixedori = yes' in the FieldTrip function ft_sourceanalysis), saving the filters computed during this step, and then multiplying the time series data by these filters for every trial; the output of which is a single channel of time series data that resembles sensor-space data. This virtual sensor can then be analysed for frequency (ft_freqanalysis) or ERF (ft_timelockanalysis) outcomes, and then interrogated using inferential statistics.

3.2.6 Statistical analysis

Inferential statistics performed at the source or sensor level can both be evaluated by the use of classical statistical methods for interval data in FieldTrip (ft_xxxxstatistics). Conventional statistical analysis can be as simple as peak amplitude or mean values across a particular time window or frequency band, though this requires prior knowledge of component latencies and can miss more nuanced data (Huang and Zhang, 2017). Point-wise comparison of larger time/frequency windows enables greater detail in the output, but requires each point to be tested for statistical significance, which falls prey to the multiple comparisons problem. This is exacerbated by the analysis of this data over many voxels or sensors.

MEG statistical analysis can solve the multiple comparisons problem with traditional methods such as Bonferonni and False Discovery Rate corrections, though these are often overly harsh – especially when used with time series data that have high sample rates (Maris and Oostenveld, 2007). Cluster permutation provides effective control of the false error rate when comparing between groups (or conditions) without over-correcting for multiple comparisons. To define clusters, every sample of interest (time point, frequency, voxel etc.) has its test statistic calculated by T-test with another condition or group. All samples that meet significance at $\alpha = 0.05$ (or 0.025 depending on the tailing of the study design) are grouped by adjacency in time, spectra, or location. These clusters have their statistic values summed, which is referred to as their cluster-level statistic (they can also be clustered by size, sum, or a weighting of both). The Monte Carlo method is then used to identify the significance probability of the largest cluster statistic in this original test statistic by comparing it to a random distribution generated by permuting the data. Samples are randomly assigned (permuted) between one of two groups, after which a statistical test is performed. This is repeated many times ('cfg.numrandomization = 2000') to generate a normal distribution of cluster statistics, against which the original cluster statistic is compared. If the original cluster statistic is within the bounds defined by the α threshold the null hypothesis can be rejected. This type of analysis can be computationally expensive, but requires no prior knowledge of the distribution of the data or whether it meets assumptions for specific statistical tests (and can therefore be referred to as non-parametric (Maris & Oostenveld, 2007; Chaumon, Puce and George, 2021)). Cluster-based permutation analysis is considered the most powerful method for correcting for multiple comaprisons, though it is limited by its potential insensitivity to smaller clusters (Huang & Zhang, 2017). Once performed in FieldTrip, these measures create masks that can be applied to plots to

visualise the clusters that contributed to the outcome of the test; these clusters must be interpreted by the investigator, as with all statistical testing, as permutation analysis is principally a test of whether or not a null hypothesis can be rejected, not at which data points the difference is significant (Maris and Oostenveld, 2007; Sassenhagen and Draschkow, 2019).

4. Study 1: Spinal Cord Stimulation in MEG

4.1 Introduction

Conventional Spinal Cord Stimulation (SCS) (also known as 'tonic' or 'paraesthesia-based SCS') is an invasive therapy, most commonly used for intractable neuropathic pain conditions, such as Persistent Spinal Pain Syndrome (PSPS) and Complex Regional Pain Syndrome (CRPS; Visnjevac et al., 2017; Rigoard et al., 2021), in which patients have electrical pulses applied to the dorsal column of their spinal cord by leads surgically implanted in the epidural space. To be eligible for the surgery, patients must undergo a trial period using a percutaneous lead and external generator, during which their quality of life, activities of daily living and pain relief are tracked; patients for which SCS achieves a reduction in pain of at least 50% are considered for permanent implants (alongside anatomical and technical considerations; Deer et al., 2022), though the utility of these trials is contested and can introduce an additional risk of infections (Eldabe et al., 2020; Jeon and Huh, 2009). Patients receiving SCS have reported significantly improved pain relief when compared to conventional medical management for intractable pain at 6, 10 and 12 months of follow-up (Duarte et al., 2021; Kumar et al., 2006).

The dorsal columns stimulated by SCS are comprised primarily of Aβ neuronal fibres, thick myelinated fibre tracts that carry action potentials for innocuous somatosensory inputs to the cerebrum; external stimulation of these fibres coincides with suppression of evoked potentials recorded in the brain, which has led to theories that incoming nociceptive signals are attenuated by way of antidromic activation of inhibitory interneurons connected to Wide Dynamic Range (WDR) projecting neurons (Caylor et al., 2019). These dorsal column fibres also propagate signals in an orthodromic manner to the thalamus before projecting to

the somatosensory cortices. This means that stimulation of the dorsal column can influence brain activity directly and indirectly through two neural pathways (a thorough description of SCS mechanisms is provided in chapter 2.1). The full picture of how SCS achieves its antinociceptive effect is not well elucidated, it is especially unclear why some patients receive greater pain reduction than others, why some patients receive no benefits, why it is not effective in all pain conditions, and where any cortical modulation occurs in the time and frequency domains.

Identifying the effects of SCS on the brain is crucial to understanding its supraspinal mechanisms. The majority of functional brain imaging studies in humans have used methods with a low temporal resolution, such as functional Magnetic Resonance Imaging (fMRI)– which are only able to observe very low-frequency fluctuations (0-0.75 Hz) in brain activity as a function of blood oxygenation or cerebral blood flow. Most oscillatory components are thought to range within the boundaries of 1-100 Hz, much higher than is obtainable by fMRI. Electromagnetic imaging techniques such as electroencephalography (EEG) and magnetoencephalography (MEG) use sensors around the head to record electric or magnetic activity, and can do so at very high temporal resolutions, enabling the sampling of data that reflects high-frequency brain oscillations. MEG is evidenced as having a greater spatial resolution, the ability to delineate temporal characteristics that are otherwise absent in EEG recordings (Fardo et al., 2017), and some systems benefit from advanced artefact rejection techniques. MEG is less accessible due to its required magnetic shielding, high initial price, and price per session, but boasts vastly reduced set-up time. In addition, movement compensation methods support data collection in clinical populations where protracted recording sessions may be uncomfortable (Stolk et al., 2013).

To observe brain activity, EEG or MEG data is acquired during tasks or whilst participants are at rest. In SCS research, participants have an innate experimental resting-state condition as the ability to switch on/off the implantable pulse generator facilitates the exploration of its short-term, long-term, and residual mechanisms. Painful stimuli have been used to demonstrate a suppression of nociceptive inputs by SCS (Bocci et al., 2018; Hylands-White et al., 2016; Pluijms et al., 2015b), though the majority of SCS research using time-locked stimuli has focused on somatosensory evoked potentials (SSEPs). SSEPs are effective as a mode of exploring the alleged suppressive effect of SCS on ascending somatosensory signals as they propagate through Aβ fibres, where the antidromic effect of SCS should be most acutely observed. Systematic reviews performed by Bentley et al. (2016), Sivanesan et al, (2019) and Caylor et al. (2019) have documented the suppressive effect of SCS on SSEPs and other evoked waveforms in electromagnetic recordings, with the majority of identified studies showing a decreased amplitude as a result of therapeutic stimulation (de Andrade et al., 2010; Buonocore et al., 2012; Buonocore and Demartini, 2016; Lang et al., 1989; Larson et al., 1974; Stančák et al., 2007; Theuvenet et al., 1999; Urasaki et al., 2014; Weigel et al., 2015; Wolter et al., 2013), with only a few studies finding no effect (Doerr et al., 1978; Mazzonea et al., 1994; Niso et al., 2021). Median nerve SSEPs do not collide with antidromic dorsal column stimulations at the lower thoracic spine, and would instead reflect general somatosensory processing; evidence of altered median nerve SSEPs in the cortex as a result of SCS in the lower spine would demonstrate a supraspinal modulatory action of ascending SCS, or possible “first-come, first-served” collateral processing, in which ascending somatosensory afferents compete with, and diminish ascending nociceptive afferent processing (Testani et al., 2015).

Few studies combining SCS and MEG analysis exist (Witjes et al., 2022), and none of them adequately evaluate the source characteristics of spectral features of resting-state (Pahapill and Zhang, 2014; Schulman et al., 2005; Theuvenet et al., 1999). Only one MEG study explored SSEPs, and did so using only sensor-level topography analysis of collisions (Theuvenet et al., 1999); since this article was published, more advanced techniques have been developed with vastly improved spatial resolution. No whole-brain source reconstruction analyses of SSEPs exist using EEG or MEG, despite the limitations of sensor-space analysis (Schaworonkow and Nikulin, 2022).

The acquisition of resting-state data facilitates the exploration of underlying oscillatory activity that may act as a marker for a condition or participant group. Resting-state analysis of SCS at the sensor level in the frequency domain has revealed mixed results: some studies have demonstrated a normalisation of spectral power (i.e. suppression of dysfunctionally enhanced broad-band frequency power; Pahapill and Zhang, 2014; Schulman et al., 2005), showing that moderation of dysregulated cortical activity could be a mechanism by which SCS achieves its anti-nociceptive effect; consistent with this, Sufianov et al. (2014) demonstrated a relative suppression of delta, theta, and beta band synchrony three months after SCS implantation compared to baseline and healthy controls. De Ridder & Vanneste (2016) found beta and gamma were suppressed in the posterior cingulate gyrus and parahippocampus when SCS was enabled. More recently, Goudman et al. (2019) explored frequency power spectrum averaged across 32 EEG sensors during resting-state in no SCS, conventional SCS and high-frequency SCS; they observed that conventional SCS suppressed delta, theta and beta frequency bands when compared to high-frequency SCS, though neither were significantly different from the no-SCS control. Despite heterogeneous study design, stimulation parameters and participant conditions (Witjes et al., 2022), there is

evidence for the suppression of delta, theta, beta and gamma frequencies during SCS in EEG research: Identifying the cortical sources for any significant differences in processing underlying SCS during stimulation may highlight therapeutic targets for deep brain stimulation, as well as inform us on the contribution of ascending mechanisms and characteristics of SCS responders.

To date, only one of the existing studies that explore the cortical changes associated with ongoing conventional SCS has attempted to localise oscillatory power in source-space (De Ridder & Vanneste, 2016), using electrophysiological techniques that might be improved with whole-head magnetoencephalography. An exploratory analysis of modulation of broadband frequency at rest is warranted, as is an investigation into the frequency dynamics and field strength of cortical processing of SSEPs following SCS. This study will attempt to localise SCS-dependent frequency power across all frequency bands.

4.1.1 Aims and hypotheses:

This experiment aims to elucidate changes in the brain that result from conventional SCS in chronic pain patients in MEG somatosensory evoked potential and resting-state paradigms.

It is hypothesised that baseline (SCS-off) and SCS-on datasets will demonstrate significant differences in brain activity at rest, producing source reconstructions of locations responsible for the supraspinal processing of ascending SCS inputs. It is also hypothesised that reconstructions of SSEPs will be suppressed in SCS-on compared to SCS-off, representing the suppression of SSEPs by ascending SCS signals. The null hypotheses are that the SCS-on condition will result in no statistically significant changes when compared to SCS-off.

4.2 Methods:

4.2.1 Objectives

By performing a DICS beamformer (by using cfg.method = 'dics' in the ft_sourceanalysis function of FieldTrip^{TM}) on resting activity during SCS-on and SCS-off states within-individuals, differences in global changes in oscillatory power distribution can be localised which will elucidate any supraspinal effects of SCS. Performing a Linearly Constrained Minimum Variance (LCMV; performed by using cfg.method = 'lcmv' in the ft_sourceanalysis function of FieldTrip^{TM}) beamformer on SSEP data will enable the reconstruction and statistical comparison of the waveforms at the voxel with greatest field strength; this will demonstrate any suppression of the SSEP waveform by SCS. Additionally, performing a DICS beamformer on the SSEP dataset will demonstrate frequency distribution changes in SSEP activity as a result of SCS. Statistical analysis of source-level and power spectra will be achieved using cluster-based permutation analysis; event-related field strength will be tested using average field strength over a specified time window.

4.2.2 Dataset

This dataset was acquired at the Institute of Health and Neurodevelopment in 2014 by Lisa Bentley. This data was acquired for the purposes of a study exploring SCS, SSEPs and transcutaneous electrical nerve stimulation. No analyses beyond those reported here have been performed upon it. No published studies exist using this dataset.

4.2.3 Participants

Participants were approached and invited to participate in this study during their SCS review clinic at the Regional Centre for Neuromodulation Pain Therapies at Russells Hall Hospital, Dudley. The inclusion and exclusion criteria were as follows:

Inclusion criteria:

- Must be aged 18-70
- Must have fully implanted SCS for treatment of their chronic pain disorder
- Evidence from visual analogue or numerical rating scores indicating ≥50% pain relief with SCS treatment

Exclusion criteria:

- Patient refusal to participate in the study
- Patients with other implanted metal devices (e.g., pacemakers)
- Patients suffering from surface hyperalgesia

Four participants were recruited (2 male), with an age range of 46-52 years (Mean: 50, SD: 2.5). During screening participants reported, on average, an SCS pain reduction of 4.38 (SD: 1.52; equivalent to an average reduction of 60%) as measured on a 10-point numerical rating score (NRS). Informed consent was obtained from all participants, and the study protocol was approved by local ethics committees at Institute of Health and Neurodevelopment and Birmingham City University, as well as the Research Ethics Committee and Research & Development Office for the Dudley Group of Hospitals NHS Foundation Trust.

Two participants were diagnosed with PSPS, one with cauda equina syndrome and one with spinal fusions and disc collapse. Parameters that define the SCS stimulation for each individual can be found in Table 4.1. These stimulation parameters describe the

characteristics of the electrical current applied to the spine, and are set and adjusted by clinicians during check-ups to provide the most pain relief.

Table 4.1: SCS parameters for included participants

Participant	Pulse width	Hz	mA	Position	Coverage	Leads (contacts)	Age of implant (years)
1	350	40	1.8	T12	100%	1 (8)	6
2	500	130	2.9	T11	100%	2 (8)	5
3	340	60	1.9	T10	100%	2 (8)	4
4	440	40	3	T10	90%	1 (8)	7

4.2.4 Stimulus

During the recordings, SSEPs were delivered via electrodes on the median nerve. These were delivered to their non-dominant hand (three left, one right) in blocks of 50 s; these were trains of 100 stimuli with an inter-stimulus interval of 0.5 seconds. The amplitude of the stimuli was tailored to be 70% motor threshold, obtained by stimulating the median nerve until a finger twitch was observed, facilitating clear sensation without movement or pain (Mean: 6.51 mA, SD = 1.88) (Table 2). Stimuli were delivered using a Digitimer Constant Current Pulse Stimulator (DS7A; Digitimer Ltd, Welwyn Garden City) at 300V, 7 Hz with a pulse duration of 0.2 ms to ensure the stimulus was perceivable but short, and were connected to the MEG to mark epochs via trigger.

Table 4.2: Side and intensity of median nerve SSEP by participant, at 70% of motor threshold

Participant	Stimulation intensity (location)
1	5.6mA (Right)
2	9.59mA (Left)
3	4.55mA (Left)
4	6.3mA (Left)

4.2.5 MEG acquisition

MEG data were acquired using an Elekta TRIUX 306-channel MEG system, at a sampling rate of 2000 Hz, within an MSR at Institute of Health and Neurodevelopment. Participants were recorded at rest and during SSEP stimulation blocks in the two conditions (SCS-on and SCS-off) whilst in a sitting position (22˚ recline). Participants were asked to turn off their SCS generators 12 hours before attending the research session. SCS-off preceded SCS-on as a baseline for comparison, but also to avoid any lasting effects of SCS. Participants had their head shape digitized by a Polhemus Isotrak System (Kaiser Aerospace Inc.) and had five Head Position Indicator (HPI) coils attached to their forehead and bilateral mastoids to track head movement. No active online noise reduction techniques were used. Participants were asked to report their back pain during MEG acquisition via a Numerical Rating Scale (NRS; a scale of 0-10); participants were prompted to report their pain every 1-3 minutes by the investigator over an intercom. Participants blinding was impossible due to the nature of parasthesia-based SCS.

4.2.6 MEG data processing

tSSS was applied using MaxFilter (Elekta Neuromag Oy, version 2.2.10) to clean the data before processing and remove any signal noise created by the implanted pulse generators or SCS electrodes (0.98 Correlation limit, 9s buffer; Taulu & Hari, 2009). Preprocessing of

MEG data was performed offline using the M/EEG MATLAB toolbox FieldTrip (Oostenveld et al., 2011; build 20200513), and involved a discrete Fourier transform (DFT) filter of 50 Hz, 100 Hz and 150 Hz at a width of 0.5 Hz to minimise line noise without reducing the quality of the data; a high-pass filter of 1 Hz and a low-pass filter of 200 Hz were applied to remove slow and very fast spectra attributable to physiological phenomena outside our frequencies of interest, and the data were additionally detrended to control for slow drifts in magnetic fields. SSEP epochs were defined by their trigger, affording a 0.25 second baseline and 0.4 second post-stimulus window. There was an average of 850 SSEP trials in the SCS-on and 475 trials in the SCS-off condition, and an average of 850s of resting data was acquired for SCS-on and 481s for SCS-off. Continuous resting-state data was split into two-second trials with 50% overlap. Head movement was checked by performing ft_qualitycheck in the FieldTrip MATLAB toolbox.

Bad channels identified by MaxFilter were removed from all analyses for consistency. ICA was performed using the RUNICA method (Bell & Sejnowski, 1995), both magnetometers and gradiometers, and an upper limit of 60 components to adjust for reduced dimensionality introduced by tSSS. Using ICA, signal components for eye blinks and heartbeats were removed (Mean: 3, range: 2-4). Artefact outlier trials were removed separately for magnetometers and gradiometers, to avoid bias in trial rejection; further analysis used only gradiometers, as is commonplace in MEG analysis due to magnetometers and gradiometers recording different metrics (Garcés et al., 2017).

Datasets were aligned with template T1 MRIs from within the FieldTrip toolbox, which was then segmented. Template models of source grids 5 mm in resolution were warped to match the MRIs to facilitate group analysis, from which lead field matrices were computed

with the sensor configuration. For LCMV beamforming, sensor covariance matrices were calculated for averaged epochs, as well as pre- and post-stimulus windows independently; these were used to obtain source analysis outputs for both stimulus windows whilst using the filters computed for the whole time window. For DICS beamforming of SSEP epochs, processed data went through Fourier analysis of delta (0-4 Hz), theta (4-8 Hz), alpha (8-14 Hz), beta (14-30 Hz) and gamma (30+ Hz) frequency bands from -0.25s to 0.4s with the smoothing of 1, 2, 3, 9, and 33 Hz, respectively. In resting-state analysis, the full time window of 2s was utilised and compared to a 2s window in SCS-off resting-state recording.

Beamforming outputs were obtained using a regularisation parameter of λ=5% and a κ value set by the rank of the dataset (~58-60; described in more detail in chapter 3.2.4). The λ of 5% was chosen to account for poor signal-to-noise ratio in participant 2, and applied to all participant datasets for consistency. Relative change in the experimental (post-stimulus or SCS-on resting) time window was then calculated by subtracting the baseline from the experimental time window to remove centre-of-head noise bias innate to beamforming spatial weighting, and then dividing by the baseline to estimate the ratio of field strength between the baseline and window of interest (Quraan, 2011).

Virtual sensors were obtained by multiplying the processed time series data by a beamformer filter (in the form of an array containing spatial weights for each point in the 5mm resolution 3D source space, demonstrated previously in Figure 3.8) created specifically for the position with the maximal value in the LCMV source analysis output, resulting in time series data that is reconstructed for that specific voxel of the source model. This data was then averaged over trials to obtain the SSEP event-related field waveform, upon which

statistical analysis was performed; this was to circumvent the lack of consistency in the stimulation side and facilitate statistical comparisons regardless of handedness.

4.2.7 Statistical analysis

Non-parametric cluster-based statistical analysis was performed on virtual sensor power spectra: one-tailed within-participant T-tests were used to compare SCS-on and SCS-off conditions. This method corrects for multiple comparisons by clustering and permutation with the Monte Carlo method to determine significance: data points (individual frequencies) that met $p \leq 0.05$ when comparing SCS-on and SCS-off were clustered by temporal adjacency, and their combined 'cluster' T-value summed – which was then used to determine if a cluster was significant against a normal distribution generated by permuting and testing data points 2000 times (described in more detail in chapter 3.2.6). SSEP ERF statistical comparisons were made for the time window of 0.001-0.2s; statistical analysis of power spectra was performed on frequencies 1-100 Hz with a 1 Hz step. Timeseries data were analysed from an average of data from 0.001-0.2s and required no corrections for multiple comparisons (as this time-window encompassed all N2-P2 components and latencies were likely to be heterogeneous).

No group statistical test was possible for source-space data, as one participant's SSEP electrodes were placed on an inconsistent side; cluster-based permutation analysis enabled the statistical comparison of source-space reconstructions of resting-state data with a two-tailed design. Locations were identified using the Automated Anatomical Labelling (AAL) atlas (Tzourio-Mazoyer et al., 2002).

4.3 Results

4.3.1 Pain rating during SCS

The average reported pain during SCS-off was 6.18/10 (SD: 1.35), compared to 3.43/10 (SD: 1.14) for SCS-on (Figure 4.1). A paired samples t-test found this difference to be significant ($t(3) = 2.840$, $p<0.05$). It is noteworthy that participant #3 experienced a -22% change in pain score during the SCS-on portion of their MEG recording, as opposed to the average of -55% in the other three participants (range: -48-73%), which was not near the values reported in their screening questionnaire (-50%), and which would not meet initial screening criteria for inclusion in the study at recruitment.

4.3.2 MEG data quality

Quality checks were performed on the data using FieldTrip's ft_qualitycheck function to inspect line noise and head movements; this did not reveal any need to correct or remove data from any participants. No participants had head movements greater than 5mm during scanning. Two channels (MEG0531 and MEG0111) were removed from the analysis of all datasets after being flagged for SQUID jump artefacts by MaxFilter during data cleaning.

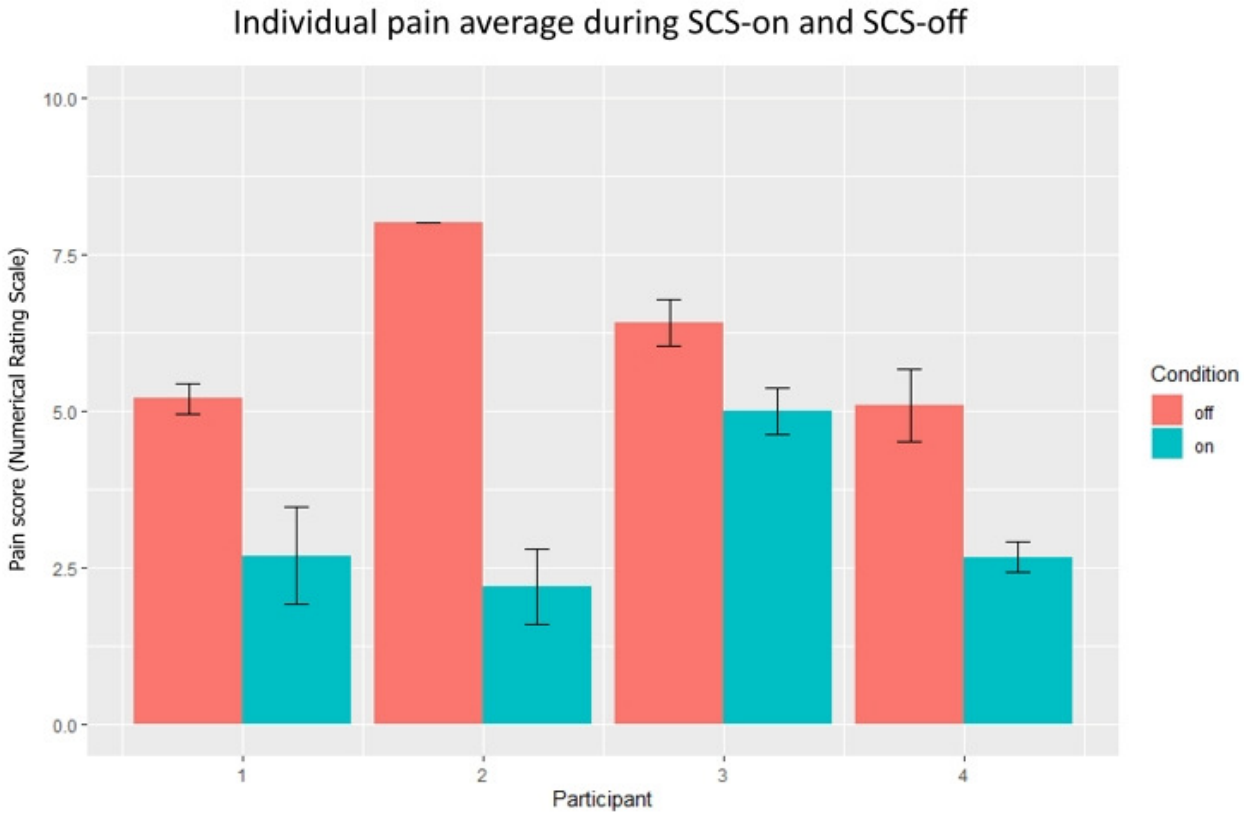

Figure 4.1: Subjective pain score by individual, as rated on a scale of 0-10 (0 = no pain, 10 = most pain imaginable) during SCS-on and SCS-off MEG recordings. Error bars represent standard deviation.

4.3.3 SSEP virtual sensors

LCMV SSEP outputs for SCS-on and SCS-off conditions are outlined in 4.2. A 5% regularisation was necessary to reconstruct data for participant 2, which was then applied to all other participants' source reconstructions. Presented below are reconstructions of relative field strength in the 0.001-0.2s time window after removal of and subsequent division by pre-stimulus activity in the -0.25s-0.01s time window, and therefore display values that express the change in field strength relative to the baseline in arbitrary units (Figure 4.2). On average, SCS-off had a mean relative change in field strength (fT/cm) from baseline of 67% (SD: 50%), and SCS-on had a mean of 67% (SD: 61%). The average difference when SCS was turned on was 0.25% (SD: 12%). No source statistics were performed on the

LCMV outcomes, as one participant's data was acquired with stimulation of the right median nerve, in contrast to three participants being stimulated on the left median nerve, though their source analysis outputs are displayed below (Figure 4.2). Voxels with maximal values for each individual were identified in the somatosensory cortices: these voxels were selected for virtual sensor reconstruction. Interindividual variability in magnitude across participants (such as the difference between participants 1 and 2) is to be expected, especially with individually adapted stimuli that require subjective reporting, and may reflect a myriad of physiological or psychological variables.

4.3.3.1 Virtual sensor evoked waveforms

Virtual sensors were computed with the LCMV beamformer weights and singular value decomposition (determined by defining the parameter 'cfg.fixedori =yes' in ft_sourceanalysis). This enabled the reconstruction of time series information in the voxel of peak magnitude identified in the previous step, though the orientation of the dipole is voxel-specific, and as such, can appear inconsistent across individuals. Virtual sensors for the peak voxels were reconstructed by multiplying the raw time series data by the spatial beamformer weights generated by the beamformer, on which statistical testing could be performed (Figure 4.3).

The majority of literature exploring SSEPs in SCS demonstrates suppression of incoming signals and the resulting cortical waveform in the somatosensory cortex. As such, statistical hypothesis-testing in this comparison was one-tailed, with the null hypothesis that SSEPs would not be reduced in the SCS-on condition. No clusters attained significance ($t(3) = -0.687$, $p=0.271$) when comparing SCS-off to SCS-on SSEP waveforms in the 0.001-0.2s time window.

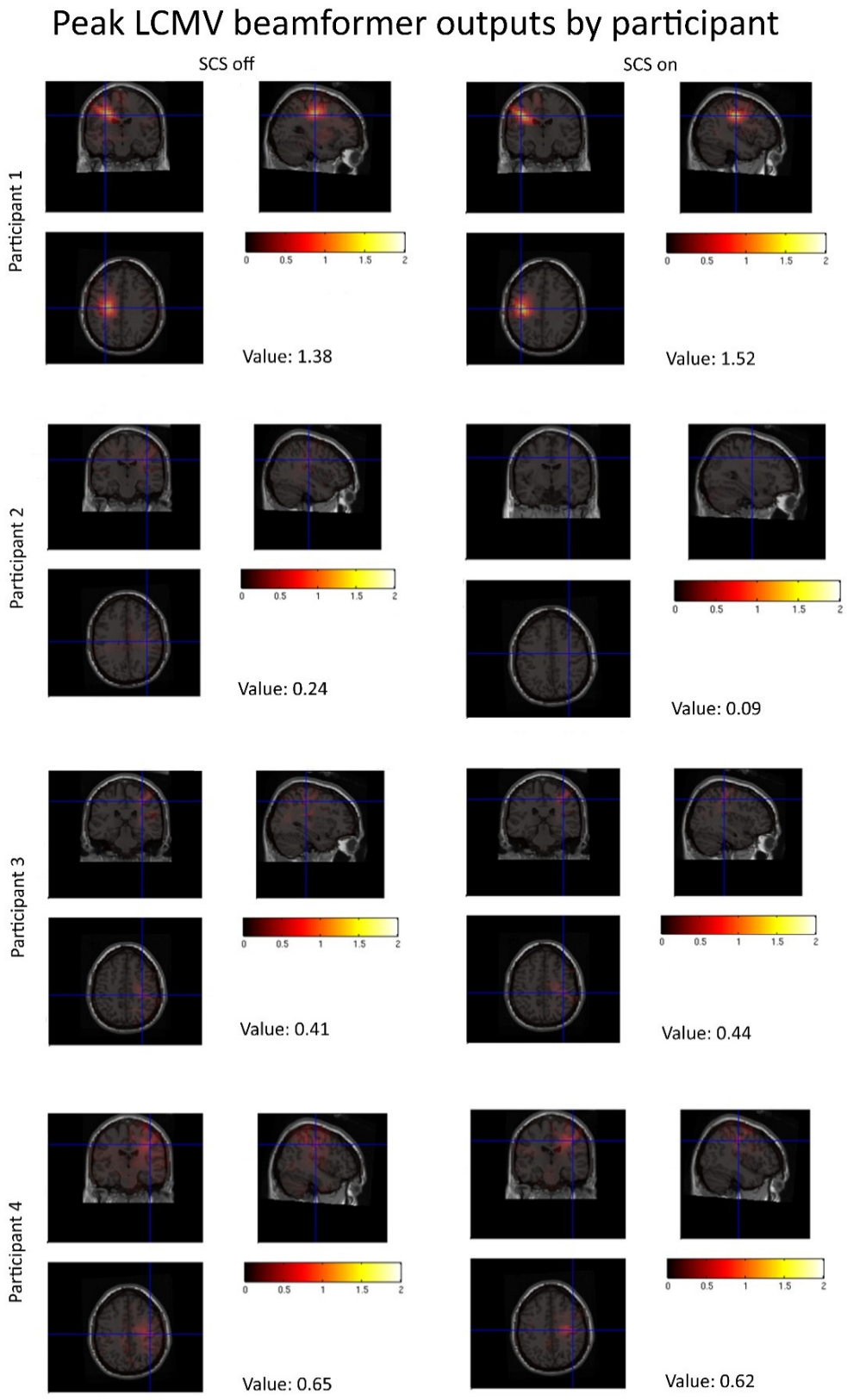

Figure 4.2: Peak beamformer plots generated within FieldTrip with the 'slice' method, a crossbar highlighting the Neuromag coordinates of peak brain activity. The value represents % change vs baseline (i.e. 1.51 is 151%). Colour bars are on the same scale for each Figure.

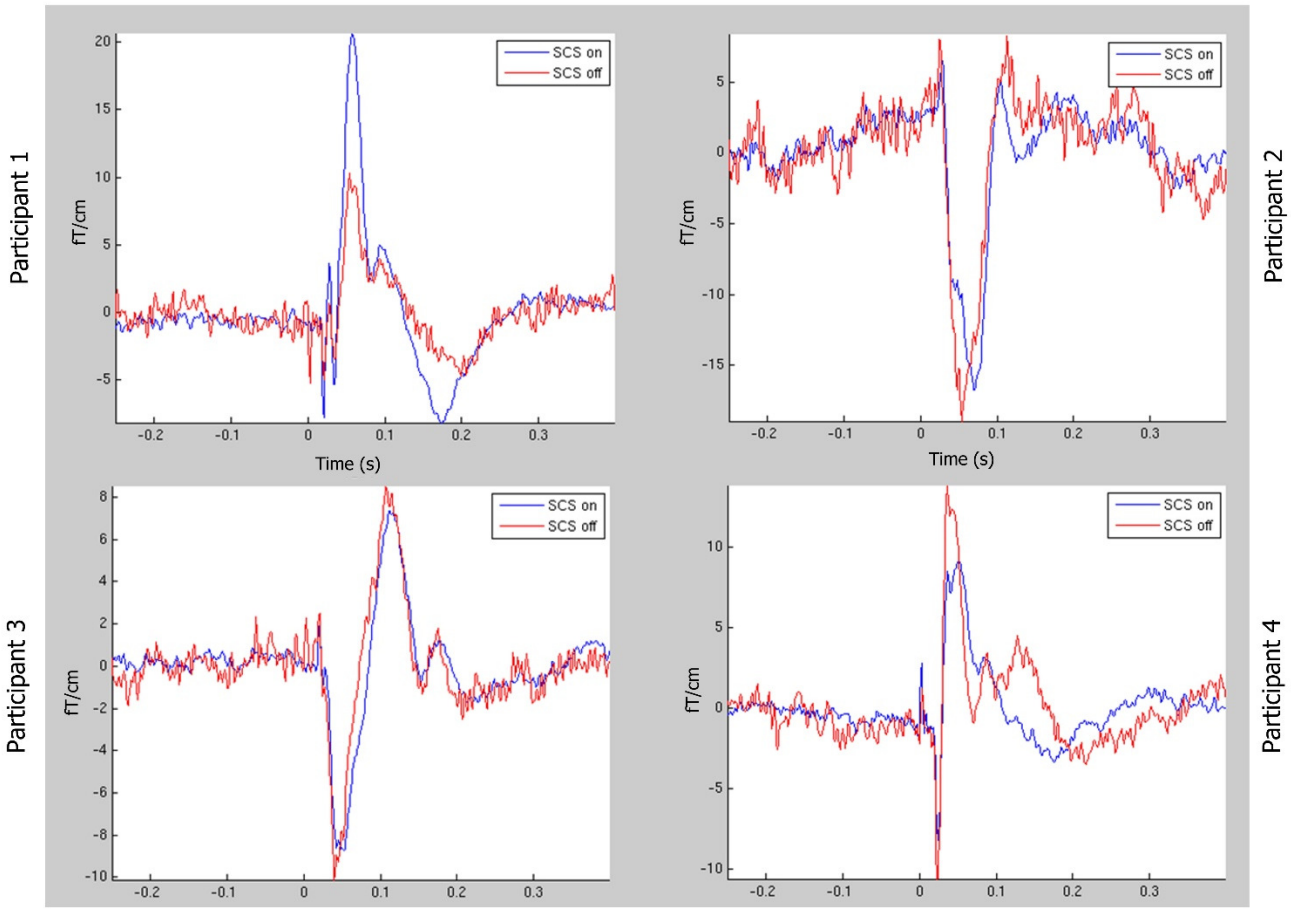

Figure 4.3: The difference in SSEP waveforms with SCS turned on and off, by participant and SCS-condition. Virtual sensors were reconstructed by multiplying time series data by spatial filters generated by the LCMV beamformer. Singular value decomposition was applied to the lead field matrix; hence the shapes of the different waveforms.

4.3.3.2 Virtual sensor power spectra analysis

Fourier analysis of the virtual sensors demonstrated frequency differences between conditions: with SCS-on, a clear reduction in oscillatory power is evident across all bands. A non-parametric cluster-based permutation analysis with corrections for multiple comparisons confirms a notable change: a significant difference was identified by the analysis as significant after permutation analysis at $p<0.001$, with a medium-to-large effect size as measured by Cohen's D at the largest cluster (t=-1.503; d = 0.74). Though cluster-based permutation analysis in this context does not make any conclusions regarding the significance of individual frequencies, the sole cluster that contributed to the rejection of the null hypothesis at 3 Hz is highlighted in Figure 4.4, widened in the Figure by 1 Hz for visualisation purposes.

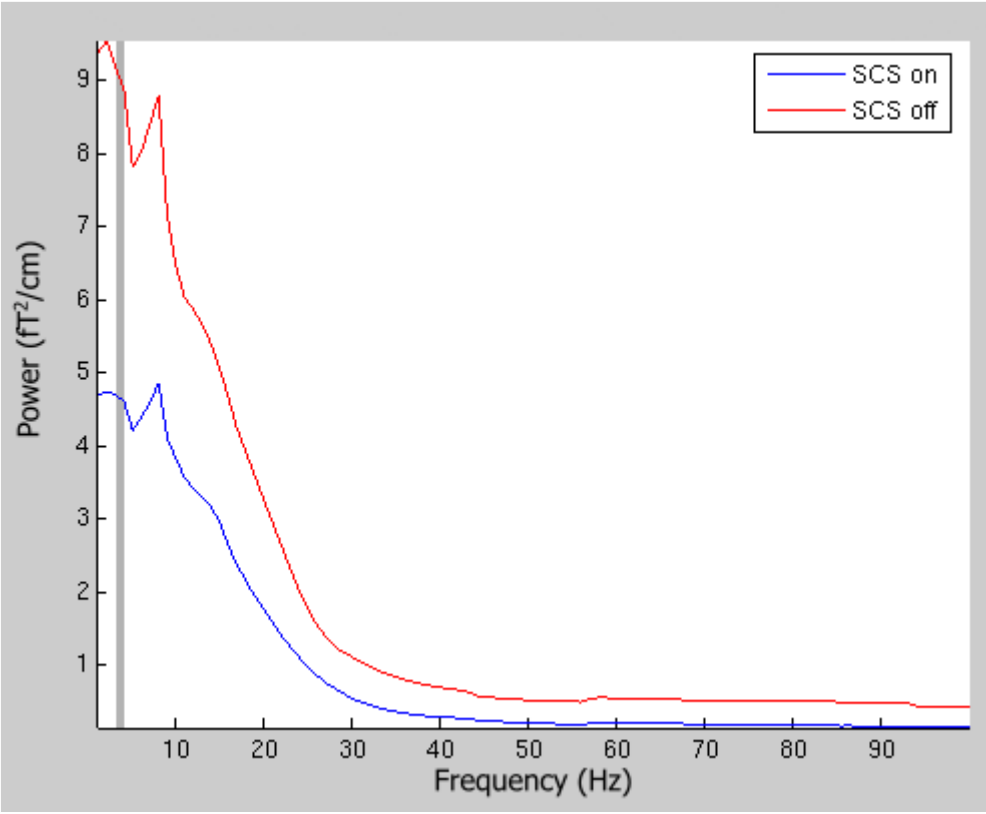

Figure 4.4: Power spectrum of the averaged virtual sensor SSEP waveforms of all participants. The grey box indicates where the significant cluster was identified by statistical analysis (3 Hz), and is widened by 1 Hz for visualisation.

4.3.4 Resting DICS

DICS was performed on all frequency bands by comparing SCS-on and SCS-off resting-state data. Grand averages were generated for visualisation, and statistics were performed. Here, statistically significant enhancement of synchrony in theta and delta frequency bands are observed, as opposed to the desynchronisation seen in SSEPs.

4.3.4.1 Theta resting DICS

Clusters that met the threshold for significance were identified in the theta frequency band, with greater activity in the SCS-on condition, demonstrating a statistically significant difference between conditions .Using this method for statistical analysis does not allow for spatial conclusions, however; instead, the cluster-based permutation analysis enables the rejection of the null hypothesis for the differences between SCS-on and SCS-off. Clusters that contributed to this rejection of the null hypothesis were identified in the left superior temporal gyrus, bilateral middle cingulate and right anterior cingulate cortices (Figure 4.5; greatest cluster $t = 2991$, $p<0.0001$), with the largest T-values localised to the right dorsal anterior cingulate cortex and left middle cingulate cortex, where theta power was greater in SCS-on than SCS-off; though it must not be misunderstood to suggest that only (or primarily) these areas were significantly different. The effect size of the greatest significant cluster was $d = 1.59$.

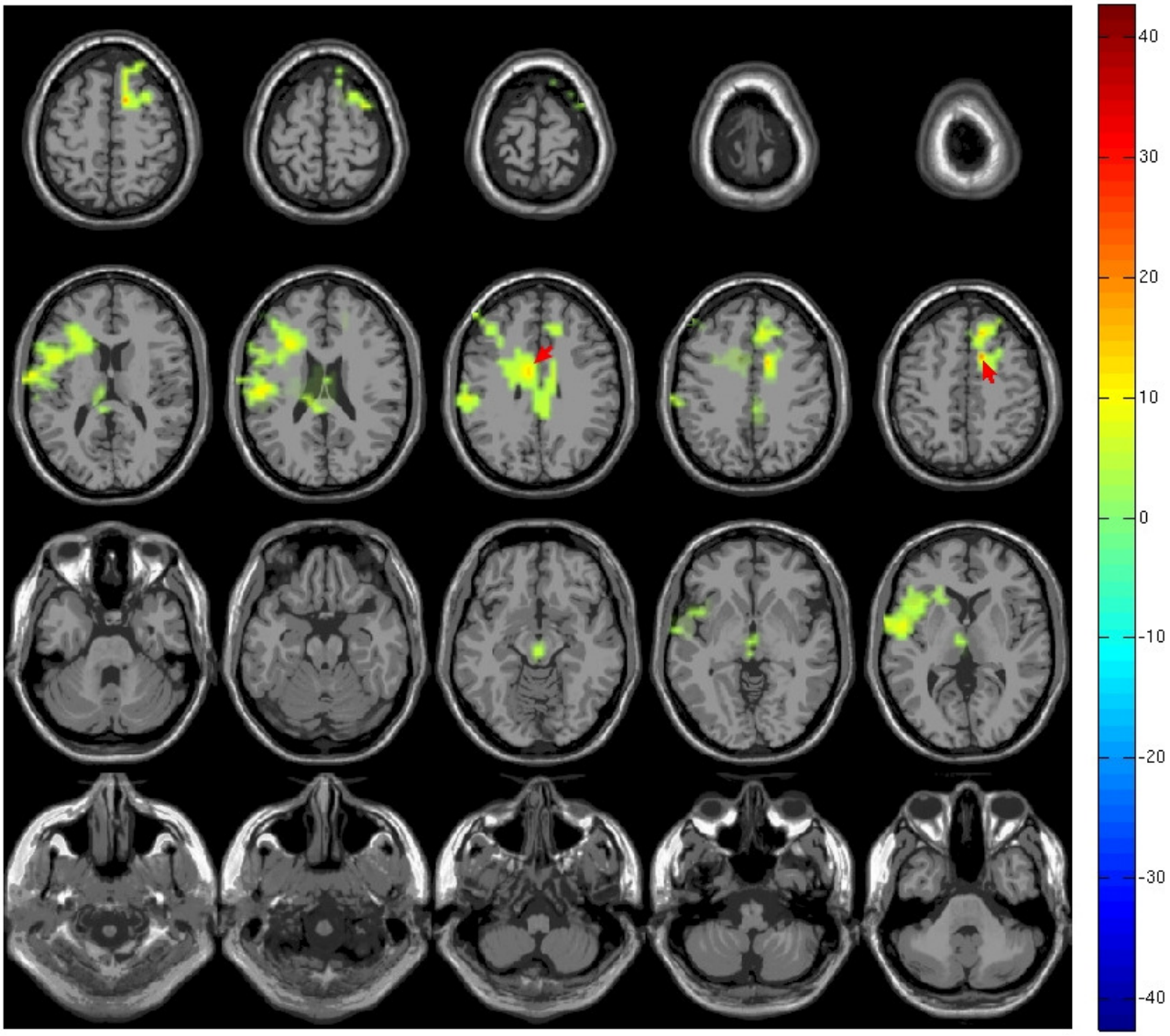

Figure 4.5: A statistical map showing T-values for clusters of theta-band activity thresholded at p<0.05. Red arrows point to the clusters with the highest T-values.

4.3.4.2 Delta resting DICS

Clusters that met the threshold for significance were identified in the theta frequency band, with greater activity in the SCS-on condition, demonstrating a statistically significant difference between conditions (t = 6269, p<0.0001). As described above, cluster-based permutation analysis only enables the rejection of the null hypothesis based on differences across conditions; Figure 4.6 demonstrates clusters that met a significance threshold for visualisation purposes. High-value clusters that contributed to the rejection of the null

hypothesis were localised to the left superior temporal gyrus, left insula, and left caudate nucleus, where delta power was greater in SCS-on than SCS-off. The largest cluster had an effect size of d = 1.6 and was located in the left insula.

4.3.4.3 Alpha, beta and gamma resting DICS

Some notable increases in power of frequency bands can be observed in the alpha and beta frequency bands in the left somatosensory cortices (Figure 4.7). Weak suppression of gamma activity is observable in bilateral somatosensory cortices; none of these changes were statistically significant at $p<0.05$ (Largest gamma cluster: t = 1248; Largest beta cluster: t = 951, Largest alpha cluster: t = 3563).

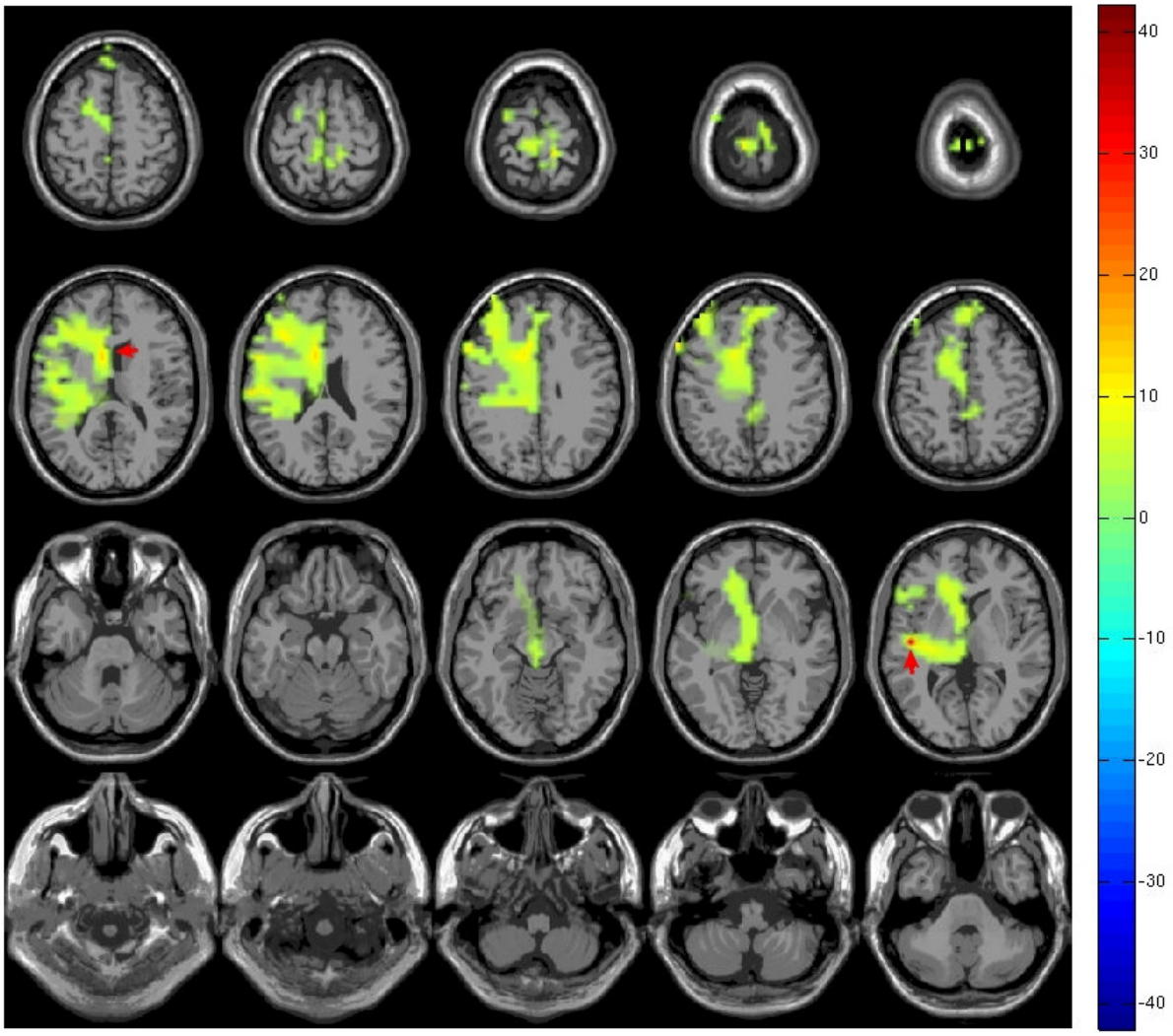

Figure 4.6: Statistical map showing T-values for clusters of delta-band activity, thresholded at $p<0.05$. Red arrows point towards the clusters with the greatest T-values.

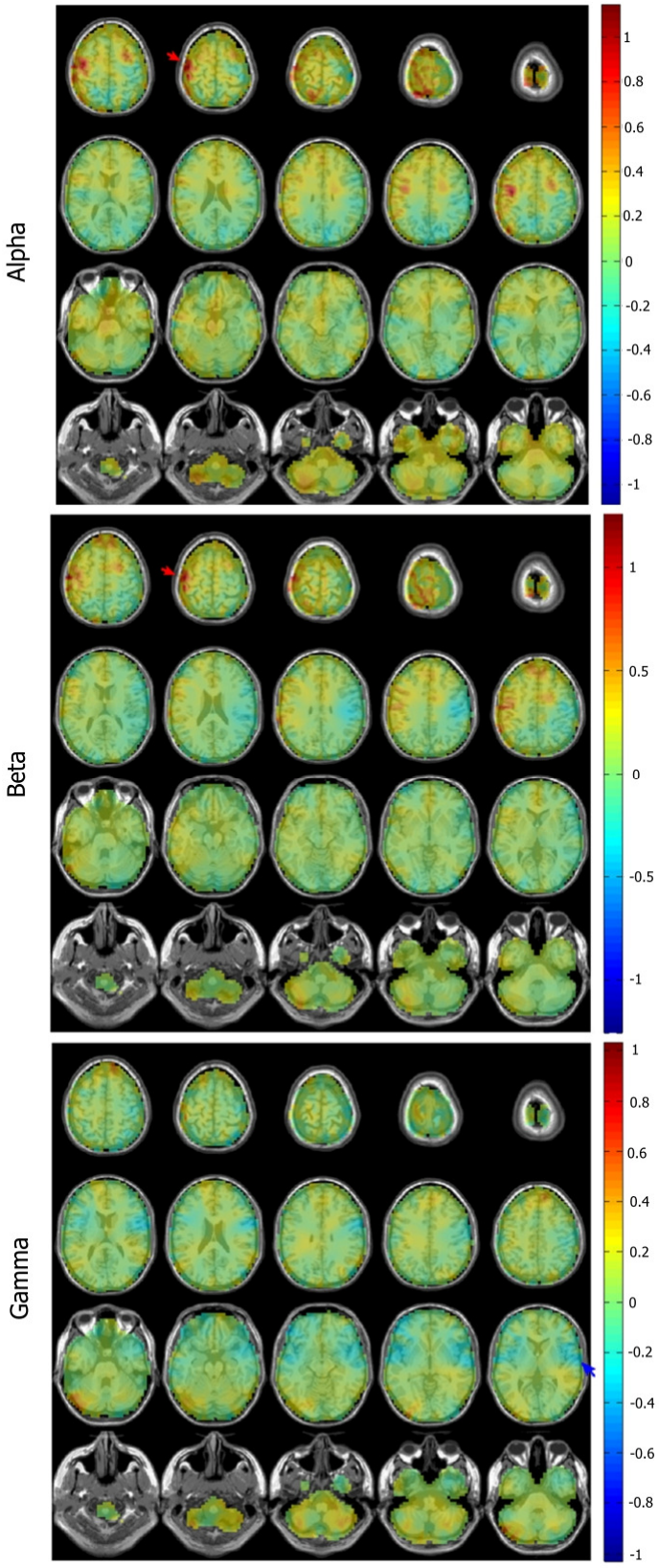

Figure 4.7: Ratio of change in synchronisation between SCS-off and SCS-on conditions averaged across all participants. The colour bar represents the % change between the two conditions, with a value of 1 indicating a 100% increase. Increase in alpha and beta and suppression of gamma highlighted with red and blue arrows respectively.

4.4 Discussion

4.4.1 Resting-state

The results of this study show a significant difference in resting-state activity at delta and theta frequencies when comparing SCS-on and SCS-off conditions in a group of four SCS participants. The clusters that contributed to the rejection of the null hypothesis were mostly localised to the left hemisphere, most notably the left posterior insula, caudate nucleus and superior temporal gyrus; it is likely that the enhancement of power in delta and theta frequencies in these areas are a result of ascending stimulation of the dorsal columns via the medial pathway, as suggested by de Ridder & Vanneste (2016), and the slowing of processing in areas associated with higher pain processing and pain-related memory. The current findings fail to replicate the findings of several studies that observed suppressive effects of SCS on spectral power in the brain at rest (Schulman et al., 2005; Sufianov et al., 2014; Goudman et al., 2019); most notably De Ridder & Vanneste (2016), whose investigations of conventional SCS versus a control baseline identified suppression in beta and gamma frequency bands in the posterior cingulate cortex and the parahippocampus, respectively.

The current study identified localised enhancement of theta band activity in the bilateral mid-cingulate cortex (MCC) and right anterior cingulate cortex (ACC). The cingulate cortices are regularly associated with pain experience, especially its link to affective, emotional and planning processing in pain and pain anticipation (Moseley, 2003; Nevian, 2017). Only the ACC and posterior cingulate cortex (PCC) have been identified as locations for altered brain activity during SCS so far (De Ridder & Vanneste, 2016; Moens et al., 2012), and not yet in MEG; SCS's interaction with the ACC could correspond to suppression in the otherwise

increased baseline activity in chronic pain patients (Bliss et al., 2016; Gungor and Johansen, 2019; Meda et al., 2019). MCC activation has been implicated in modulating pain sensitivity and descending pain facilitation in mice (Nevian, 2017; Tan et al., 2017) and has been associated with nociception, negative affect, and cognitive control (Shackman et al., 2011). Event-related theta frequency enhancement has been associated with increased pain empathy (Mu et al., 2008), and resting-state analysis has demonstrated enhancement of theta activity in chronic pain patients in the pain neuromatrix (Fallon et al., 2018; González-Roldán et al., 2016; Hsiao et al., 2017; Lim et al., 2016; Stern et al., 2006). Previous works consider ACC theta enhancement as hallmarks of disturbed thalamocortical networks (Stern, Jeanmonod and Sarnthein, 2006), or contributors to ongoing chronic pain neurocircuitry (Fallon et al., 2018). In this study, theta enhancement is seen in the MCC and ACC resulting from conventional SCS in resting-state; these findings instead suggest that theta synchronisation may reflect the slowing of processing in areas responsible for affective pain components in the presence of ongoing pain.

The superior temporal gyrus is not part of the classic pain neuromatrix, but pain-related changes in this region are identified in some studies. It has been linked with experimental pain (Cleve et al., 2017; Song et al., 2006), chronic pain conditions (Van Ettinger-Veenstra et al., 2019; Han et al., 2013; De Pauw et al., 2019), pain anticipation (Palermo et al., 2015), and the maintenance of unpleasant pain-related memories (Houde et al., 2020; Luo et al., 2016), though it has not yet been identified as a candidate for underlying SCS activity. In MEG research, delta enhancement in the left superior temporal gyrus was recently identified as negatively correlating with subjective pain levels in low back pain patients before and after selective nerve root blocks (Shigihara et al., 2021); the current study also identified significant delta enhancement in the superior temporal gyrus in resting-state SCS-

on conditions, which complements Shigihara et al.'s findings. Together, it is apparent that greater resting-state delta power is associated with pain relief. Further research is required, however, to determine the exact nature of this delta component: it is possible that the SCS-linked delta enhancement in this region contributes to pain suppression by disrupting painful memory exaggeration with slowing of brain activity, a recognised contributor to pain sensitivity and chronic pain in this area of the cortex (Houde et al., 2020; McCarberg and Peppin, 2019).

Increased delta synchrony in the insula and the caudate nucleus has not been identified by previous SCS studies; though low-gamma suppression has previously been observed, it was not found in this study (De Ridder et al., 2013). The insula and caudate nucleus their involvement in salience processing and somatosensory processing is well established (Garcia-Larrea, 2012), and its ongoing activation likely represents the attentional and localisation processes linked to the presence of paraesthesia; though it is noteworthy that the insula and cingulate cortices are connected to the PAG and can assert control over descending inhibitory projections of the RVM, which are likely candidates for the therapeutic effect of SCS.

The primary difference to note between currently published studies and the presented works here is that prior research has almost entirely utilised EEG. It is widely acknowledged that MEG and EEG acquire functionally similar data – but also, that EEG suffers from greater volume conduction, and less advanced suppression of external electromagnetic noise. It is possible that utilising MEG with signal cleaning methods like tSSS (Taulu and Hari, 2009) effectively minimised spectral components from the SCS generator that have been found to be invested in EEG recordings (Buentjen et al., 2021). It is also worth noting that many

studies exploring SCS do so with a relatively small number of participants and a highly heterogeneous sample of stimulation parameters and chronic pain conditions, such is the nature of the participant population (Mode average = 5; Witjes et al., 2022), and that utilising such a small sample is recognised to result in reduced power.

4.4.2 Beamforming SSEPs in SCS

This is the first MEG study to contribute to the discourse surrounding the effect of SCS on SSEPs since Theuvenet et al. (1999) published their exploration of SSEPs in a sensor-level analysis using a system with only 19 magnetometers. In the current experiment, 204 gradiometers were used to obtain spatial weights by which to multiply the time series, thereby reconstructing activity at the location in the brain with the highest field strength, rather than at the sensor. Previous studies observing SSEPs in SCS have done so to evaluate the hypothesis that SCS pain-relief is due to antidromic stimulations of the Aβ fibres inhibiting ascending wide dynamic range (WDR) neurons; any suppression of SSEPs in the presence of SCS stimulation is possible evidence for the collision of these antidromic stimulations with ascending Aβ activation, and ability of SCS antidromic stimulation to inhibit WDR signals. Most studies report significant attenuation following SCS (de Andrade et al., 2010; Buonocore et al., 2012; Buonocore and Demartini, 2016; Lang et al., 1989; Larson et al., 1974; Poláček et al., 2007; Theuvenet et al., 1999; Urasaki et al., 2014; Weigel et al., 2015; Wolter et al., 2013), though it is not a unanimous finding (Doerr et al., 1978; Mazzonea et al., 1994), and not necessary for pain suppression (Urasaki et al., 2014). This study observes SSEPs generated by median nerve stimulation, an action potential that cannot collide at the dorsal column. This experimental design instead evaluates any suppressive effect by orthodromic dorsal column stimulation on the processing of

somatosensory stimuli. A change in SSEP field strength was not identified in the participants recruited for this study at the virtual sensor level, despite three of four participants reporting successful pain reductions in the SCS-on condition. Anecdotally, some reduced field strength is noticeable in participants one, two and four (and notably not participant three, who reported lesser pain relief), but not at group level, and not to the extent of the drastic attenuation demonstrated in the studies identified above.

Virtual sensor comparisons of power spectra of SSEPs in SCS-on and SCS-off conditions revealed a significant difference using cluster-based permutation analysis; the corresponding cluster was a narrow band at 3 Hz in the delta frequency band. Visual inspection suggests a broader difference between the SCS-induced suppression of the power spectra in the post-SSEP evoked waveform. This difference in power spectra during SSEPs is noteworthy especially because it cannot be explained by any significant differences in the overall strength of the ERF, and that it contrasts the enhancement of delta in the resting-state analysis above. The power spectra resulting from SSEPs have not yet been explored in any of the current literature, and warrants exploration with proper time-frequency analysis. Evoked delta power in sensation has been linked to relative stimulus intensity (Fardo et al., 2017; Hauck et al., 2015), and is thought to be linked to decision making and signal detection (Başar et al., 2001); this is perhaps a greater indicator of the ascending effect of SCS in the absence of SSEP collision but requires statistical evaluation with time-frequency analysis.

Together, the virtual sensor power spectra and the lack of SSEP field strength attenuation somewhat elucidate the somatosensory processing changes as a result of ascending orthodromic dorsal column SCS. It is clear from these findings that SCS influences

somatosensory processing in the frequency domain, even without attenuation of overall field strength. This could be explained by a similar “first-come first-served” mechanism described by Tesani et al., (2015) who showed that competing ascending noxious stimuli were diminished when processed collaterally with ascending somatosensory stimuli, though such a claim would require further study. As the effect of SCS is known to last between pulses and beyond stimulation, it is likely that the timing of the stimuli is not the only phenomenon responsible for the anti-nociceptive effect, though it is possible that entrained rhythms last beyond the initial stimulation. As demonstrated by the resting-state findings, ascending SCS can slow the rhythms in the insula, MCC, ACC, caudate nucleus, and superior temporal gyrus, which could disrupt somatosensory processes, though their facilitation of descending antinociception is unlikely to contribute to the suppression of somatosensation. Future research exploring connectivity and networks of these areas during SSEPs unrelated to collision could elucidate directionality of the relationships between these brain areas responsible for the modulation of SSEPs in the somatosensory cortex.

It is important to note that the statistical methods used on the source localisation data here enable the rejection of the null hypothesis (that the power and location of SCS-on and SCS-off resting-state brain oscillations are the same), but do not facilitate drawing absolute conclusions on the location of the significant differences. That being said, clusters that contribute to the rejection of a null hypothesis can be indicators for future research using statistical methods that do enable these deductions (Sassenhagen and Draschkow, 2019).

4.4.3 Limitations

The primary limitation of this study is the small sample. SCS is reserved for chronic pain patients for whose pain is intractable, and for those who respond to the treatment after a

screening trial. The range of participants in conventional SCS M/EEG studies as recorded by the Bentley et al. (2016) systematic review of brain activity following SCS is between 1-30, with an average of 10 participants. The only MEG studies of SCS conducted thus far had between one and five participants (Schulman et al., 2005; Theuvenet et al., 1999), demonstrating how difficult it is to recruit in this particular field, and why the results are worthwhile contributions to the literature.

One of the four participants only experienced minimal SCS pain relief during their MEG recording. This participants' dataset was included in the statistical analyses, and thusly the results must be interpreted as significant differences in SCS-on and SCS-off conditions, but not as significant differences between SCS-off and SCS-analgesic conditions. The participant in question reported that their usual SCS-on pain relief was at least 50%, suggesting that their SCS implant would usually function adequately; it is possible that the long-term suppressive effect of their SCS implant might not have yet begun during their data acquisition (as implicated by long-term SCS effects, see chapter 2). Their data still serves to inform us as to the ascending effects on the brain, though it is possible that the effects identified here would be greater with a stronger responder.

In the dataset analysed in this chapter, the median nerve was stimulated in blocks of 15, with an inter-stimulus interval (ISI) of 0.5s. This limited the potential for time-frequency analysis, but also likely diminished the signal-to-noise ratio of ERFs (Theuvenet et al., 1999). Future studies would benefit from allowing for greater ISIs, to enable high-resolution time-frequency analysis and better elucidation of brain activity.

4.4.4 Future directions

This study has highlighted potential avenues for research in conventional SCS, MEG and SSEPs. An exploration of time-frequency changes in peak virtual sensor SSEPs as a result of SCS could elucidate the evoked and induced oscillations suppressed in the therapeutic condition identified by cluster-based permutation analysis in a way that was not possible in this study. Resting-state analysis of virtual sensors specifically observing delta and theta oscillations in the left ACC, MCC, insula, and the superior temporal gyrus as a result of SCS would enable researchers to evaluate these spectral power enhancements with more specific and powerful statistical methods, which is not possible when using cluster-based permutation for whole-brain analysis. Directional connectivity analysis of the regions of interested highlighted here during collision-free SSEPs could demonstrate any temporally correlated networks responsible for the power spectra changes in somatosensory processes, or whether the effect is primarily restricted to the processes of the somatosensory cortex. Additionally, single-trial analysis of virtual sensor data may reveal oscillatory components that are not phase-locked, and otherwise obscured by the averaging process.

When observing the data, participants that responded to the SCS whilst in the MEG showed some decreases in SSEP beamformer magnitude, whilst the participant that did not demonstrate any real reduction in pain showed no change at all. Future research with a larger dataset could consider the responsiveness to SCS in the modulation of non-collision SSEP processing in the somatosensory cortex.

Advanced SCS methods that focus on patterned stimulation and closed-loop systems are becoming popular in neurostimulation techniques, as they boost pain relief for a greater

number of those implanted (Mekhail et al., 2020); there is evidence to suggest the supraspinal effects of new techniques are separate to those of conventional SCS (Bocci et al., 2018; Goudman et al., 2019; Telkes et al., 2020), though the extent to which they are different is contended (Goudman et al., 2021) and may benefit from future exploration using MEG.

4.4.5 Conclusion

For the first time, this study reports the effect of SCS on SSEP and resting-state electromagnetic brain activity in chronic pain states using MEG data cleaned with temporal signal space separation, and MEG beamforming source analysis. This enabled analysis of evoked fields and power spectra at virtual sensors, as well as whole-brain source localisation of resting-state frequency modulation as a result of SCS. Significant resting-state enhancements were identified using cluster-based permutation analysis in delta and theta frequencies in source analysis. Virtual sensors identified significant suppression of power spectra as a result of SCS stimulation in SSEPs when stimuli were applied without collision in the dorsal columns, but no changes were observable in the field strength of ERFs. These findings demonstrate slowing of frequencies in the resting state in the ACC, MCC, insula, caudate nucleus, and superior temporal gyrus, and also provide evidence for the disruption of somatosensory processing in the frequency domain during SCS.

5. Study 2: The Cold Pressor Test and pain sensitivity in MEG

5.1 Introduction

Pain is a sensory experience that is comprised of cognitive, physiological, and affective components; it is a complex phenomenon that changes from person to person. Individuals experiencing the same objective stimuli strength, under the same conditions, can subjectively report pain starting at different thresholds, and interpersonal variability in the amounts of perceived pain from objectively consistent stimuli. The differing thresholds for pain and the resulting intensity from a standardised stimulus across individuals is one's pain sensitivity. Much of the research explaining interindividual variability in pain sensitivity has focused on genetics: Whilst specific pain modalities can be linked to transduction at the nociceptor (Dubin and Patapoutian, 2010), pain pathways are made of many stages, each of which can be associated with multiple different genetic variations (Nielsen et al., 2009). Nielsen, Staud and Price (2009) studied monozygotic and dizygotic twin pairs to explore the genetic influence on cold pressor and heat pain, and concluded that as much as 60% of cold pressor pain could be explained by genetic mediation, and 26% in heat pain – whilst as little as 5% of the variance was explained by environmental factors. It is clear that genetics is not the sole factor in explaining differences between individuals

Sensitivity to pain can be increased pathologically through the mechanisms of peripheral or central pain sensitisation. Peripheral sensitisation is an enhancement of nociceptive signals as a result of inflammation or tissue damage, and can result in painful stimuli becoming more painful (hyperalgesia) and non-painful stimuli becoming painful (allodynia; Gangadharan and Kuner, 2013). Similarly, central sensitisation can elicit these symptoms as a result of neuronal changes at the second-order synapse, such as dysfunctional long-term potentiation and receptor up-regulation initiated by ectopic or prolonged neuronal firing at

wide dynamic range neurons, though this is usually implicated in chronic pain conditions (Campbell and Meyer, 2006). Atypical reduced pain sensitivity is demonstrated in congenital hyposensitivity to pain, autism spectrum disorder and idiopathic cases of mechanical nerve damage, but is also associated with older age, exercise, and stress (Belavy et al., 2021; Weingarten et al., 2006; Yasuda et al., 2016). Transiently, pain intensity can be reduced by fatigue and reduction in stimulus novelty when presented in short timeframes to Aδ nociceptors (Treede, 2016), but augmented by temporal summation in C-fibres (Dengler-Crish et al., 2011); temporal summation of pain is often observed with tonic thermal stimuli, and works to function as a measure of pain sensitivity in experimental settings.

Research has shown differences in pain sensitivity to be associated with gender (Bulls et al., 2015; Esterlis et al., 2013; Ravn et al., 2012), age (Yezierski, 2012, El Tumi et al., 2017) gender role-conformity (Alabas et al., 2012), menstrual cycle phase (Iacovides et al., 2015), ethnic identity (Ostrom et al., 2017; Rahim-Williams et al., 2007), handedness (Pud et al., 2009), cortical density (Emerson et al., 2014; Erpelding et al., 2012), genes (Nielsen et al., 2009) and neurotransmitter levels (Zunhammer et al., 2016). Increased pain sensitivity is a possible characteristic of many disorders, including those that are not defined by pain, including panic disorder (Lautenbacher et al., 1999), sleep disorders (Sivertsen et al., 2015), and Brown-Sequard and Wallenberg syndromes (Bromm and Treede, 1991). Psychological factors such as stress (Timmers et al., 2018; Vachon-Presseau et al., 2013), depression (Schwier et al., 2010), anxiety and anxiety sensitivity (Dodo and Hashimoto, 2017), fear of pain (Timmers et al., 2018), pain catastrophising (Banozic et al., 2018), attention (Miron et al., 1989), audience composition (Vigil and Coulombe, 2011) and cognitive inhibition (Oosterman et al., 2010) have also been identified as influencing pain sensitivity. Identifying common neural markers of pain sensitivity could impact many fields of physiology,

psychology, and pathology research, with possible therapeutic applications using deep brain or transcranial alternating current stimulators. Neural biomarkers could assist in treatment selection, effectiveness and responsiveness or diagnosis, risk, stage, or progression of disease (Lleó, 2021; Mouraux and Iannetti, 2018).

Pain sensitivity has been explored using time-frequency analysis of evoked potentials acquired using EEG (Hu and Iannetti, 2019; Schulz et al., 2012), source analysis of evoked potentials (Goffaux et al., 2013), tonic and resting-state frequency analyses (Furman et al., 2018; Nir et al., 2010, 2012; Valentini et al., 2022), and alpha connectivity (Modares-Haghighi et al., 2021). Notably, alpha and gamma frequency enhancement in laser evoked potentials have been implicated as predictors of pain sensitivity (Schulz et al., 2012; Hu & Iannetti, 2019), and do so selectively (Valentini et al., 2022). In tonic pain research, Nir et al. (2010) observed that peak alpha frequency (PAF) at rest and during noxious heat stimulation correlated with subjective pain scores. In a follow-up study, Nir et al. (2012) identified significant correlations between numerical pain scores and slow (7-10 Hz) alpha during Contact Heat Evoked Potential (CHEP) stimulation and at baseline. PAF in the sensorimotor cortex has since been implicated in variation in inter-individual pain sensitivity in phasic heat (CHEPS) and tonic capsaicin pain (Furman et al., 2018; Furman et al., 2020), but with opposing findings depending on the width of the alpha band (Valentini et al., 2022). It is clear that alpha is a component with a strong relationship to pain sensation, and it is well implicated in pain sensitivity specifically. Its associations with subjective pain experience are well-documented in tonic and evoked pain experiments, and whilst evoked pain models have been criticised due to their phase-locked nature and recruitment of salience networks not selectively reflecting pain (Mouraux and Iannetti, 2018), tonic pain models are more able to emulate the experience of the chronic pain patients; this makes

their findings more applicable to clinical cases, and reduces the impact of novelty on the stimuli. One experimental stimulus that has been suggested to mimic chronic pain is the Cold Pressor Test (Chang et al., 2002; Chen et al., 1989).

5.1.1 Cold Pressor Test

Originally designed and validated by Hines & Brown (1932) as a method by which to observe blood pressure changes, the Cold Pressor Test (CPT) is a task that requires the participant to submerge their hand or arm in chilled water. Submerging one's limb in cold water quickly causes unpleasant and painful sensations in most participants; as the temperature of the skin drops, nociceptors signal the painful stimulus, ramping temporal summation of nociceptive input signals the intensity of this sensation. After some time, pain intensity plateaus, likely due to the recruitment of descending antinociceptive systems (Tesarz et al., 2013). In experimental pain settings, the task outcome is usually how long the participant can endure the low temperature or the time at which the experience becomes painful, and is sometimes paired with ongoing pain intensity ratings. Pain intensity outcomes over time in these studies can separate high and low pain sensitivity individuals, and their outcomes are consistent over time (Koenig, Marc N. Jarczok, et al., 2014; Gram et al., 2015).

fMRI studies observing participants during CPT have highlighted SI, SII, prefrontal cortex, insula and cingulate cortices as brain areas that are active during experimentation, which is consistent with the network commonly associated with pain processing (La Cesa et al., 2014; Frankenstein et al., 2001; Lapotka et al., 2017). Other studies exploring the power spectra of EEG recordings during CPT data have identified consistent alpha desynchronisation in the earliest stages, followed by increased synchronisation of beta, delta, and theta oscillations (Chen et al., 1989; Backonja et al., 1991; Ferracuti et al., 1994; Chang, Arendt-Nielsen and

Chen, 2002; Dowman, Rissacher and Schuckers, 2008; Shao et al., 2012; Gram et al., 2015). Shao et al. (2012) and Hansen et al. (2017) used source localisation techniques and identified decreased alpha synchronisation in the central gyri, with increases in prefrontal cortices, insula, temporal, cingulate regions across beta and gamma bands.

An overview of CPT-induced pain data compared to resting-state brain recordings in EEG published by Wang et al. (2020) demonstrated significant enhancement of delta, theta, alpha, beta, and gamma frequency synchrony over central and occipital electrodes – with gamma showing enhanced synchrony across all electrodes during pain. Their study highlights the primary concern with CPT neuroimaging: participants with higher pain sensitivity will endure the pain for a shorter duration, therefore having fewer epochs to analyse and reducing the power of the statistical comparisons. In these scenarios, it is beneficial to have CPT temperatures that are less painful, but still able to discern differences between groups. Fortunately, alternatives to the traditional ice water bath that better suit neuroimaging exist – namely cooled gel wraps and contact thermodes – and have been validated as analogous to the traditional cold-water bath (Lapotka et al., 2017; Porcelli, 2014; Ruscheweyh et al., 2010). Though some research has shown that CPT-associated muscle activity can confound data analysis, these issues are successfully omitted in beamforming analysis.

No comparisons of the brain activity across pain sensitivity groups during CPT have been attempted, and despite demonstrating its ability to delineate the temporal characteristics of thermosensation (Fardo et al., 2017), studies using MEG and CPT analogues are lacking. The following experiment compares the MEG data of pain-sensitive and pain tolerant participants during tonic pain to elucidate any differences in alpha and gamma-band

oscillations, and the localisation of these differences in the brain. Regions of interest identified here will inform future studies, and enable powerful statistical analyses that could identify targets for therapies in conditions with increased pain sensitivity.

5.1.2 Aims and hypotheses:

This experiment aims to delineate the neural correlates of pain sensitivity during the cold pressor test, specifically within the alpha and gamma frequency bands, in MEG and healthy controls.

It is hypothesised that high pain sensitivity and low pain sensitivity participant groups will demonstrate significantly different synchrony in alpha and gamma frequency bands during the maximal and late CPT time windows: This will be tested with cluster-based permutation analysis of Dynamic Imaging of Coherent Sources beamforming. The null hypothesis of this experiment is that there is no significant difference in alpha or gamma synchrony during maximal or late CPT pain time windows.

5.2 Methodology

5.2.1 Objectives

This study will use MEG DICS whole-brain beamforming to localise frequency differences between pain-sensitive and pain-insensitive participants during the Cold Pressor Test; this will be achieved by comparing peak (15s) and late (200-300s) epochs to a control baseline window at both frequencies. Primary study outcomes compare the relative difference between the baseline and the epoch of interest, which is then contrasted between pain sensitivity groups for alpha and gamma bands separately.

5.2.2 Dataset

This dataset was acquired and analysed at the Institute of Health and Neurodevelopment for a separate project in 2008. The purpose of the study this data was collected for was to compare tonic pain to a resting control condition. No published studies exist using this dataset, and the following analysis has not been performed by any others.

5.2.3 Participants

Participants were recruited from the Aston University community. The inclusion and exclusion criteria were as follows:

Inclusion criteria

- Must be aged 18+

Exclusion criteria

- Neurological or pain disorders
- Taking medication at the time of study
- Implanted with any metal devices (E.g., pacemakers)

12 healthy participants (five male), with an age range of 24-42 years were recruited. Three of the participants were left-handed. Informed consent was obtained from all participants, and the study protocol was approved by local ethics committees at Institute of Health and Neurodevelopment. Participants were divided into low pain-sensitivity and high pain-sensitivity groups based on the peak of their numerical rating scores during CPT. Participants whose peak pain was above the average of the sample were classified as ‘high pain sensitivity;’ all others were ‘low pain sensitivity.’

5.2.4 Stimulus

An ice pack measuring 20cm x 20cm x 3cm was used as a MEG-appropriate alternative to the traditional cold water bath CPT method, similar in effect to the gel packs utilised by others (Ruscheweyh et al., 2010; Laptoka et al., 2016; Porcelli, 2014). The ice packs were cooled by being placed in a -20˚C freezer before use. In the control condition, a room-temperature ice pack was used (12cm x 12cm x 3cm). During data acquisition, participants rested their right hand on top of the freezer-cooled ice packs, and a room-temperature ice pack was placed on top to ensure contact with the stimulus. Participants were briefed, and instructed to remove the ice pack from their hand if the pain became unbearable.

5.2.5 MEG acquisition and MRI acquisition

MEG data were acquired using a 275-channel CTF whole-head MEG system (CTF Systems Inc.) within a magnetically shielded room at Institute of Health and Neurodevelopment, using a sampling rate of 600 Hz due to file storage limitations. A MEG-compatible trigger box (Lumina LP-300, Cambridge Research Systems) operated by an investigator inside the MSR marked the data with triggers reflecting participant self-reported pain states and phases of the acquisition protocol (e.g., 'Control', 'maximal', 'late'). Participants had Head Position Indicator coils attached to them at nasion and bilateral mastoids to record head movement during the acquisition. Their head shapes were digitized by a Polhemus Isotrak System (Kaiser Aerospace Inc.) for co-registration with MRIs.

Participants were sat upright in the MEG chair with the investigator in the room, a cold or room-temperature icepack placed underneath their right hand. In the baseline condition, participants were recorded for three minutes. In the experimental condition, participants were recorded for five minutes. During the experimental condition, participants were

instructed to verbally rate the pain they were experiencing on a scale of 0-10 (0 = no change, 1 = slightly cool, 2 = cool, 3 = cold, 4 = slight pain, 5 = mild pain, 6 = moderate pain, 7 = moderate-strong pain, 8 = strong pain, 9 = severe pain, 10 = unbearable pain; Chang et al., 2002). In the experimental condition, participants were informed that they could move their hand away from the ice pack if the pain became intolerable.

T1 MRIs were obtained for eight of the participants at the Institute of Health and Neurodevelopment, and later used for co-registration. Surrogate template brains from the FieldTrip toolbox (Holmes et al., 1998) were used for the other four participants.

5.2.6 MEG data processing

Data were denoised online by 3rd order synthetic gradiometry obtained during acquisition, to remove passive background magnetic fields and SQUID artefacts. Preprocessing was performed using the FieldTrip MATLAB toolbox (Oostenveld et al., 2011; build 20200513). A 4 Hz width discrete band-stop filter was performed at 48-52 Hz and 98-102 Hz to account for line noise that was resistant to standard discrete Fourier transforms; data were high-pass filtered at 1 Hz and low-pass filtered at 200 Hz to attenuate slow and very fast spectral components that are the result of environmental and physiological spectra outside of our frequencies of interest. Before the dataset was split into 5-minute continuous baseline and 5-minute CPT data, ICA was performed to remove eyeblinks and ECG components using the RUNICA method (Bell & Sejnowski, 1995). Head movement was checked by performing ft_qualitycheck in the FieldTrip MATLAB toolbox. Bad channels were removed from all participants' data for consistency, then fixed using 'ft_channelrepair' and 'cfg.method = 'weighted'.

Sensor and MRI data were co-registered to individual MRIs for eight of the participants; those that had incomplete MRI recordings were co-registered with a template MRI (Holmes et al., 1998). All participants had 5 mm resolution template source models warped to their segmented MRI and registered to a head model for lead field matrix construction.

Data were split into control, CPT-late and CPT-max time series. Control data was three minutes of resting-state data acquired with a room-temperature ice pack. CPT data was five minutes of experimental data. CPT-late was the last 100s of the 5-minute recording, where the pain intensity is plateaued for most participants. CPT-max was defined by the 15s time window trigger that marked the maximum verbal rating scale score the participant reported on the aforementioned scale of 0-10. These continuous data segments were split into trials of 2s with 50% overlap.

DICS beamformers were performed on alpha (7-14 Hz) and gamma-frequency (33-97 Hz) Fourier-transformed time series data with a smoothing of 4 Hz and 33 Hz respectively using discrete prolate spheroidal sequence tapers with zero-padding of the maximal trial length rounded up to the next power of two (cfg.pad = 'nextpow2'; 4s). Final beamformer source reconstructions were computed for CPT-late and CPT-max by determining the relative difference between the baseline and time window of interest, as is conventional to remove centre-of-head bias: source analysis was performed on the baseline, CPT-late and CPT-max windows, then the relative difference between the baseline and active time windows was then computed for CPT-late or CPT-max (as discussed in chapter 3; Fig 3.9). λ5% regularisation was used, and a κ value for component inclusion was calculated from the rank of the dataset (approximately 260).

5.2.7 Statistical analysis

Non-parametric cluster-based permutation analysis was performed on alpha (7-14 Hz) and gamma-band (33-97 Hz) source reconstructions of maximal pain (15s) and late (last 100s) pain CPT epochs, in which a two-tailed between-groups T-test (high pain sensitivity vs low pain sensitivity) was performed for each voxel with multiple comparison corrections made using the Monte Carlo method (See chapter 3). The data was permuted 2000 times with a $p \leq 0.025$ alpha threshold for significance.

5.3 Results

Pain scores for participants are displayed in Figure 5.2. All participants endured the full 300s of the CPT. Median pain scores over 300s were five on a scale of 0-10 (IQR = 3). Participants whose pain peaked over the median (>5 in the first 100s) were assigned to the high pain sensitivity group, all others were assigned to the low pain sensitivity group. One participant's pain score was identified as an outlier upon visual inspection (Pt2), as can be seen in Figure 5.2: low pain values that slowly increased over time, without the 'peak' that characterises all other participants' pain scores. Another participant's dataset (Pt4) was confounded with a steadily worsening head movement of over 5mm that could not be resolved with available offline techniques, hence their dataset was not included in further analyses; head movements over 5mm negatively impact the quality of the beamformer and statistical analyses (Messaritaki et al., 2017).

5.3.1 Analysis of maximal pain epoch (15s)

Visualisation of the relative difference of frequency by group in the maximal pain epoch in comparison to baseline activity is shown in Figure 5.3.

5.3.1.1 Alpha band

To show the contrast between groups, the actual differences between high and low pain sensitivity final source reconstructions are visualised in Figure 5.4: By subtracting the source reconstruction of the low pain sensitivity group from the high pain sensitivity group, we can observe the actual difference between their relative difference values in the maximal pain CPT epoch. The high pain sensitivity group has an observably greater alpha change in the ipsilateral temporal lobe and cerebellum (Values: 0.6 and 1.18 respectively). No statistically significant clusters were identified after multiple corrections when comparing high and low sensitivity groups in the alpha band in the maximal pain epoch (Largest positive cluster statistic, t = 167.429, p = 0.825; largest negative cluster statistic = -60.6893, p = 1).

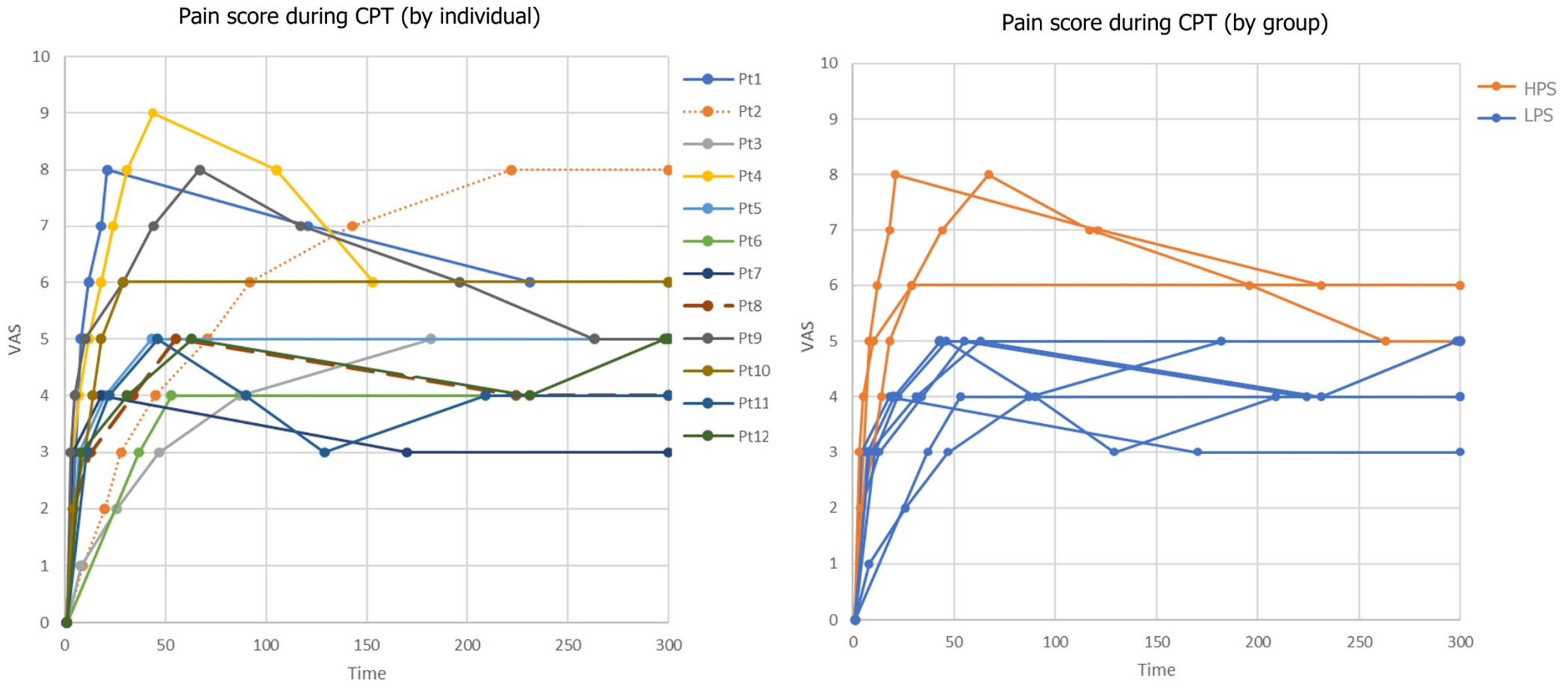

Figure 5.2: Subjective pain ratings as reported by participants during Cold Pressor Test MEG acquisition, as scored by a Verbal Rating Scale over time in seconds. Pain scores are displayed by the individual (left) and pain sensitivity groups minus removed participants (right). HPS = High Pain Sensitivity. LPS = Low Pain Sensitivity.

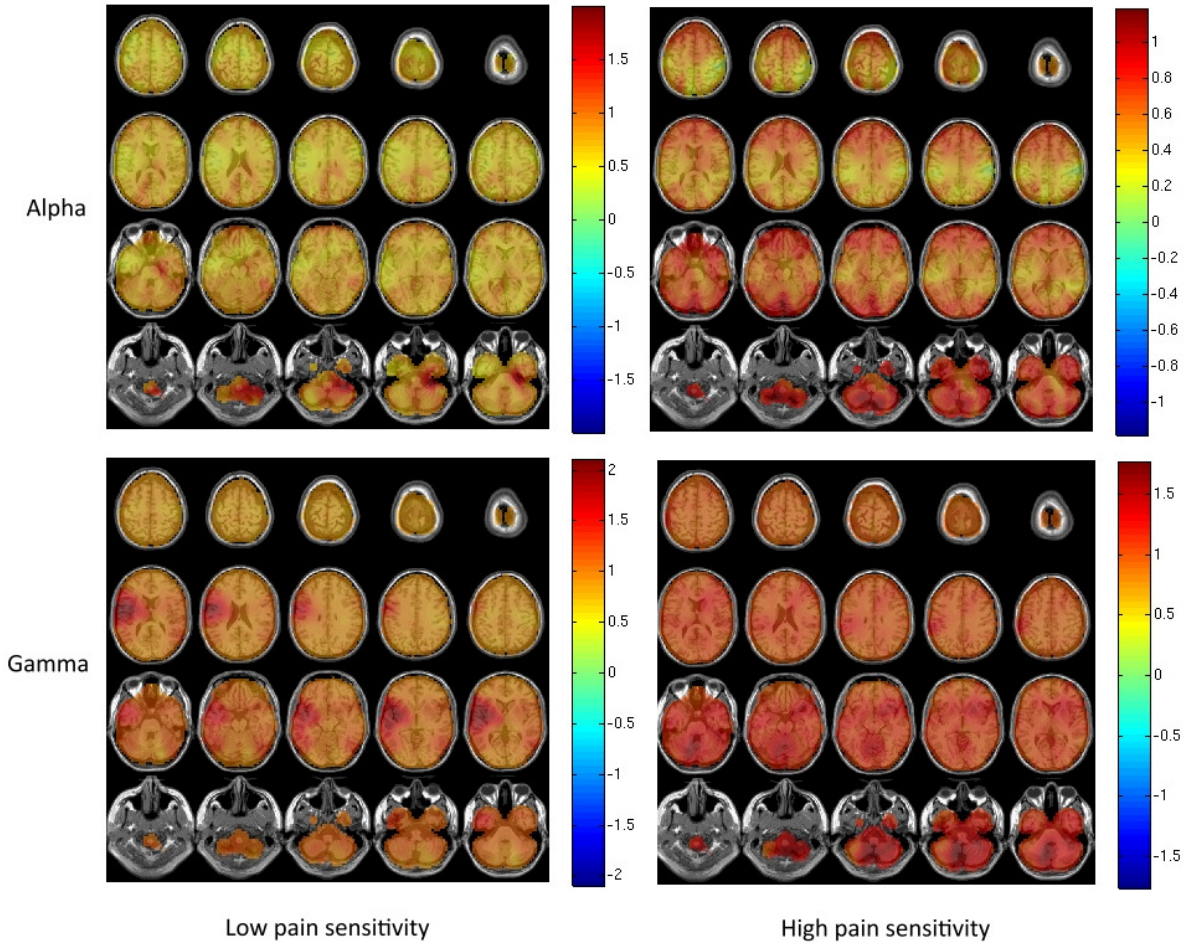

Figure 5.3: Ratio of change in frequency band synchronisation in the maximal pain epoch when compared to the control baseline. Displayed by frequency of interest (alpha, gamma) and pain sensitivity group averages. The colour bar indicates the ratio of change (%) relative to the baseline. These figures are for visualisation of the brain activity in the maximal window compared to baseline by group membership and frequency. Between-group comparison in figures 5.4 and 5.5.

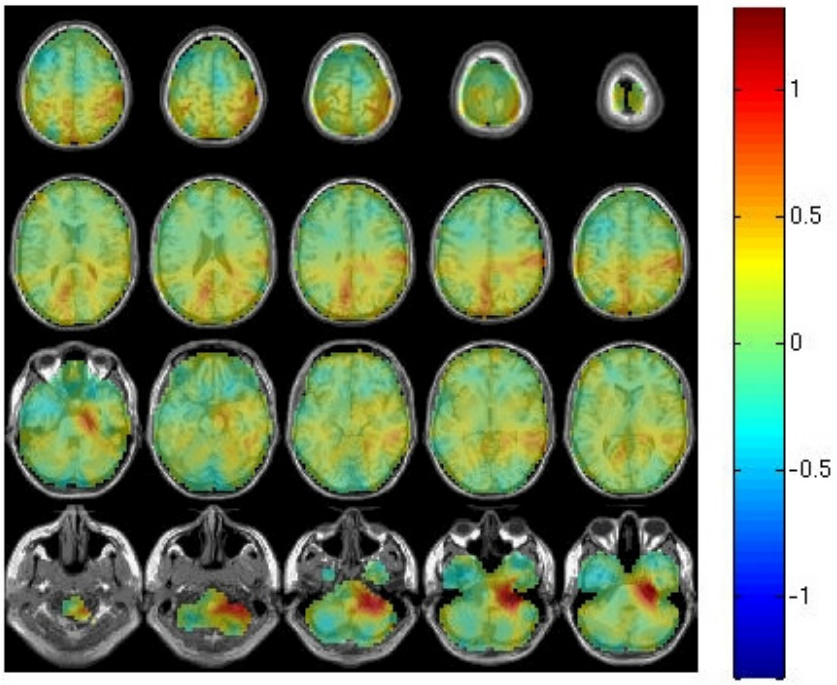

Figure 5.4: Source analysis of the relative difference between high and low pain sensitivity groups in alpha synchronisation in the maximal pain time window. The colour bar indicates the ratio of change (%) relative to the baseline.

5.3.1.2 Gamma band

Subtracting the source reconstruction of the low sensitivity group grand average from the high sensitivity grand average facilitated the visualisation of actual differences in relative synchrony change: lesser synchronisation can be observed in the contralateral temporal cortex (absolute difference value = -1.1) in the high pain sensitivity group, and a greater synchronisation is observable in the midline cerebellum (absolute difference value = 0.68; Fig 5.5). In the gamma band, no clusters were identified as statistically significant in the maximal pain epoch following cluster-based permutation analysis and corrections for multiple comparisons (Largest positive cluster statistic t = 524.2865, p = 0.2779; No negative clusters were identified).

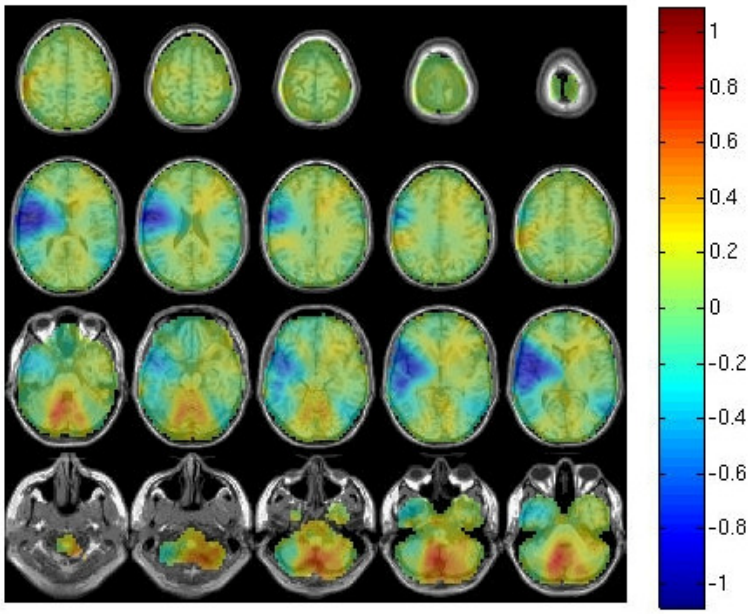

Figure 5.5: Source analysis of the relative difference between high and low pain sensitivity groups in gamma synchronisation in the maximal pain time window. The colour bar indicates the ratio of change (%) relative to the baseline.

5.3.2 Analysis of late CPT epoch

Figure 5.6 shows the source reconstructions for alpha and gamma by pain sensitivity group separately.

5.3.2.1 Alpha band

Figure 5.7 demonstrates the relative change in alpha frequency power when subtracting low sensitivity reconstructions from high sensitivity. Subtracting the source reconstruction of the low sensitivity group grand average from the high sensitivity grand average facilitated the visualisation of actual differences in relative synchrony change: the high pain sensitivity group displayed a greater enhancement of alpha (absolute difference value = 0.16) across temporal,

parietal, and occipital cortices. In the alpha band, no significant clusters were identified in the CPT-late epoch by statistical analysis after multiple comparisons (Largest positive cluster, t = 190.45, p = 0.82; no negative clusters were identified).

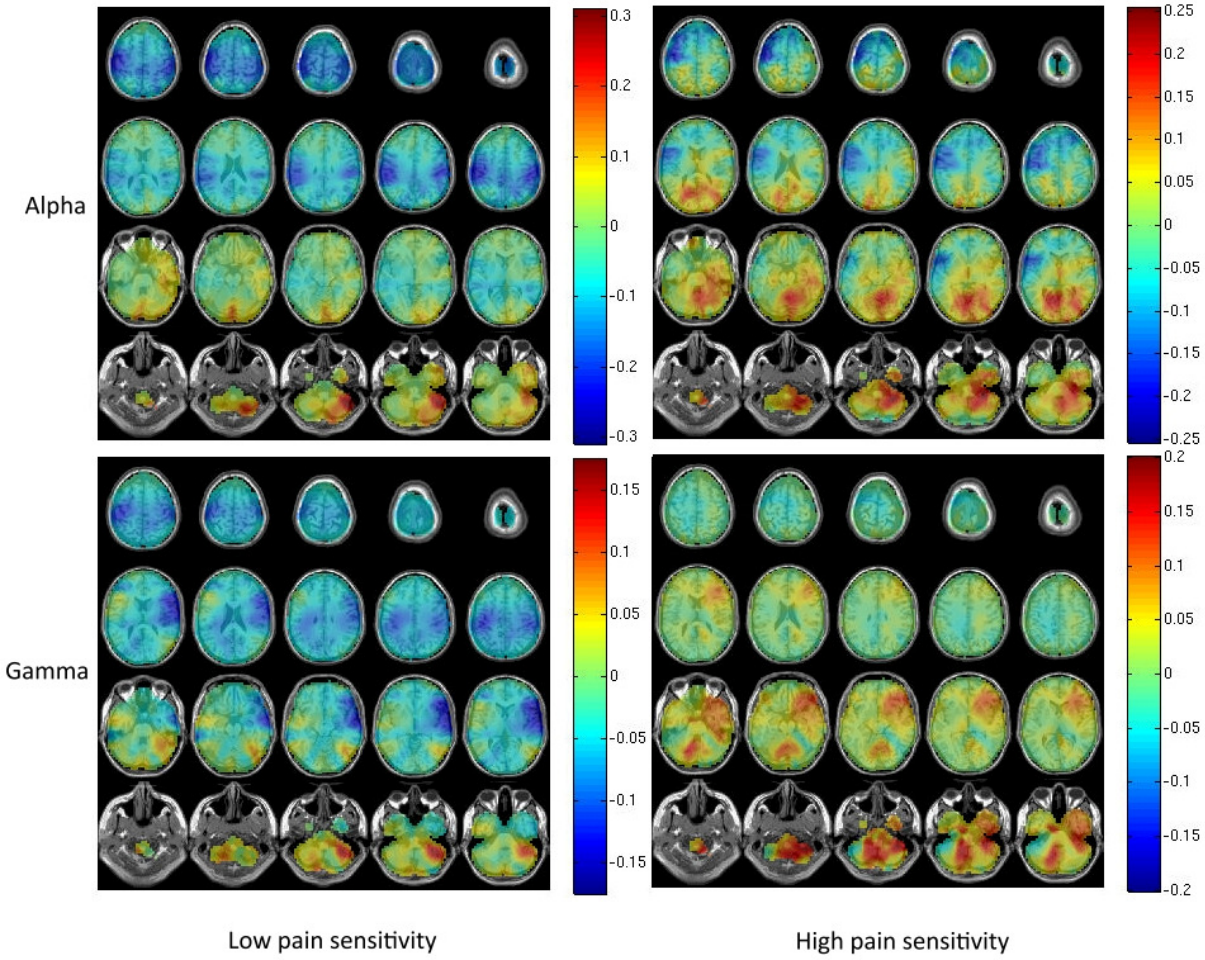

Figure 5.6: Ratio of change in frequency band synchronisation in the late (last 100s) CPT time window, calculated by comparison with the control baseline. Alpha and gamma synchrony are plotted in low pain sensitivity and high pain sensitivity groups. The colour bar indicates the ratio of change (%) relative to the baseline.

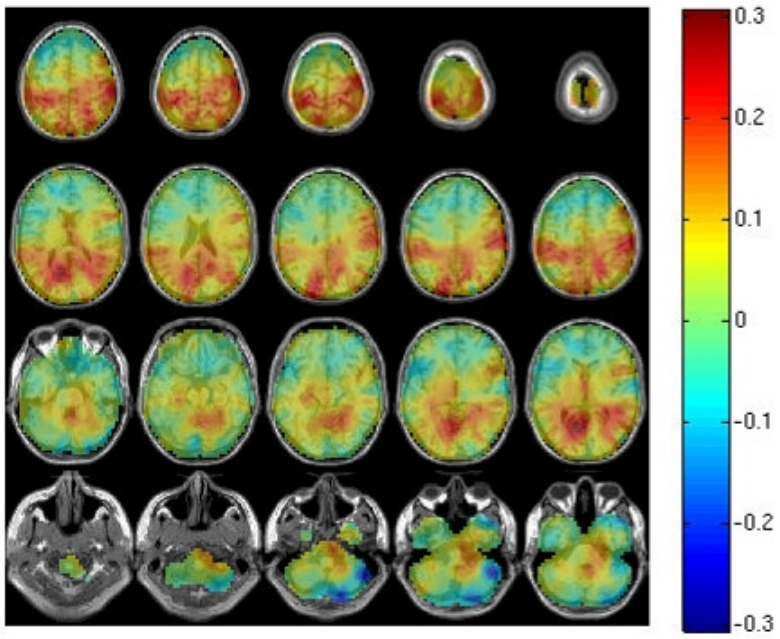

Figure 5.7: Source analysis of the relative difference in alpha power between high and low pain sensitivity groups during the late CPT epoch.

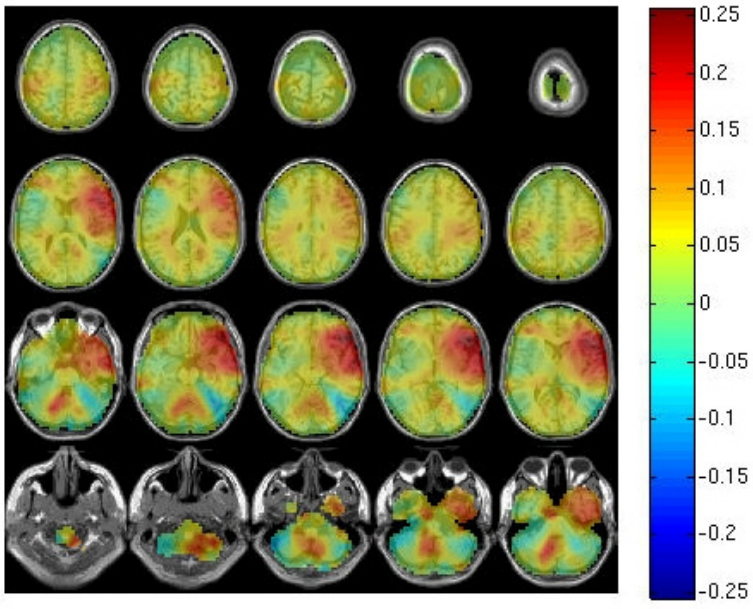

Figure 5.8: Source analysis of the difference in gamma synchrony between high and low pain sensitivity groups during the late CPT epoch.

5.3.2.2 Gamma band

Subtracting the source reconstruction of the low sensitivity group grand average from the high sensitivity grand average facilitated the visualisation of actual differences in relative synchrony change: in the high pain sensitivity group a relative increase is observable in the ipsilateral temporal lobe (absolute difference value = 0.21; Figure 5.8). In the gamma band, no clusters were identified as statistically significant in the maximal pain epoch following cluster-based permutation analysis and corrections for multiple comparisons (Largest positive cluster statistic, t = 2161.5, p = 0.29; No negative clusters were identified).

5.4 Discussion

Alpha and gamma oscillations are primary candidates for underlying biomarkers of pain sensitivity in EEG analysis, though changes within their frequency bands are most often observed in resting-state or evoked potentials (Furman et al., 2018; Hu and Iannetti, 2019; Mayhew et al., 2013; Nir et al., 2010, 2012; Schulz et al., 2012; Valentini et al., 2022). In chronic pain models, where many conditions are accompanied by increased pain sensitivity, slowing of peak EEG alpha oscillations has been identified in comparison to healthy groups (Lim et al., 2016; de Vries et al., 2013), alongside the regularly reported thalamocortical dysrhythmia noted in fibromyalgia (Schulman et al., 2005; Sufianov et al., 2014). In healthy controls, experimental observations of healthy controls in fMRI have identified the primary somatosensory, anterior cingulate, prefrontal, insula cortices and cerebellum as networks whose connectivity explains some variations in pain sensitivity between individuals (Coghill et al., 2003; Sevel et al., 2016; Spisak et al., 2020; Veréb et al., 2021).

As enhanced synchrony at alpha frequency has been linked with blood oxygenation level dependency levels (Jann et al., 2009), regions identified by fMRI research may have been expected to demonstrate some changes between pain sensitivity groups at the alpha band in MEG. Previous studies exploring the scalp topography of spectral power in the cold pressor test have localised suppression of alpha synchrony to the contralateral temporal, the fronto-central and central scalp (Chang et al., 2002; Dowman et al., 2008), with some cortical source localisation techniques showing decreased alpha synchrony in central gyri (Shao et al., 2012; Hansen et al., 2017), and tonic pain stimulus intensity has been negatively correlated with alpha synchrony in the contralateral cortex (Nickel et al., 2017). Though the literature exploring the localisation of alpha frequency synchronisation changes in tonic pain sensitivity specifically was too sparse and poorly localised to enable a one-tailed analysis or region of interest approach, it was hypothesised that there would be a significant difference in alpha or gamma frequency activity between high and low pain sensitivity participants during tonic pain either due to the difference in perceived pain intensity, or a biomarker for the difference in processing at the cortical level; and, were these differences present, they might be likely to be localised to one of the aforementioned brain areas.

Gamma band oscillations are recognised to reflect localised processing, and have been shown to reflect pain intensity specifically in experimental tonic pain (Nickel et al., 2017) and affective pain response in evoked pain EEG research (Lyu et al., 2022). Though some research suggests gamma band synchronisation can predict inter-individual pain sensitivity in humans and rodents in electrical and laser stimulation paradigms (Schulz et al., 2012; Hu and Iannetti, 2019), its role during tonic pain processing had not yet been evaluated as a marker for pain sensitivity.

The results in this analysis conclude that, at the source level, gamma oscillatory synchronisation does not significantly differ between pain sensitivity groups in a CPT paradigm; this suggests that gamma enhancement is a marker for pain sensitivity in evoked stimuli alone, which implies that gamma enhancement in pain sensitivity may reflect greater recruitment of attention, as opposed to altered processing of nociception.

In a between-groups analysis of high and low pain-sensitive participant groups, no significant source-level differences were identified in alpha or gamma frequency bands during maximal pain or plateau windows in any clusters. These findings indicate that the alpha and gamma frequencies do not significantly reflect changes associated with pain sensitivity group membership during tonic cold pressor pain at either epoch; though the low number of participants in the high pain sensitivity group is likely to mean that the statistical analyses presented here are under-powered. The results of this study result in the acceptance of the null hypothesis that there are no differences in alpha or gamma synchronisation during peak or late CPT that are identifiable using MEG beamforming. The findings here imply that alpha and gamma oscillations' ability to predict pain sensitivity biomarkers may be limited to evoked pain and connectivity paradigms, when contrasted to gamma synchronisation found in evoked laser and electrical stimulation studies (Schulz et al., 2012; Hu and Iannetti, 2019): this may suggest that the gamma synchronisation identified in evoked paradigms are associated with stimulus salience and presentation, as opposed to pain or nociception. This highlights the importance of elucidating neural biomarkers for pain sensitivity in tonic and evoked models, and an increased focus on tonic pain stimuli when aiming to generalise to clinical populations. Grand average visualisations highlighted an enhancement of alpha in bilateral temporal and somatosensory

cortices, and gamma suppression in the right temporal cortex in pain-sensitive participants that future studies with more statistical power may find to be significant.

5.4.1 Limitations

This dataset contained two participants that necessitated omission from the analysis: one due to head movements, and another due to an abnormal CPT pain response curve. These omissions reduced the number of pain-sensitive participants to three, contrasted to a group of seven pain-tolerant participants. This disparity likely negatively impacted the power of the statistical testing (Groppe et al., 2011). The likelihood of type-II errors is exaggerated by the necessity of correction for multiple comparisons when performing statistical analysis across every voxel of the brain, and the limited number of participants recruited by this study. Future studies should use this study to inform their design and select regions of interest identified by the grand average visualisations within, in addition to recruiting larger participant groups to avoid these limitations.

In addition to the above, this study utilised a cold ice pack to emulate the experience of a cold pressor test, as the traditional ice water bath or circulated water cooler methods were not practical for MEG recording. Whilst this method has been validated in comparison to the traditional methods (Hunt, 2008), it would be inaccurate to claim that these results are entirely comparable with all other CPT studies. This remains a problem with all CPT studies, as discussed by Mitchell, MacDonald & Brodie (2004): many centres investigating CPT use different temperatures and methods, which can result in significantly varying participant outcomes. For this study it is accurate to report that the participants were subjected to the same tonic cold

stimulus for the same duration; but, as with all CPT studies that do not use precisely controlled water circulators, it is not possible to determine the precise temperature of the ice packs during the recording.

This analysis focused on the 15s epoch at the maximal pain peak reported by the participants and the final 100s of the 300s dataset; the first epoch was chosen to selectively observe oscillations during the time window where the most pain was experienced, where classically there is a transient peak followed by a reduction in subjective pain, as such, this time window is short. The final 100s were selected for their plateau in pain scores (as demonstrated in Figure 5.2), to ensure a long time window of data with low pain variation. These choices were made to ensure the analysis reflected data that had as little between-participant variation as possible, avoiding different peak and trough latencies where possible; useful data may lie during these larger windows with greater variance.

A future study might also benefit from a control task that includes active control conditions as opposed to a passive resting-state: Dowman, Rissacher & Schuckers (2008) suggest that resting-state control comparisons fail to control for the additional attentional load that is innate in a pain task.

5.4.2 Conclusion

This was the first analysis to use MEG to explore alpha and gamma oscillations at the source level as a method to highlight oscillatory synchronisation differences between pain sensitivity groups during the Cold Pressor Test. This study did not find any significant differences in high and low pain-sensitive groups' oscillatory synchronisation at either the maximal peak or the late

plateau epoch; this suggests that previous literature that has identified these differences in evoked paradigms may in fact be observing attentional processing of salient stimuli. Future research should analyse virtual sensors in the contralateral and ipsilateral temporal lobes during the maximal pain window and plateau respectively to better evaluate if any differences exist there in alpha and gamma frequency bands.

6. Study 3: Removal of Non-fMRI Compatible Contact Heat Evoked Potential Stimulator Artefact in Magnetoencephalography

6.1 Introduction:

The PATHWAY Contact Heat Evoked Potential Stimulator (referred to here simply as CHEPS to avoid confusion with the evoked potential sharing the same acronym; Medoc Ltd., Ramat-Yoshai, Israel) is a computer-controlled Peltier thermode that is most often used in quantitative sensory testing for neuropathic pain conditions. In that setting, contact heat is a technique to assess thermal sensory functioning: Warmth detection thresholds, heat detection thresholds and pain detection thresholds are determined by ramping temperature and self-report; cooling and cold configurations are available also, though the latter requires a license. The CHEPS in heating configuration is capable of reaching destination temperatures at the speed of 70˚C/s; as the name suggests, this speed facilitates the generation of evoked potential waveforms to assess amplitude and latency in-clinic as well as in research, potentially identifying exaggerated or diminished nerve responses in experimental conditions or patient populations.

Contact heat is often compared to lasers, as they are both noxious thermal stimuli that have been used to evaluate evoked nervous system activity in experimental neuroscience. In one study that compared CHEPS and LEP waveforms, significant differences were identified in N1, N2 and P2 amplitude and latencies, with mean N2 latencies being almost 200ms later (392±37ms and 221±19ms respectively; De Schoenmacker et al., 2021). This is most likely because of earlier, more simultaneous recruitment of nociceptors by radiation as opposed to contact heat permeation (Iannetti et al., 2006), but this rapid onset comes at a cost. LEP equipment is costly and cumbersome, requires regular movement of the stimulus by the

investigator to avoid damage to the skin, necessitates greater safety precautions for experimenter and participant, and the most common technique stimulates an area as small as 4mm in diameter (Schoenmacker et al., 2021). In comparison, the CHEPS thermode covers an area of skin that is more representative of pain one might experience outside of a laboratory (with a diameter of 27mm), poses a significantly lessened risk to skin health and is not influenced by skin reflectance (Frahm et al., 2020).

The CHEPS has great potential as a stimulus in pain research, as it can be used as a tonic or phasic stimulus, and has proven its utility in EEG and fMRI research in experimental and clinical settings (Lugo et al., 2018; Opsommer et al., 2021; Sun et al., 2022). As demonstrated in the systematic review above (see chapter 2), there is a dearth of literature utilising the CHEPS in a MEG environment; this is despite evidence demonstrating its utility in identifying cooling CHEPS-related activity that was absent in simultaneous EEG analysis (Fardo, 2017). One explanation for this is that the CHEPS thermode generates a significant electromagnetic field when active, though others have demonstrated the effective removal of this artefact using tSSS and Damped Sinusoid Modelling preprocessing techniques (Gopalakrishnan et al., 2013) and unregularized beamforming (Adjamian et al., 2009). For combined use in magneto-sensitive environments such as fMRI and MEG, it is recommended to use an fMRI-compatible thermode to mitigate signal artefacts, and it is assumed that all studies to date have used these thermodes, though few have reported such. However, the fMRI-compatible thermode has a greater cost, and signal artefacts remain in the raw data (Gopalakrishnan et al., 2013). Exploring the utility of standard CHEPS thermodes in MEG analysis could facilitate the expansion of

research into this combination of methods, and test the limits of current signal cleaning and spatial filter source reconstruction techniques.

Gopalakrishnan et al. (2013) have demonstrated that removing signal artefacts associated with the fMRI-compatible CHEPS thermode is possible by using bespoke, in-house Damped Sinusoid Modelling methods, or the more commonly available temporal Signal Space Separation (tSSS) for Elekta™ MEG systems (Taulu & Hari, 2009) (MEGIN UK Ltd, Surrey). Prior to this, Adjamian et al. (2009) had found that Synthetic Aperture Magnetometry (SAM) beamforming performed on fMRI-compatible CHEPS data balanced with 3rd order synthetic gradiometry sufficiently suppressed the CHEPS noise with spatial filtering, and highlighted that omitting regularisation provided better spatial accuracy. Beamforming and tSSS techniques separately have shown their effectiveness at attenuating the signal artefact. Both methods aim to filter out noise that is generated outside of the head (See chapter 3), but it is unclear if their combined or separate effects are sufficient to enable the use of the standard, fMRI-incompatible thermodes.

This chapter will outline attempts at attenuating the artefact generated by the standard fMRI-incompatible CHEPS thermode in a recording of one healthy control participant. The goal is to determine whether any combination of ICA, beamforming and tSSS of varying parameters are capable of facilitating the analysis of CHEPS artefact-contaminated MEG data acquired using this equipment. It is hoped that the MEG research community may benefit from more accessible research equipment, and centres and clinics that have standard CHEPS systems may contribute to the collection of, or salvage previously acquired, MEG datasets.

6.2 Method

6.2.1 Datasets

These datasets were acquired at Institute of Health and Neurodevelopment, using an Elekta ™ Neuromag TRIUX 306 (MEGIN UK Ltd, Surrey), sampled at 2000 Hz. Three datasets were acquired: one using a participant (F, 22, left-handed) stimulated by the CHEPS thermode; one of an empty room, with the thermode resting on a cushion to mimic the placement of a participant's arm, recorded whilst the CHEPS was heating and cooling in the identical protocol of the participant dataset (Figure 6.1, henceforth the 'active' dataset); one recording of the thermode powered and in the same position, but not heating and cooling (henceforth the 'passive' dataset).

Figure 6.1: The MEG system with PATHWAY CHEPS thermode positioned to mimic the pilot participant's resting arm

6.2.2 Stimulation and acquisition

The stimulator for this was the PATHWAY CHEPS ™ (Medoc Ltd, Ramat-Yoshai, Israel), stimulating at an inter-stimulus-interval (ISI) of 8-12s, a peak temperature of 50˚C at 70˚C/s. Overshoot attenuation, a feature that can stop the thermode from exceeding the target temperature by cooling the thermode by a set variable, was disabled. No holding duration was set, with a peak temperature being met at roughly 250ms. No active shielding of the magnetically shielded room was applied. For participant data, the head shape was digitised using a Polhemus Isotrak System™ (Kaiser Aerospace Inc.) and head position was recorded by five Head Position Index (HPI) coils attached across the forehead and bilateral mastoids. Participant data was recorded from a seated position inside the Magnetically Shielded Room (MSR). CHEPS stimulation was applied to the dorsal surface of the left hand. In empty room recordings, the CHEPS thermode was attached to an MSR-suitable cushion in a position and orientation that matched the participant recording.

6.2.3 Data cleaning methods

Attempts to attenuate the electromagnetic artefact were made using Signal Space Separation (SSS), temporal SSS, Independent Component Analysis (ICA), and beamforming of the post-stimulus time window. All processing and analyses were performed using gradiometers only.

SSS and tSSS (See chapter 2) were applied using MaxFilter (MEGIN UK, version 2.2.10). tSSS parameters include correlation limit and buffer size, where 0.98 is the default correlation setting and 0.6 is the lowest recommended value (Medvedovsky et al., 2009); correlation limit

is the parameter by which signals external to the MEG dewar helmet must correlate with those inside the dewar helmet before being projected out of the dataset, and buffer window describes the duration of segments that are analysed at a time, controlling for slow drifts. The buffer window was set at 30 seconds to ensure that the window contained multiple stimulations (as demonstrated by Fardo et al., 2017). Throughout this chapter, 'raw' data will refer to data that is not cleaned by SSS or tSSS, though in other contexts this might be considered data that has not yet been filtered or processed at all. The goal of SSS is to project out signals which have an origin outside of the dewar helmet signal space; in tSSS, this process is extended to the time domain.

RUNICA (Bell & Sejnowski, 1995) was the chosen method for ICA (See chapter 3), with a component limit set at the rank of the dataset after tSSS to account for its effect on dimensionality. The goal of ICA was to decompose the MEG data into unique components; in average datasets, this is often reserved for the rejection of ocular movements and heartbeat artefacts, but in this dataset the ICA algorithm was used to identify components unique to the CHEPS in empty room and pilot datasets.

The goal of minimum variance beamforming is the reconstruction of activity within source space using spatial filtering and unit-gain constraint to suppress activity arising from adjacent and distant voxels. Due to the way the spatial weights are computed, voxels near the centre of the head are over-represented and present their own artefacts. This is circumvented by calculating the ratio of change between a time series of interest and baseline data, at each given voxel (Quraan, 2011). This would also minimise any baseline 'passive' artefact the CHEPS introduces. Regularisation is commonly used in source reconstruction, and involves introducing

noise to a dataset by a specified percentage to minimise the effect of rank deficiency, smooth source estimates and improve signal-to-noise ratio in cases of poor sensor covariance estimates. Beamforming outcomes after tSSS are sensitive to regularisation in CHEPS datasets (Adjamian et al., 2009), which reduces spatial resolution as part of its functionality. Without prior rationale for a specific regularisation parameter, this study explored beamformer outcomes with a broad spectrum of values. Beamformers with regularisation parameters of 0%, 5%, 10%, 25%, 50%, 75% and 100% values were performed (signified by λ). Rank deficiency can also be managed by truncating the covariance matrix at the rank of the data (see chapter 3). In this analysis, the truncation value (κ) was set at the rank of the data (60 or 200, depending on the preprocessing performed) or at a more conservative value (50). A distant baseline epoch (-5 -4s) was chosen for comparison against the post-stimulus window (0s 1s) to avoid any immediate effects of the CHEPS stimulator ramping in temperature before 0s.

6.2.4 Pre-processing of data

All data were pre-processed using the FieldTrip MATLAB toolbox (Oostenveld et al., 2011; build 20200513). Data were low-pass filtered at 200 Hz and high-pass filtered at 1 Hz. A discrete Fourier transform at 50 Hz and 100 Hz at a width of 1 Hz was applied to attenuate line noise. Epochs were created around CHEPS triggers with a baseline of 6s and a post-stimulus window of 6s. Detrending and demeaning were performed on all epochs.

6.3 What does the artefact look like?

In this section, the electromagnetic signal artefact generated by the CHEPS and recorded by the MEG in a passively shielded room is outlined. To properly describe the artefact, the two empty-room recordings were first analysed. The magnetic field strength (fT/cm) of the passive and active datasets were compared. A t-test was performed using the mean field strength values of one second of the passive dataset, with one second of the active dataset's baseline (-5 to -4s); a significant difference in mean values over all channels at each time point was found ($t(1999)=2.5722$, $p=0.01$), demonstrating a greater level of baseline noise in the active dataset, even 5s before the stimulation. From this we can deduce that even a distant baseline time window has an increased noise field strength when the CHEPS is in an active configuration, meaning that comparison of the post-stimulus time window with the passive configuration baseline would not adequately reflect the stimulus activity, and that the ongoing mechanisms of the CHEPS can contribute to electromagnetic field recordings even when not stimulating: This shows that a passive dataset control would not effectively work as an alternative baseline if the active dataset includes stimulus artefacts in the pre-stimulus window.

In sensor space, a timelock analysis was performed to observe the evoked waveform: in a perfectly empty room, the evoked waveform should be averaged to 0. To evaluate the frequency components over time, time-frequency analysis was performed using the multi-taper convolution method implemented in the FieldTrip MATLAB Toolbox (Oostenveld et al., 2011; build 20200513). Hanning tapers from -6-6s in steps of 0.01s were applied using a sliding window 0.5s long, with a frequency resolution of 2 Hz in the range of 2-100 Hz.

6.3.1 Timelocked waveform

Fig 6.2 shows an average of all sensors over the entire epoch, and fig 6.3 shows a butterfly plot of all sensors. As is evident in these images, the time-locked evoked waveform is not limited spatially and appears in all sensors. Some sensors demonstrate time-locked components as early as -1.2 seconds before the trigger and 2.40s after it. When averaged over all channels, the Event-Related field (ERF) is clearly of great magnitude relative to the expected zero average.

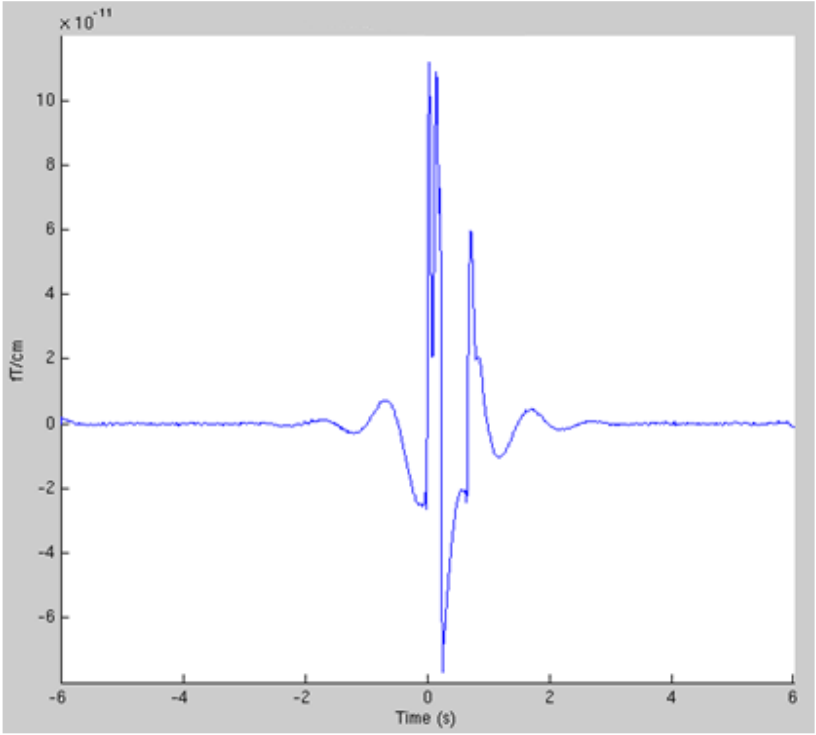

Figure 6.2: Evoked waveform of the active empty room recording, averaged over all channels and trials

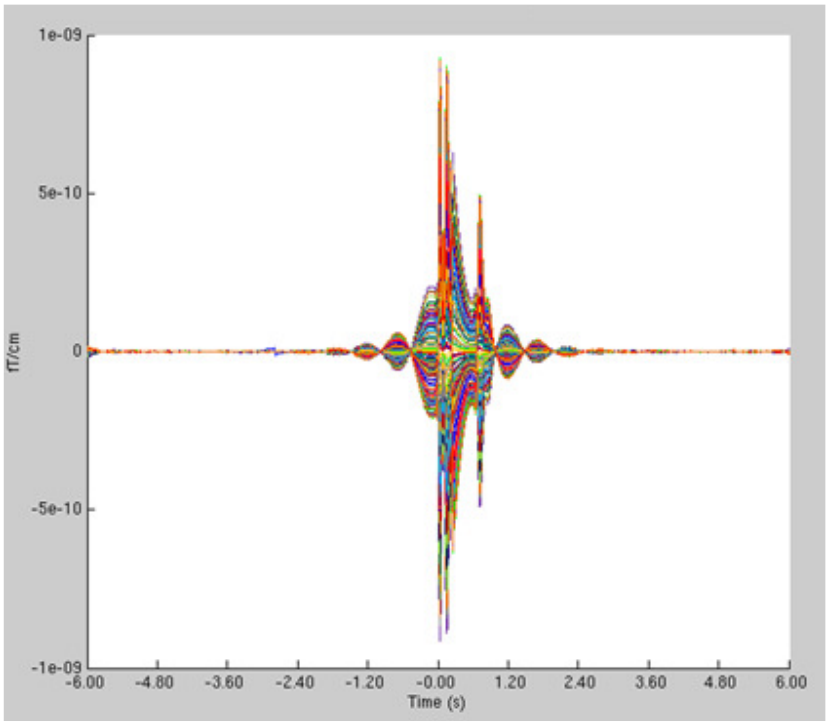

Figure 6.3: A butterfly plot of all sensors, averaged over trials

6.3.2 Time-frequency representation

Figure 6.4 shows the average time-frequency representation for all sensors in decibels (dB), baseline-corrected against the -5s to -4s time window. It is clear from these Figures that the raw artefact is pervasive in time, space and across a broad range of frequencies. When averaged, all channels have some form of evoked activity or time-frequency component. Similar to Gopalakrishnan et al.'s (2013) work with an fMRI-compatible thermode, it is demonstrated that the heating of the standard CHEPS thermode generates an electromagnetic field that has can be seen up to 2s before a stimulus trigger. This is possibly due to applied filters, but likely represents the ramping of the stimulus temperature. Time-frequency representations demonstrate an immediate evoked enhancement across 1-60 Hz that lasts for 200ms, with suppression from 5-100 Hz at around 250ms post-stimulation. Low-frequency activity in the raw

data appears to precede the stimulus trigger by 1s and continue for 2s after, with a post-suppression rebound up to 15 Hz. This timeframe is consistent with the activity seen in a butterfly plot of all sensors.

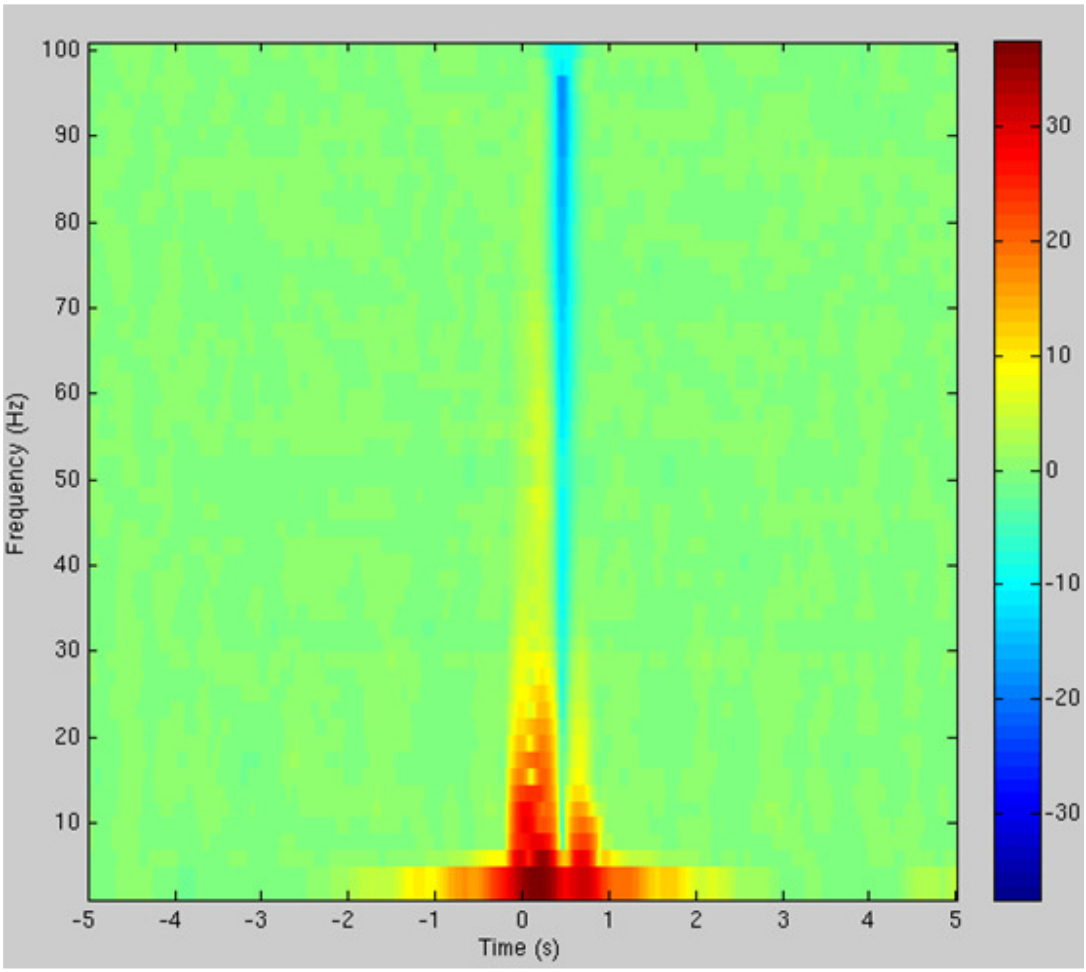

Figure 6.4: Averaged time-frequency plot for all sensors over all trials, normalised using a baseline of -5 to -4s. Colour bar represents frequency power in dB.

Stimulus-related activity that is not time-locked is often referred to as 'induced,' and is occasionally accessed by removing an averaged waveform from a time series trial individually, before analysing the time-frequency characteristics. If the empty-room ERF was constant across

trials, removing the evoked waveform from each trial should completely remove its presence in time-frequency representation. Removing the averaged waveform significantly changed the time-frequency characteristics of the empty-room recording (Fig 6.5), but did not entirely attenuate it. This is to be expected, as the averaged waveform will reflect components from imperfectly opposing dipolar sources. By defining the artefact in an empty room, the efficacy of attenuation attempts can be evaluated; and evoked and time-frequency data can be evaluated further.

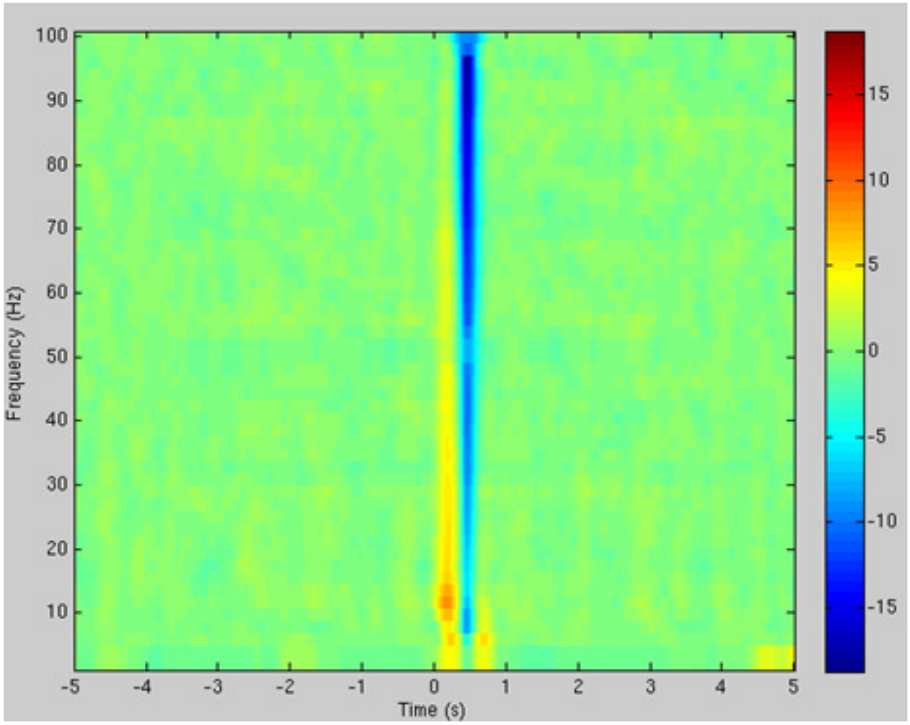

Figure 6.5: Averaged time-frequency plot for all sensors over all trials after removing averaged waveform, normalised using a baseline of -5 to -4s. Colour bar represents frequency power in dB.

6.4 Attenuating the artefact

In this section, commonly utilised MEG data cleaning methods are used to suppress the artefact described above. As outlined in chapter three, there are several techniques available to remove

artefacts in M/EEG data. Primarily afforded to Neuromag Elekta™ (MEGIN) MEG acquisition hardware, signal space separation and temporal signal space separation (SSS; tSSS; Taulu, Kajola & Simola, 2004; Taulu & Hari, 2009) are part of the MaxFilter (Elekta Neuromag Oy) software package and attenuate noise by projecting out components that originate from outside of the dewar helmet's immediate signal space; in theory, this should separate signals generated by the CHEPS, as the CHEPS thermode was positioned outside of the dewar helmet. Independent Component Analysis (ICA) breaks raw data down into separate time series that compromise the dataset; it is ideally suited for removing heartbeats and eye blinks. If the CHEPS artefact could be isolated as components in an empty-room recording and effectively removed from the dataset, it might be possible to achieve that same resolution in a participant recording. Beamformer techniques rely on inverse models of source spaces that have weighted spatial filters for positions throughout the brain; they reconstruct time series for each voxel in a given lead-field using a unit-gain constraint (See chapter 3), minimising the effect of adjacent voxels. Beamformers are, by nature, effective at mitigating the effect of outside sources on brain activity, and may prove to be capable of suppressing the CHEPS artefact.

6.4.1 SSS and tSSS

SSS and tSSS were applied before pre-processing using MaxFilter (Elekta Neuromag Oy, version 2.2.10), with default expansion order parameters. For tSSS, the buffer limit was set to 30s. This is long enough to contain at least two stimulations (as performed in Fardo et al., 2017), and the correlation limits were manipulated to observe which was most effective. A lower correlation limit of 0.6 has been validated in experimental studies, so was set as the most rigorous limit

(Medvedovsky et al., 2009); the higher, default correlation limit of 0.98 was used as an alternative control for its effectiveness.

All forms of signal space separation reduced the raw signal field strength. SSS attenuated it to the smallest extent, followed by tSSS with a 0.98 correlation limit. A correlation limit of 0.6 suppressed the artefact to the greatest extent. Figure 6.6 shows the averaged waveforms for raw, SSS, tSSS 0.98 and tSSS 0.6. Figure 6.7 displays the averaged waveforms for tSSS 0.6 and 0.98, for better visualisation. It is clear that the overall field strength of the evoked waveform is attenuated by signal space separation, but as demonstrated in the induced waveform above, the induced components are resistant.

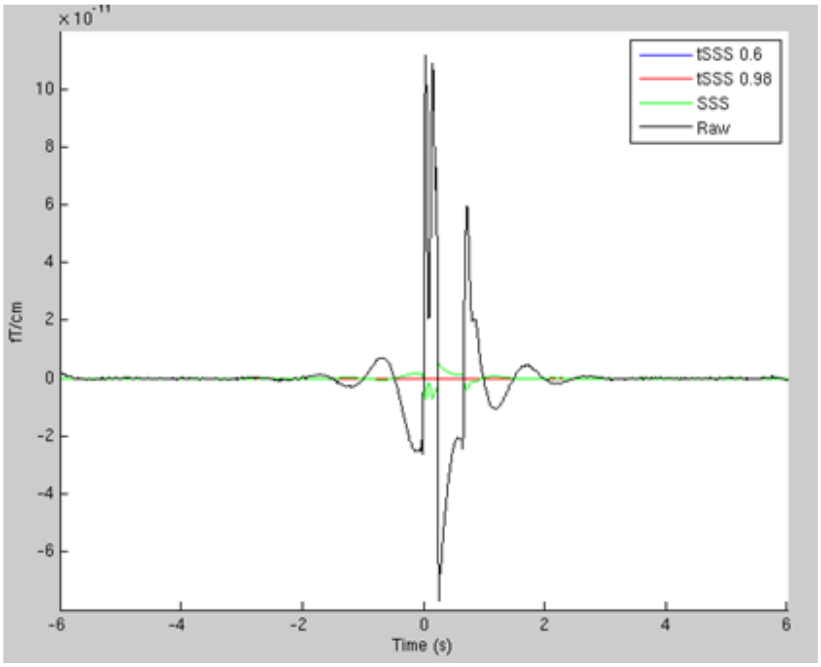

Fig 6.6: Event-Related fields averaged over all trials and gradiometers for all three data cleaning methods, compared to the raw dataset

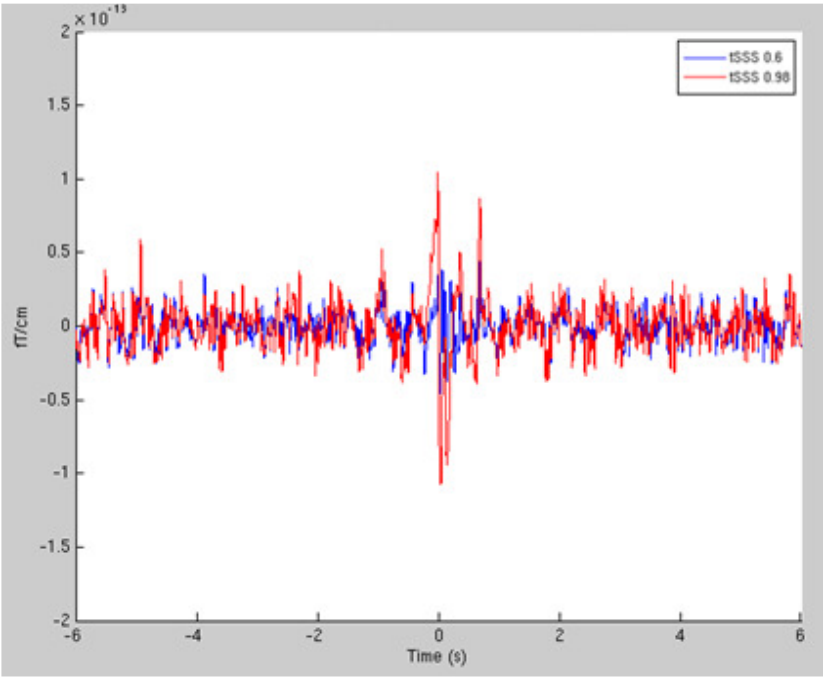

Fig 6.7: Event-Related fields averaged over all trials and gradiometers for all tSSS at 0.6 and 0.98 correlation limit

Figure 6.8 is a time-frequency plot of the cleaned data. In this figure, frequency power is plotted for each frequency from 1 to 100 Hz, -5s to 5s, with colours representing power in decibels relative to the baseline of -5s to -4s. TFR of cleaned data (Figure 6.8) demonstrates that the artefact is pervasive through the time-frequency domain even after cleaning. SSS also appears to introduce new characteristics to the data that were not in the raw recordings. SSS data cleaning lowers the signal field strength by 5 dB, but also generates a broad-band peak from -2.5s to -3s that does not appear in the raw dataset. tSSS with a 0.98 correlation limit significantly reduces the magnitude of the artefact to a peak of 7 dB, whilst retaining the evoked component of 0-25 Hz at 0-1s, with a broadband suppression at 500ms. A correlation limit of 0.6 reduces the field strength one further decibel and removes the pre-trigger delta-

band enhancement. However, tSSS of any type also appears to suppress the line-noise frequency of 50 Hz; something that is not a reported side-effect of tSSS in the literature. It is clear that less conservative tSSS can attenuate the CHEPS artefact significantly, demonstrating an overall reduction of 30 dB. Caution is necessary when interpreting results around the 50 Hz frequency band. No data cleaning methods alone were sufficient to suppress the artefact fully. Even the least stringent correlation limit observed time-frequency components across all sensors.

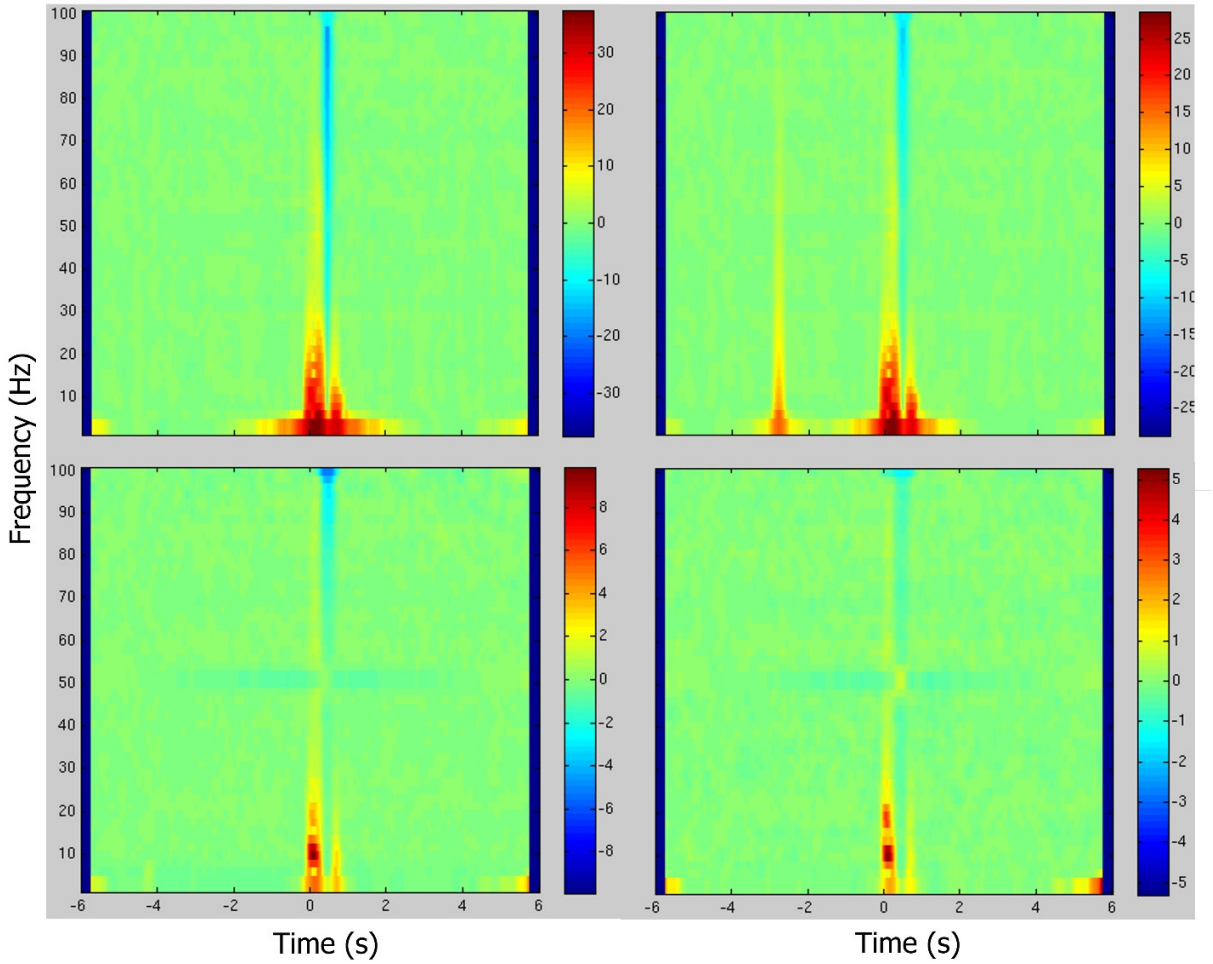

Figure 6.8: Time-frequency plots calculated by averaging all trials over all sensors, baseline-corrected with -5s to -4s. Synchrony is plotted in decibels (dB), as demonstrated by the colour bar. Top left: 'Raw' empty room data. Top right: Data cleaned using SSS. Bottom left: Data cleaned using tSSS with a correlation limit of 0.98. Bottom right: Data cleaned using tSSS with a more aggressive correlation limit of 0.6.

6.4.2 Independent component analysis

Usually performed to isolate and reject eye movements and heart-beat components, ICA was performed on raw, SSS and both tSSS datasets to identify and remove components that corresponded to the CHEPS. Components of interest were defined as being time-locked (i.e., time series that had apparent peaks centred at 0s), or demonstrating regular deflections above noise level (examples in appendix C.1). In the raw dataset, only two components were identified that could be attributed to the CHEPS; ICA of SSS data had at least 13 components with CHEPS characteristics, and ICA of tSSS had 10 and five components in 0.98 and 0.6 correlation limit data, respectively. Components in the tSSS datasets were less easily identifiable than in SSS and raw datasets, as their magnitude was much closer to that of signal noise. Figure 6.9 demonstrates the resulting change in averaged waveform after the removal of components identified in ICA. ICA greatly reduced the magnitude of the evoked waveforms in raw and SSS-cleaned data: a difference of 1.075E-10 fT/cm is observable between raw and ICA-raw, and 3.9E-12 fT/cm is observable in between SSS and ICA-SSS. The additional attenuation of field strength in both forms of tSSS is less obvious, but still notable.

In Figures 6.10 and 6.11, time-frequency representations are shown for each stage of data cleaning, with the ICA-cleaned form for comparison. In all cases, the maximum field strength of the evoked components is reduced. The greatest change is in the raw dataset. Removing components with visually apparent time-locked features demonstrated a similar line-noise suppression of 50 Hz in the raw and SSS data, suggesting a temporal 50 Hz component in the artefact that is being attenuated. Even removing 10 components with time-locked phenomena

did not significantly reduce the evoked theta-beta enhancement; in the SSS data, the pre-stimulus artefact that was generated was comparatively enhanced.

ICA, much like (t)SSS, demonstrated some attenuation of frequency power, most notably in the raw dataset. In raw data, a substantial decrease in field strength is observable, emulating much of the effectiveness of tSSS and including the 50 Hz suppression. In SSS, the pre-stimulation enhancement at -3s across all frequencies is made more apparent by the relative decrease in the power of the evoked components. The effectiveness of ICA in the raw dataset is note-worthy because it attains a similar level of attenuation as tSSS with a 0.98 correlation limit, but the data is not excessively de-ranked, and the components are much easier to identify. However, the artefact is evidently not fully removed even by the combination of these methods.

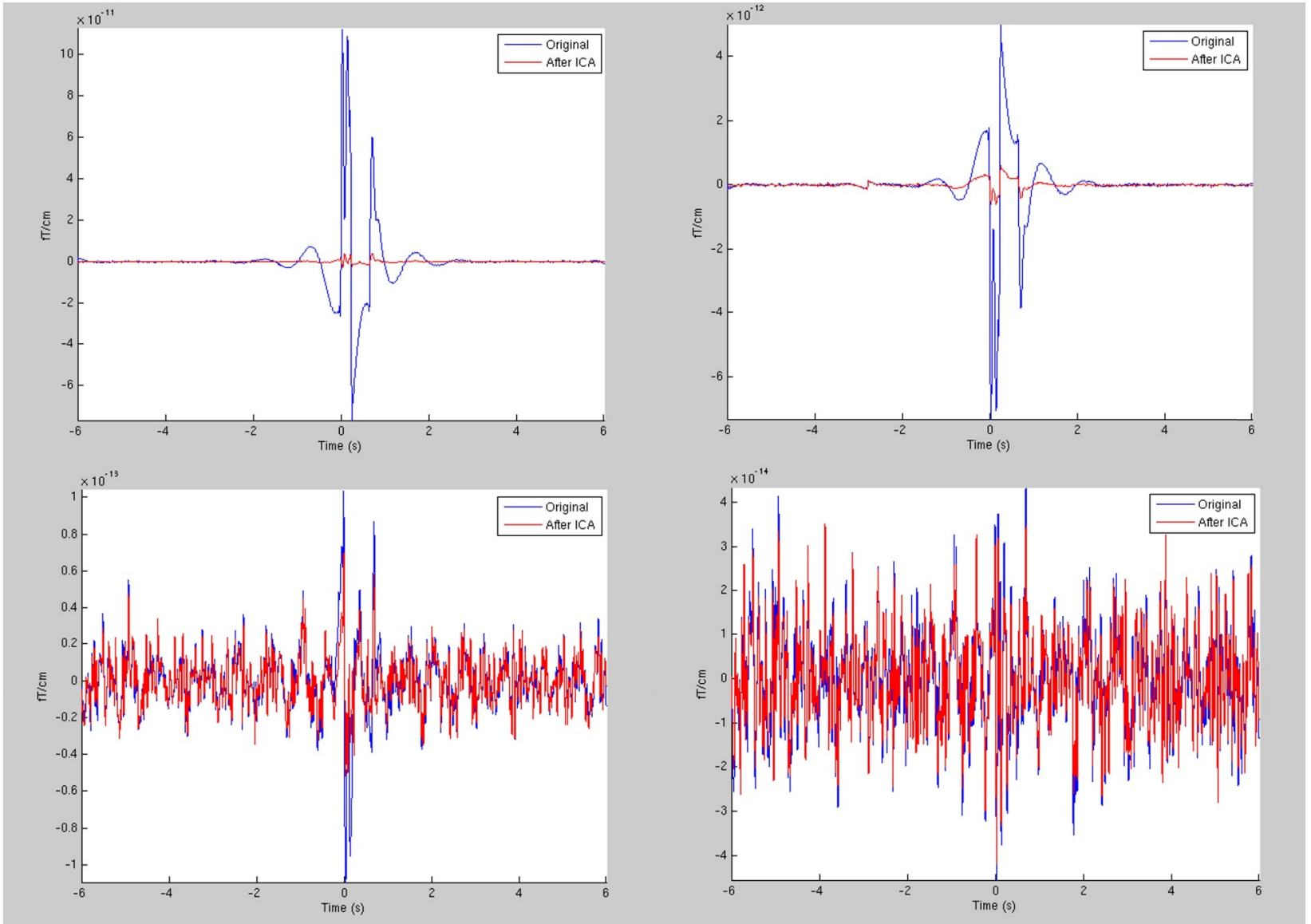

Figure 6.9: Averaged waveform of all gradiometers and trials before and after ICA, band-pass filtered at 1-30 Hz. A: 'Raw' data before and after ICA. B: Data cleaned by SSS before and after ICA. C: Data cleaned by tSSS with a correlation limit of 0.98 before and after ICA. D: Data cleaned by tSSS with a more aggressive correlation limit of 0.6 before and after ICA. Note the scale of the Y axis between C and D.

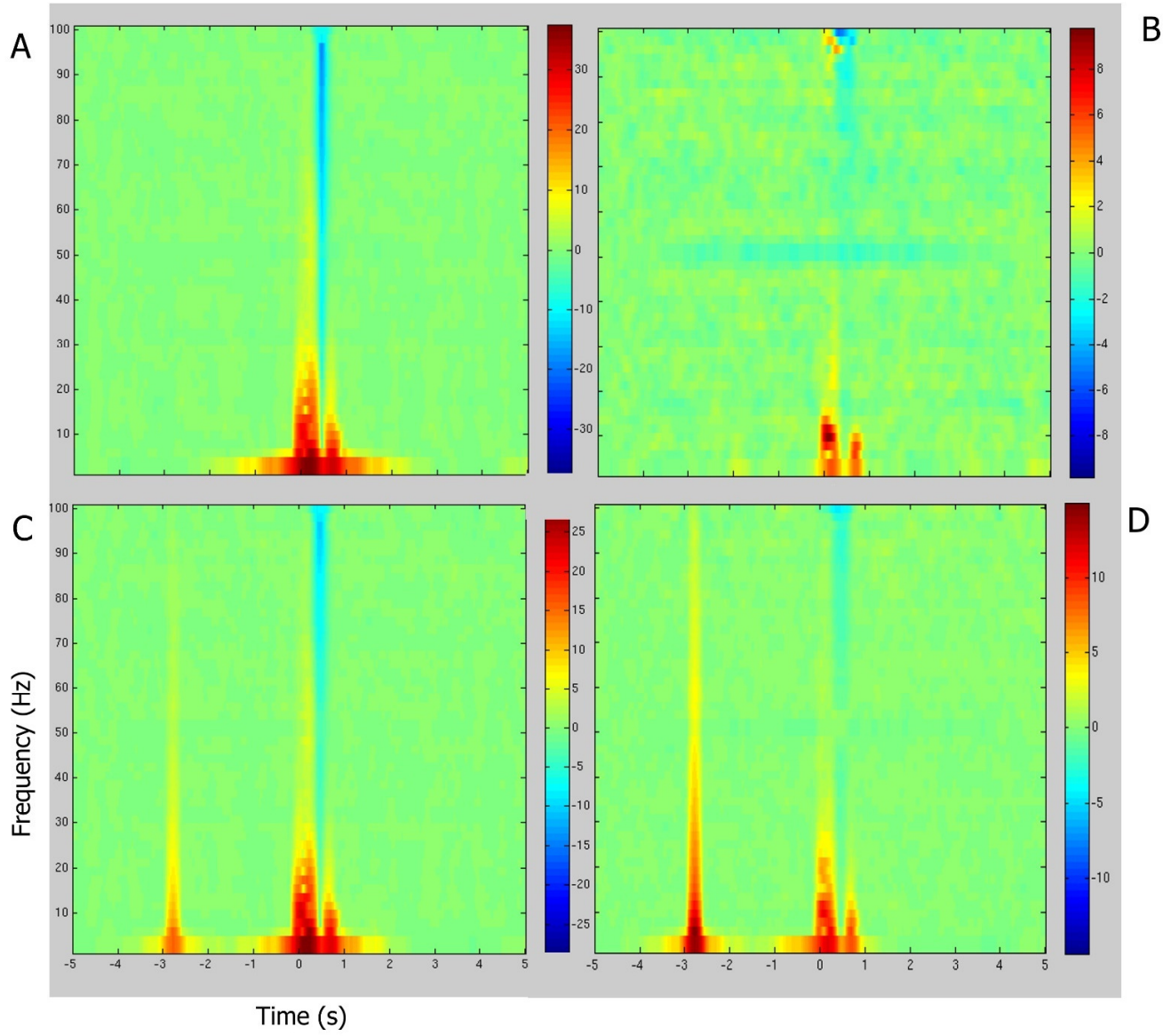

Figure 6.10: Time-frequency plots generated by averaging all trials over all gradiometers on all datasets before and after ICA for comparison. Power is plotted in dB, baseline-corrected with -5s to -4s. 'Raw' data before (A) and after ICA (B). Data cleaned with SSS before (C) and after ICA (D). Note the plotted dB scales after ICA – with the greatest difference being raw-ICA at -36dB.

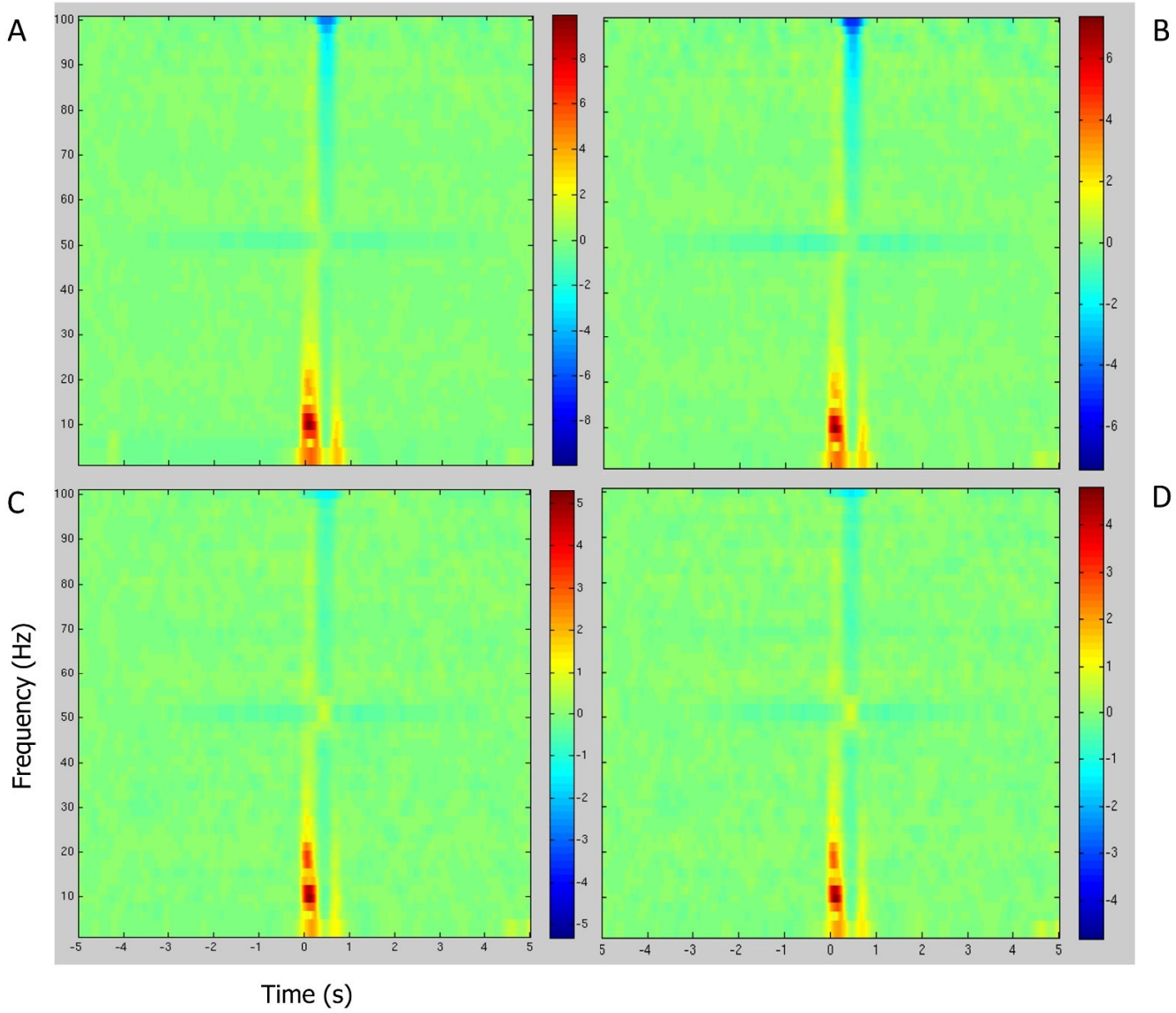

Figure 6.11: Time-frequency plots generated by averaging all trials over all gradiometers on all datasets before and after ICA for comparison. Power is plotted in dB, baseline-corrected with -5s to -4s. Data cleaned by tSSS with correlation limit 0.98 before (A) and after ICA (B). Data cleaned by tSSS with the more aggressive correlation limit of 0.6 before (C) and after ICA (D).

6.5 Beamforming

In this section, raw and cleaned data from empty room and participant datasets are analysed using beamforming; the goal of which is to assess whether the beamformer's innate suppression of source generators outside of a given point can adequately suppress the artefact generated by the CHEPs. Beamformers have multiple configuration parameters (See chapter 3) that can influence their outputs, and as such they are controlled for here.

Lead field spatial weights defined in the beamforming process are purposed to suppress magnetic fields that originate outside any given source point, which could potentially filter out any fields generated by the CHEPS (see chapter 3). Unit-gain minimum-variance beamformers are robust in the presence of random noise, and achieve the highest spatial resolution source reconstructions (Quraan, 2011). Beamformers have certain limitations, however, that may restrict their usefulness in this case: beamformers can suffer from leakage when presented with strong signals outside of their region of interest, which can eventually dominate over weaker sources that might be of interest, and they can be biased by strong correlations across space (Quraan, 2011). These limitations have thus far been described in relation to the brain's source space, however, and not that of an externally generated field.

Beamformers are often spatially whitened by regularisation of the covariance matrix (λ%, See chapter 3). Ranging from 0-100%, a λ of 0.01-5% is common in MEG beamforming, though previous research by Adjamian et al. (2009) has demonstrated that using regularisation can reduce the accuracy of reconstruction methods. Source analysis can also be limited to a

particular number of components (κ, see chapter 3), and as such reduce the dimensionality of the data; this is commonplace in fMRI and principal component analysis, but especially necessary when using MEG data cleaned with signal space separation. The application of signal space separation of any kind reduces the rank of the data to roughly 64 components from 306 (the number of combined gradiometers and magnetometers, reduced to a greater extent when components are removed by ICA; Westner et al., 2022) by removing those that originate outside the dewar; this induced rank-deficiency leaves roughly 140 components that do not accurately reflect sensor recordings, instead only representing noise. These are included in the covariance matrix used in further MEG analysis, and must be accounted for when beamforming by pruning the rank of the data by setting a κ value that describes the number of spatial components to be included in the source reconstruction. In Elekta Neuromag 306 gradiometer data that has not been cleaned, the maximum κ value is 204 (102 of the sensors are magnetometers, as described in chapter 2); the maximum κ value of tSSS data can vary, but is usually between 60-70 (Westner et al., 2022). It is possible that the higher dimensionality of raw data might improve attenuation, or that purposefully limiting the dimensionality may omit some of the noisier components. For these reasons, κ and λ parameters were manipulated in an empty-room dataset to evaluate whether suppression was possible.

6.5.1 Beamforming an empty room recording

Several combinations of datasets and parameters were obtained using the empty-room recording (Table 6.1); the purpose of this was to observe the effectiveness of beamforming and manipulation of κ and λ parameters in attenuating the CHEPS artefact without the participant's brain activity present. Raw and tSSS-cleaned versions of the same dataset were processed

before and after ICA cleaning for comparison. Beamforming of the empty-room dataset was source-reconstructed using a standard MRI, and as such beamforming outputs are presented as if reconstructed in a brain (see Figure 6.10). Exhaustive Figures are found in appendix C.2. Beamforming the raw dataset after ICA resulted in a complete suppression of the artefact, resulting in a completely clear beamformer output, but only with nearly-full dimensionality retained (i.e., no ICA, SSS or tSSS, $\kappa = 202$) and no regularisation ($\lambda = 0$). No other combination of dataset and beamforming parameter successfully attenuated the CHEPS artefact in the empty-room dataset. Figure 6.10 displays the failed attenuation of the artefact by LCMV beamforming ($\kappa = 60$, $\lambda = 0$) in a dataset cleaned using tSSS (0.6) in the FieldTrip LCMV beamformer output using the plotting method 'slice' for a complete perspective in comparison to the effective attenuation of the artefact. This is a promising finding suggesting that it is possible to use beamformers to suppress the CHEPS artefact using spatial weights under specific circumstances.

6.5.2 Beamforming a participant dataset

In this section, the previously identified steps to successfully suppress the CHEPS artefact were replicated in a participant dataset. Following the successful attenuation of the CHEPS artefact in an empty room dataset, an LCMV beamformer was performed on a dataset acquired from one participant whilst they were being stimulated by the CHEPS. The participant was stimulated on their left-hand dorsum in the same position as was emulated in the empty-room recording, using the same stimulation parameters. The LCMV beamformer was performed using the parameters that successfully attenuated the artefact in the empty-room analysis, with the aim to suppress the artefact but also reconstruct the expected source activity reflecting the

sensation of a painful thermal stimulus. A successful reconstruction should show a minimum of a positive peak in the right sensorimotor cortex. The participant dataset required the subtraction of eye movement and heartbeat artefacts alongside the CHEPS components

Table 6.1: All beamformer and data cleaning parameter combinations

Dataset	κ 50				κ 60				κ 200+			
	λ0	λ5	λ15	λ25	λ0	λ5	λ15	λ25	λ0	λ5	λ15	λ25
Raw	x	x	x	x	x	x	x	x	x	x	x	x
Raw (ICA)	x	x	x	x	x	x	x	x	S	x	x	x
tSSS (0.6)	x	x	x	x	x	x	x	x	*	*	*	*
tSSS (0.6, ICA)	x	x	x	x	x	x	x	x	*	*	*	*
tSSS (0.98)	x	x	x	x	x	x	x	x	*	*	*	*
tSSS (0.98, ICA)	x	x	x	x	x	x	x	x	*	*	*	*

A table of all combinations of data types (raw data, tSSS-cleaned data of varying levels, and data that had been cleaned by ICA), lambda and kappa values for beamforming. X = no successful elimination of artefact. * = no analysis possible due to rank insufficiency at this level. S = Successful elimination.

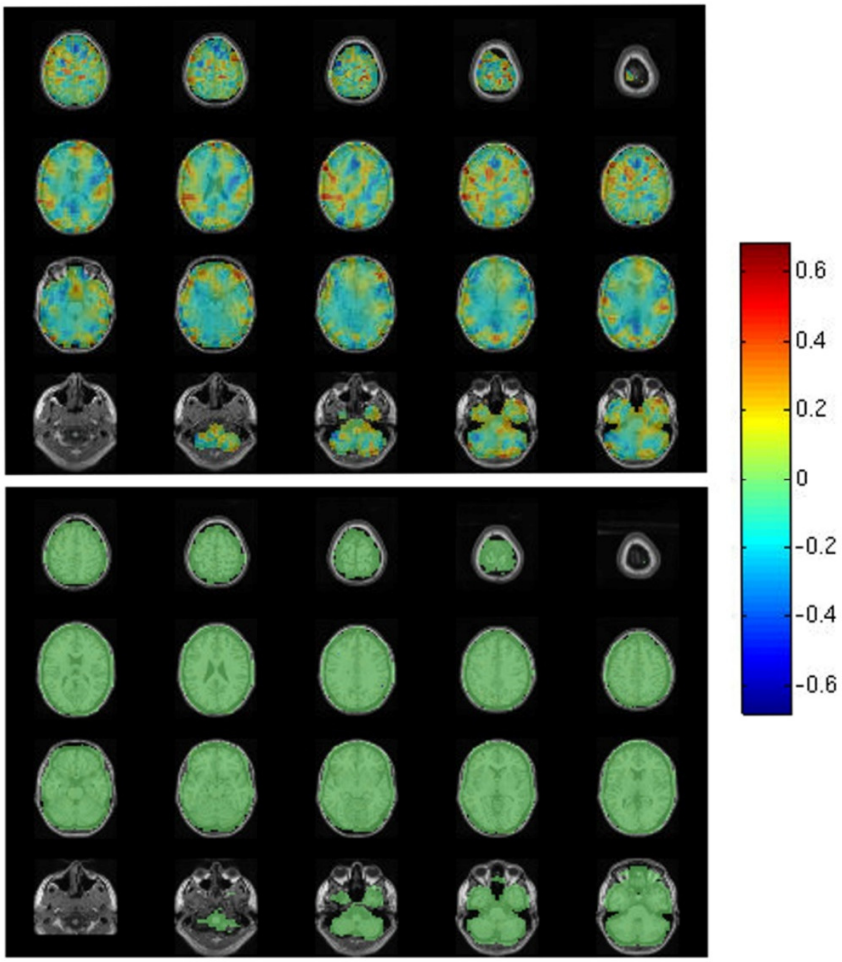

Figure 6.12: LCMV beamformer outputs for empty room recordings, displaying the relative activity in the post-stimulus time window (0 to 1s) compared to the baseline (-5 to -4s), interpolated and plotted on a model of a brain (MNI). The colour bar represents the ratio of change in field strength when the CHEPS thermode is active, compared to its baseline. Left: Source analysis of the tSSS 0.6 dataset, performed using κ = 202 and λ = 0. Right: A beamformer performed on raw data using κ = 202 and λ = 0. This shows complete suppression of the CHEPS artefact, as demonstrated by a value of 0 in all voxels.

As demonstrated in Figure 6.12, the LCMV beamformer of raw participant data after ICA-cleaning using the highest possible number of spatial components (κ = 191) and no

regularisation (λ = 0) did not successfully reconstruct a classic CHEPS source, despite suppressing the artefact in an empty room dataset.

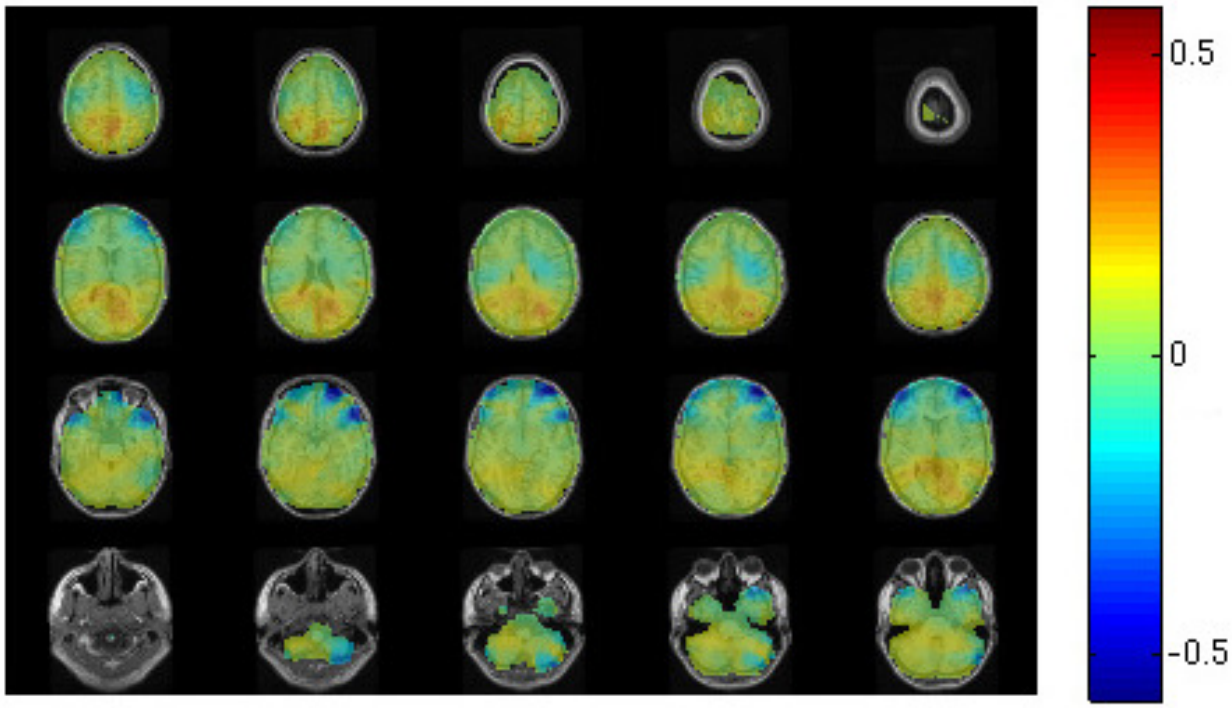

Figure 6.13: LCMV beamformer output of a participant, displaying the ratio of change in field strength in the 0-1s window, as contrasted against a -5 to -4s baseline. Typically, a sensory or nociceptive stimulus elicits a positive peak in the contralateral somatosensory cortex.

6.5.3 DICS beamforming an extended post-stimulus window

As observed in previous sections, the initial time-frequency components of the CHEPS artefacts are limited to the 0-1s time window, but it is well documented that pain processing can last beyond this time. This is reflected by alpha suppression well into the 1 to 2s time window

(Schulz et al., 2012). Dynamic Imaging of Coherent Source (DICS) beamformers can be used to reconstruct frequency-specific activity, and plot the ratio of change between two time windows much like the LCMV plots above. In this final analysis, empty-room DICS analyses are performed to determine whether alpha is present in the extended post-stimulus time window (1 to 2s), and whether it is stronger than the distant baseline (-5s to -4s). Then, the pilot dataset will be analysed to attempt to beamform any suppressed alpha. This analysis aims to determine whether more distant time series data are unaffected by the artefact we are otherwise unable to attenuate.

Figure 6.14 displays the DICS beamformer performed on the raw participant dataset after the removal of time-locked CHEPS components by ICA. The DICS beamformer reconstructs suppressed alpha activity in the bilateral sensory cortices and enhanced alpha in the occipital lobe, which might be expected in a participant experiencing a painful stimulus. However, this reconstruction demonstrates an alpha suppression that is very similar to the negative field strength in the frontal lobe seen in Figure 6.13; in fact, the map of the activity is almost identical. Because of these similarities, it can be concluded that the source reconstruction has not successfully suppressed the CHEPS artefact. This analysis was also performed using the previous combinations of κ and λ parameters on the raw data with and without ICA of the time-locked components (see Appendix C.2), with no reconstructions that convincingly suppress the CHEPS artefact. Whilst virtual sensor reconstruction of time series data at the voxels of interest is possible, the analysis of the empty room demonstrates that the noise suppression has not successfully extended to this timewindow, and that any time series reconstruction in the participant data would also be corrupted.

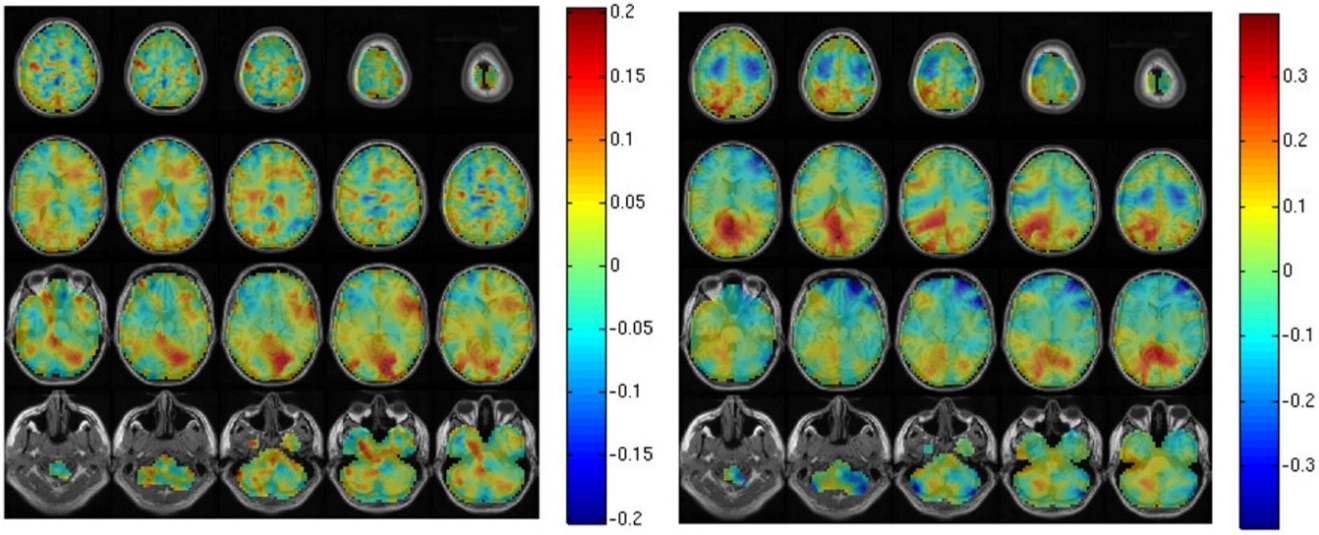

Figure 6.14: DICS beamformer outputs for the 1-2s time window, with alpha-frequency synchronisation plotted in contrast to a -5 to -4s baseline, the highest respective κ value and zero regularisation. Left: Empty room dataset. Right: Participant dataset.

6.6 Discussion and conclusion

The CHEPS artefact is present even when using fMRI-compatible thermodes; though it has been demonstrated that the attenuation of the fMRI-compatible thermode artefact is possible with the use of temporal signal space separation, beamforming, and bespoke damped sinusoid modelling (Gopalakrishnan et al., 2013; Adjamian et al., 2009). fMRI-compatible thermodes for the CHEPS are more expensive, and unnecessary for standardised testing that is used by pain clinicians. This study aimed to assess the feasibility of using the standard apparatus in MEG acquisition, for its improved spatial resolution and clinical utility, and to evaluate the limits of MEG signal cleaning methods. Here for the first time, attempts have been made to suppress the electromagnetic signal that confounds CHEPS recordings in MEG for thermodes that are not specifically shielded for magnetic field recordings.

Primary observations described the nature of the stimulation artefact, and demonstrated that the noise floor is significantly raised in an 'active' state, even in a distant baseline. This is consistent with the findings of Gopalakrishnan et al. (2013), who observed increases in noise in the baseline, though it was not compared to the passive state. Gopalakrishnan et al. used a stimulation with a ramp-and-hold duration of 2s, as opposed to the brief evoked nature of the stimulus used in this chapter, which limits the comparisons regarding time-locked waveforms in the post-stimulus time window; though it is clear that gradiometers record opposing dipole waveforms, as is also evident in Gopalakrishnan's analysis.

Initial attempts to reduce the artefact's influence on the sensor-level data included the application of SSS, and two different levels of tSSS. SSS and tSSS suppressed the field strength of the evoked waveform, which is consistent with Gopalakrishnan's findings. Less conservative tSSS (using a correlation limit of 0.6 as opposed to the default 0.98) had not yet been explored using either CHEPS thermode in heating configuration, and here showed a greater degree of artefact suppression in the evoked time domain. ICA of time-locked components attenuated the waveform further, but has a greater risk of altering the representation of brain signals when applied to a participant dataset.

This study was the first to explore the time-frequency characteristics of the CHEPS artefact regardless of thermode. Time-frequency analysis of raw data showed that pre-stimulus enhancements of low frequencies (2-5 Hz) were apparent up to 2s before the stimulus, though these were smoothed in the time domain somewhat by the parameters of the filters applied. The application of tSSS showed a suppression of the magnitude of these components in time and frequency, with a greater attenuation with less conservative methods. SSS suppressed

some of the field strength of the primary evoked activity, but introduced a strong broadband enhancement at -3s in the pre-stimulus time window that was not present in the raw dataset.

ICA of datasets cleaned by these methods proved challenging after tSSS: in the raw dataset, time-locked components that could be clearly attributed to the CHEPS artefact were few; the ICA of tSSS-cleaned data had a much greater distribution of field strength across components, and at a lesser field strength. This suggests that the reduced rank of the data or the removal of a large amount of the activity via tSSS projection split the remnants of the original component into many, which complicated its identification and resulted in further dimensionality reduction through the process of ICA. The permeation of the artefact was made clearer by observing the time-frequency representation after ICA, where the field strength of the artefact was suppressed in all datasets, but not entirely removed at the sensor level. This additional complexity was enhanced in the participant dataset, where the introduction of physiological data had spread the CHEPS artefact energy across many more components even in the raw dataset.

Beamforming of the evoked waveform was performed by reconstructing the field strength at each voxel of the brain and calculating the ratio of change in the activity in the 0 to 1s time window with a distant baseline of -5 to -4s. The regularisation and number of spatial components were manipulated to evaluate optimum parameters, and raw data, cleaned data, and post-ICA datasets were evaluated for the presence of the CHEPS thermode artefact. The construction of a lead field for beamforming involves the suppression of magnetic fields that originate outside of any given voxel by spatial filtering which, though sensitive to highly correlated activity, has been demonstrated to effectively attenuate fMRI-compatible CHEPS

artefacts (Adjamian et al., 2009). In the empty room dataset, an LCMV beamformer was able to attenuate all activity in the 0-1s epoch and reconstructed no activity; this does support its ability to effectively remove the extraneous signal, but only when performed on a raw dataset after ICA, with no regularisation and high-rank data. This was not successfully replicated in a dataset with a participant present: no brain activity resembling an evoked somatosensory stimulus was apparent, demonstrating the failure to successfully reconstruct underlying brain activity in the presence of the CHEPS artefact. The inclusion of a participant in the MSR introduced additional noise and signal components that thwarted the effective cleaning of the electromagnetic signal artefact; indeed, simply identifying the CHEPS artefact in the participant dataset was significantly more difficult during ICA, with time-locked waveforms visible across many more independent components (See appendix C.1).

The limitations of unit-gain constrained beamforming likely impacted the effectiveness of the artefact suppression. As described by Quraan et al., (2011), beamformers are limited in their reconstruction of sources that are smaller in field strength than other more dominant sources, and can additionally fail to suppress sources that are highly correlated in the time domain.

Incidentally, this study identified a significant erroneous broadband frequency component produced by applying SSS to the empty room artefact recording, but this was not replicated when applying tSSS. It should be noted that SSS may confound signal recordings when used to suppress large electromagnetic artefacts, potentially influencing the characteristics of cleaned data: tSSS is recommended in its stead.

6.6.1 Limitations

The CHEPS stimulus was recorded using an ISI of 8-12s, but it is possible that a longer ISI would have provided a cleaner baseline for comparisons. In the above analyses, a baseline time window was chosen that would otherwise be considered extremely distant and adequately long for a somatosensory stimulus, and therefore an exemplary reflection of baseline activity. However, statistical comparison of the passive empty-room dataset (i.e., with the CHEPS powered, but not stimulating) and the active -5 to -4s time window showed significant differences. This demonstrates that the noise floor is significantly increased in the baseline of the stimulation dataset, even at a distant time window. It is possible, then, that baseline correction of time-frequency representations was polluted by a baseline that was not entirely stationary despite best efforts. Contrasting the CHEPS stimulations to the active empty-room dataset would not have provided appropriate baseline correction, given the significantly different baseline activity.

This study could not explore the effectiveness of synthetic gradiometers, as was done in Adjamian et al. (2009), as the MEG system used does not facilitate such a mechanism. It is possible that 3rd order or greater synthetic gradiometers would be capable of suppressing the CHEPS artefact further.

A final limitation of this exploration of the CHEPS artefact is the lack of painful control stimulus. It is possible, though unlikely, that the brain activity observed in the participant after artefact suppression attempts were genuine brain activity. The participant was noted as not finding the

stimulation to be remarkably painful, though one would still expect representation of the somatosensory processing in the cortex.

6.6.2 Conclusions

Ultimately, the outcomes of this study demonstrate that signal space separation, independent component analysis and MEG beamforming methods are insufficient for the removal of CHEPS artefacts produced by standard CHEPS thermodes, even when combined with a thorough exploration of beamforming parameters. These findings complement those of Gopalakrishnan et al. (2013) and Adjamian et al. (2009) by highlighting the necessity of an fMRI-compatible thermode for combining CHEPS and MEG methodologies, and demonstrate the limitations of signal space separation and beamforming methods, but do not draw any conclusions about synthetic gradiometry. It is hoped that future research will not be stymied by these methodological concerns, and that CHEPS and MEG studies going forward will benefit from the clarity provided by a thorough investigation of the methods and parameters herein; it is recommended that investigators invest in fMRI-compatible CHEPS thermodes for MEG research. It is also recommended that MEG data cleaning should be performed with both tSSS and SSS to evaluate any possible signal artefacts generated by the application of SSS.

7. Thesis conclusion

The following is a concluding chapter, which provides summaries of the key findings, original contributions, and implications of each piece of research presented in this thesis. The primary goal of this thesis was to use MEG source reconstruction to identify the neural correlates of ongoing pain, and to investigate future avenues for tonic pain research using MEG beamforming. In pursuit of this goal, two experimental studies, one systematic review, and one technical exploration of signal cleaning methods were performed.

The first chapter of this thesis explores chronic pain through the therapeutic intervention of SCS. Neuroimaging studies are often utilised to explore the underlying mechanisms of the antinociceptive effect of SCS, as they are poorly understood, and it is recognised that identifying regions involved with the production of pain attenuation may inform future therapeutic advances. Many studies record SSEPs to evaluate the modulation of ascending signals during SCS, hypothesising that the antidromic dorsal column current suppresses nociceptive signalling at the WDR neurons: Most literature has shown the reduction of SSEP amplitude at the sensor or channel level, though it is not unanimous. No studies before this had used MEG to explore the effect of SCS on somatosensory processing distinct from collision in the dorsal column, and no MEG studies have used source reconstruction methods to identify the brain areas affected by paraesthesia-based SCS during SSEP or rest.

4 SCS patients were recruited from Russell's Hall Hospital, and participated in a MEG recording session at rest and during SSEP stimulation of their median nerve, after 12 hours with their SCS disabled, and once again after their SCS has been re-enabled. Participants demonstrated

significantly reduced pain scores during the SCS-on condition, indicating that the antinociceptive effect had taken effect. Source analysis of resting-state activity identified significant clusters of enhanced synchrony in the theta frequency band throughout the left superior temporal gyrus, bilateral mid-cingulate and right anterior cingulate cortices, and delta enhancement throughout the left superior temporal gyrus, left insula and caudate nucleus, implying entrainment by spinal cord stimulation. The involvement of the mid and anterior cingulate cortices in pain processing has been identified by previous functional imaging studies, and associated with pain unpleasantness, anticipation, and disturbed thalamocortical networks in chronic conditions (Caylor et al., 2019), and theta enhancement in these areas especially has been tied to chronic pain experience (Fallon et al., 2018; González-Roldán et al., 2016; Stern et al., 2006). An enhancement as a result of SCS represents the involvement of these areas in the antinociceptive moderation of ascending stimuli, likely through the disruption of local processes by entraining slower neural activity. Whilst other studies have observed theta band normalisation in SCS research, they have done so using alternative (high frequency, burst) SCS that could have shown significantly different patterns of activity in the brain (Caylor et al., 2019). It is possible that the findings in theta and delta frequency power as identified by this study were due to alternative data acquisition techniques (i.e. MEG and EEG) or advanced signal cleaning methods, as others have shown an entrainment SCS stimulation frequency recorded in sensor space (Buentjen et al., 2021); but it is also worth noting that both studies recruited a small number of participants (4-5), as is common in the literature (Witjes et al., 2022), and are using techniques with limited utility in deep subcortical brain areas. This research would benefit from using a more powerful statistical analysis, which could be achieved

using the regions of interest identified within this thesis. Delta enhancement in the left superior temporal gyrus, insula and the caudate nucleus had not been identified by previous studies, but their involvement in memory formation, salience processing and somatosensory processing is well established (Garcia-Larrea, 2012; Houde et al., 2020; McCarberg and Peppin, 2019), and its activation could represent the disruption of processes related to the recruitment of memory, attentional and painful components of ongoing pain, or a contribution to the activation of descending inhibitory projections in the PAG and RVM.

Statistical evaluation of the evoked fields resulting from somatosensory stimulation demonstrated no significant reduction in field strength when comparing SCS-on and SCS-off conditions. Previous studies have used sensor- or channel-level analysis, in which data is analysed superficially, the underlying neural currents or fields superimposed on one another. The evoked fields acquired in this thesis were obtained via reconstruction of virtual sensors at the voxel with peak field strength during the post-stimulus SSEP window. It is well understood that accessing source-level reconstructions is an enhanced perspective of underlying sources, with a more accurate representation of underlying neural activity – especially following MaxFilter and temporal signal space separation (Taulu and Hari, 2009) – and virtual sensors have demonstrated high levels of accuracy when compared to intracortical recording electrodes even deep in the cortex (Korczyn et al., 2013). For the first time, this study uses SSEPs that would not be susceptible to collision in the dorsal column to evaluate the cortical effects of SCS on ascending somatosensory signals recorded by MEG. Notably, post-stimulus SSEP power spectra at the virtual sensor were significantly reduced during SCS, providing evidence of disruption of cortical processing in the somatosensory cortex, where clusters contributing to

the rejection of the null hypothesis were identified in the delta frequency band. Future analysis of frequency changes in the time domain will likely elucidate these differences, with more powerful statistical analysis possible due to the identification of this cluster. The present thesis was unable to explore the time-frequency domain in adequate resolution because of the short ISI of the SSEP stimuli, nor was it able to utilise source-level statistics, as one of the participants was stimulated at a heterogeneous stimulus location.

The second experimental chapter in this thesis explored the frequency correlates of pain sensitivity groups as operationalised by pain scores during a cold pressor test analogue. This was the first study to analyse the source localisation of the neural correlates of pain sensitivity in MEG. Though previous research has identified changes in alpha and gamma frequency power during experimental pain and clinical pain groups (Schulz et al., 2012; Hu & Iannetti, 2019), most experimental pain studies have used acute pain stimuli and stimuli that do not effectively reflect pain experienced day-to-day. Utilising the CPT to access pain sensitivity and ongoing pain during data acquisition, participants were divided into high or low pain sensitivity groups by their peak pain score during the recording. Time series data were split into peak and late epochs, reflecting the first 15 seconds of the greatest pain score and the last 100 seconds, where the pain had plateaued.

Source localisation of gamma and alpha frequencies during CPT did not reveal significant differences between sensitivity groups during the peak pain or the late time window, possibly due to lack of power in the statistical method and imbalance in final group sizes. Though not significant, suppression of alpha and gamma frequencies revealed areas of interest that would be worthy of investigation with greater sample sizes and more powerful statistical methods;

alpha and gamma suppression were greater in the low pain sensitivity group in bilateral somatosensory cortices during the late epoch – but most notably, a relatively large suppression of gamma in the contralateral somatosensory cortex was observed during the peak pain epoch.

The systematic review in chapter six explored the literature combining the Contact Heat Evoked Potentials System (CHEPS) and MEG using a systematic search; the CHEPS uses a Peltier thermode that is capable of achieving a ramping speed of 70˚C/s, enabling its use in evoked potential research, and also holding a temperature of up to 51˚C for an extended duration; it is a good candidate for an evoked or tonic pain stimulus in MEG, but few studies combine the two methods. A systematic search was performed by accessing records from MEDLINE, The Cochrane Library (CENTRAL), Embase, CINAHL, PsycINFO, SportDISCUS, Scopus and Google Scholar, in addition to bibliographic coupling graphs generated by the ConnectedPapers search engine. Of the initial 646 articles identified, 58 texts were evaluated in their entirety for inclusion, and eight were included in a qualitative synthesis. Six of the eight studies identified were performed by one group of researchers studying the anticipation of pain. Of the six studies from this group, one study investigated the suppression of electromagnetic signals generated by the fMRI-compatible CHEPS thermode in MEG, and the other five studied anticipation of pain in various healthy control and chronic pain participant groups. Of the remaining two studies, one studied the effectiveness of synthetic gradiometry and beamforming in the suppression of electromagnetic noise, and the other observed cold thermosensation in healthy controls. The findings of the systematic review highlight the paucity of the literature combining the two methods: of all CHEPS and MEG studies, only one identified in the review aimed to evaluate the post-stimulus time window: all other studies were

methodological or observed a distant pre-stimulus time window. This paucity is surprising, given that two studies exist to show that the combination of these novel methods is possible despite the presence of a strong electromagnetic signal, where they show its attenuation with modern signal cleaning methods. A likely explanation for this paucity is the necessity for an fMRI-compatible thermode, a more expensive piece of equipment that is not otherwise necessary for EEG imaging. Despite this, Fardo et al. (2017) utilised simultaneous EEG and MEG with CHEPS to identify the underlying neural generators of cold sensation in sensor-level and source-level analyses; even highlighting that MEG is capable of obtaining more precise temporal dynamics of sensory processing.

Informed by the systematic review in the previous chapter, the final chapter of this thesis was an extensive methodological study of the suppression of the electromagnetic signal artefact produced by the standard CHEPS thermode. Whilst active in the MSR, the standard (i.e., non-fMRI compatible) thermode produces an electromagnetic field which contaminates MEG data, making analysis of brain activity impossible. While some studies have been able to combine MEG and CHEPS, most published articles opt to use the pre-stimulus time window where the artefact is less prevalent, as was identified in the systematic review above. Others have likely attempted the combination of CHEPS and MEG with a standard CHEPS thermode and been flummoxed by the challenges this presents. Electrophysiological data is routinely cleaned of physiological or external artefacts that might otherwise contaminate the signal presented by the brain, and modern source analysis techniques are effective in reducing the contribution of external signals. This chapter utilised traditional and advanced data cleaning methods in conjunction with modern beamforming analysis to determine whether using the standard

CHEPS thermode is possible in an empty room and a pilot participant dataset. A thorough evaluation of possible combinations of these methods and their various configurations eventually successfully removed the artefact from an empty room dataset, but not that of a participant. Incidentally, the analysis identified a large signal artefact that was not identified in the raw dataset which was introduced by Signal Space Separation (SSS; Taulu and Simola, 2006) alone. Whilst the concluding study of this thesis does not present an exciting climax, its contribution to the literature is original, and will inform future researchers hoping to pursue the aforementioned paucity in the MEG and CHEPS literature.

7.1 Concluding statement

The research presented within this thesis demonstrates the utility of MEG source reconstruction in the evaluation of brain activity in ongoing pain. Initially, novel evidence for the supraspinal enhancement of theta and delta frequency bands in spinal cord stimulation resting-state was presented, alongside statistically significant suppression of power spectra during somatosensory evoked fields, elucidating the contribution of SCS to somatosensory processing, and demonstrating that SSEP processing is disrupted by its ascending currents even without any possible collision in the dorsal column. Whilst comparisons between pain sensitivity groups in healthy controls did not find significant source-level differences at gamma or alpha frequency, it is possible that the areas identified in the analysis would benefit from further study with a greater number of participants and more powerful statistical analysis: something possible thanks to the research included here. A systematic review revealed the significant paucity in the literature that combines MEG and CHEPS techniques, and not only that the combination is possible, but also that it could contribute more effectively to the delineation

of neural mechanisms. Finally, a methodological study explored the attenuation of a large electromagnetic signal artefact produced by standard (i.e., non-fMRI compatible) CHEPS thermodes in MEG data acquisition; it was found to be possible in an empty room dataset, but not possible with most modern signal cleaning techniques. It is hoped that this thorough examination of the equipment's limitations will inform future CHEPS-MEG researchers, saving time, datasets, and money.

8. Reference list

Abdallat, M., Saryyeva, A., Blahak, C., Wolf, M.E., Weigel, R., Loher, T.J., Runge, J., Heissler, H.E., Kinfe, T.M. and Krauss, J.K. (2021) Centromedian–Parafascicular and Somatosensory Thalamic Deep Brain Stimulation for Treatment of Chronic Neuropathic Pain: A Contemporary Series of 40 Patients. *Biomedicines*, 9(7).

Abhang, P.A., Gawali, B.W. and Mehrotra, S.C. (2016) Technological Basics of EEG Recording and Operation of Apparatus.in *Introduction to EEG- and Speech-Based Emotion Recognition*. Elsevier, pp. 19–50.

Abrishami, A., Chan, J., Chung, F., Wong, J. and Warner, D.S. (2011) Preoperative Pain Sensitivity and Its Correlation with Postoperative Pain and Analgesic Consumption. *Anesthesiology*, 114(2).

Adjamian, P., Worthen, S.F., Hillebrand, A., Furlong, P.L., Chizh, B.A., Hobson, A.R., Aziz, Q. and Barnes, G.R. (2009) Effective electromagnetic noise cancellation with beamformers and synthetic gradiometry in shielded and partly shielded environments. *Journal of Neuroscience Methods*, 178(1).

Al'absi, M., Nakajima, M. and Bruehl, S. (2021) Stress and pain: modality-specific opioid mediation of stress-induced analgesia. *Journal of Neural Transmission*, 128.

Alabas, O.A., Tashani, O.A., Tabasam, G. and Johnson, M.I. (2012) Gender role affects experimental pain responses: A systematic review with meta-analysis. *European Journal of Pain*, 16(9).

de Andrade, D.C., Bendib, B., Hattou, M., Keravel, Y., Nguyen, J.P. and Lefaucheur, J.P. (2010) Neurophysiological assessment of spinal cord stimulation in failed back surgery syndrome. *Pain*, 150(3).

Apkarian, A.V., Bushnell, M.C., Treede, R.-D.D., Zubieta, J.-K.K., Vania, A.A., Catherine, B.M., Rolf-Detlef, T. and Jon-Kar, Z. (2005) Human brain mechanisms of pain perception and regulation in health and disease. *European Journal of Pain*, 9(4).

Arendt-Nielsen, L. and Chen, A.C.N.C.N. (2003) Lasers and other thermal stimulators for activation of skin nociceptors in humans. *Clinical Neurophysiology*, 33(6).

Backonja, M., Howland, E.W., Wang, J., Smith, J., Salinsky, M. and Cleeland, C.S. (1991) Tonic changes in alpha power during immersion of the hand in cold water. *Electroencephalography and Clinical Neurophysiology*, 79(3).

Banozic, A., Miljkovic, A., Bras, M., Puljak, L., Kolcic, I., Hayward, C. and Polasek, O. (2018) Neuroticism and pain catastrophizing aggravate response to pain in healthy adults: An experimental study. *Korean Journal of Pain*, 31(1).

Barchini, J., Tchachaghian, S., Shamaa, F., Jabbur, S.J., Meyerson, B.A., Song, Z., Linderoth, B. and Saadé, N.E. (2012) Spinal segmental and supraspinal mechanisms underlying the pain-relieving effects of spinal cord stimulation: An experimental study in a rat model of neuropathy. *Neuroscience*, 215.

Başar, E., Başar-Eroglu, C., Karakaş, S. and Schürmann, M. (2001) Gamma, alpha, delta, and theta oscillations govern cognitive processes. *International Journal of Psychophysiology*, 39(2–3).

Belavy, D.L., Van Oosterwijck, J., Clarkson, M., Dhondt, E., Mundell, N.L., Miller, C.T. and Owen, P.J. (2021) Pain sensitivity is reduced by exercise training: Evidence from a systematic review and meta-analysis. *Neuroscience and biobehavioral reviews*, 120.

Bell, A.J. and Sejnowski, T.J. (1995) An information-maximization approach to blind separation and blind deconvolution. *Neural computation*, 7(6).

Bentley, L.D., Duarte, R. V, Furlong, P.L., Ashford, R.L. and Raphael, J.H. (2016) Brain activity modifications following spinal cord stimulation for chronic neuropathic pain: A systematic review. *European Journal of Pain*, 20(4).

Berg, C.J., Snyder, C.R. and Hamilton, N. (2008) The Effectiveness of a Hope Intervention in Coping with Cold Pressor Pain. *Journal of Health Psychology*, 13(6).

Bliss, T.V.P., Collingridge, G.L., Kaang, B.K. and Zhuo, M. (2016) Synaptic plasticity in the anterior cingulate cortex in

acute and chronic pain. *Nature Reviews Neuroscience 2016 17:8*, 17(8).

Boccard, S.G.J., Fitzgerald, J.J., Pereira, E.A.C., Moir, L., Van Hartevelt, T.J., Kringelbach, M.L., Green, A.L. and Aziz, T.Z. (2014a) Targeting the Affective Component of Chronic Pain. *Neurosurgery*, 74(6).

Boccard, S.G.J., Pereira, E.A.C., Moir, L., Van Hartevelt, T.J., Kringelbach, M.L., Fitzgerald, J.J., Baker, I.W., Green, A.L. and Aziz, T.Z. (2014b) Deep brain stimulation of the anterior cingulate cortex: targeting the affective component of chronic pain. *Neuroreport*, 25(2).

Bocci, T., De Carolis, G., Paroli, M., Barloscio, D., Parenti, L., Tollapi, L., Valeriani, M. and Sartucci, F. (2018) Neurophysiological Comparison Among Tonic, High Frequency, and Burst Spinal Cord Stimulation: Novel Insights Into Spinal and Brain Mechanisms of Action. *Neuromodulation*, 21(5).

Boly, M., Balteau, E., Schnakers, C., Degueldre, C., Moonen, G., Luxen, A., Phillips, C., Peigneux, P., Maquet, P. and Laureys, S. (2007) Baseline brain activity fluctuations predict somatosensory perception in humans. *Proceedings of the National Academy of Sciences*, 104(29).

Bornhövd, K., Quante, M., Glauche, V., Bromm, B., Weiller, C. and Büchel, C. (2002) Painful stimuli evoke different stimulus–response functions in the amygdala, prefrontal, insula and somatosensory cortex: a single-trial fMRI study. *Brain*, 125(6).

Borsook, D. and Becerra, L. (2011) CNS animal fMRI in pain and analgesia. *Neuroscience and Biobehavioral Reviews*, 35(5).

Bouin, M., Plourde, V., Boivin, M., Riberdy, M., Lupien, F., Laganière, M., Verrier, P. and Poitras, P. (2002) Rectal distention testing in patients with irritable bowel syndrome: Sensitivity, specificity, and predictive values of pain sensory thresholds. *Gastroenterology*, 122(7).

Bromm, B. and Treede, R.D. (1991) Laser-evoked cerebral potentials in the assessment of cutaneous pain sensitivity in normal subjects and patients. *Revue neurologique*, 147(10).

Brookes, M.J., Vrba, J., Robinson, S.E., Stevenson, C.M., Peters, A.M., Barnes, G.R., Hillebrand, A. and Morris, P.G. (2008) Optimising experimental design for MEG beamformer imaging. *NeuroImage*, 39(4).

Brooks, J. and Tracey, I. (2005) From nociception to pain perception: imaging the spinal and supraspinal pathways. *Journal of Anatomy*, 207(1).

Brown, D., Schenk, S., Genent, D., Zernikow, B. and Wager, J. (2021) A scoping review of chronic pain in emerging adults. *PAIN Reports*, 6(1).

Buchgreitz, L., Lyngberg, A.C., Bendtsen, L. and Jensen, R. (2008) Increased pain sensitivity is not a risk factor but a consequence of frequent headache: A population-based follow-up study. *Pain*, 137(3).

Buentjen, L., Vicheva, P., Chander, B.S., Beccard, S.A., Coutts, C., Azañón, E., Stenner, M.P. and Deliano, M. (2021) Spatial Filtering of Electroencephalography Reduces Artifacts and Enhances Signals Related to Spinal Cord Stimulation (SCS). *Neuromodulation: Technology at the Neural Interface*, 24(8).

Bulls, H.W., Freeman, E.L., Anderson, A.J., Robbins, M.T., Ness, T.J. and Goodin, B.R. (2015) Sex differences in experimental measures of pain sensitivity and endogenous pain inhibition. *Journal of pain research*, 8.

Buonocore, M., Bodini, A., Demartini, L. and Bonezzi, C. (2012) Inhibition of somatosensory evoked potentials during spinal cord stimulation and its possible role in the comprehension of antalgic mechanisms of neurostimulation for neuropathic pain. *Minerva Anestesiologica*, 78(3).

Buonocore, M. and Demartini, L. (2016) Inhibition of Somatosensory Evoked Potentials During Different Modalities of Spinal Cord Stimulation: A Case Report. *Neuromodulation*, 19(8).

Burgess, R.C. (2020) Recognizing and Correcting MEG Artifacts. *Journal of clinical neurophysiology : official publication of the American Electroencephalographic Society*, 37(6).

Bushnell, M.C., Čeko, M. and Low, L.A. (2013) Cognitive and emotional control of pain and its disruption in chronic pain. *Nature Reviews Neuroscience*, 14(7).

Butler, S., Draleau, K., Heinrich, R., Nguyen, L., Shbeeb, D., Sigalovsky, D., Koh, W.Y., Hull, S.Z. and Cao, L. (2020) Evaluation of Using the Sphygmomanometer Test to Assess Pain Sensitivity in Chronic Pain Patients vs Normal Controls. *Pain Medicine*, 21(11).

Campbell, J.N. and Meyer, R.A. (2006) Mechanisms of neuropathic pain. *Neuron*, 52(1).

Caylor, J., Reddy, R., Yin, S., Cui, C., Huang, M., Huang, C., Rao, R., Baker, D.G., Simmons, A., Souza, D., Narouze, S., Vallejo, R. and Lerman, I. (2019) Spinal cord stimulation in chronic pain: evidence and theory for mechanisms of action. *Bioelectronic Medicine*, 5(1).

La Cesa, S., Tinelli, E., Toschi, N., Di Stefano, G., Collorone, S., Aceti, A., Francia, A., Cruccu, G., Truini, A. and Caramia, F. (2014) fMRI pain activation in the periaqueductal gray in healthy volunteers during the cold pressor test. *Magnetic Resonance Imaging*, 32(3).

Chang, P.F., Arendt-Nielsen, L. and Chen, A.C.N. (2002) Dynamic changes and spatial correlation of EEG activities during cold pressor test in man. *Brain Research Bulletin*, 57(5).

Chaumon, M., Puce, A. and George, N. (2021) Statistical power: Implications for planning MEG studies. *NeuroImage*, 233.

Chen, A.C.N., Dworkin, S.F., Haug, J. and Gehrig, J. (1989) Human pain responsivity in a tonic pain model: Psychological determinants. *Pain*, 37(2).

Cheyne, D.O. and Papanicolaou, A.C. (2015) Magnetoencephalography and Magnetic Source Imaging.in Papanicolaou, A.C. (ed.) *The Oxford Handbook of Functional Brain Imaging in Neurpsychology and Cognitive Neurosciences*. Oxford University Press.

Choi, S., Park, S.-G. and Lee, H.-H. (2018) The analgesic effect of music on cold pressor pain responses: The influence of anxiety and attitude toward pain. *PLOS ONE*. Edited by U.M. Nater, 13(8).

Cleve, M., Gussew, A., Wagner, G., Bär, K.J. and Reichenbach, J.R. (2017) Assessment of intra- and inter-regional interrelations between GABA+, Glx and BOLD during pain perception in the human brain – A combined 1H fMRS and fMRI study. *Neuroscience*, 365.

Coghill, R.C., McHaffie, J.G. and Yen, Y.-F.Y.F. (2003) Neural correlates of interindividual differences in the subjective experience of pain.in *Proceedings of the National Academy of Sciences of the United States of America*. National Academy of Sciences, pp. 8538–8542.

Compton, P., Halabicky, O.M., Aryal, S. and Badiola, I. (2022) Opioid Taper is Associated with Improved Experimental Pain Tolerance in Patients with Chronic Pain: An Observational Study. *Pain and Therapy*, 11(1).

Coronado, R.A., George, S.Z., Devin, C.J., Wegener, S.T. and Archer, K.R. (2015) Pain Sensitivity and Pain Catastrophizing Are Associated With Persistent Pain and Disability After Lumbar Spine Surgery. *Archives of Physical Medicine and Rehabilitation*, 96(10).

Cui, J.G., Linderoth, B. and Meyerson, B.A. (1996) Effects of spinal cord stimulation on touch-evoked allodynia involve GABAergic mechanisms. An experimental study in the mononeuropathic rat. *Pain*, 66(2–3).

Cui, J.G., O'Connor, W.T., Ungerstedt, U., Linderoth, B. and Meyerson, B.A. (1997) Spinal cord stimulation attenuates augmented dorsal horn release of excitatory amino acids in mononeuropathy via a GABAergic mechanism. *Pain*, 73(1).

Dahlquist, L.M., Weiss, K.E., Dillinger Clendaniel, L., Law, E.F., Ackerman, C.S. and McKenna, K.D. (2009) Effects of Videogame Distraction using a Virtual Reality Type Head-Mounted Display Helmet on Cold Pressor Pain in Children. *Journal of Pediatric Psychology*, 34(5).

Damme, S., Crombez, G., Wever, K.N. and Goubert, L. (2008) Is distraction less effective when pain is threatening? An experimental investigation with the cold pressor task. *European Journal of Pain*, 12(1).

Deer, T.R., Russo, M., Grider, J.S., Pope, J., Hagedorn, J.M., Weisbein, J., Abd-Elsayed, A., Benyamin, R., Raso, L.J., Patel, K. V., Provenzano, D., Kim, P.S., Amirdelfan, K., Bolash, R., Steegers, M., Sullivan, R., Verrills, P., Carlson, J.,

Kapural, L., Diwan, S., Barolat, G., Pahapill, P.A., De Andres, J., Raslan, A.M., Lopez, J.A., Leong, M.S., Attias, M.B., Teddy, P., Green, A.L., Dario, A., Piedimonte, F., Chapman, K.B., Tomycz, N.D., FitzGerald, J., Gatzinsky, K., Varshney, V., Gish, B., Lindsey, B.L., Buvanendran, A., Lamer, T.J., Slavin, K. V. and Levy, R.M. (2022) The Neurostimulation Appropriateness Consensus Committee (NACC): Recommendations on Best Practices for Cervical Neurostimulation. *Neuromodulation : journal of the International Neuromodulation Society*, 25(1).

Deer, T.R., Skaribas, I.M., Haider, N., Salmon, J., Kim, C., Nelson, C., Tracy, J., Espinet, A., Lininger, T.E., Tiso, R., Archacki, M.A. and Washburn, S.N. (2014) Effectiveness of Cervical Spinal Cord Stimulation for the Management of Chronic Pain. *Neuromodulation*, 17(3).

Dengler-Crish, C.M., Bruehl, S. and Walker, L.S. (2011) Increased wind-up to heat pain in women with a childhood history of functional abdominal pain. *Pain*, 152(4).

Dodo, N. and Hashimoto, R. (2017) The effect of anxiety sensitivity on psychological and biological variables during the cold pressor test. *Autonomic Neuroscience*, 205.

Doerr, M., Krainick, J.U. and Thoden, U. (1978) Pain perception in man after long term spinal cord stimulation. *Journal of Neurology*, 217(4).

Dowman, R., Rissacher, D. and Schuckers, S. (2008) EEG indices of tonic pain-related activity in the somatosensory cortices. *Clinical Neurophysiology*, 119(5).

Duarte, R. V., McNicol, E., Colloca, L., Taylor, R.S., North, R.B. and Eldabe, S. (2020a) Randomized Placebo-/Sham-Controlled Trials of Spinal Cord Stimulation: A Systematic Review and Methodological Appraisal. *Neuromodulation : journal of the International Neuromodulation Society*, 23(1).

Duarte, R. V., Nevitt, S., Maden, M., Meier, K., Taylor, R.S., Eldabe, S. and de Vos, C.C. (2021) Spinal cord stimulation for the management of painful diabetic neuropathy: a systematic review and meta-analysis of individual patient and aggregate data. *Pain*, 162(11).

Duarte, R. V., Nevitt, S., McNicol, E., Taylor, R.S., Buchser, E., North, R.B. and Eldabe, S. (2020b) Systematic review and meta-analysis of placebo/sham controlled randomised trials of spinal cord stimulation for neuropathic pain. *Pain*, 161(1).

Dubin, A.E. and Patapoutian, A. (2010) Nociceptors: The sensors of the pain pathway. *Journal of Clinical Investigation*, 120(11).

Dum, R.P., Levinthal, D.J. and Strick, P.L. (2009) The Spinothalamic System Targets Motor and Sensory Areas in the Cerebral Cortex of Monkeys. *Journal of Neuroscience*, 29(45).

Edwards, R.R., Fillingim, R.B. and Ness, T.J. (2003) Age-related differences in endogenous pain modulation: a comparison of diffuse noxious inhibitory controls in healthy older and younger adults. *Pain*, 101(1–2).

Eichhorn, N., Treede, R.-D. and Schuh-Hofer, S. (2018) The Role of Sex in Sleep Deprivation Related Changes of Nociception and Conditioned Pain Modulation. *Neuroscience*, 387.

El-Khoury, C., Hawwa, N., Baliki, M., Atweh, S.., Jabbur, S.. and Saadé, N.. (2002) Attenuation of neuropathic pain by segmental and supraspinal activation of the dorsal column system in awake rats. *Neuroscience*, 112(3).

Eldabe, S., Duarte, R. V, Gulve, A., Thomson, S., Baranidharan, G., Houten, R., Jowett, S., Sandhu, H., Chadwick, R., Brookes, M., Kansal, A., Earle, J., Bell, J., Robinson, J., Walker, S., Rhodes, S. and Taylor, R.S. (2020) Does a screening trial for spinal cord stimulation in patients with chronic pain of neuropathic origin have clinical utility and cost-effectiveness (TRIAL-STIM)? A randomised controlled trial. *Pain*, 161(12).

Emerson, N.M., Zeidan, F., Lobanov, O. V, Hadsel, M.S., Martucci, K.T., Quevedo, A.S., Starr, C.J., Nahman-Averbuch, H., Weissman-Fogel, I., Granovsky, Y., Yarnitsky, D. and Coghill, R.C. (2014) Pain sensitivity is inversely related to regional grey matter density in the brain. *Pain*, 155(3).

Erpelding, N., Moayedi, M. and Davis, K.D. (2012) Cortical thickness correlates of pain and temperature sensitivity. *Pain*, 153(8).

Esterlis, I., McKee, S.A., Kirk, K., Lee, D., Bois, F., Stiklus, S.M., Seibyl, J.P., Krishnan-Sarin, S., O'Malley, S.S., Staley, J.K. and Cosgrove, K.P. (2013) Sex-specific differences in GABA A -benzodiazepine receptor availability: relationship with sensitivity to pain and tobacco smoking craving. *Addiction Biology*, 18(2).

Van Ettinger-Veenstra, H., Lundberg, P., Alföldi, P., Södermark, M., Graven-Nielsen, T., Sjörs, A., Engström, M. and Gerdle, B. (2019) Chronic widespread pain patients show disrupted cortical connectivity in default mode and salience networks, modulated by pain sensitivity. *Journal of Pain Research*, 12.

Fallon, N., Chiu, Y., Nurmikko, T. and Stancak, A. (2018) Altered theta oscillations in resting EEG of fibromyalgia syndrome patients. *European Journal of Pain*, 22(1).

Fardo, F., Vinding, M.C., Allen, M., Jensen, T.S. and Finnerup, N.B. (2017) Delta and gamma oscillations in operculo-insular cortex underlie innocuous cold thermosensation. *Journal of Neurophysiology*, 117(5).

Fayaz, A., Croft, P., Langford, R.M., Donaldson, L.J. and Jones, G.T. (2016) Prevalence of chronic pain in the UK: a systematic review and meta-analysis of population studies. *BMJ Open*, 6(6).

Ferracuti, S., Seri, S., Mattia, D. and Cruccu, G. (1994) Quantitative EEG modifications during the cold water pressor test: hemispheric and hand differences. *International Journal of Psychophysiology*, 17(3).

Fitzcharles, M.A., Cohen, S.P., Clauw, D.J., Littlejohn, G., Usui, C. and Häuser, W. (2021) Nociplastic pain: towards an understanding of prevalent pain conditions. *The Lancet*, 397(10289).

Frahm, K.S., Gervasio, S., Arguissain, F. and Mouraux, A. (2020) New Insights into Cutaneous Laser Stimulation – Dependency on Skin and Laser Type. *Neuroscience*, 448.

Frankenstein, U.N., Richter, W., McIntyre, M.C. and Remy, F. (2001) Distraction modulates anterior cingulate gyrus activations during the cold pressor test. *Neuroimage*, 14(4).

Frot, M., Mauguiere, F., Magnin, M. and Garcia-Larrea, L. (2008) Parallel Processing of Nociceptive A- Inputs in SII and Midcingulate Cortex in Humans. *Journal of Neuroscience*, 28(4).

Fuchs, P.N., Peng, Y.B., Boyette-Davis, J.A. and Uhelski, M.L. (2014) The anterior cingulate cortex and pain processing. *Frontiers in Integrative Neuroscience*, 8.

Furman, A.J., Meeker, T.J., Rietschel, J.C., Yoo, S., Muthulingam, J., Prokhorenko, M., Keaser, M.L., Goodman, R.N., Mazaheri, A. and Seminowicz, D.A. (2018) Cerebral peak alpha frequency predicts individual differences in pain sensitivity. *NeuroImage*, 167.

Furman, A.J., Prokhorenko, M., Keaser, M.L., Zhang, J., Chen, S., Mazaheri, A. and Seminowicz, D.A. (2020) Sensorimotor Peak Alpha Frequency Is a Reliable Biomarker of Prolonged Pain Sensitivity. *Cerebral Cortex*, 30(12).

Furman, A.J., Thapa, T., Summers, S.J., Cavaleri, R., Fogarty, J.S., Steiner, G.Z., Schabrun, S.M. and Seminowicz, D.A. (2019) Cerebral peak alpha frequency reflects average pain severity in a human model of sustained, musculoskeletal pain. *Journal of Neurophysiology*, 122(4).

Gangadharan, V. and Kuner, R. (2013) Pain hypersensitivity mechanisms at a glance. *Disease Models & Mechanisms*, 6(4).

Garcés, P., López-Sanz, D., Maestú, F. and Pereda, E. (2017) Choice of Magnetometers and Gradiometers after Signal Space Separation. *Sensors*, 17(12).

Garcia-Larrea, L. (2012) The posterior insular-opercular region and the search of a primary cortex for pain. *Clinical Neurophysiology*, 42(5).

Garcia-Larrea, L., Peyron, R., Mertens, P., Laurent, B., Mauguiere, F. and Sindou, M. (2000) Functional imaging and neurophysiological assessment of spinal and brain therapeutic modulation in humans. *Archives of Medical Research*, 31(3).

Gauriau, C. and Bernard, J. (2004) Posterior Triangular Thalamic Neurons Convey Nocicepive Messages to the Secondary Somatosensory and Insular Cortices in the Rat. *Journal of Neuroscience*, 24(3).

George, S., Dannecker, E. and Robinson, M. (2006) Fear of pain, not pain catastrophizing, predicts acute pain intensity, but neither factor predicts tolerance or blood pressure reactivity: An experimental investigation in pain-free individuals. *European Journal of Pain*, 10(5).

Goffaux, P., Girard-Tremblay, L., Marchand, S., Daigle, K. and Whittingstall, K. (2013) Individual Differences in Pain Sensitivity Vary as a Function of Precuneus Reactivity. *Brain Topography 2013 27:3*, 27(3).

Gogolla, N. (2017) The insular cortex. *Current Biology*, 27(12).

González-Roldán, A.M., Cifre, I., Sitges, C. and Montoya, P. (2016) Altered Dynamic of EEG Oscillations in Fibromyalgia Patients at Rest. *Pain Medicine*, 17(6).

Gopalakrishnan, R., Burgess, R.C., Lempka, S.F., Gale, J.T., Floden, D.P. and Machado, A.G. (2016a) Pain anticipatory phenomena in patients with central poststroke pain: a magnetoencephalography study. *Journal of neurophysiology*, 116(3).

Gopalakrishnan, R., Burgess, R.C., Malone, D.A., Lempka, S.F., Gale, J.T., Floden, D.P., Baker, K.B. and Machado, A.G. (2018) Deep brain stimulation of the ventral striatal area for poststroke pain syndrome: a magnetoencephalography study. *Journal of neurophysiology*, 119(6).

Gopalakrishnan, R., Burgess, R.C., Plow, E.B., Floden, D.P. and Machado, A.G. (2015) A magnetoencephalography study of multi-modal processing of pain anticipation in primary sensory cortices. *Neuroscience*, 304.

Gopalakrishnan, R., Burgess, R.C., Plow, E.B., Floden, D.P. and Machado, A.G. (2016b) Early event related fields during visually evoked pain anticipation. *Clinical Neurophysiology*, 127(3).

Gopalakrishnan, R., Machado, A.G., Burgess, R.C. and Mosher, J.C. (2013) The use of contact heat evoked potential stimulator (CHEPS) in magnetoencephalography for pain research. *Journal of neuroscience methods*, 220(1).

Goudman, L., De Groote, S., Linderoth, B., De Smedt, A., Eldabe, S., Duarte, R. V. and Moens, M. (2021) Exploration of the supraspinal hypotheses about spinal cord stimulation and dorsal root ganglion stimulation: A systematic review. *Journal of Clinical Medicine*, 10(13).

Goudman, L., Linderoth, B., Nagels, G., Huysmans, E. and Moens, M. (2019) Cortical Mapping in Conventional and High Dose Spinal Cord Stimulation: An Exploratory Power Spectrum and Functional Connectivity Analysis With Electroencephalography. *Neuromodulation: Technology at the Neural Interface*, 23(1).

Gram, M, Graversen, C., Olesen, A.E. and Drewes, A.M. (2015) Machine learning on encephalographic activity may predict opioid analgesia. *European Journal of Pain (United Kingdom)*, 19(10).

Gram, M., Graversen, C., Olesen, S. and Drewes, A.M. (2015) Dynamic spectral indices of the electroencephalogram provide new insights into tonic pain. *Clinical Neurophysiology*, 126(4).

Granot, M., Granovsky, Y., Sprecher, E., Nir, R.-R. and Yarnitsky, D. (2006) Contact heat-evoked temporal summation: Tonic versus repetitive-phasic stimulation. *Pain*, 122(3).

Granovsky, Y., Matre, D., Sokolik, A., Lorenz, J. and Casey, K.L. (2005) Thermoreceptive innervation of human glabrous and hairy skin: a contact heat evoked potential analysis. *Pain*, 115(3).

Granovsky, Y., Raz, N. and Defrin, R. (2017) Electrophysiological and psychophysical correlates of spatial summation to noxious heat: the possible role of A-delta fibers. *Experimental Brain Research*, 235(2).

Greffrath, W., Baumgärtner, U. and Treede, R.-D. (2007) Peripheral and central components of habituation of heat pain perception and evoked potentials in humans. *Pain*, 132(3).

De Groote, S., De Jaeger, M., Van Schuerbeek, P., Sunaert, S., Peeters, R., Loeckx, D., Goudman, L., Forget, P., De Smedt, A., Moens, M., Schuerbeek, P. Van, Sunaert, S., Peeters, R., Loeckx, D., Goudman, L. and Forget, P. (2018) Functional magnetic resonance imaging : cerebral function alterations in subthreshold and suprathreshold spinal cord stimulation. *Journal of Pain Research*, 11.

Groppe, D.M., Urbach, T.P. and Kutas, M. (2011) Mass Univariate Analysis of Event-Related Brain Potentials/Fields II: Simulation Studies. *Psychophysiology*, 48(12).

Gross, J., Baillet, S., Barnes, G.R., Henson, R.N., Hillebrand, A., Jensen, O., Jerbi, K., Litvak, V., Maess, B., Oostenveld, R., Parkkonen, L., Taylor, J.R., van Wassenhove, V., Wibral, M. and Schoffelen, J.-M. (2013) Good practice for conducting and reporting MEG research. *NeuroImage*, 65(100).

Gross, J., Kujala, J., Hämäläinen, M., Timmermann, L., Schnitzler, A. and Salmelin, R. (2001) Dynamic imaging of coherent sources: Studying neural interactions in the human brain. *Proceedings of the National Academy of Sciences of the United States of America*, 98(2).

Gross, J., Schnitzler, A., Timmermann, L. and Ploner, M. (2007) Gamma Oscillations in Human Primary Somatosensory Cortex Reflect Pain Perception. *PLoS Biology*, 5(5).

Gungor, N.Z. and Johansen, J. (2019) A Chronic Pain in the ACC. *Neuron*, 102(5).

Han, S., Buchman, A.S., Arfanakis, K., Fleischman, D.A. and Bennett, D.A. (2013) Functional connectivity networks associated with chronic musculoskeletal pain in old age. *International Journal of Geriatric Psychiatry*, 28(8).

Hansen, T.M., Mark, E.B., Olesen, S.S., Gram, M., Frøkjær, J.B. and Drewes, A.M. (2017) Characterization of cortical source generators based on electroencephalography during tonic pain. *Journal of Pain Research*, 10.

Hanssen, M.M., Vancleef, L.M.G., Vlaeyen, J.W.S. and Peters, M.L. (2014) More optimism, less pain! The influence of generalized and pain-specific expectations on experienced cold-pressor pain. *Journal of behavioral medicine*, 37(1).

Harat, A., Sokal, P., Zielinski, P., Harat, M., Rusicka, T. and Herbowski, L. (2012) Assessment of Economic Effectiveness in Treatment of Neuropathic Pain and Refractory Angina Pectoris Using Spinal Cord Stimulation. *Advances in Clinical and Experimental Medicine*, 21(5).

Hari, R. and Puce, A. (2017) *MEG-EEG Primer*. New York: Oxford University Press.

Hari, R. and Salmelin, R. (1997) Human cortical oscillations: a neuromagnetic view through the skull. *Trends in Neurosciences*, 20(1).

Hauck, M., Domnick, C., Lorenz, J., Gerloff, C. and Engel, A.K. (2015) Top-down and bottom-up modulation of pain-induced oscillations. *Frontiers in human neuroscience*, 9.

Haumann, N.T., Parkkonen, L., Kliuchko, M., Vuust, P. and Brattico, E. (2016) Comparing the Performance of Popular MEG/EEG Artifact Correction Methods in an Evoked-Response Study. *Computational Intelligence and Neuroscience*, 2016.

Head, H., Rivers, W.H.R., Holmes, G., Sherren, J., Thompson, T. and Riddoch, G. (1920) *Studies in neurology*. 2nd edn. Frowde & Hodder: London.

Hellström, B. and Lundberg, U. (2000) Pain perception to the cold pressor test during the menstrual cycle in relation to estrogen levels and a comparison with men. *Integrative Physiological and Behavioral Science*, 35(2).

Hines, E. and Brown, G. (1932) A Standard Stimulant for Measuring Vasomotor Reactions: Its Application in the Study of Hypertension.in *Proceedings of the Staff Meetings of the Mayo Clinic*, pp. 325–332.

Hirsh, A.T., George, S.Z., Bialosky, J.E. and Robinson, M.E. (2008) Fear of Pain, Pain Catastrophizing, and Acute Pain Perception: Relative Prediction and Timing of Assessment. *The Journal of Pain*, 9(9).

Hjermstad, M.J., Fayers, P.M., Haugen, D.F., Caraceni, A., Hanks, G.W., Loge, J.H., Fainsinger, R., Aass, N. and Kaasa, S. (2011) Studies Comparing Numerical Rating Scales, Verbal Rating Scales, and Visual Analogue Scales for Assessment of Pain Intensity in Adults: A Systematic Literature Review. *Journal of Pain and Symptom Management*, 41(6).

Holmes, C.J., Hoge, R., Collins, L., Woods, R., Toga, A.W. and Evans, A.C. (1998) Enhancement of MR images using registration for signal averaging. *Journal of computer assisted tomography*, 22(2).

Holsheimer, J. (1998) Computer modelling of spinal cord stimulation and its contribution to therapeutic efficacy. *Spinal cord*, 36(8).

Houde, F., Martel, M., Coulombe-Lévêque, A., Harvey, M.P., Auclair, V., Mathieu, D., Whittingstall, K., Goffaux, P. and Léonard, G. (2020) Perturbing the activity of the superior temporal gyrus during pain encoding prevents the exaggeration of pain memories: A virtual lesion study using single-pulse transcranial magnetic stimulation. *Neurobiology of Learning and Memory*, 169.

Hsiao, F.J., Wang, S.J., Lin, Y.Y., Fuh, J.L., Ko, Y.C., Wang, P.N. and Chen, W.T. (2017) Altered insula–default mode network connectivity in fibromyalgia: a resting-state magnetoencephalographic study. *Journal of Headache and Pain*, 18(1).

Hu, L. and Iannetti, G.D. (2019) Neural indicators of perceptual variability of pain across species. *Proceedings of the National Academy of Sciences of the United States of America*, 116(5).

Huang, G. and Zhang, Z. (2017) Improving sensitivity of cluster-based permutation test for EEG/MEG data.in *International IEEE/EMBS Conference on Neural Engineering, NER*. IEEE Computer Society, pp. 9–12.

Hudspith, M.J. (2016) Anatomy, physiology and pharmacology of pain. *Anaesthesia & Intensive Care Medicine*, 17(9).

Hüllemann, P., Nerdal, A., Sendel, M., Dodurgali, D., Forstenpointner, J., Binder, A. and Baron, R. (2019) Cold-evoked potentials versus contact heat-evoked potentials—Methodological considerations and clinical application. *European Journal of Pain*, 23(6).

Hunt, A. (2008) *Investigating activity changes in the brain in response to tonic pain stimulation*. Aston University.

Hutchison, W.D., Davis, K.D., Lozano, A.M., Tasker, R.R. and Dostrovsky, J.O. (1999) Pain-related neurons in the human cingulate cortex. *Nature Neuroscience*, 2(5).

Hylands-White, N., Duarte, R. V., Beeson, P., Mayhew, S.D. and Raphael, J.H. (2016) Electroencephalographic evoked pain response is suppressed by spinal cord stimulation in complex regional pain syndrome: a case report. *Journal of Clinical Monitoring and Computing*, 30(6).

Iacovides, S., Avidon, I. and Baker, F.C. (2015) Does pain vary across the menstrual cycle? A review. *European Journal of Pain*, 19(10).

Iannetti, G.D., Hughes, N.P., Lee, M.C. and Mouraux, A. (2008) Determinants of laser-evoked EEG responses: pain perception or stimulus saliency? *Journal of neurophysiology*, 100(2).

Iannetti, G.D., Zambreanu, L., Cruccu, G. and Tracey, I. (2005) Operculoinsular cortex encodes pain intensity at the earliest stages of cortical processing as indicated by amplitude of laser-evoked potentials in humans. *Neuroscience*, 131(1).

Iannetti, G.D., Zambreanu, L. and Tracey, I. (2006) Similar nociceptive afferents mediate psychophysical and electrophysiological responses to heat stimulation of glabrous and hairy skin in humans. *Journal of Physiology*, 577(1).

Inui, K., Tran, T.D., Qiu, Y., Wang, X., Hoshiyama, M. and Kakigi, R. (2003) A comparative magnetoencephalographic study of cortical activations evoked by noxious and innocuous somatosensory stimulations. *Neuroscience*, 120(1).

Ioannides, A.A., Liu, M.J., Liu, L.C., Bamidis, P.D., Hellstrand, E. and Stephan, K.M. (1995) Magnetic field tomography of cortical and deep processes: examples of 'real-time mapping' of averaged and single trial MEG signals. *International Journal of Psychophysiology*, 20(3).

Irvine, K.A. and David Clark, J. (2018) Chronic pain after traumatic brain injury: Pathophysiology and pain mechanisms. *Pain Medicine*, 19(7).

Iwamoto, S., Tamura, M., Sasaki, A. and Nawano, M. (2021) Dynamics of neuronal oscillations underlying nociceptive response in the mouse primary somatosensory cortex. *Scientific Reports*, 11.

Jaiswal, A., Nenonen, J., Stenroos, M., Gramfort, A., Dalal, S.S., Westner, B.U., Litvak, V., Mosher, J.C., Schoffelen, J.M., Witton, C., Oostenveld, R. and Parkkonen, L. (2020) Comparison of beamformer implementations for MEG source localization. *NeuroImage*, 216.

Jann, K., Dierks, T., Boesch, C., Kottlow, M., Strik, W. and Koenig, T. (2009) BOLD correlates of EEG alpha phase-locking and the fMRI default mode network. *NeuroImage*, 45(3).

Jardín, I., López, J.J., Diez, R., Sánchez-Collado, J., Cantonero, C., Albarrán, L., Woodard, G.E., Redondo, P.C., Salido, G.M., Smani, T. and Rosado, J.A. (2017) TRPs in pain sensation. *Frontiers in Physiology*, 8.

Jasrotia, R., Kanchan, A., Harsoda, J., Saini, R. and Agarwal, M. (2018) Pain sensitivity and cardiovascular reactivity to the experimental induced cold pressor pain during different phases of menstrual cycle in young Indian females. *National Journal of Physiology, Pharmacy and Pharmacology*, 8(5).

Jensen, O. and Hesse, C. (2010) Estimating Distributed Representations of Evoked Responses and oscillatory Brain Activity.in Hansen, P., Kringelbach, M., and Salmelin, R. (eds) *MEG: An Introduction to Methods*. New York: Oxford University Press.

Jeon, Y. and Huh, B.K. (2009) Spinal Cord Stimulation for Chronic Pain. *Annals Academy of Medicine Singapore*, 38(11).

Jin, Y., Meng, Q., Mei, L., Zhou, W., Zhu, X., Mao, Y., Xie, W., Zhang, X., Luo, M.H., Tao, W., Wang, H., Li, Jie, Li, Juan, Li, X. and Zhang, Z. (2020) A somatosensory cortex input to the caudal dorsolateral striatum controls comorbid anxiety in persistent pain. *Pain*, 161(2).

Jones, A., Spindler, H., Jørgensen, M.M. and Zachariae, R. (2002) The effect of situation–evoked anxiety and gender on pain report using the cold pressor test. *Scandinavian Journal of Psychology*, 43(4).

Kakeda, T., Ogino, Y., Moriya, F. and Saito, S. (2010) Sweet taste-induced analgesia: An fMRI study. *NeuroReport*, 21(6).

Kasch, H., Qerama, E., Bach, F.W. and Jensen, T.S. (2005) Reduced cold pressor pain tolerance in non-recovered whiplash patients: a 1-year prospective study. *European Journal of Pain*, 9(5).

Kay, A.D., McIntyre, M.D., Macrae, W.A. and Varma, T.R.K. (2001) Spinal cord stimulation - a long-term evaluation in patients with chronic pain. *British Journal of Neurosurgery*, 15(4).

Kim, H.J., Lee, J.I., Kang, K.T., Chang, B.S., Lee, C.K., Ruscheweyh, R., Kang, S.S. and Yeom, J.S. (2015) Influence of pain sensitivity on surgical outcomes after lumbar spine surgery in patients with lumbar spinal stenosis. *Spine*, 40(3).

Kim, J.A. and Davis, K.D. (2021) Neural Oscillations: Understanding a Neural Code of Pain. *The Neuroscientist*, 27(5).

Kim, J.Y., Kim, Seong Ho, Seo, J., Kim, Sang Hyon, Han, S.W., Nam, E.J., Kim, S.K., Lee, H.J., Lee, S.J., Kim, Y.T. and Chang, Y. (2013) Increased power spectral density in resting-state pain-related brain networks in fibromyalgia. *Pain*, 154(9).

Kishima, H., Saitoh, Y., Oshino, S., Hosomi, K., Ali, M., Maruo, T., Hirata, M., Goto, T., Yanagisawa, T., Sumitani, M., Osaki, Y., Hatazawa, J. and Yoshimine, T. (2010) Modulation of neuronal activity after spinal cord stimulation for neuropathic pain; (H2O)-O-15 PET study. *Neuroimage*, 49(3).

Klein, C. (2015) What Pain Asymbolia Really Shows. *Mind*, 124(494).

Koenig, J., Jarczok, M.N., Ellis, R.J., Bach, C., Thayer, J.F. and Hillecke, T.K. (2014a) Two-Week Test-Retest Stability of the Cold Pressor Task Procedure at two different Temperatures as a Measure of Pain Threshold and Tolerance. *Pain Practice*, 14(3).

Koenig, J., Jarczok, M.N., Ellis, R.J., Hillecke, T.K. and Thayer, J.F. (2014b) Heart rate variability and experimentally induced pain in healthy adults: a systematic review. *European Journal of Pain*, 18(3).

Korczyn, A.D., Schachter, S.C., Brodie, M.J., Dalal, S.S., Engel, J., Guekht, A., Hecimovic, H., Jerbi, K., Kanner, A.M., Johannessen Landmark, C., Mares, P., Marusic, P., Meletti, S., Mula, M., Patsalos, P.N., Reuber, M., Ryvlin, P., Štillová, K., Tuchman, R. and Rektor, I. (2013) Epilepsy, cognition, and neuropsychiatry (Epilepsy, Brain, and Mind, part 2). *Epilepsy & Behavior*, 28(2).

Kowalczyk, W.J., Evans, S.M., Bisaga, A.M., Sullivan, M.A. and Comer, S.D. (2006) Sex differences and hormonal

influences on response to cold pressor pain in humans. *The Journal of Pain*, 7(3).

Kramer, J.L.K., Taylor, P., Haefeli, J., Blum, J., Zariffa, J., Curt, A. and Steeves, J. (2012) Test–Retest Reliability of Contact Heat-Evoked Potentials From Cervical Dermatomes. *Journal of Clinical Neurophysiology*, 29(1).

Kropf, E., Syan, S.K., Minuzzi, L. and Frey, B.N. (2018) From anatomy to function: the role of the somatosensory cortex in emotional regulation. *Brazilian Journal of Psychiatry*, 41(3).

Kumar, K., Taylor, R.S., Jacques, L., Eldabe, S., Meglio, M., Molet, J., Thomson, S., O'Callaghan, J., Eisenberg, E., Milbouw, G., Buchser, E., Fortini, G., Richardson, J. and North, R.B. (2008) The effects of spinal cord stimulation in neuropathic pain are sustained: A 24-month follow-up of the prospective randomized controlled multicenter trial of the effectiveness of spinal cord stimulation. *Neurosurgery*, 63(4).

Kumar, K., Wilson, J.R., Taylor, R.S. and Gupta, S. (2006) Complications of spinal cord stimulation, suggestions to improve outcome, and financial impact. *Journal of Neurosurgery-Spine*, 5(3).

Kwan, C.L., Crawley, A.P., Mikulis, D.J. and Davis, K.D. (2000) An fMRI study of the anterior cingulate cortex and surrounding medial wall activations evoked by noxious cutaneous heat and cold stimuli. *Pain*, 85(3).

Lang, E., Krainick, J.U. and Gerbershagen, H.U. (1989) Spinal cord transmission of impulses during high spinal anesthesia as measured by cortical evoked potentials. *Anesthesia and Analgesia*, 69(1).

Lapotka, M., Ruz, M., Ballesteros, A.S. and Hernández, O.O. (2017) Cold pressor gel test: A safe alternative to the cold pressor test in fMRI. *Magnetic Resonance in Medicine*, 78(4).

Larson, S.J., Sances, A., Riegel, D.H., Meyer, G.A., Dallmann, D.E. and Swiontek, T. (1974) Neurophysiological effects of dorsal column stimulation in man and monkey. *Journal of Neurosurgery*, 41(2).

Lautenbacher, S., Spernal, J., Schreiber, W. and Krieg, J.C. (1999) Relationship between clinical pain complaints and pain sensitivity in patients with depression and panic disorder. *Psychosomatic medicine*, 61(6).

Lenz, F.A., Rios, M., Zirh, A., Chau, D., Krauss, G. and Lesser, R.P. (1998) Painful Stimuli Evoke Potentials Recorded Over the Human Anterior Cingulate Gyrus. *Journal of Neurophysiology*, 79(4).

Levi, V., Cordella, R., D'Ammando, A., Tringali, G., Dones, I., Messina, G. and Franzini, A. (2019) Dorsal anterior cingulate cortex (ACC) deep brain stimulation (DBS): a promising surgical option for the treatment of refractory thalamic pain syndrome (TPS). *Acta neurochirurgica*, 161(8).

Li, C., Liu, S., Lu, X., Feng, T. (2019) Role of Descending Dopaminergic Pathways in Pain Modulation. *Current Neuropharmacology*, 17(12).

Liberati, G., Algoet, M., Santos, S.F., Ribeiro-Vaz, J.G., Raftopoulos, C. and Mouraux, A. (2019) Tonic thermonociceptive stimulation selectively modulates ongoing neural oscillations in the human posterior insula: Evidence from intracerebral EEG. *NeuroImage*, 188.

Liberati, G., Klöcker, A., Algoet, M., Mulders, D., Maia Safronova, M., Ferrao Santos, S., Ribeiro Vaz, J.-G., Raftopoulos, C. and Mouraux, A. (2018) Gamma-Band Oscillations Preferential for Nociception can be Recorded in the Human Insula. *Cerebral cortex*, 28(10).

Lighthall, N.R., Sakaki, M., Vasunilashorn, S., Nga, L., Somayajula, S., Chen, E.Y., Samii, N. and Mather, M. (2012) Gender differences in reward-related decision processing under stress. *Social Cognitive and Affective Neuroscience*, 7(4).

Lim, M., Kim, J.S., Kim, D.J. and Chung, C.K. (2016) Increased low-and high-frequency oscillatory activity in the prefrontal cortex of fibromyalgia patients. *Frontiers in Human Neuroscience*, 10.

Linde, L.D., Haefeli, J., Jutzeler, C.R., Rosner, J., McDougall, J., Curt, A. and Kramer, J.L.K. (2020) Contact Heat Evoked Potentials Are Responsive to Peripheral Sensitization: Requisite Stimulation Parameters. *Frontiers in Human Neuroscience*, 13.

Linderoth, B., Cui, J.-G., Yakhnitsa, V., Shi, T.-J.S., Stiller, C.-O., O'Connor, W.T., Holmin, S., Mathiesen, T., Sollevi, A., Hökfelt, T. and Meyerson, B.A. (2000) Neurotransmitter and Inflammatory Correlates in Experimental Neuropathy:

Modulation by Electric Spinal Cord Stimulation.in Saade, N.E., Apkarian, A. V, and Jabbur, S.J. (eds) *Pain and Neuroimmune Interactions*. Boston, MA: Springer US, pp. 57–68.

Linderoth, B. and Foreman, R.D. (2017) Conventional and Novel Spinal Stimulation Algorithms: Hypothetical Mechanisms of Action and Comments on Outcomes. *Neuromodulation: Technology at the Neural Interface*, 20(6).

Lindholm, P., Lamusuo, S., Taiminen, T., Pesonen, U., Lahti, A., Virtanen, A., Forssell, H., Hietala, J., Hagelberg, N., Pertovaara, A., Parkkola, R. and Jääskeläinen, S. (2015) Right secondary somatosensory cortex-a promising novel target for the treatment of drug-resistant neuropathic orofacial pain with repetitive transcranial magnetic stimulation. *Pain*, 156(7).

Liu, Y., Latremoliere, A., Li, X., Zhang, Z., Chen, M., Wang, X., Fang, C., Zhu, J., Alexandre, C., Gao, Z., Chen, B., Ding, X., Zhou, J.-Y., Zhang, Y., Chen, C., Wang, K.H., Woolf, C.J. and He, Z. (2018) Touch and tactile neuropathic pain sensitivity are set by corticospinal projections. *Nature*, 561(7724).

Lleó, A. (2021) Biomarkers in neurological disorders: a fast-growing market. *Brain Communications*, 3(2).

Lockwood, P.L., Iannetti, G.D. and Haggard, P. (2013) Transcranial magnetic stimulation over human secondary somatosensory cortex disrupts perception of pain intensity. *Cortex*, 49(8).

Lugo, A., Ferrer-Fuertes, A., Isabel Correa, L., Campolo, M., Casanova-Molla, J. and Valls-Sole, J. (2018) Clinical utility of contact heat evoked potentials (CHEPs) in a case of mentalis nerve lesion. *Clinical Neurophysiology Practice*, 3.

Lundeland, B., Toennis, M., Züchner, M., Janerås, L., Stubhaug, A. and Hansson, P. (2021) Spinal cord stimulation for the treatment of peripheral neuropathic pain. *Tidsskrift for Den norske legeforening*, 141(9).

Luo, Y., Yan, C., Huang, T., Fan, M., Liu, L., Zhao, Z., Ni, K., Jiang, H., Huang, X., Lu, Z., Wu, W., Zhang, M. and Fan, X. (2016) Altered Neural Correlates of Emotion Associated Pain Processing in Persistent Somatoform Pain Disorder: An fMRI Study. *Pain Practice*, 16(8).

Lyu, Y., Zidda, F., Radev, S.T., Liu, H., Guo, X., Tong, S., Flor, H. and Andoh, J. (2022) Gamma Band Oscillations Reflect Sensory and Affective Dimensions of Pain. *Frontiers in Neurology*, 12.

Machado, A.G., Gopalakrishnan, R., Plow, E.B., Burgess, R.C. and Mosher, J.C. (2014) A magnetoencephalography study of visual processing of pain anticipation. *Journal of neurophysiology*, 112(2).

Majedi, H., Dehghani, S.S., Soleyman-Jahi, S., Tafakhori, A., Emami, S.A., Mireskandari, M. and Hosseini, S.M. (2019) Assessment of Factors Predicting Inadequate Pain Management in Chronic Pain Patients. *Anesthesiology and Pain Medicine*, 9(6).

Maris, E. and Oostenveld, R. (2007) Nonparametric statistical testing of EEG- and MEG-data. *Journal of Neuroscience Methods*, 164(1).

Martin, R.M. (2019) Influence of biological sex, trait gender, and state gender on pain threshold, pain tolerance, and ratings of pain severity. *Personality and Individual Differences*, 138.

Mayhew, S.D., Hylands-White, N., Porcaro, C., Derbyshire, S.W.G.G. and Bagshaw, A.P. (2013) Intrinsic variability in the human response to pain is assembled from multiple, dynamic brain processes. *Neuroimage*, 75.

Mazzola, L., Isnard, J. and Mauguière, F. (2006) Somatosensory and Pain Responses to Stimulation of the Second Somatosensory Area (SII) in Humans. A Comparison with SI and Insular Responses. *Cerebral Cortex*, 16(7).

Mazzola, L., Isnard, J., Peyron, R. and Mauguière, F. (2012) Stimulation of the human cortex and the experience of pain: Wilder Penfield's observations revisited. *Brain*, 135(2).

Mazzonea, P., Pisania, R., Piziob, N., Arrigoc, A. and Nobilic, F. (1994) Cerebral blood flow and somatosensory evoked response changes induced by spinal cord stimulation: Preliminary follow-up observations. *Stereotactic and Functional Neurosurgery*, 62(1–4).

McCarberg, B. and Peppin, J. (2019) Pain Pathways and Nervous System Plasticity: Learning and Memory in Pain. *Pain Medicine*, 20(12).

McCarthy, K.F., Connor, T.J. and McCrory, C. (2013) Cerebrospinal Fluid Levels of Vascular Endothelial Growth Factor Correlate With Reported Pain and Are Reduced by Spinal Cord Stimulation in Patients With Failed Back Surgery Syndrome. *Neuromodulation*, 16(6).

McClure, J.J., Desai, B.D., Ampie, L., You, W., Smith, J.S. and Buchholz, A.L. (2021) A Systematic Review of the Cost-Utility of Spinal Cord Stimulation for Persistent Low Back Pain in Patients With Failed Back Surgery Syndrome. *Global Spine Journal*, 11.

McMahon, S., Koltzenburg, M., Tracey, I. and Turk, D. (2013) *Wall and Melzack's Textbook of Pain*. 6th edn. Saunders.

Meda, K.S., Patel, T., Braz, J.M., Malik, R., Turner, M.L., Seifikar, H., Basbaum, A.I. and Sohal, V.S. (2019) Microcircuit Mechanisms through which Mediodorsal Thalamic Input to Anterior Cingulate Cortex Exacerbates Pain-Related Aversion. *Neuron*, 102(5).

Medvedovsky, M., Taulu, S., Bikmullina, R., Ahonen, A. and Paetau, R. (2009) Fine tuning the correlation limit of spatio-temporal signal space separation for magnetoencephalography. *Journal of Neuroscience Methods*, 177(1).

Mekhail, N., Levy, R.M., Deer, T.R., Kapural, L., Li, S., Amirdelfan, K., Hunter, C.W., Rosen, S.M., Costandi, S.J., Falowski, S.M., Burgher, A.H., Pope, J.E., Gilmore, C.A., Qureshi, F.A., Staats, P.S., Scowcroft, J., Carlson, J., Kim, C.K., Yang, M.I., Stauss, T., Poree, L., Brounstein, D., Gorman, R., Gmel, G.E., Hanson, E., Karantonis, D.M., Khurram, A., Kiefer, D., Leitner, A., Mugan, D., Obradovic, M., Parker, J., Single, P. and Soliday, N. (2020) Long-term safety and efficacy of closed-loop spinal cord stimulation to treat chronic back and leg pain (Evoke): a double-blind, randomised, controlled trial. *The Lancet Neurology*, 19(2).

Melzack, R. (1990) Phantom limbs and the concept of a neuromatrix. *Trends in Neurosciences*, 13(3).

Melzack, R. (1999) From the gate to the neuromatrix. *Pain*, 82(Supplement 1).

Melzack, R. and Wall, P.D. (1965) Pain mechanisms: a new theory. *Science (New York, N.Y.)*, 150(3699).

Mendell, L.M. (2022) The Path to Discovery of Windup and Central Sensitization. *Frontiers in Pain Research*, 3.

Messaritaki, E., Koelewijn, L., Dima, D.C., Williams, G.M., Perry, G. and Singh, K.D. (2017) Assessment and elimination of the effects of head movement on MEG resting-state measures of oscillatory brain activity. *NeuroImage*, 159.

Meuwissen, K.P.V., Toorn, A. van der, Gu, J.W., Zhang, T.C., Dijkhuizen, R.M. and Joosten, E.A.J. (2020) Active Recharge Burst and Tonic Spinal Cord Stimulation Engage Different Supraspinal Mechanisms: A Functional Magnetic Resonance Imaging Study in Peripherally Injured Chronic Neuropathic Rats. *Pain Practice*, 20(5).

Meyerson, B., Sagher, O., North, R.B., Kumar, K., Hunter, G., Demeria, D., Krishna, K. and Demeria, D. (2006) Spinal cord stimulation in treatment of chronic benign pain: Challenges in treatment planning and present status, a 22-year experience. *Neurosurgery*, 58(3).

Miller, J.P., Eldabe, S., Buchser, E., Johanek, L.M., Guan, Y. and Linderoth, B. (2016) Parameters of Spinal Cord Stimulation and Their Role in Electrical Charge Delivery: A Review. *Neuromodulation*, 19(4).

Miron, D., Duncan, G.H. and Catherine Bushnell, M. (1989) Effects of attention on the intensity and unpleasantness of thermal pain. *Pain*, 39(3).

Mitchell, L.A., MacDonald, R.A.R. and Brodie, E.E. (2004) Temperature and the cold pressor test. *The journal of pain*, 5(4).

Mitsi, V. and Zachariou, V. (2016) Modulation of pain, nociception, and analgesia by the brain reward center. *Neuroscience*, 338.

Modares-Haghighi, P., Boostani, R., Nami, M. and Sanei, S. (2021) Quantification of pain severity using EEG-based functional connectivity. *Biomedical Signal Processing and Control*, 69.

Montgomery, S.A. and Asberg, M. (1979) A new depression scale designed to be sensitive to change. *British Journal of Psychiatry*, 134(4).

Moseley, G.L. (2003) A pain neuromatrix approach to patients with chronic pain. *Manual Therapy*, 8(3).

Mouraux, A. and Iannetti, G.D. (2009) Nociceptive Laser-Evoked Brain Potentials Do Not Reflect Nociceptive-Specific Neural Activity. *Journal of Neurophysiology*, 101(6).

Mouraux, A. and Iannetti, G.D. (2018) The search for pain biomarkers in the human brain. *Brain*, 141(12).

Mouraux, A., De Paepe, A.L., Marot, E., Plaghki, L., Iannetti, G.D. and Legrain, V. (2013) Unmasking the obligatory components of nociceptive event-related brain potentials. *Journal of Neurophysiology*, 110(10).

Mouraux, A. and Plaghki, L. (2006) Are the processes reflected by late and ultra-late laser evoked potentials specific of nociception? *Supplements to Clinical neurophysiology*, 59.

Mu, Y., Fan, Y., Mao, L. and Han, S. (2008) Event-related theta and alpha oscillations mediate empathy for pain. *Brain research*, 1234.

Nagamachi, S., Fujita, S., Nishii, R., Futami, S., Wakamatsu, H., Yano, T., Kodama, T., Tamura, S., Kunitake, A., Uno, T. and Takasaki, M. (2006) Alteration of regional cerebral blood flow in patients with chronic pain - Evaluation before and after epidural spinal cord stimulation. *Annals of Nuclear Medicine*, 20(4).

National Heart, Lung and Blood Institute (2021) Study Quality Assessment Tools. Available at: https://www.nhlbi.nih.gov/health-topics/study-quality-assessment-tools [Accessed 22 January 2023].

Nevian, T. (2017) The cingulate cortex: divided in pain. *Nature Neuroscience*, 20(11).

Nickel, M.M., May, E.S., Tiemann, L., Schmidt, P., Postorino, M., Ta Dinh, S., Gross, J. and Ploner, M. (2017) Brain oscillations differentially encode noxious stimulus intensity and pain intensity. *Neuroimage*, 148.

Nielsen, C.S., Staud, R. and Price, D.D. (2009) Individual Differences in Pain Sensitivity: Measurement, Causation, and Consequences. *The Journal of Pain*, 10(3).

Nielsen, C.S., Stubhaug, A., Price, D.D., Vassend, O., Czajkowski, N. and Harris, J.R. (2008) Individual differences in pain sensitivity: Genetic and environmental contributions. *Pain*, 136(1).

Nim, C.G., Kawchuk, G.N., Schiøttz-Christensen, B. and O'Neill, S. (2020) The effect on clinical outcomes when targeting spinal manipulation at stiffness or pain sensitivity: a randomized trial. *Scientific Reports 2020 10:1*, 10(1).

Nir, R.R., Sinai, A., Moont, R., Harari, E. and Yarnitsky, D. (2012) Tonic pain and continuous EEG: Prediction of subjective pain perception by alpha-1 power during stimulation and at rest. *Clinical Neurophysiology*, 123(3).

Nir, R.R., Sinai, A., Raz, E., Sprecher, E. and Yarnitsky, D. (2010) Pain assessment by continuous EEG: association between subjective perception of tonic pain and peak frequency of alpha oscillations during stimulation and at rest. *Brain research*, 1344.

Niso, G., Tjepkema-Cloostermans, M.C., Lenders, M.W.P.M. and de Vos, C.C. (2021) Modulation of the Somatosensory Evoked Potential by Attention and Spinal Cord Stimulation. *Frontiers in Neurology*, 12.

Oaks, Z., Stage, A., Middleton, B., Faraone, S. and Johnson, B. (2018) Clinical Utility of the Cold Pressor Test: Evaluation of Pain Patients and Treatment of Opioid-Induced Hyperalgesia and Fibromyalgia with Low Dose Naltrexone. *Discovery Medicine*, 26(114).

Okada, T., Kato, D., Nomura, Y., Obata, N., Quan, X., Morinaga, A., Yano, H., Guo, Z., Aoyama, Y., Tachibana, Y., Moorhouse, A.J., Matoba, O., Takiguchi, T., Mizobuchi, S. and Wake, H. (2021) Pain induces stable, active microcircuits in the somatosensory cortex that provide a therapeutic target. *Science Advances*, 7(12).

Oostenveld, R., Fries, P., Maris, E. and Schoffelen, J.M. (2011) FieldTrip: Open source software for advanced analysis of MEG, EEG, and invasive electrophysiological data. *Computational Intelligence and Neuroscience*, 2011.

Oosterman, J.M., Dijkerman, H.C., Kessels, R.P.C. and Scherder, E.J.A. (2010) A unique association between cognitive inhibition and pain sensitivity in healthy participants. *European journal of pain*, 14(10).

Opsommer, E., Korogod, N., Stockinger, L. and Landmann, G. (2021) Multimodal sensory evaluation of neuropathic spinal cord injury pain: an experimental study. *Spinal Cord*, 59(8).

Ossipov, M.H., Morimura, K. and Porreca, F. (2014) Descending pain modulation and chronification of pain. *Current Opinion in Supportive and Palliative Care*, 8(2).

Ostrom, C., Bair, E., Maixner, W., Dubner, R., Fillingim, R.B., Ohrbach, R., Slade, G.D. and Greenspan, J.D. (2017) Demographic Predictors of Pain Sensitivity: Results From the OPPERA Study. *The Journal of Pain*, 18(3).

Page, M.J., McKenzie, J.E., Bossuyt, P.M., Boutron, I., Hoffmann, T.C., Mulrow, C.D., Shamseer, L., Tetzlaff, J.M., Akl, E.A., Brennan, S.E., Chou, R., Glanville, J., Grimshaw, J.M., Hróbjartsson, A., Lalu, M.M., Li, T., Loder, E.W., Mayo-Wilson, E., McDonald, S., McGuinness, L.A., Stewart, L.A., Thomas, J., Tricco, A.C., Welch, V.A., Whiting, P. and Moher, D. (2021) The PRISMA 2020 statement: an updated guideline for reporting systematic reviews. *BMJ*, 372.

Pahapill, P.A. and Zhang, W.B. (2014) Restoration of Altered Somatosensory Cortical Representation With Spinal Cord Stimulation Therapy in a Patient With Complex Regional Pain Syndrome: A Magnetoencephalography Case Study. *Neuromodulation*, 17(1).

Pahapill and Zhang (2014) Restoration of altered somatosensory cortical representation with spinal cord stimulation therapy in a patient with complex regional pain syndrome: a magnetoencephalography case study. *Neuromodulation : journal of the International Neuromodulation Society*, 17(1).

Palermo, S., Benedetti, F., Costa, T. and Amanzio, M. (2015) Pain anticipation: An activation likelihood estimation meta-analysis of brain imaging studies. *Human Brain Mapping*, 36(5).

Panchuelo, R.M.S., Eldeghaidy, S., Marshall, A., McGlone, F., Francis, S.T. and Favorov, O. (2020) A nociresponsive specific area of human somatosensory cortex within BA3a: BA3c? *NeuroImage*, 221.

Parkkonen, L. and Salmelin, R. (2010) Measurements.in Hansen, P., Kringelbach, M., and Salmelin, Riitta (eds) *MEG: An Introduction to Methods*. Oxford University Press, pp. 1–448.

Patanwala, A.E., Norwood, C., Steiner, H., Morrison, D., Li, M., Walsh, K., Martinez, M., Baker, S.E., Snyder, E.M. and Karnes, J.H. (2019) Psychological and Genetic Predictors of Pain Tolerance. *Clinical and Translational Science*, 12(2).

Patestas, M. and Gartner, L. (2006) *A Textbook of Neuroanatomy*. 2nd edn. Hoboken: Wiley-Blackwell.

De Pauw, R., Coppieters, I., Caeyenberghs, K., Kregel, J., Aerts, H., Lenoir, D. and Cagnie, B. (2019) Associations between brain morphology and motor performance in chronic neck pain: A whole-brain surface-based morphometry approach. *Human Brain Mapping*, 40(14).

Peciña, M., Love, T., Stohler, C.S., Goldman, D. and Zubieta, J.-K. (2015) Effects of the Mu Opioid Receptor Polymorphism (OPRM1 A118G) on Pain Regulation, Placebo Effects and Associated Personality Trait Measures. *Neuropsychopharmacology*, 40(4).

Peckerman, A., Saab, P.G., McCabe, P.M., Skyler, J.S., Winters, R.W., Llabre, M.M. and Schneiderman, N. (1991) Blood pressure reactivity and perception of pain during the forehead cold pressor test. *Psychophysiology*, 28(5).

Peng, W. and Tang, D. (2016) Pain Related Cortical Oscillations: Methodological Advances and Potential Applications. *Frontiers in computational neuroscience*, 10.

Petkova, M. and Nikolov, V. (2018) Gender Differences in Perception of Pain and Body Awareness in Athletes and Normally Active Subjects. *LUMEN Proceedings*, 3.

Peyron, R. and Fauchon, C. (2019) The posterior insular-opercular cortex: An access to the brain networks of thermosensory and nociceptive processes? *Neuroscience letters*, 702.

Peyron, R., Laurent, B. and Garcia-Larrea, L. (2000) Functional imaging of brain responses to pain. A review and meta-analysis. *Clinical Neurophysiology*, 30.

Ploghaus, A., Tracey, I., Gati, J.S., Clare, S., Menon, R.S., Matthews, P.M., Rawlins, J.N., Rose, R.M. and Cohen, J.D. (1999) Dissociating Pain from Its Anticipation in the Human Brain. *Science*, 284(5422).

Ploner, M., Gross, J., Timmermann, L. and Schnitzler, A. (2002) Cortical representation of first and second pain sensation in humans. *Proceedings of the National Academy of Sciences of the United States of America*, 99(19).

Ploner, M., Schmitz, F., Freund, H.-J. and Schnitzler, A. (1999) Parallel Activation of Primary and Secondary Somatosensory Cortices in Human Pain Processing. *Journal of Neurophysiology*, 81(6).

Pluijms, W.A., Slangen, R., van Kleef, M., Joosten, E.A. and Reulen, J.P.H. (2015a) Increased Contact Heat Evoked Potential Stimulation Latencies in Responders to Spinal Cord Stimulation for Painful Diabetic Polyneuropathy. *Neuromodulation: Technology at the Neural Interface*, 18(2).

Pluijms, W.A., Slangen, R., Van Kleef, M., Joosten, E.A. and Reulen, J.P.H. (2015b) Increased contact heat evoked potential stimulation latencies in responders to spinal cord stimulation for painful diabetic polyneuropathy. *Neuromodulation*, 18(2).

Poláček, H., Kozák, J., Vrba, I., Vrána, J. and Stančák, A. (2007) Effects of spinal cord stimulation on the cortical somatosensory evoked potentials in failed back surgery syndrome patients. *Clinical Neurophysiology*, 118(6).

Porcelli, A.J. (2014) An Alternative to the Traditional Cold Pressor Test: The Cold Pressor Arm Wrap. *Journal of Visualized Experiments*, (83).

Pralong, E., Pollo, C., Bloch, J., Villemure, J.-G., Daniel, R.T., Tétreault, M.-H. and Debatisse, D. (2004) Recording of ventral posterior lateral thalamus neuron response to contact heat evoked potential in patient with neurogenic pain. *Neuroscience Letters*, 367(3).

Price, D.D. (2000) Psychological and Neural Mechanisms of the Affective Dimension of Pain. *Science*, 288(5472).

Pud, D., Golan, Y. and Pesta, R. (2009) Hand dominancy—A feature affecting sensitivity to pain. *Neuroscience Letters*. 467(3).

Quraan, M. (2011) Characterization of Brain Dynamics Using Beamformer Techniques: Advantages and Limitations.in Pang, E. (ed.) *Magnetoencephalography*. London: InTech, pp. 67–92.

Rahim-Williams, F.B., Riley, J.L., III, Herrera, D., Campbell, C., Hastie, B.A. and Fillingim, R.B. (2007) Ethnic Identity Predicts Experimental Pain Sensitivity In African Americans and Hispanics. *Pain*, 129(1–2).

Rainville, P. (2002) Brain mechanisms of pain affect and pain modulation. *Current Opinion in Neurobiology*, 12(2).

Rasche, D., Siebert, S., Stippich, C., Kress, B., Nennig, E., Sartor, K. and Tronnier, N.M. (2005) Spinal cord stimulation in Failed-Back-Surgery-Syndrome. Preliminary study for the evaluation of therapy by functional magnetic resonance imaging (fMRI). *Schmerz*, 19(6).

Ravn, P., Frederiksen, R., Skovsen, A.P., Christrup, L.L. and Werner, M.U. (2012) Prediction of pain sensitivity in healthy volunteers. *Journal of Pain Research*, 5.

Rees, H. and Roberts, M.H. (1989) Antinociceptive effects of dorsal column stimulation in the rat: involvement of the anterior pretectal nucleus. *The Journal of Physiology*, 417(1).

De Ridder, D. and Vanneste, S. (2016) Burst and Tonic Spinal Cord Stimulation: Different and Common Brain Mechanisms. *Neuromodulation: Technology at the Neural Interface*, 19(1).

Rigoard, P., Ounajim, A., Goudman, L., Bouche, B., Roulaud, M., Page, P., Lorgeoux, B., Baron, S., Nivole, K., Many, M., Adjali, N., Charrier, E., Rannou, D., Poupin, L., Wood, C., David, R., Héraud, D., Moens, M. and Billot, M. (2021) The Added Value of Subcutaneous Peripheral Nerve Field Stimulation Combined with SCS, as Salvage Therapy, for Refractory Low Back Pain Component in Persistent Spinal Pain Syndrome Implanted Patients: A Randomized Controlled Study (CUMPNS Study) Based on 3. *Journal of Clinical Medicine*, 10(21).

Riley 3rd, J.L., King, C.D., Wong, F., Fillingim, R.B. and Mauderli, A.P. (2010) Lack of endogenous modulation and reduced decay of prolonged heat pain in older adults. *Pain*, 150(1).

Roberts, K., Papadaki, A., Gonçalves, C., Tighe, M., Atherton, D., Shenoy, R., McRobbie, D. and Anand, P. (2008) Contact heat evoked potentials using simultaneous EEG and fMRI and their correlation with evoked pain. *BMC Anesthesiology*, 8(1).

Roebuck, G.S., Urquhart, D.M., Knox, L., Fitzgerald, P.B., Cicuttini, F.M., Lee, S. and Fitzgibbon, B.M. (2018) Psychological Factors Associated With Ultramarathon Runners' Supranormal Pain Tolerance: A Pilot Study. *The*

Journal of Pain, 19(12).

Rosner, J., Hostettler, P., Scheuren, P.S., Sirucek, L., Rinert, J., Curt, A., Kramer, J.L.K., Jutzeler, C.R. and Hubli, M. (2018a) Normative data of contact heat evoked potentials from the lower extremities. *Scientific Reports*, 8(1).

Rosner, J., Hubli, M., Hostettler, P., Scheuren, P.S., Rinert, J., Kramer, J.L.K., Hupp, M., Curt, A. and Jutzeler, C.R. (2018b) Contact heat evoked potentials: Reliable acquisition from lower extremities. *Clinical Neurophysiology*, 129(3).

Rossiter, H.E., Worthen, S.F., Witton, C., Hall, S.D. and Furlong, P.L. (2013) Gamma oscillatory amplitude encodes stimulus intensity in primary somatosensory cortex. *Frontiers in Human Neuroscience*, 7.

Ruscheweyh, R., Dany, K., Marziniak, M. and Gralow, I. (2015) Basal Pain Sensitivity does not Predict the Outcome of Multidisciplinary Chronic Pain Treatment. *Pain Medicine*, 16(8).

Ruscheweyh, R., Stumpenhorst, F., Knecht, S. and Marziniak, M. (2010) Comparison of the Cold Pressor Test and Contact Thermode-Delivered Cold Stimuli for the Assessment of Cold Pain Sensitivity. *The Journal of Pain*, 11(8).

Saber, M., Schwabe, D., Park, H.-J., Tessmer, J., Khan, Z., Ding, Y., Robinson, M., Hogan, Q.H. and Pawela, C.P. (2022) Tonic, Burst, and Burst-Cycle Spinal Cord Stimulation Lead to Differential Brain Activation Patterns as Detected by Functional Magnetic Resonance Imaging. *Neuromodulation: Technology at the Neural Interface*, 25(1).

Sankarasubramanian, V., Harte, S.E., Chiravuri, S., Harris, R.E., Brummett, C.M., Patil, P.G., Clauw, D.J. and Lempka, S.F. (2019) Objective Measures to Characterize the Physiological Effects of Spinal Cord Stimulation in Neuropathic Pain: A Literature Review. *Neuromodulation: Technology at the Neural Interface*, 22(2).

Sarlani, E. and Greenspan, J.D. (2002) Gender differences in temporal summation of mechanically evoked pain. *Pain*, 97(1–2).

Sassenhagen, J. and Draschkow, D. (2019) Cluster-based permutation tests of MEG/EEG data do not establish significance of effect latency or location. *Psychophysiology*, 56(6).

Sato, K.L., King, E.W., Johanek, L.M. and Sluka, K.A. (2013) Spinal cord stimulation reduces hypersensitivity through activation of opioid receptors in a frequency-dependent manner. *European Journal of Pain*, 17(4).

Schaworonkow, N. and Nikulin, V. V. (2022) Is sensor space analysis good enough? Spatial patterns as a tool for assessing spatial mixing of EEG/MEG rhythms. *NeuroImage*, 253.

Schmidt, N.B. and Cook, J.H. (1999) Effects of anxiety sensitivity on anxiety and pain during a cold pressor challenge in patients with panic disorder. *Behaviour Research and Therapy*, 37(4).

De Schoenmacker, I., Berry, C., Blouin, J.-S., Rosner, J., Hubli, M., Jutzeler, C.R. and Kramer, J.L.K. (2021) An intensity matched comparison of laser- and contact heat evoked potentials. *Scientific Reports*, 11(1).

Schulman, J., Ramirez, R., Zonenshayn, M., Ribary, U. and Llinas, R. (2005) Thalamocortical dysrhythmia syndrome: MEG imaging of neuropathic pain. *Thalamus and Related Systems*, 3(01).

Schulz, E., Zherdin, A., Tiemann, L., Plant, C. and Ploner, M. (2012) Decoding an Individual's Sensitivity to Pain from the Multivariate Analysis of EEG Data. *Cerebral Cortex*, 22(5).

Schwier, C., Kliem, A., Boettger, M.K. and Bär, K.-J. (2010) Increased cold-pain thresholds in major depression. *The Journal of Pain*, 11(3).

Sdrulla, A.D., Xu, Q., He, S.-Q., Tiwari, V., Yang, F., Zhang, C., Shu, B., Shechter, R., Raja, S.N., Wang, Y., Dong, X. and Guan, Y. (2015) Electrical stimulation of low-threshold afferent fibers induces a prolonged synaptic depression in lamina II dorsal horn neurons to high-threshold afferent inputs in mice. *Pain*, 156(6).

Seeley, W.W., Menon, V., Schatzberg, A.F., Keller, J., Glover, G.H., Kenna, H., Reiss, A.L. and Greicius, M.D. (2007) Dissociable Intrinsic Connectivity Networks for Salience Processing and Executive Control. *Journal of Neuroscience*, 27(9).

Sevel, L.S., Letzen, J.E., Staud, R. and Robinson, M.E. (2016) Interhemispheric Dorsolateral Prefrontal Cortex

Connectivity is Associated with Individual Differences in Pain Sensitivity in Healthy Controls. *Brain Connectivity*, 6(5).

Shackman, A.J., Salomons, T. V., Slagter, H.A., Fox, A.S., Winter, J.J. and Davidson, R.J. (2011) The integration of negative affect, pain and cognitive control in the cingulate cortex. *Nature Reviews Neuroscience*, 12(3).

Shao, S., Shen, K., Yu, K., Wilder-Smith, E.P.V. V and Li, X. (2012) Frequency-domain EEG source analysis for acute tonic cold pain perception. *Clinical Neurophysiology*, 123(10).

Shealy, C., Mortimer, J. and Reswick, J. (1967) Electrical inhibition of pain by stimulation of the dorsal columns: preliminary clinical report. *Anesthesia & Analgesia*, 46(4).

Shiers, S.I., Sankaranarayanan, I., Jeevakumar, V., Cervantes, A., Reese, J.C. and Price, T.J. (2021) Convergence of peptidergic and non-peptidergic protein markers in the human dorsal root ganglion and spinal dorsal horn. *Journal of Comparative Neurology*, 914(10).

Shigihara, Y., Hoshi, H., Fukasawa, K., Ichikawa, S., Kobayashi, M., Sakamoto, Y., Negishi, K., Haraguchi, R. and Konno, S. (2021) Resting-State Magnetoencephalography Reveals Neurobiological Bridges Between Pain and Cognitive Impairment. *Pain and Therapy*, 10(1).

Shils, J.L. and Arle, J.E. (2018) Neuromonitoring for Spinal Cord Stimulation Lead Placement Under General Anesthesia. *Journal of Clinical Neurology*, 14(4).

Sindou, M.P., Mertens, P., Bendavid, U., García-Larrea, L. and Mauguière, F. (2003) Predictive value of somatosensory evoked potentials for long-lasting pain relief after spinal cord stimulation: practical use for patient selection. *Neurosurgery*, 52(6).

Singh, S. (2014) Magnetoencephalography: Basic principles. *Annals of Indian Academy of Neurology*, 17(5).

Sivanesan, E., Maher, D.P., Raja, S.N., Linderoth, B. and Guan, Y. (2019) Supraspinal Mechanisms of Spinal Cord Stimulation for Modulation of Pain: Five Decades of Research and Prospects for the Future. *Anesthesiology*. Lippincott Williams and Wilkins, pp. 651–665.

Sivertsen, B., Lallukka, T., Petrie, K.J., Steingrímsdóttir, Ó.A., Stubhaug, A. and Nielsen, C.S. (2015) Sleep and pain sensitivity in adults. *Pain*, 156(8).

Snyder, C.R., Berg, C., Woodward, J.T., Gum, A., Rand, K.L., Wrobleski, K.K., Brown, J. and Hackman, A. (2005) Hope Against the Cold: Individual Differences in Trait Hope and Acute Pain Tolerance on the Cold Pressor Task. *Journal of Personality*, 73(2).

Song, G.H., Venkatraman, V., Ho, K.Y., Chee, M.W.L., Yeoh, K.G. and Wilder-Smith, C.H. (2006) Cortical effects of anticipation and endogenous modulation of visceral pain assessed by functional brain MRI in irritable bowel syndrome patients and healthy controls. *Pain*, 126(1–3).

Song, Z., Ansah, O.B., Meyerson, B.A., Pertovaara, A. and Linderoth, B. (2013) Exploration of supraspinal mechanisms in effects of spinal cord stimulation: Role of the locus coeruleus. *Neuroscience*, 253.

Song, Z., Meyerson, B.A. and Linderoth, B. (2011) Spinal 5-HT receptors that contribute to the pain-relieving effects of spinal cord stimulation in a rat model of neuropathy. *Pain*, 152(7).

Song, Z., Ultenius, C., Meyerson, B.A. and Linderoth, B. (2009) Pain relief by spinal cord stimulation involves serotonergic mechanisms: An experimental study in a rat model of mononeuropathy. *Pain*, 147(1).

Spisak, T., Kincses, B., Schlitt, F., Zunhammer, M., Schmidt-Wilcke, T., Kincses, Z.T. and Bingel, U. (2020) Pain-free resting-state functional brain connectivity predicts individual pain sensitivity. *Nature Communications*, 11(1).

Stančák, A., Kozák, J., Vrba, I., Tintěra, J., Vrána, J., Poláček, H., Stančák, M., Stancak, A., Kozak, J., Vrba, I., Tintera, J., Vrana, J., Polacek, H. and Stancak, M. (2008) Functional magnetic resonance imaging of cerebral activation during spinal cord stimulation in failed back surgery syndrome patients. *European Journal of Pain*, 12(2).

Stančák, A., Poláček, H., Vrána, J. and Mlynář, J. (2007) Cortical oscillatory changes during warming and heating in humans. *Neuroscience*, 147(3).

Staud, R., Godfrey, M.M., Mejia, M., Ramanlal, R., Riley, J.L. and Robinson, M.E. (2020) Usefulness of Ramp & Hold Procedures for Testing of Pain Facilitation in Human Participants: Comparisons With Temporal Summation of Second Pain. *Journal of Pain*, 21(3–4).

Steeds, C.E. (2016) The anatomy and physiology of pain. *Surgery*, 34(2).

Stening, K., Eriksson, O., Wahren, L., Berg, G., Hammar, M. and Blomqvist, A. (2007) Pain sensations to the cold pressor test in normally menstruating women: comparison with men and relation to menstrual phase and serum sex steroid levels. *American Journal of Physiology-Regulatory, Integrative and Comparative Physiology*, 293(4).

Stephens, R., Atkins, J. and Kingston, A. (2009) Swearing as a response to pain. *NeuroReport*, 20(12).

Stern, J., Jeanmonod, D. and Sarnthein, J. (2006) Persistent EEG overactivation in the cortical pain matrix of neurogenic pain patients. *Neuroimage*, 31(2).

Stiller, C.O., Linderoth, B., T. O'Connor, W., Franck, J., Falkenberg, T., Ungerstedt, U. and Brodin, E. (1995) Repeated spinal cord stimulation decreases the extracellular level of γ-aminobutyric acid in the periaqueductal gray matter of freely moving rats. *Brain Research*, 699(2).

Stolk, A., Todorovic, A., Schoffelen, J.M. and Oostenveld, R. (2013) Online and offline tools for head movement compensation in MEG. *NeuroImage*, 68.

Sufianov, A., Shapkin, A., Sufianova, G., Elishev, V., Barashin, D., Berdichevskii, V. and Churkin, S. (2014) Functional and Metabolic Changes in the Brain in Neuropathic Pain Syndrome against the Background of Chronic Epidural Electrostimulation of the Spinal Cord. *Bulletin of Experimental Biology and Medicine*, 157(4).

Sullivan, M., Bishop, S. and Pivik, J. (1995) The pain catastrophizing scale: development and validation. *Psychological assessment*, 7(4).

Sun, B., Wang, H., Chen, Z., Cui, F., Yang, F. and Huang, X. (2022) Contact Heat Evoked Potentials in China: Normal Values and Reproducibility. *Frontiers in Human Neuroscience*, 15.

Sung, S., Vijiaratnam, N., Chan, D.W.C., Farrell, M. and Evans, A.H. (2018) Pain sensitivity in Parkinson's disease: Systematic review and meta-analysis. *Parkinsonism & Related Disorders*, 48.

Tan, L.L., Oswald, M.J., Heinl, C., Retana Romero, O.A., Kaushalya, S.K., Monyer, H. and Kuner, R. (2019) Gamma oscillations in somatosensory cortex recruit prefrontal and descending serotonergic pathways in aversion and nociception. *Nature communications*, 10(1).

Tan, L.L., Pelzer, P., Heinl, C., Tang, W., Gangadharan, V., Flor, H., Sprengel, R., Kuner, T. and Kuner, R. (2017) A pathway from midcingulate cortex to posterior insula gates nociceptive hypersensitivity. *Nature neuroscience*, 20(11).

Tarkka, I.M. and Treede, R.-D. (1993) Equivalent Electrical Source Analysis of Pain-Related Somatosensory Evoked Potentials Elicited by a CO2 Laser. *Journal of Clinical Neurophysiology*, 10(4).

Taulu, S. (2008) *Processing of Weak Magnetic Multichannel Signals: The Signal Space Separation Method*. Helsinki University of Technology.

Taulu, S. and Hari, R. (2009) Removal of magnetoencephalographic artifacts with temporal signal-space separation: Demonstration with single-trial auditory-evoked responses. *Human Brain Mapping*, 30(5).

Taulu, S. and Simola, J. (2006) Spatiotemporal signal space separation method for rejecting nearby interference in MEG measurements. *Physics in Medicine and Biology*, 51(7).

Taulu, S., Simola, J. and Kajola, M. (2004) MEG recordings of DC fields using the signal space separation method (SSS). *Neurology & Clinical Neurophysiology*, 35.

Tazawa, T., Kamiya, Y., Kobayashi, A., Saeki, K., Takiguchi, M., Nakahashi, Y., Shinbori, H., Funakoshi, K. and Goto, T. (2015) Spinal cord stimulation modulates supraspinal centers of the descending antinociceptive system in rats with unilateral spinal nerve injury. *Molecular Pain*, 11.

Telkes, L., Hancu, M., Paniccioli, S., Grey, R., Briotte, M., Mccarthy, K., Raviv, N. and Pilitsis, J.G. (2020) Differences in EEG patterns between tonic and high frequency spinal cord stimulation in chronic pain patients. *Clinical Neurophysiology*, 131.

Tesarz, J., Gerhardt, A., Schommer, K., Treede, R.-D. and Eich, W. (2013) Alterations in endogenous pain modulation in endurance athletes: An experimental study using quantitative sensory testing and the cold-pressor task. *Pain*, 154(7).

Testani, E., Le Pera, D., Del Percio, C., Miliucci, R., Brancucci, A., Pazzaglia, C., De Armas, L., Babiloni, C., Rossini, P.M. and Valeriani, M. (2015) Cortical inhibition of laser pain and laser-evoked potentials by non-nociceptive somatosensory input. *European Journal of Neuroscience*, 42(7).

Theuvenet, P.J., Dunajski, Z., Peters, M.J., Van Ree, J.M., Dunajskh, Z., Petersa, M.J. and Van Ree, J.M. (1999) Responses to median and tibial nerve stimulation in patients with chronic neuropathic pain. *Brain Topography*, 11(4).

Tiemann, L., Schulz, E., Gross, J. and Ploner, M. (2010) Gamma oscillations as a neuronal correlate of the attentional effects of pain. *Pain*, 150(2).

Tilley, D.M., Vallejo, R., Kelley, C.A., Benyamin, R. and Cedeno, D.L. (2015) A Continuous Spinal Cord Stimulation Model Attenuates Pain-Related Behavior In Vivo Following Induction of a Peripheral Nerve Injury. *Neuromodulation*, 18(3).

Timmermann, L., Ploner, M., Haucke, K., Schmitz, F., Baltissen, R. and Schnitzler, A. (2001) Differential Coding of Pain Intensity in the Human Primary and Secondary Somatosensory Cortex. *Journal of Neurophysiology*, 86(3).

Timmers, I., Kaas, A.L., Quaedflieg, C.W.E.M., Biggs, E.E., Smeets, T. and de Jong, J.R. (2018) Fear of pain and cortisol reactivity predict the strength of stress-induced hypoalgesia. *European Journal of Pain*, 22(7).

Todd, A.J. (2010) Neuronal circuitry for pain processing in the dorsal horn. *Nature Reviews Neuroscience*, 11(12).

Tracey, I. and Mantyh, P.W. (2007) The cerebral signature for pain perception and its modulation. *Neuron*, 55(3).

Treede, R.D. (2016) Gain control mechanisms in the nociceptive system. *Pain*, 157(6).

El Tumi, H., Johnson, M.I., Dantas, P.B.F., Maynard, M.J. and Tashani, O.A. (2017) Age-related changes in pain sensitivity in healthy humans: A systematic review with meta-analysis. *European Journal of Pain*, 21(6).

Tzourio-Mazoyer, N., Landeau, B., Papathanassiou, D., Crivello, F., Etard, O., Delcroix, N., Mazoyer, B. and Joliot, M. (2002) Automated anatomical labeling of activations in SPM using a macroscopic anatomical parcellation of the MNI MRI single-subject brain. *NeuroImage*, 15(1).

Uddin, L.Q. (2015) Salience processing and insular cortical function and dysfunction. *Nature Reviews Neuroscience*, 16(1).

Urasaki, E., Tsuda, M., Nakane, S., Toyoda, K., Umeno, T. and Yamakawa, Y. (2014) Spinal cord stimulation for intractable pain evaluated by a collision study using somatosensory evoked potentials: A preliminary report. *Neuromodulation*, 17(8).

Uusitalo, M.A. and Ilmoniemi, R.J. (1997) Signal-space projection method for separating MEG or EEG into components. *Medical and Biological Engineering and Computing*, 35(2).

Vachon-Presseau, E., Martel, M.-O., Roy, M., Caron, E., Albouy, G., Marin, M.-F., Plante, I., Sullivan, M.J., Lupien, S.J. and Rainville, P. (2013) Acute Stress Contributes to Individual Differences in Pain and Pain-Related Brain Activity in Healthy and Chronic Pain Patients. *Journal of Neuroscience*, 33(16).

Valentini, E., Halder, S., McInnerney, D., Cooke, J., Gyimes, I.L. and Romei, V. (2022) Assessing the specificity of the relationship between brain alpha oscillations and tonic pain. *NeuroImage*, 255.

Valmunen, T., Pertovaara, A., Taiminen, T., Virtanen, A., Parkkola, R. and Jääskeläinena, S. (2009) Modulation of facial sensitivity by navigated rTMS in healhy subjects. *Pain*, 142(1–2).

Veréb, D., Kincses, B., Spisák, T., Schlitt, F., Szabó, N., Faragó, P., Kocsis, K., Bozsik, B., Tóth, E., Király, A., Zunhammer, M., Schmidt-Wilcke, T., Bingel, U. and Kincses, Z.T. (2021) Resting-state functional heterogeneity of the right insula contributes to pain sensitivity. *Scientific Reports*, 11(1).

Vierck, C.J., Whitsel, B.L., Favorov, O. V, Brown, A.W. and Tommerdahl, M. (2013) Role of primary somatosensory cortex in the coding of pain. *Pain*, 154(3).

Vigil, J.M. and Coulombe, P. (2011) Biological sex and social setting affects pain intensity and observational coding of other people's pain behaviors. *Pain*, 152(9).

Vigil, J.M., Rowell, L.N., Alcock, J. and Maestes, R. (2014) Laboratory personnel gender and cold pressor apparatus affect subjective pain reports. *Pain Research and Management*, 19(1).

Villemure, C. and Bushnell, M.C. (2009) Mood influences supraspinal pain processing separately from attention, 29(3).

Visnjevac, O., Costandi, S., Patel, B.A., Azer, G., Agarwal, P., Bolash, R. and Mekhail, N.A. (2017) A Comprehensive Outcome-Specific Review of the Use of Spinal Cord Stimulation for Complex Regional Pain Syndrome. *Pain Practice*, 17(4).

Vogt, B.A. (2005) Pain and emotion interactions in subregions of the cingulate gyrus. *Nature Reviews Neuroscience*, 6(7).

de Vries, M., Wilder-Smith, O.H.G., Jongsma, M.L.A., van den Broeke, E.N., Arns, M., van Goor, H. and van Rijn, C.M. (2013) Altered resting state EEG in chronic pancreatitis patients: Toward a marker for chronic pain. *Journal of Pain Research*, 6.

Wang, A.L., Mouraux, A., Liang, M. and Iannetti, G.D. (2010) Stimulus Novelty, and Not Neural Refractoriness, Explains the Repetition Suppression of Laser-Evoked Potentials. *Journal of Neurophysiology*, 104(4).

Wang, L., Xiao, Y., Urman, R.D. and Lin, Y. (2020) Cold pressor pain assessment based on EEG power spectrum. *SN Applied Sciences*, 2(12).

Weigel, R., Capelle, H.H., Flor, H. and Krauss, J.K. (2015) Event-Related Cortical Processing in Neuropathic Pain under Long-Term Spinal Cord Stimulation. *Pain Physician*, 18(2).

Weingarten, T.N., Sprung, J., Ackerman, J.D., Bojanic, K., Watson, J.C. and Dyck, P.J. (2006) Anesthesia and patients with congenital hyposensitivity to pain. *Anesthesiology*, 105(2).

Weisse, C.S., Foster, K.K. and Fisher, E.A. (2005) The Influence of Experimenter Gender and Race on Pain Reporting: Does Racial or Gender Concordance Matter? *Pain Medicine*, 6(1).

Werner, M.U., Mjöbo, H.N., Nielsen, P.R. and Rudin, Å. (2010) Prediction of Postoperative Pain. *Anesthesiology*, 112(6).

Westner, B.U., Dalal, S.S., Gramfort, A., Litvak, V., Mosher, J.C., Oostenveld, R. and Schoffelen, J.M. (2022) A unified view on beamformers for M/EEG source reconstruction. *NeuroImage*, 246.

Wiech, K., Lin, C. -s., Brodersen, K.H., Bingel, U., Ploner, M. and Tracey, I. (2010) Anterior Insula Integrates Information about Salience into Perceptual Decisions about Pain. *Journal of Neuroscience*, 30(48).

Witjes, B., Ottenheym, L.A., Huygen, F.J.P.M. and de Vos, C.C. (2023) A Review of Effects of Spinal Cord Stimulation on Spectral Features in Resting-State Electroencephalography. *Neuromodulation: Technology at the Neural Interface*, 26(1).

Wolter, T., Kieselbach, K., Sircar, R. and Gierthmuehlen, M. (2013) Spinal cord stimulation inhibits cortical somatosensory evoked potentials significantly stronger than transcutaneous electrical nerve stimulation. *Pain Physician*, 16(4).

Woolrich, M., Hunt, L., Groves, A. and Barnes, G. (2011) MEG beamforming using Bayesian PCA for adaptive data covariance matrix regularization. *NeuroImage*, 57(4).

Worthen, S.F., Hobson, A.R., Hall, S.D., Aziz, Q. and Furlong, P.L. (2011) Primary and secondary somatosensory cortex responses to anticipation and pain: a magnetoencephalography study. *European Journal of Neuroscience*, 33(5).

Yakhnitsa, V., Linderoth, B. and Meyerson, B.A. (1999) Spinal cord stimulation attenuates dorsal horn neuronal hyperexcitability in a rat model of mononeuropathy. *Pain*, 79(2).

Yasuda, Y., Hashimoto, R., Nakae, A., Kang, H., Ohi, K., Yamamori, H., Fujimoto, M., Hagihira, S. and Takeda, M. (2016) Sensory cognitive abnormalities of pain in autism spectrum disorder: A case-control study. *Annals of General Psychiatry*, 15(1).

Yezierski, R.P. (2012) The Effects of Age on Pain Sensitivity: Preclinical Studies. *Pain Medicine*, 13.

You, H.J., Lei, J. and Pertovaara, A. (2022) Thalamus: The 'promoter' of endogenous modulation of pain and potential therapeutic target in pathological pain. *Neuroscience & Biobehavioral Reviews*, 139.

Yuan, R., Di, X., Taylor, P.A., Gohel, S., Tsai, Y.-H. and Biswal, B.B. (2016) Functional topography of the thalamocortical system in human. *Brain structure & function*, 221(4).

Zahari, Z., Lee, C.S., Ibrahim, M.A., Musa, N., Mohd Yasin, M.A., Lee, Y.Y., Tan, S.C., Mohamad, N. and Ismail, R. (2016) Comparison of Pain Tolerance between Opioid Dependent Patients on Methadone Maintenance Therapy (MMT) and Opioid Naive Individuals. *Journal of Pharmacy & Pharmaceutical Sciences*, 19(1).

Zhang, J., Cavanaugh, D.J., Nemenov, M.I. and Basbaum, A.I. (2013) The modality-specific contribution of peptidergic and non-peptidergic nociceptors is manifest at the level of dorsal horn nociresponsive neurons. *The Journal of physiology*, 591(4).

Zunhammer, M., Schweizer, L.M., Witte, V., Harris, R.E., Bingel, U. and Schmidt-Wilcke, T. (2016) Combined glutamate and glutamine levels in pain-processing brain regions are associated with individual pain sensitivity. *Pain*, 157(10).

9. Appendices

Appendix A – Frequency power reconstruction of SSEP in SCS-on and SCS-off

Exploratory source visualisation was performed to localise differences in oscillatory power across frequency bands during SSEPs. Due to time window limitations, high-resolution time-frequency analysis was not possible, so a window of 0-0.3s was chosen for comparison with the pre-stimulus time window to identify any frequency changes in the SSEP source reconstruction. No statistics were performed for comparison.

In participant 1, delta and theta activity in the contralateral primary and secondary sensory cortices, the premotor cortex and temporal lobe were greater during the SSEPs. No changes were identified in any other frequency band. These changes are shown in Figure (9.1).

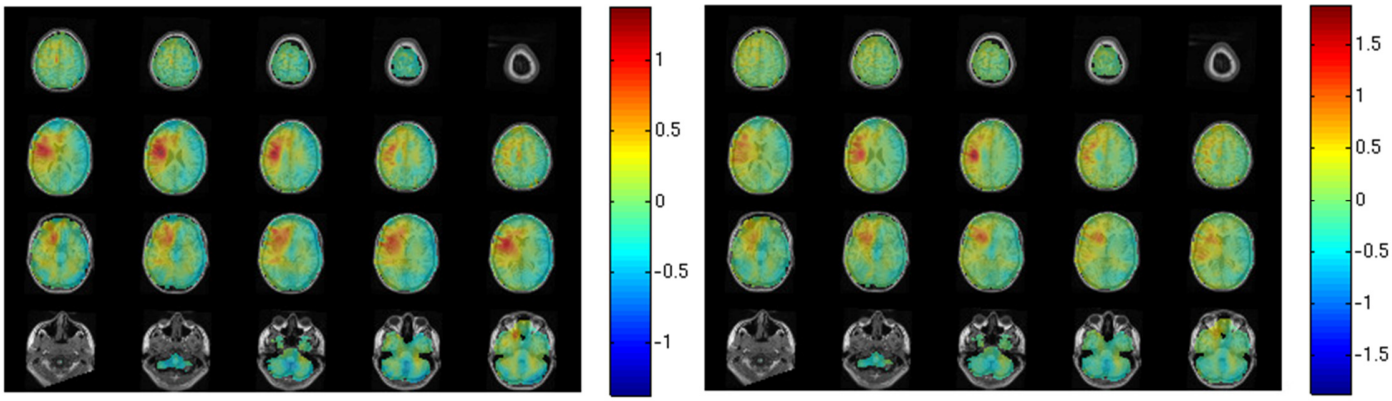

Figure 9.1: Delta (left) and theta (right) activity in the post-stimulus time window in SCS-on compared to SCS-off.

In participant 2, alpha power increased in contralateral primary and secondary sensory cortices, and temporal lobe. In participant 3, gamma power increased over the contralateral somatosensory cortex and primary motor area, with diffuse depression of alpha and theta power globally. In participant 4, beta power was enhanced in the ipsilateral somatosensory cortices, and gamma was enhanced in the ipsilateral secondary somatosensory cortex and temporal lobe. Suppression of beta and gamma power was observed in frontal cortices.

Appendix B – Systematic review appendices and supplementary table

Appendix B.1 Search strategy for systematic review:

Databases	**Date**	**Results**
MEDLINE (Ovid)	01/04/2020	120
Cochrane	01/04/2020	14
Embase (Ovid)	01/04/2020	241
CINAHL (EBSCOhost)	01/04/2020	42
PsycINFO (EBSCOhost)	01/04/2020	65
SportDISCUS (EBSCOhost)	01/04/2020	5
Scopus	01/04/2020	132
Google Scholar	01/04/2020	27
	Total	646
	Unique refs in Endnote	370
	Duplicate res in Endnote	276

Table 10.1: Search summary for systematic review

MEDLINE

1. "contact heat".af.
2. "CHEP".af.
3. "CHEPS".af.
4. "Medoc Pathway".af.
5. or/1-4
6. exp Magnetoencephalography/
7. "magnetoencephalo*".af.
8. MEG*.af.
9. exp Electroencephalography/
10. "EEG*".af.
11. electroencephalo*.af.
12. dipole.af.
13. "evoked potential*".af.
14. oscillat*.af.
15. exp evoked potentials/
16. or/6-15
17. 5 and 16
18. exp Pain/
19. pain*.af.
20. nocicept*.af.
21. or/18-20
22. 17 and 21
23. limit 22 to english language

Cochrane

#1 ("contact heat")

#2 ("CHEP")

#3 ("CHEPS")

#4 ("Medoc Pathway")

#5 {OR #1-#4}

#6 MeSH descriptor: [Magnetoencephalography] explode all trees

#7 ("magnetoencephalo*")

#8 (MEG)

#9 MeSH descriptor: [Electroencephalography] explode all trees

#10 ("EEG*")

#11 (electroencephalo*)

#12 (dipole)

#13 ("evoked potential*")

#14 (oscillat*)

#15 MeSH descriptor: [Evoked Potentials] explode all trees

#16 {OR #6-#15}

#17 #5 AND #16

EMBASE

1. "contact heat".af.

2. "CHEP".af.

3. "CHEPS".af.

4. "Medoc Pathway".af.

5. 1 or 2 or 3 or 4

6. exp magnetoencephalography/

7. "magnetoencephalo*".af.

8. MEG*.af.

9. exp electroencephalography/

10. "EEG*".af.

11. electroencephalo*.af.

12. dipole.af.
13. "evoked potential*".af.
14. oscillat*.af.
15. exp evoked response/
16. or/6-15
17. 5 and 16
18. exp pain/
19. pain*.af.
20. nocicept*.af.
21. or/18-20
22. 17 and 21
23. limit 22 to english language

CINAHL

S1 "contact heat"
S2 "CHEP"
S3 "CHEPS"
S4 "Medoc Pathway"
S5 S1 OR S2 OR S3 OR S4
S6 "magnetoencephalo*"
S7 MEG*
S8 "EEG*"
S9 electroencephalo*
S10 dipole
S11 "evoked potential*"
S12 oscillat*
S13 S6 OR S7 OR S8 OR S9 OR S10 OR S11 OR S12
S14 S5 AND S13

S15 (MH "Pain+")

S16 pain*

S17 nocicept*

S18 S15 OR S16 OR S17

S19 S14 AND S18

PsycINFO

S1 "contact heat"

S2 "CHEP"

S3 "CHEPS"

S4 "Medoc Pathway"

S5 S1 OR S2 OR S3 OR S4

S6 DE "Magnetoencephalography"

S7 "magnetoencephalo*"

S8 MEG*

S9 DE "Electroencephalography" OR DE "Alpha Rhythm" OR DE "Beta Rhythm" OR DE "Delta Rhythm" OR DE "Gamma Rhythm" OR DE "Theta Rhythm"

S10 "EEG*"

S11 electroencephalo*

S12 dipole

S13 "evoked potential*"

S14 oscillat*

S15 DE "Evoked Potentials" OR DE "Auditory Evoked Potentials" OR DE "Contingent Negative Variation" OR DE "Error-Related Negativity" OR DE "Mismatch Negativity" OR DE "Olfactory Evoked Potentials" OR DE "P300" OR DE "Somatosensory Evoked Potentials" OR DE "Visual Evoked Potentials"

S16 S6 OR S7 OR S8 OR S9 OR S10 OR S11 OR S12 OR S13 OR S14 OR S15

S17 S5 AND S16

SportDISCUS

S1 "contact heat"

S2 "CHEP"

S3 "CHEPs"

S4 "Medoc Pathway"

S5 S1 OR S2 OR S3 OR S4

S6 Magnetoencephalo*

S7 MEG*

S8 EEG*

S9 electroencephalo*

S10 dipole

S11 "evoked potential*"

S12 oscillat*

S13 DE "EVOKED potentials (Electrophysiology)"

S14 S6 OR S7 OR S8 OR S9 OR S10 OR S11 OR S12 OR S13

S15 S5 AND S13

Scopus

(TITLE-ABS-KEY ("contact heat" OR chep OR cheps OR "Medoc Pathway") AND TITLE-ABS-KEY (magnetoencephalo* OR meg* OR electroencephalo* OR eeg OR dipole OR "evoked potential*" OR oscillat*) AND TITLE-ABS-KEY (pain* OR nocicept*)) AND (LIMIT-TO (LANGUAGE , "English"))

Directory of Open Access

"contact heat" OR chep OR cheps OR "Medoc Pathway

Google Scholar

allintitle: pain chep OR cheps OR "Medoc Pathway" OR "contact heat evoked potentials"

allintitle: nociceptive chep OR cheps OR "Medoc Pathway" OR "contact heat evoked potentials"

Appendix B.2 Risk of bias assessment table

Table 10.2: Risk of bias assessment table

	1	2	3	4	5	6	7	8	9	10
Adjamian 2009	Y	N	N	CD	Y	Y	Y	Y	Y	N/A
Gopalakrishnan 2013	Y	Y	N/A	Y	Y	Y	Y	N/A	Y	N/A
Machado 2014	Y	Y	N	Y	Y	Y	Y	Y	Y	N
Gopalakrishnan 2015	Y	Y	N	Y	Y	Y	Y	Y	Y	Y
Gopalakrishnan 2016a	Y	Y	N	Y	Y	Y	Y	Y	Y	N
Gopalakrishna 2016b	Y	Y	N	Y	Y	Y	Y	Y	Y	N
Fardo 2017	Y	Y	N	Y	Y	Y	Y	Y	Y	Y
Gopalakrishnan 2018	Y	Y	N	Y	Y	Y	Y	Y	Y	N

1. Was the study question or objective clearly stated? 2 Was the study population clearly and fully described, including case definition? 3. Were the cases consecutive? 4. Were the subjects comparable? 5. Was the experimental procedure clearly described? 6. Were the outcome measures clearly defined, valid, reliable and implemented consistently across all study participants? 7. Was the duration of the experiment appropriate? 8. Were the statistical methods well-described? 9. Were the results well-described? 10. Were the conditions sufficiently counterbalanced or randomised? Y = Yes, N = No, N/A = Not applicable, CD = Cannot determine.

Appendix C – Chapter seven study four, CHEPS artefact attenuation

Appendix C.1 Independent Component Analysis outputs for various stages of data cleaning

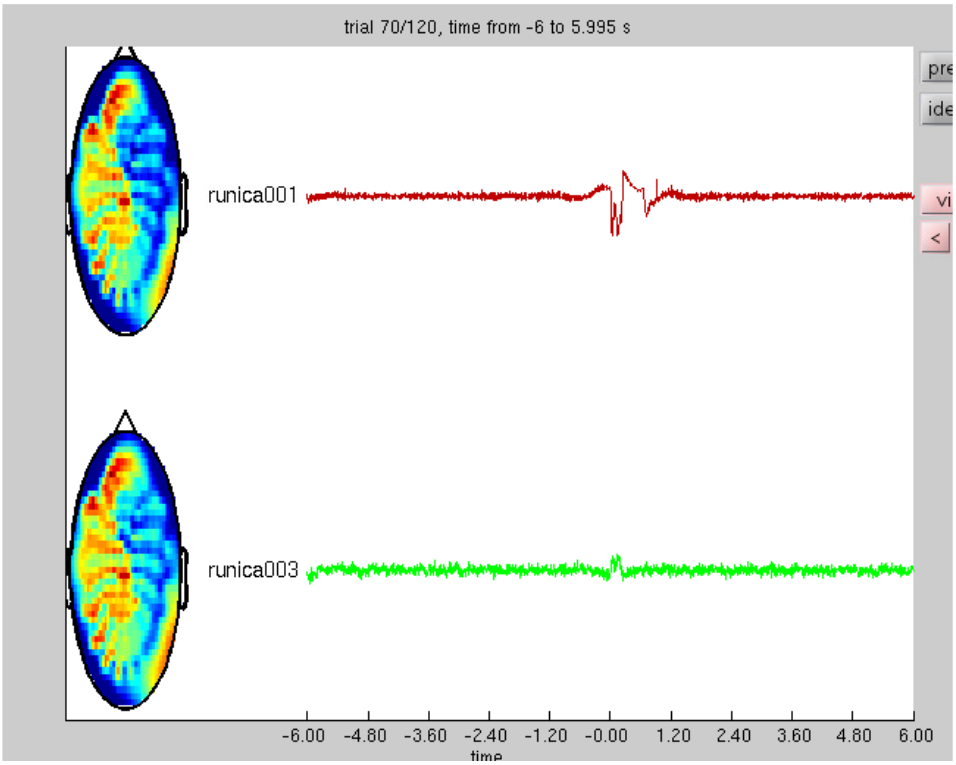

Figure 9.2: FieldTrip output of select raw empty room data components with stimulus-locked characteristics.

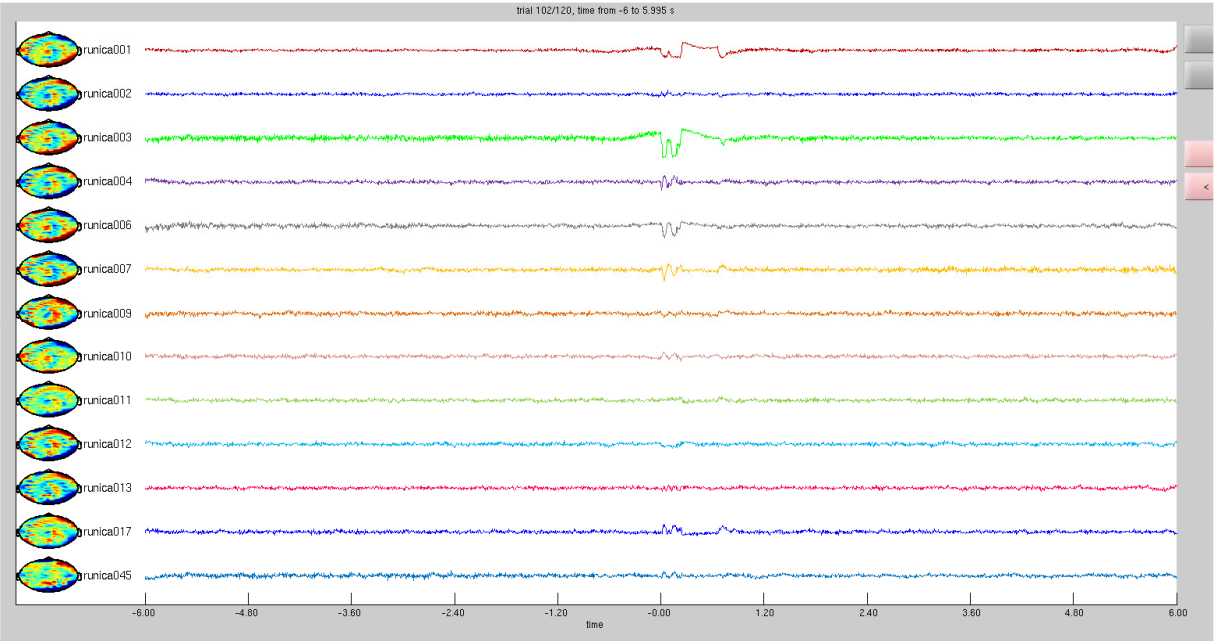

Figure 9.4: FieldTrip output of select SSS-cleaned empty room components with stimulus-locked characteristics

tSSS 0.98 components

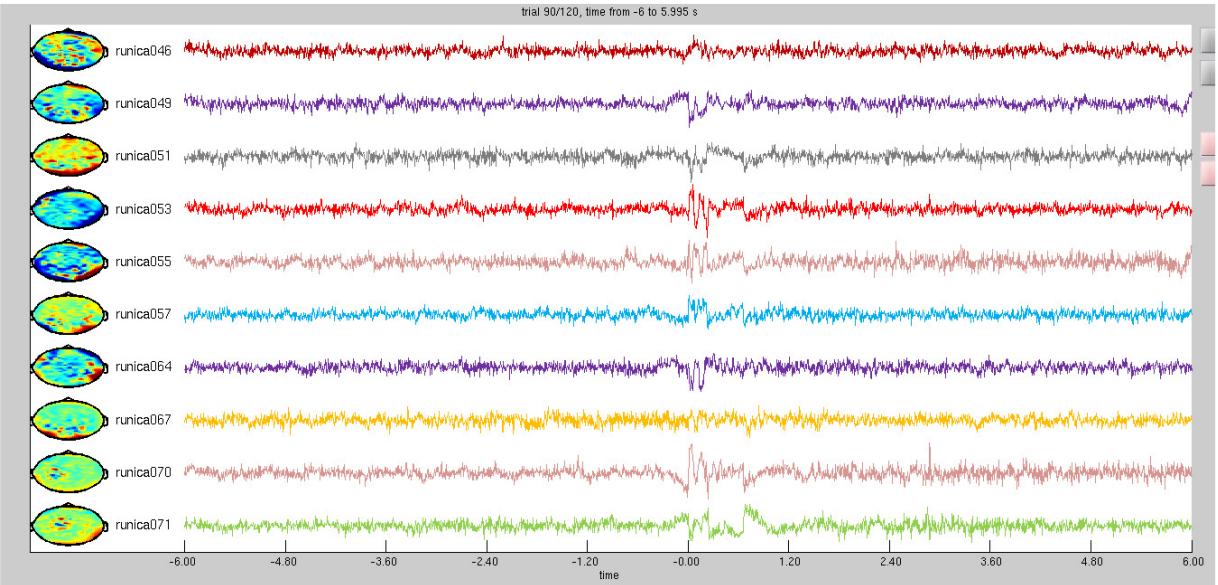

Figure 9.5: FieldTrip output of select tSSS-cleaned empty room components with stimulus-locked characteristics (correlation limit 0.98)

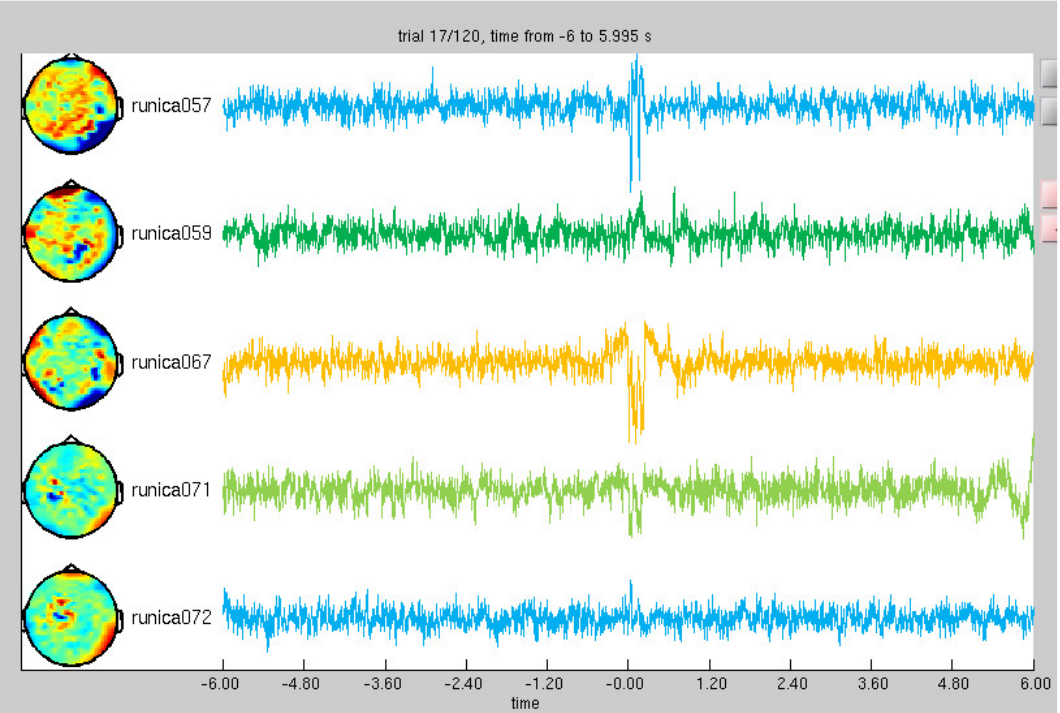

Figure 9.6: FieldTrip output of select tSSS-cleaned empty room components with stimulus-locked characteristics (correlation limit 0.6)

Participant components

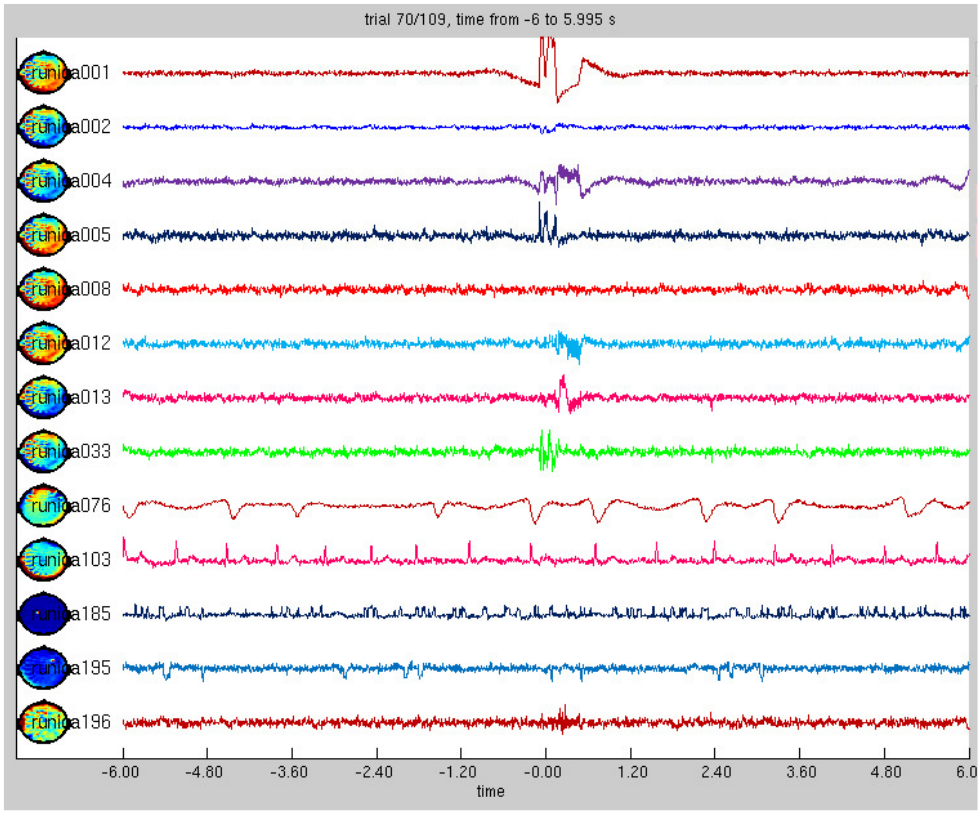

Figure 9.7: FieldTrip output of select raw participant data components with stimulus-locked characteristics. Eyeblink and heartbeat components are also visible (76 and 103). Compared to Fig 10.2, which has had the same steps applied to it, it is clear that the artefact has spread its energy over many more components.

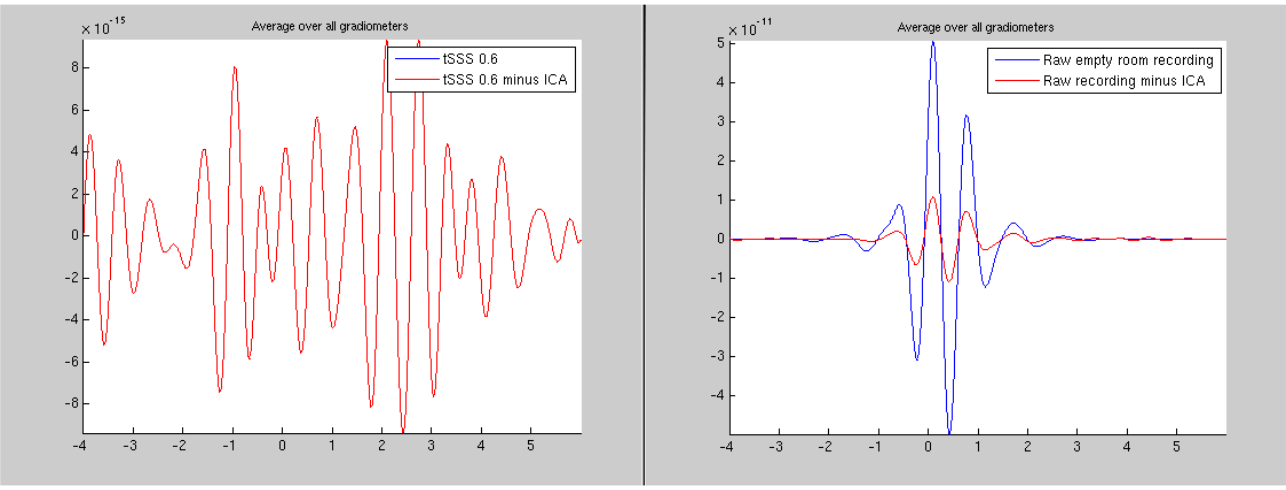

Figure 9.8: FieldTrip output for empty room data averaged over all trials and all gradiometers. Left: Empty room dataset before and after ICA (they are identical); Right: Raw data before and after ICA (a reduction of field strength is noticeable after ICA).

Appendix C.2 Beamformer outputs

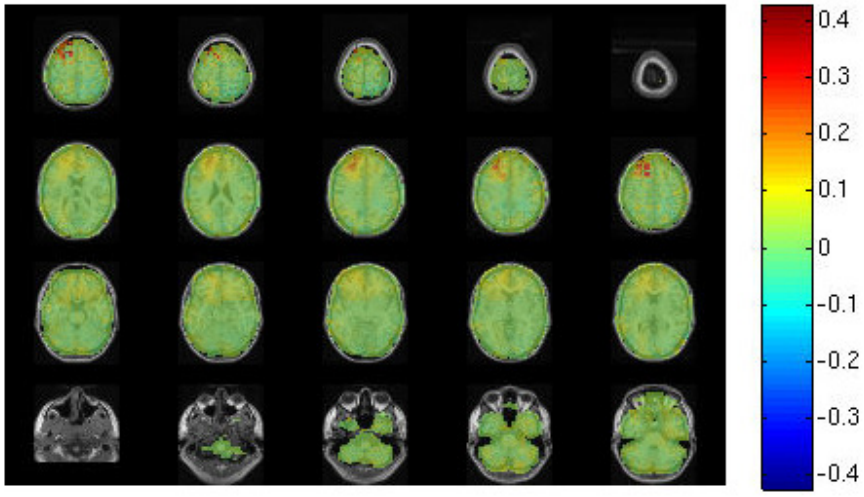

Figure 9.9: FieldTrip LCMV beamformer output for the post-stimulus time window of the raw empty-room dataset (κ = 202, λ = 0)

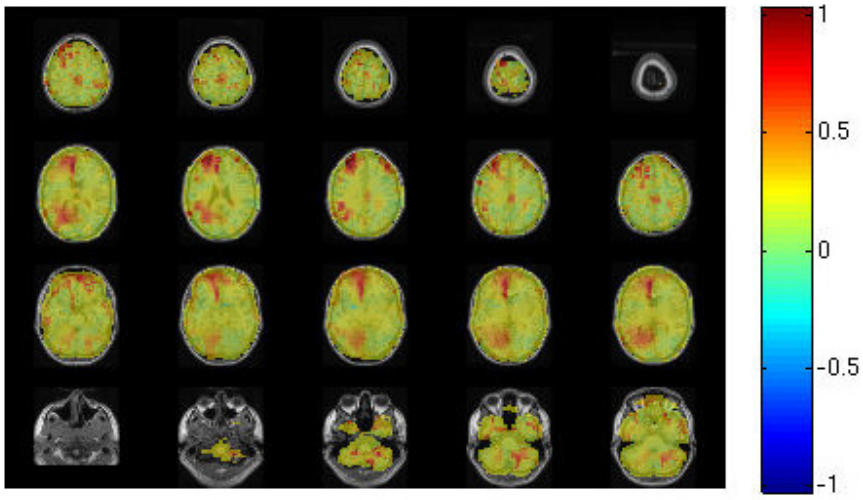

Figure 9.10: FieldTrip LCMV beamformer output for the post-stimulus time window of the raw empty-room dataset (κ = 202, λ = 5)

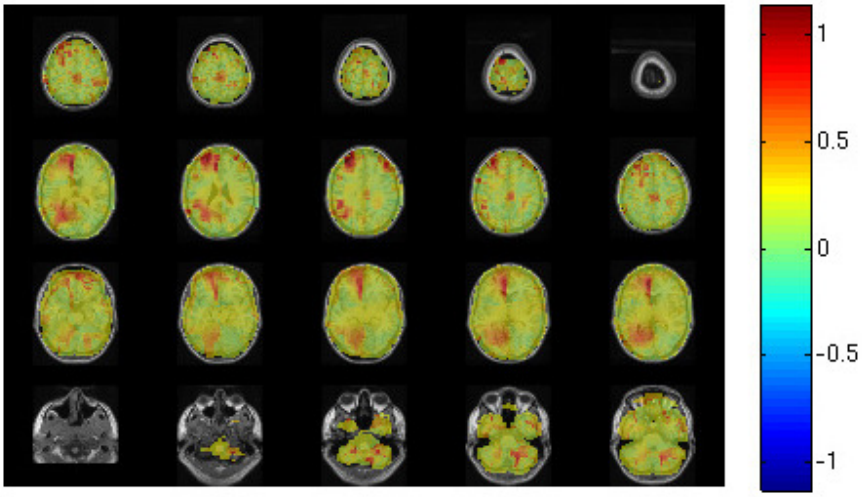

Figure 9.11: FieldTrip LCMV beamformer output for the post-stimulus time window of the raw empty-room dataset (κ = 202, λ = 10)

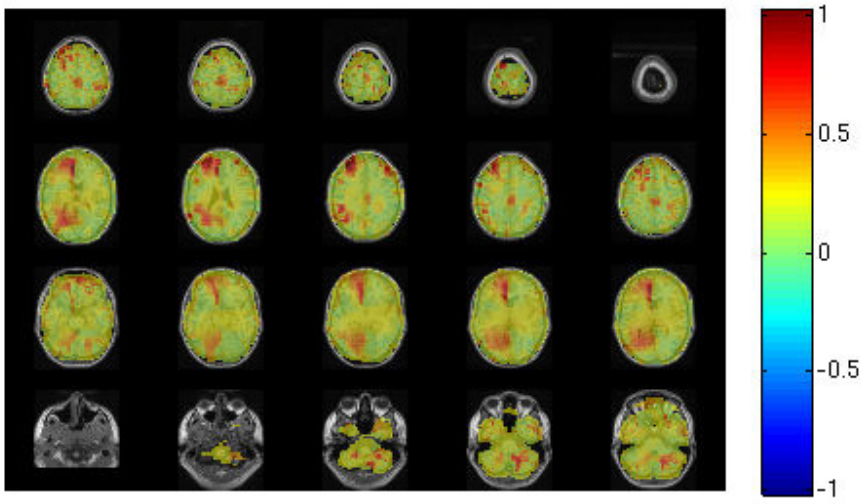

Figure 9.11: FieldTrip LCMV beamformer output for the post-stimulus time window of the raw empty-room dataset (κ = 202, λ = 25)

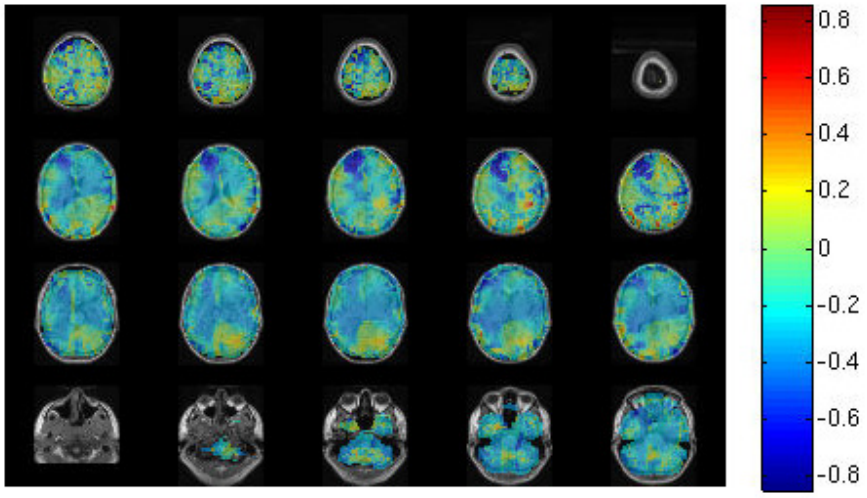

Figure 9.12: FieldTrip LCMV beamformer output for the post-stimulus time window of the raw empty-room dataset (κ = 50, λ = 0)

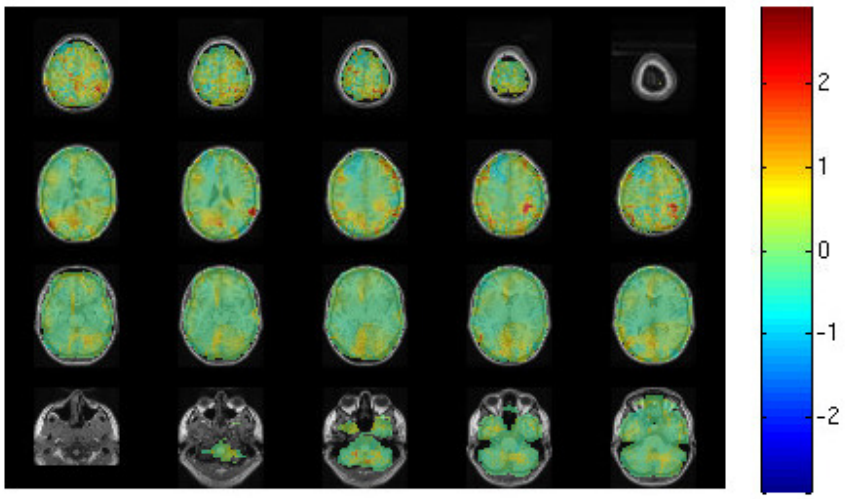

Figure 9.13: FieldTrip LCMV beamformer output for the post-stimulus time window of the raw empty-room dataset (κ = 50, λ = 5)

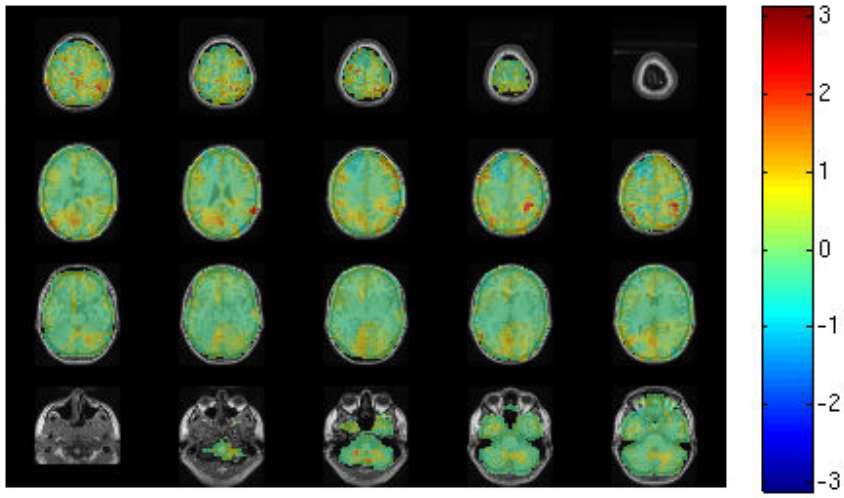

Figure 9.14: FieldTrip LCMV beamformer output for the post-stimulus time window of the raw empty-room dataset (κ = 50, λ = 10)

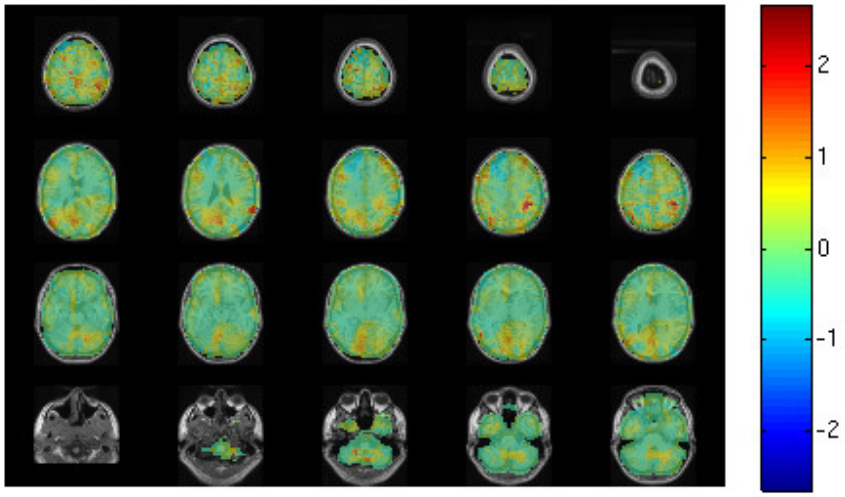

Figure 9.15: FieldTrip LCMV beamformer output for the post-stimulus time window of the raw empty-room dataset (κ = 50, λ = 25)

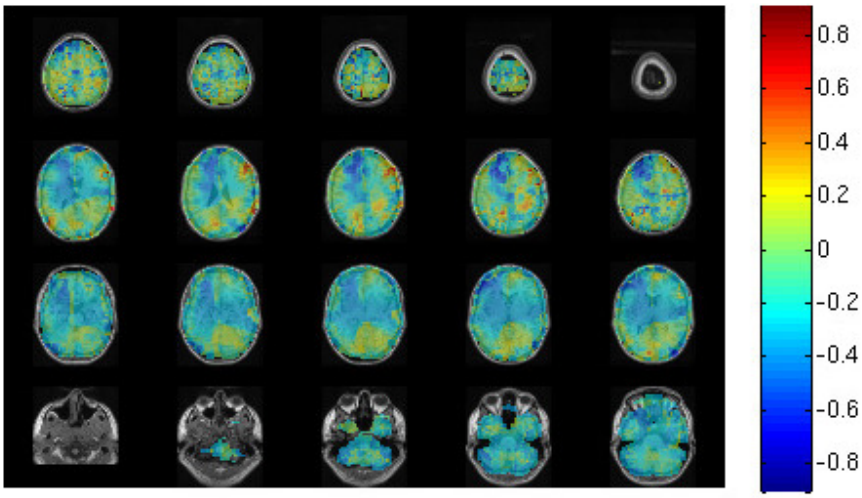

Figure 9.16: FieldTrip LCMV beamformer output for the post-stimulus time window of the raw empty-room dataset (κ = 60, λ = 0)

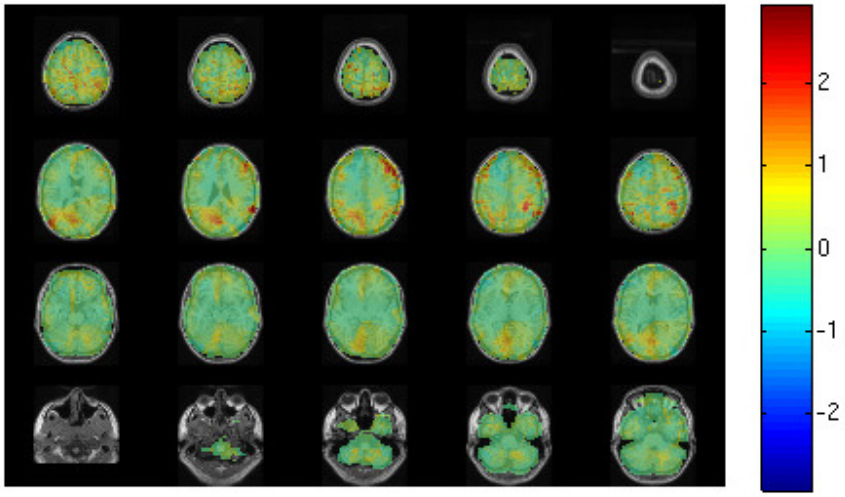

Figure 9.17: FieldTrip LCMV beamformer output for the post-stimulus time window of the raw empty-room dataset (κ = 60, λ = 5)

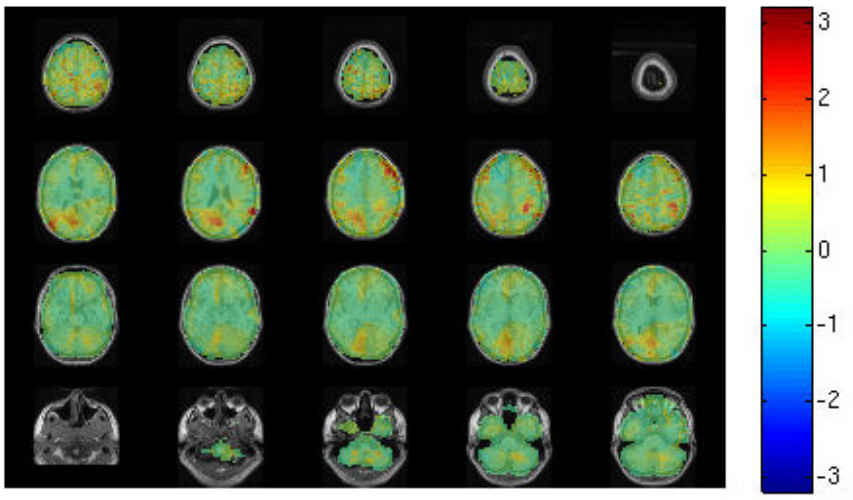

Figure 9.18: FieldTrip LCMV beamformer output for the post-stimulus time window of the raw empty-room dataset (κ = 60, λ = 10)

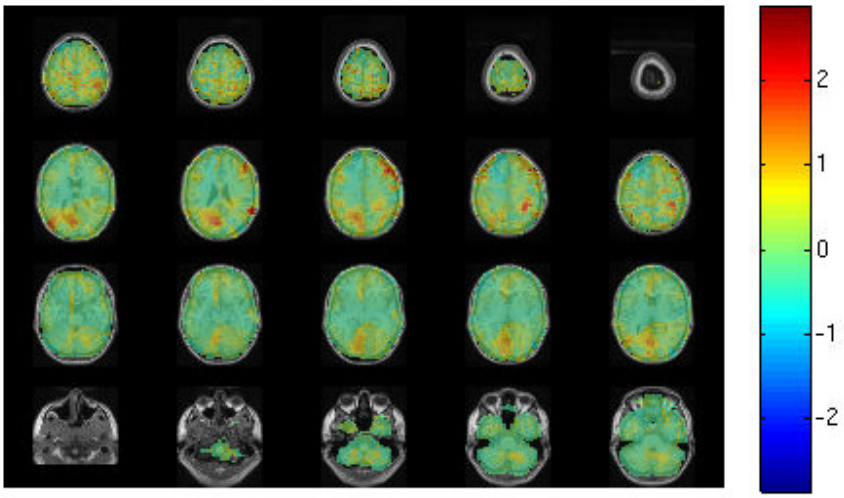

Figure 9.19: FieldTrip LCMV beamformer output for the post-stimulus time window of the raw empty-room dataset (κ = 60, λ = 25)

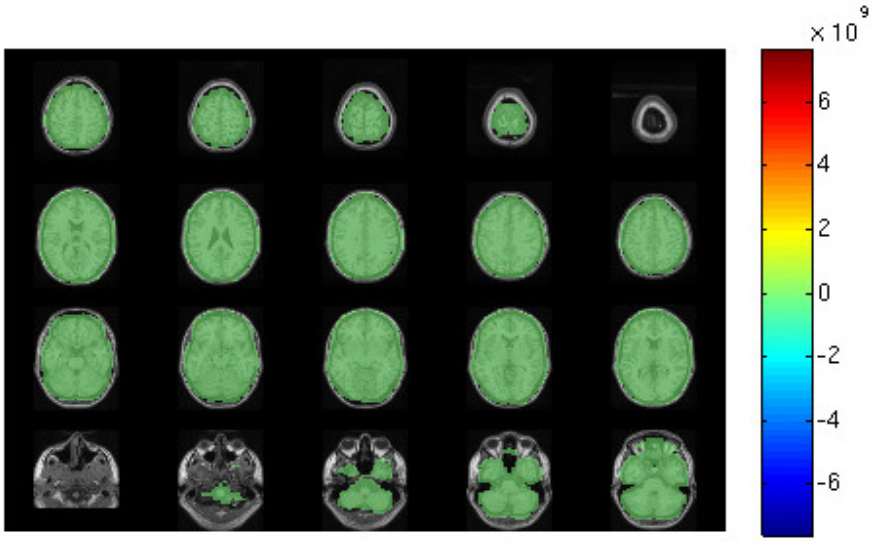

Figure 9.20: FieldTrip LCMV beamformer output for the post-stimulus time window of the raw empty-room dataset, performed after removing stimulus-locked components via ICA (κ = 60, λ = 0). This shows full suppression of the artefact.

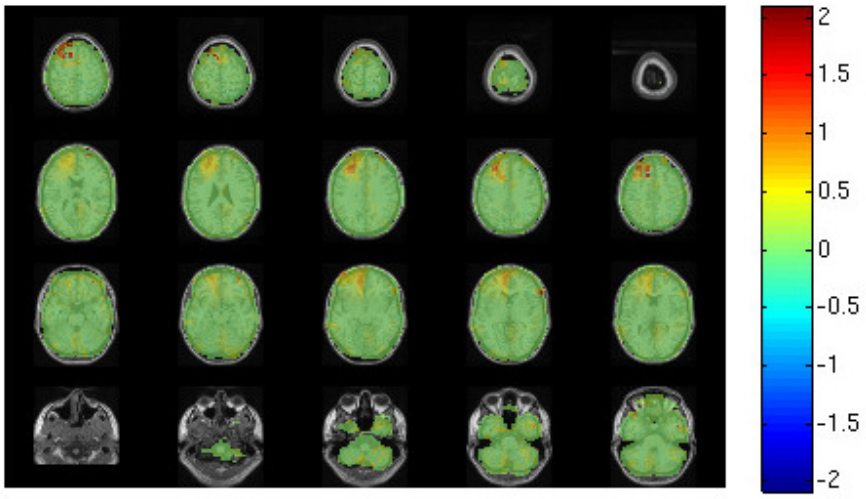

Figure 9.21: FieldTrip LCMV beamformer output for the post-stimulus time window of the raw empty-room dataset, performed after removing stimulus-locked components via ICA (κ = 60, λ = 5)

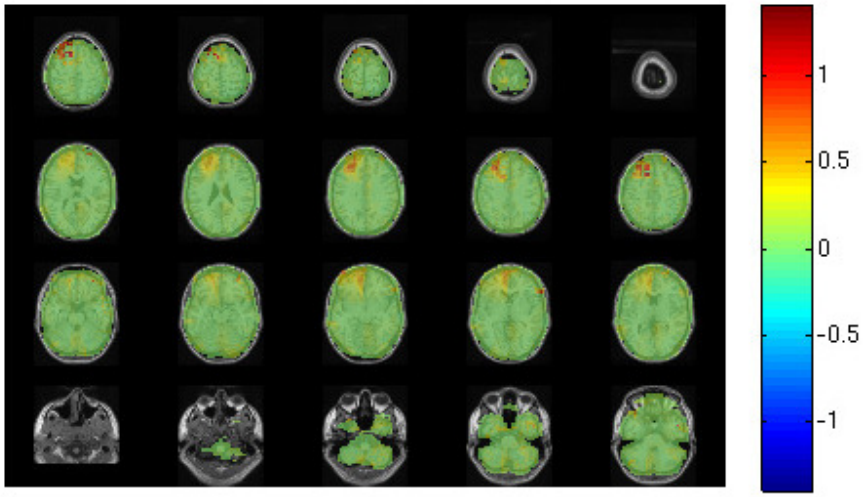

Figure 9.22: FieldTrip LCMV beamformer output for the post-stimulus time window of the raw empty-room dataset, performed after removing stimulus-locked components via ICA (κ = 60, λ = 10)

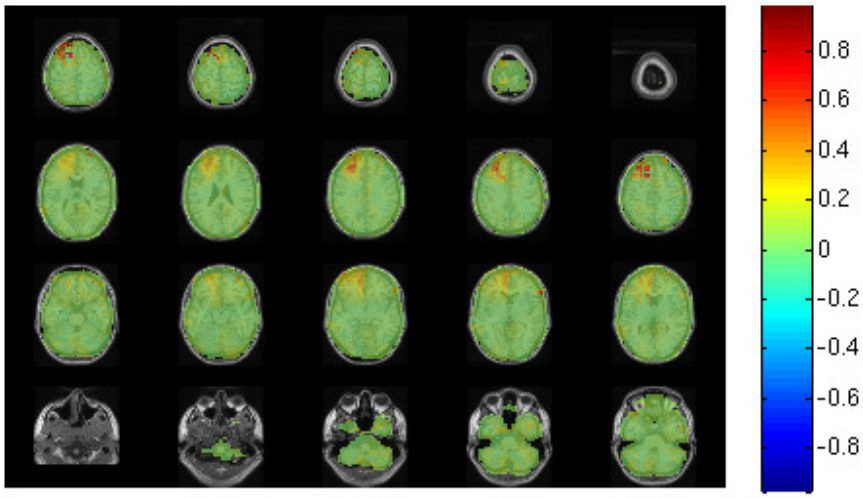

Figure 9.23: FieldTrip LCMV beamformer output for the post-stimulus time window of the raw empty-room dataset, performed after removing stimulus-locked components via ICA (κ = 60, λ = 25)

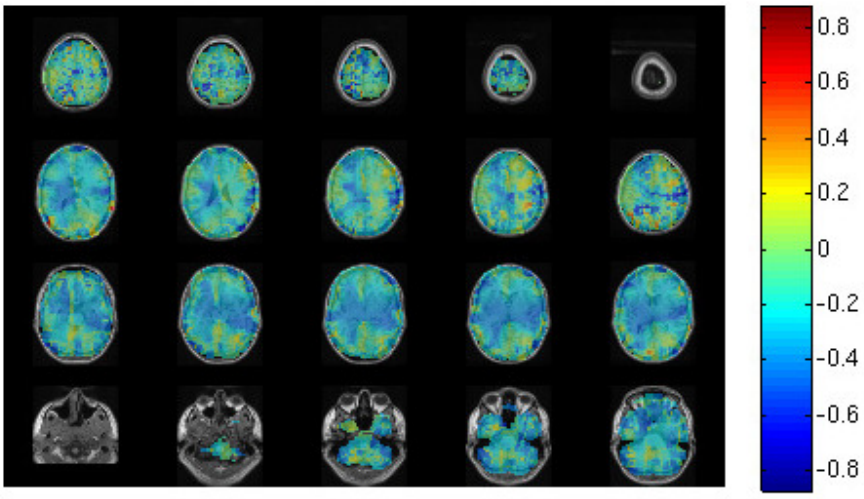

Figure 9.24: FieldTrip LCMV beamformer output for the post-stimulus time window of the raw empty-room dataset, performed after removing stimulus-locked components via ICA (κ = 50, λ = 0)

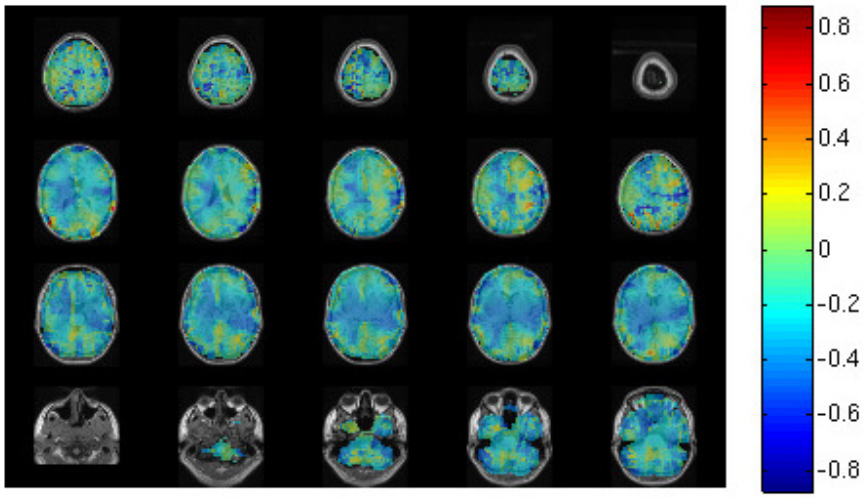

Figure 9.25: FieldTrip LCMV beamformer output for the post-stimulus time window of the raw empty-room dataset, performed after removing stimulus-locked components via ICA (κ = 50, λ = 5)

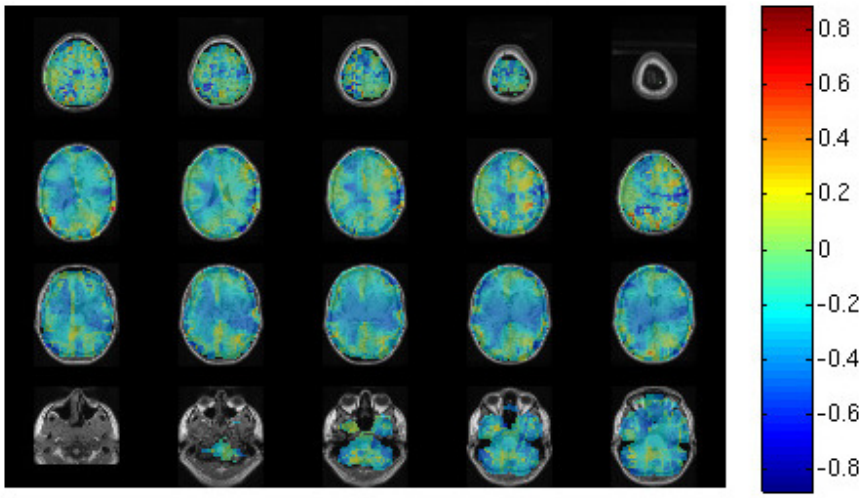

Figure 9.26: FieldTrip LCMV beamformer output for the post-stimulus time window of the raw empty-room dataset, performed after removing stimulus-locked components via ICA (κ = 50, λ = 10)

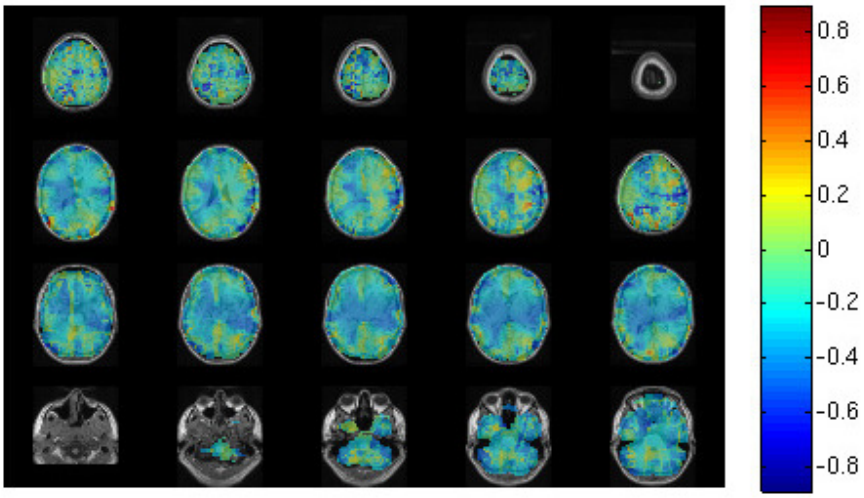

Figure 9.27: FieldTrip LCMV beamformer output for the post-stimulus time window of the raw empty-room dataset, performed after removing stimulus-locked components via ICA (κ = 50, λ = 25)

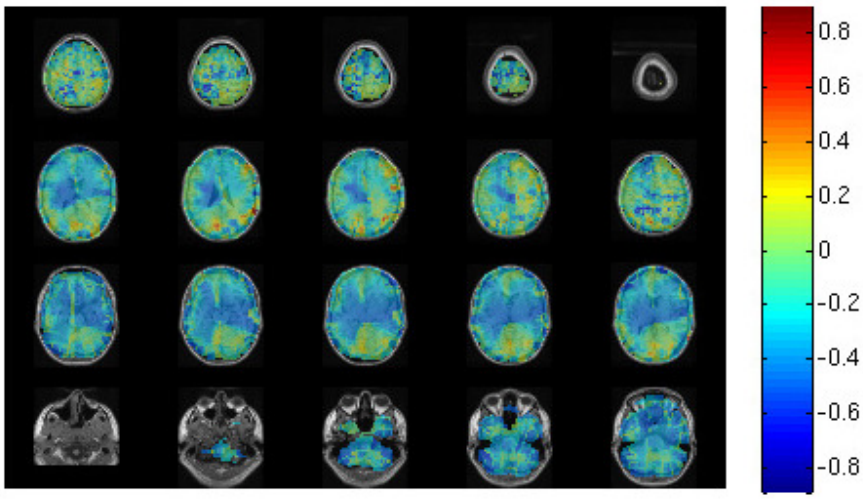

Figure 9.28: FieldTrip LCMV beamformer output for the post-stimulus time window of the raw empty-room dataset, performed after removing stimulus-locked components via ICA (κ = 60, λ = 0)

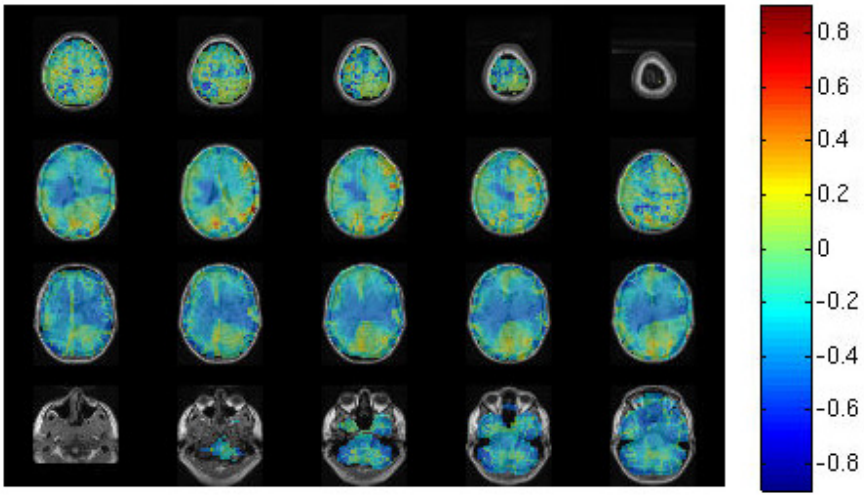

Figure 9.29: FieldTrip LCMV beamformer output for the post-stimulus time window of the raw empty-room dataset, performed after removing stimulus-locked components via ICA (κ = 60, λ = 5)

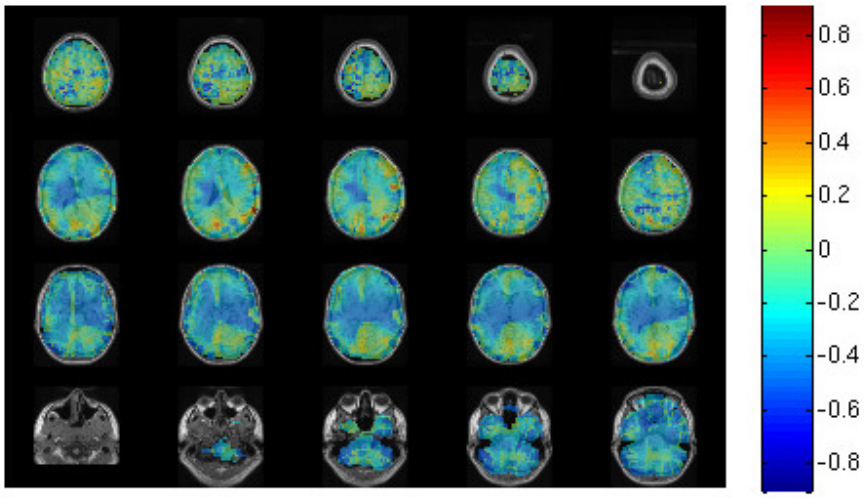

Figure 9.30: FieldTrip LCMV beamformer output for the post-stimulus time window of the raw empty-room dataset, performed after removing stimulus-locked components via ICA (κ = 60, λ = 10)

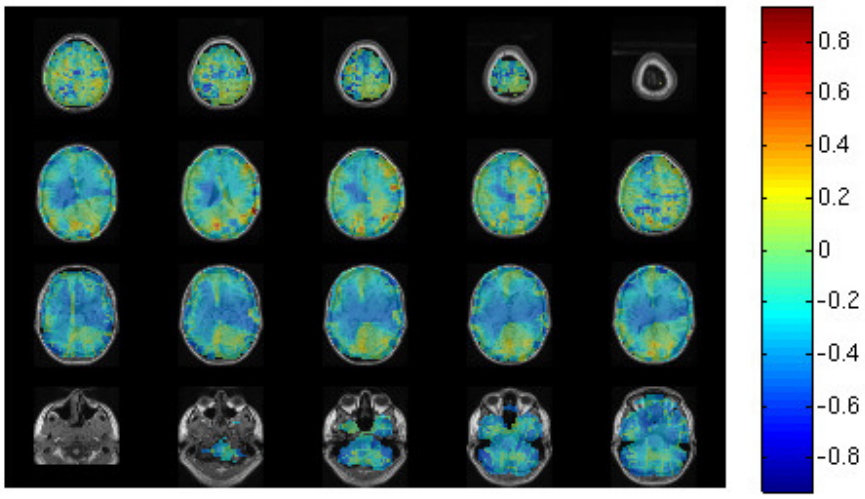

Figure 9.31: FieldTrip LCMV beamformer output for the post-stimulus time window of the raw empty-room dataset, performed after removing stimulus-locked components via ICA (κ = 60, λ = 25)

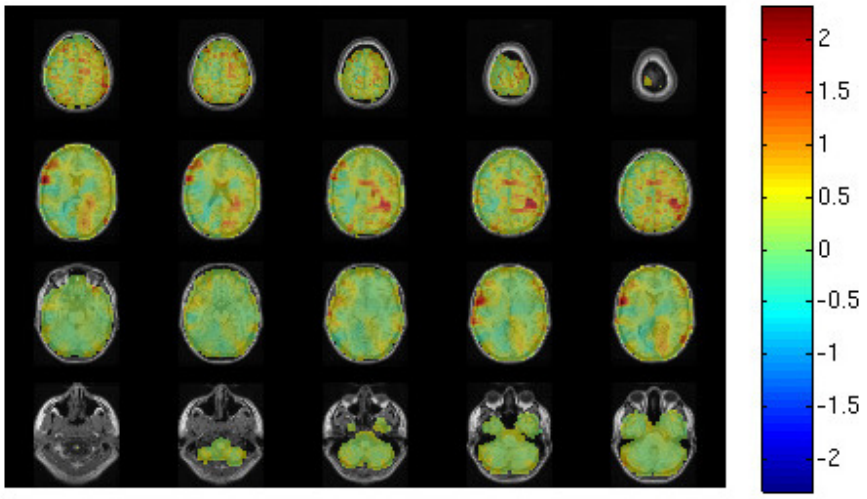

Figure 9.32: FieldTrip LCMV beamformer output for the post-stimulus time window of the tSSS-cleaned empty-room dataset (correlation limit = 0.98, κ = 50, λ = 0)

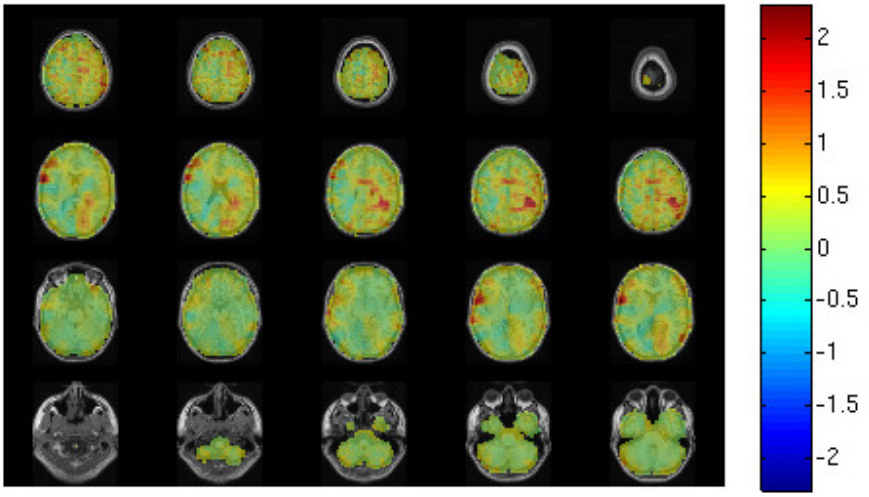

Figure 9.33: FieldTrip LCMV beamformer output for the post-stimulus time window of the tSSS-cleaned empty-room dataset (correlation limit = 0.98, κ = 50, λ = 5)

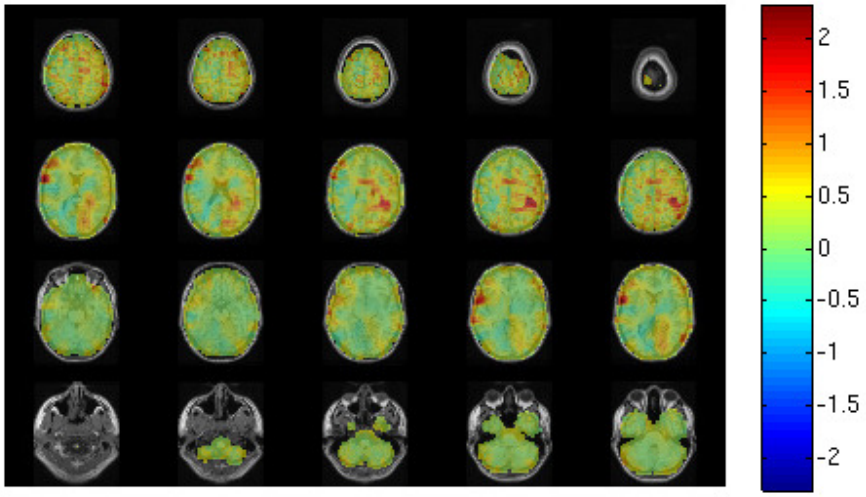

Figure 9.34: FieldTrip LCMV beamformer output for the post-stimulus time window of the tSSS-cleaned empty-room dataset (correlation limit = 0.98, κ = 50, λ = 10)

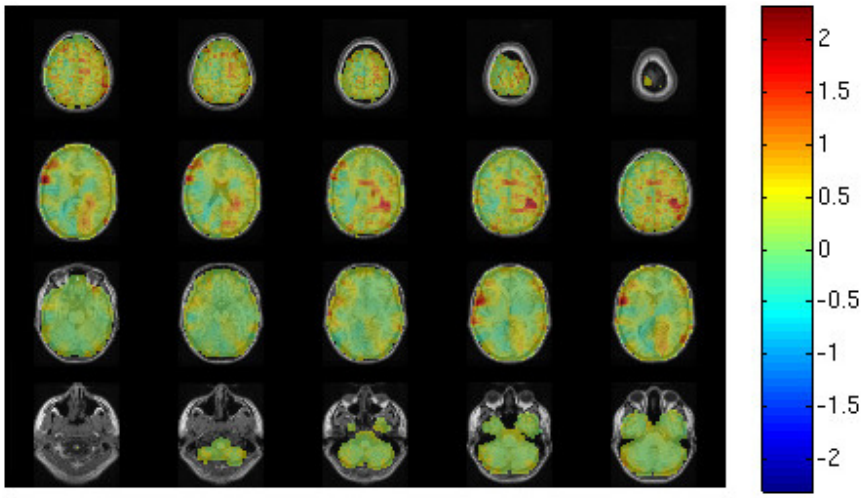

Figure 9.34: FieldTrip LCMV beamformer output for the post-stimulus time window of the tSSS-cleaned empty-room dataset (correlation limit = 0.98, κ = 50, λ = 25)

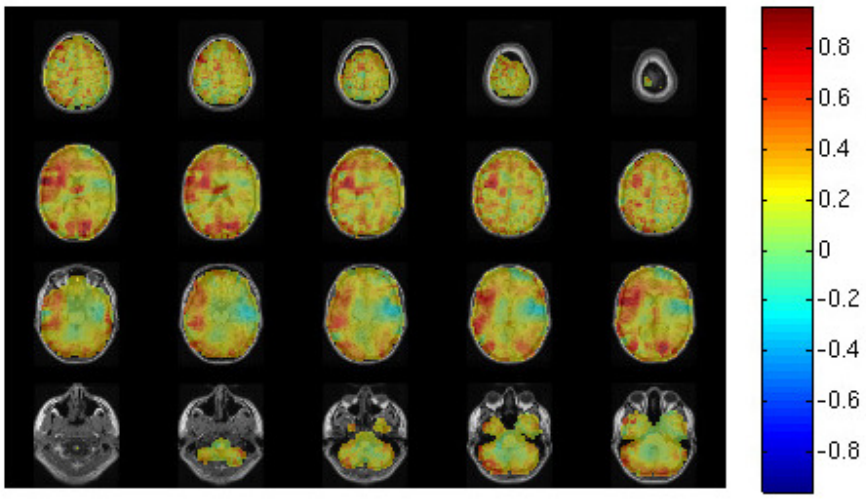

Figure 9.35: FieldTrip LCMV beamformer output for the post-stimulus time window of the tSSS-cleaned empty-room dataset (correlation limit = 0.98, κ = 60, λ = 0)

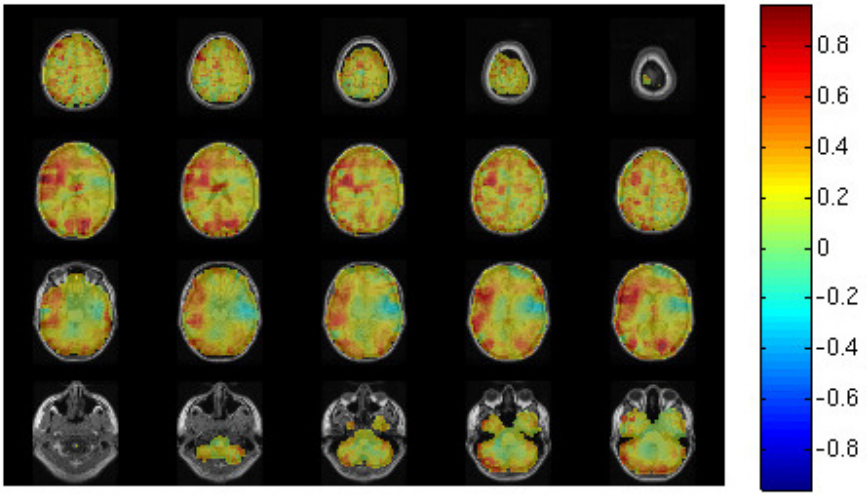

Figure 9.36: FieldTrip LCMV beamformer output for the post-stimulus time window of the tSSS-cleaned empty-room dataset (correlation limit = 0.98, κ = 60, λ = 5)

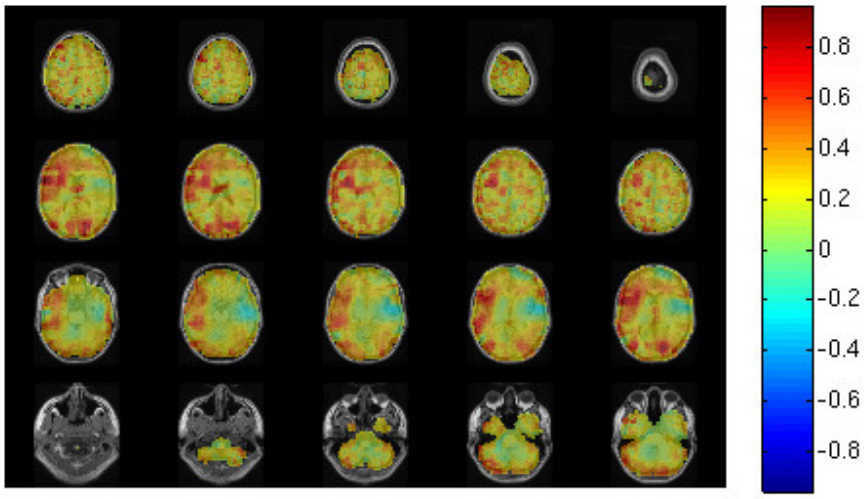

Figure 9.37: FieldTrip LCMV beamformer output for the post-stimulus time window of the tSSS-cleaned empty-room dataset (correlation limit = 0.98, κ = 60, λ = 10)

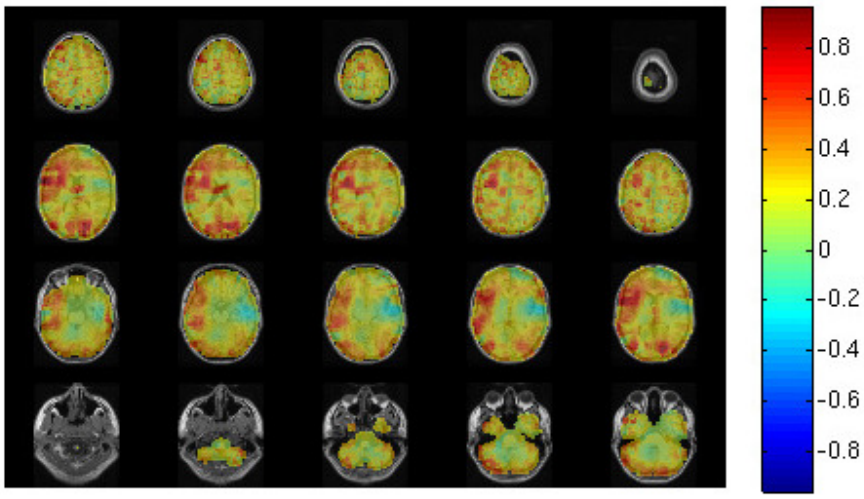

Figure 9.38: FieldTrip LCMV beamformer output for the post-stimulus time window of the tSSS-cleaned empty-room dataset (correlation limit = 0.98, κ = 60, λ = 25)

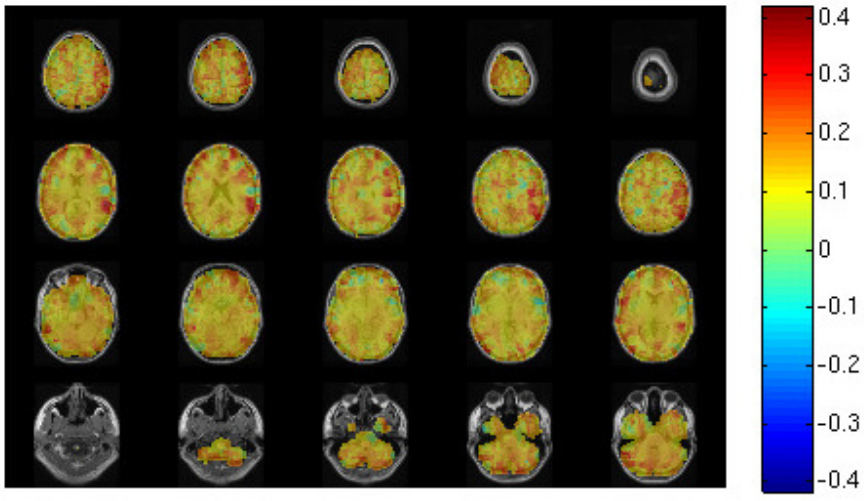

Figure 9.39: FieldTrip LCMV beamformer output for the post-stimulus time window of the tSSS-cleaned empty-room dataset, performed after removing stimulus-locked components via ICA (correlation limit = 0.98, κ = 50, λ = 0)

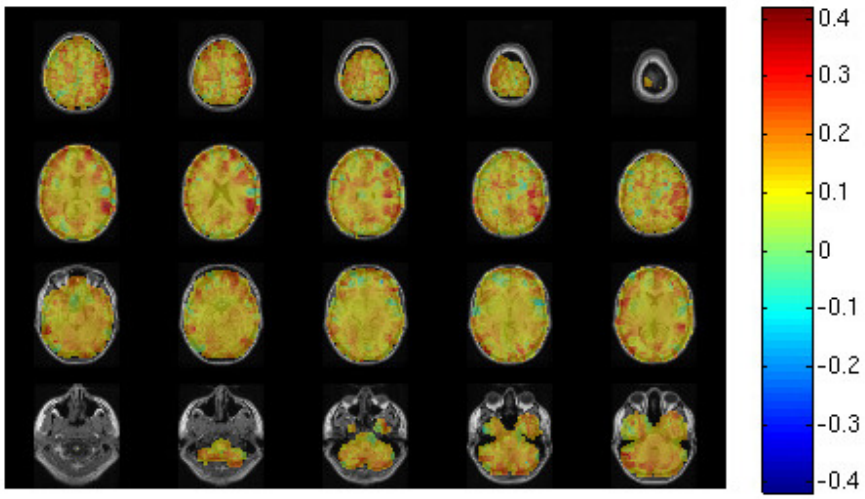

Figure 9.40: FieldTrip LCMV beamformer output for the post-stimulus time window of the tSSS-cleaned empty-room dataset, performed after removing stimulus-locked components via ICA (correlation limit = 0.98, κ = 50, λ = 5)

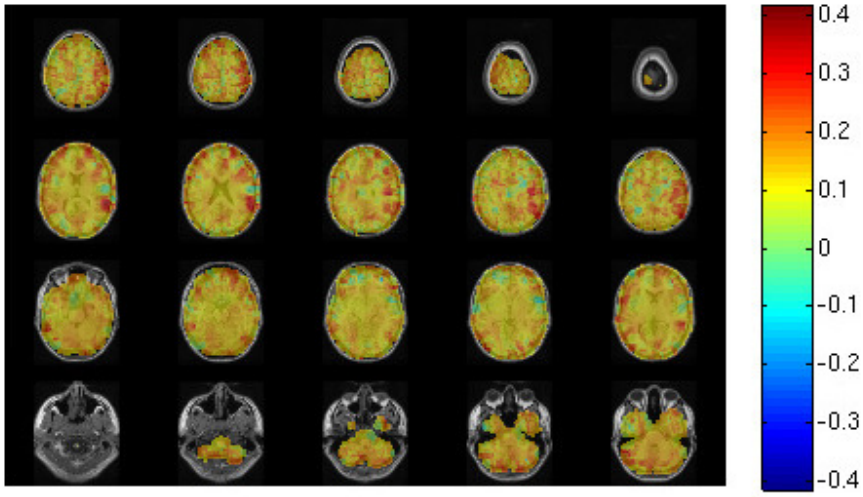

Figure 9.41: FieldTrip LCMV beamformer output for the post-stimulus time window of the tSSS-cleaned empty-room dataset, performed after removing stimulus-locked components via ICA (correlation limit = 0.98, κ = 50, λ = 10)

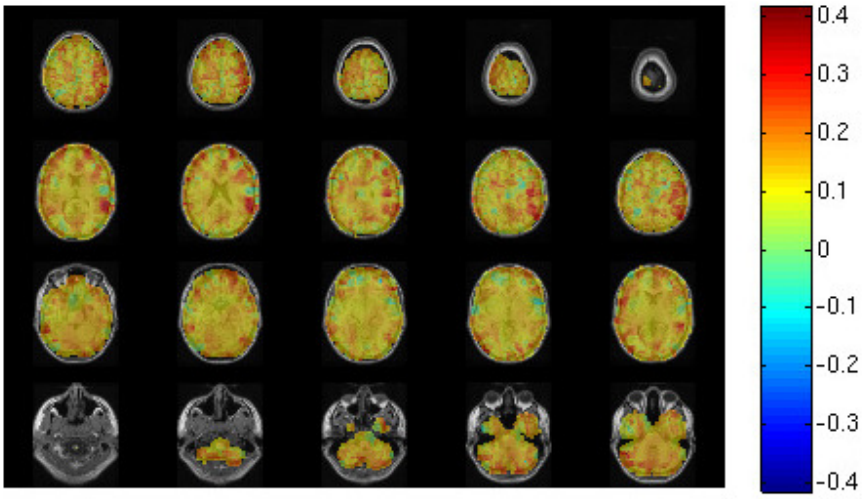

Figure 9.41: FieldTrip LCMV beamformer output for the post-stimulus time window of the tSSS-cleaned empty-room dataset, performed after removing stimulus-locked components via ICA (correlation limit = 0.98, κ = 50, λ = 25)

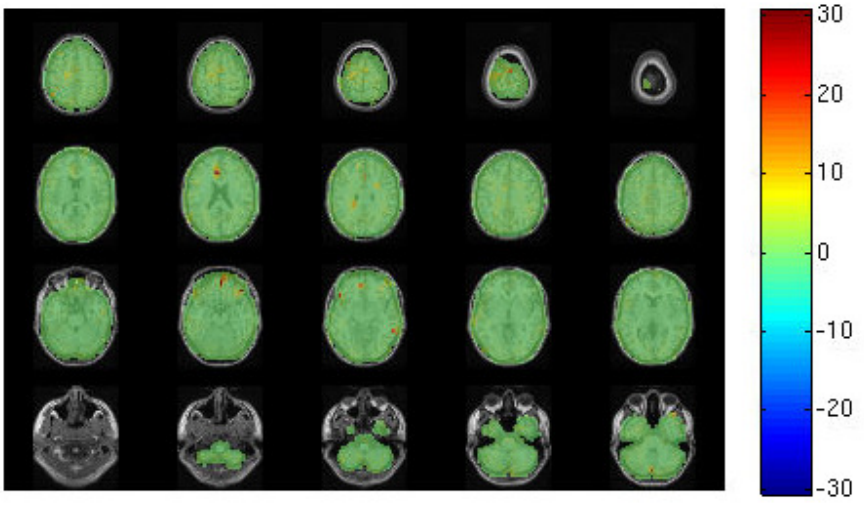

Figure 9.42: FieldTrip LCMV beamformer output for the post-stimulus time window of the tSSS-cleaned empty-room dataset, performed after removing stimulus-locked components via ICA (correlation limit = 0.98, κ = 60, λ = 0)

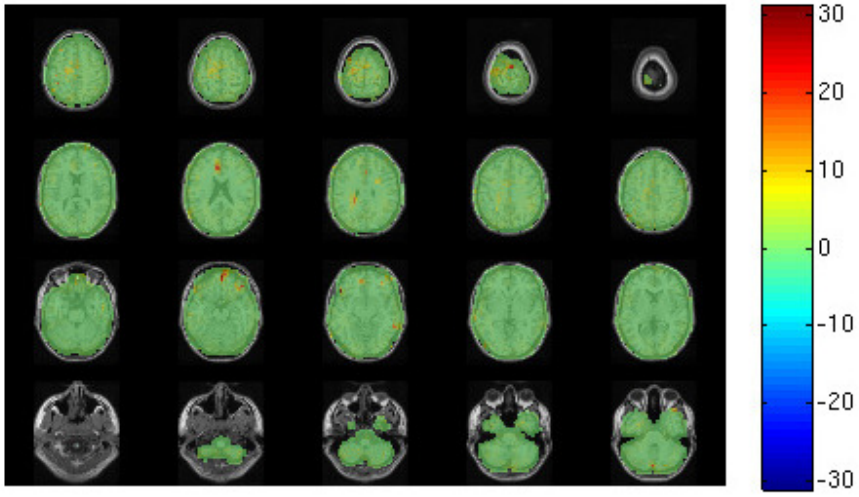

Figure 9.43: FieldTrip LCMV beamformer output for the post-stimulus time window of the tSSS-cleaned empty-room dataset, performed after removing stimulus-locked components via ICA (correlation limit = 0.98, κ = 60, λ = 5)

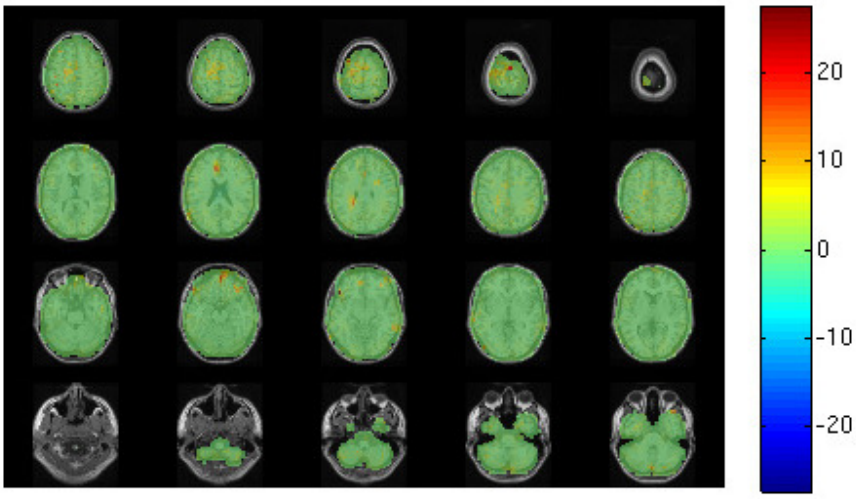

Figure 9.44: FieldTrip LCMV beamformer output for the post-stimulus time window of the tSSS-cleaned empty-room dataset, performed after removing stimulus-locked components via ICA (correlation limit = 0.98, κ = 60, λ = 10)

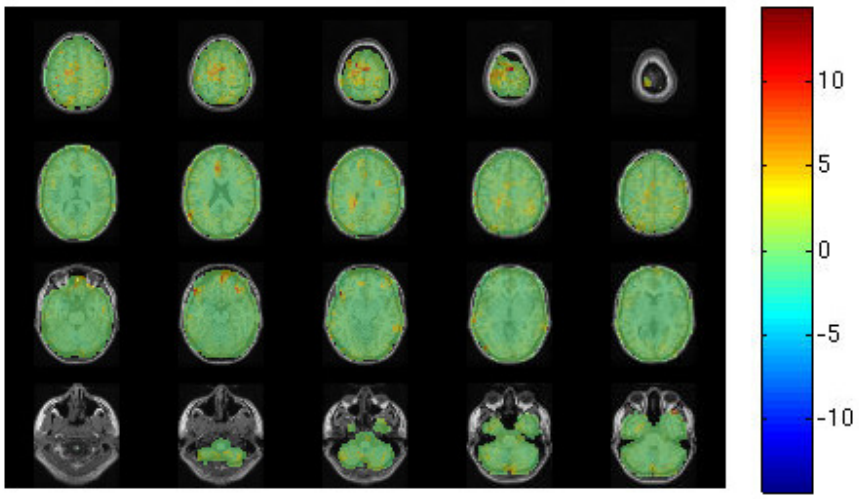

Figure 9.45: FieldTrip LCMV beamformer output for the post-stimulus time window of the tSSS-cleaned empty-room dataset, performed after removing stimulus-locked components via ICA (correlation limit = 0.98, κ = 60, λ = 25)

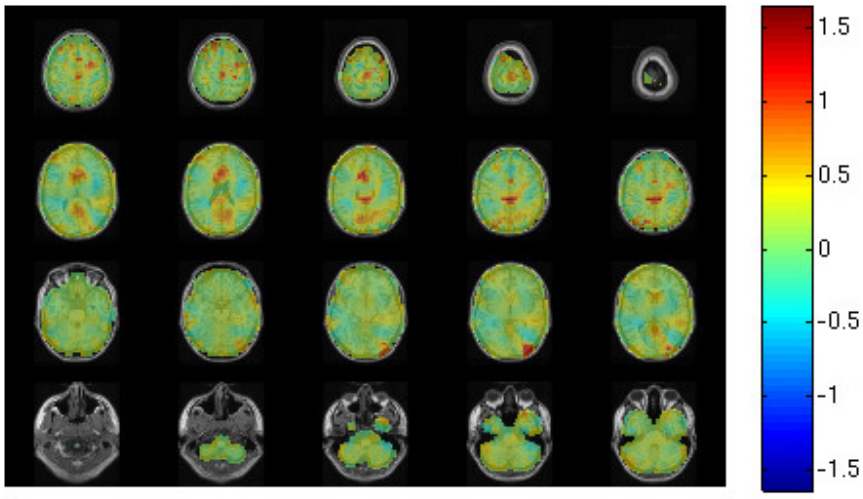

Figure 9.46: FieldTrip LCMV beamformer output for the post-stimulus time window of the tSSS-cleaned empty-room dataset (correlation limit = 0.6, κ = 50, λ = 0)

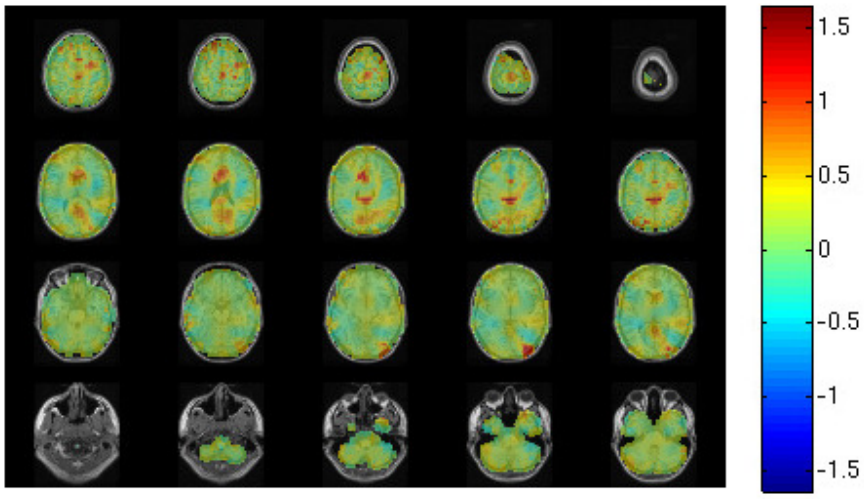

Figure 9.47: FieldTrip LCMV beamformer output for the post-stimulus time window of the tSSS-cleaned empty-room dataset (correlation limit = 0.6, κ = 50, λ = 5)

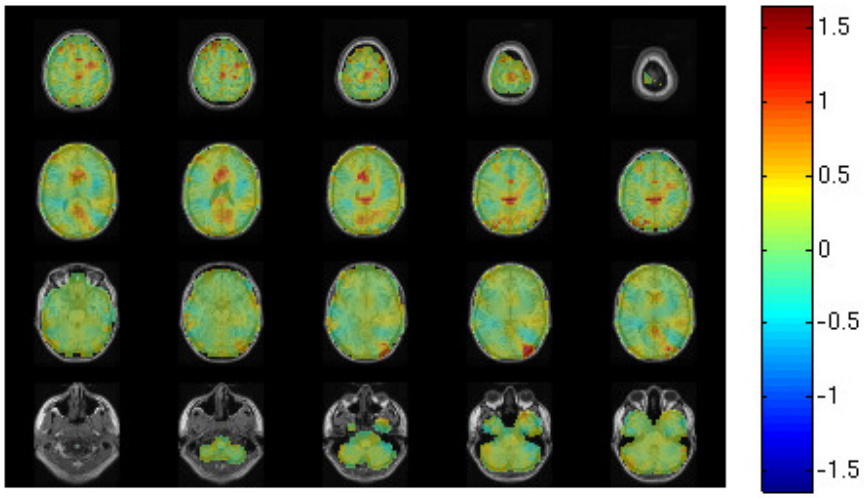

Figure 9.48: FieldTrip LCMV beamformer output for the post-stimulus time window of the tSSS-cleaned empty-room dataset (correlation limit = 0.6, κ = 50, λ = 10)

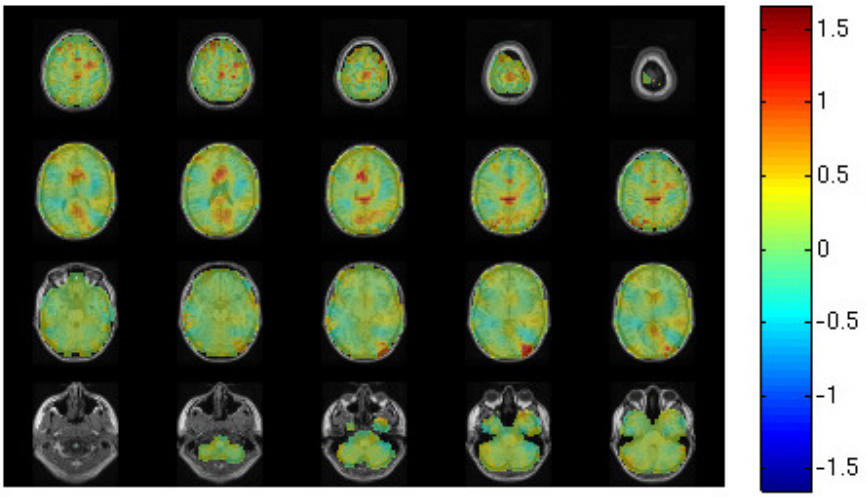

Figure 9.49: FieldTrip LCMV beamformer output for the post-stimulus time window of the tSSS-cleaned empty-room dataset (correlation limit = 0.6, κ = 50, λ = 25)

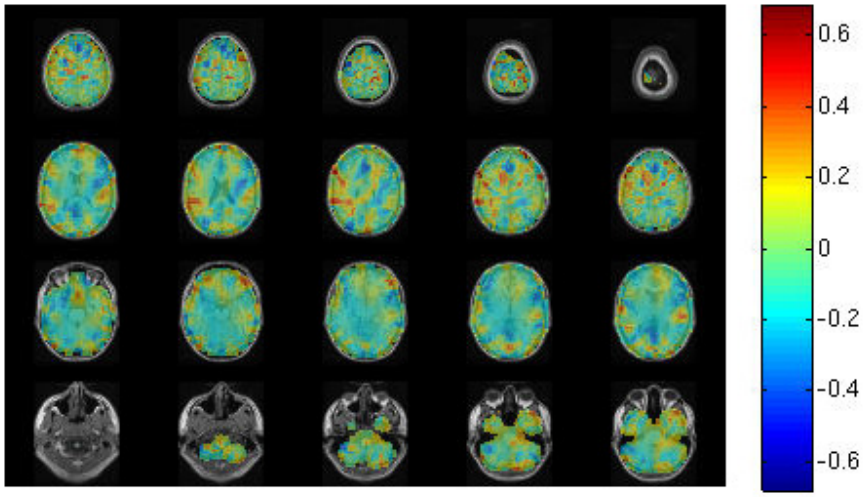

Figure 9.50: FieldTrip LCMV beamformer output for the post-stimulus time window of the tSSS-cleaned empty-room dataset (correlation limit = 0.6, κ = 60, λ = 0)

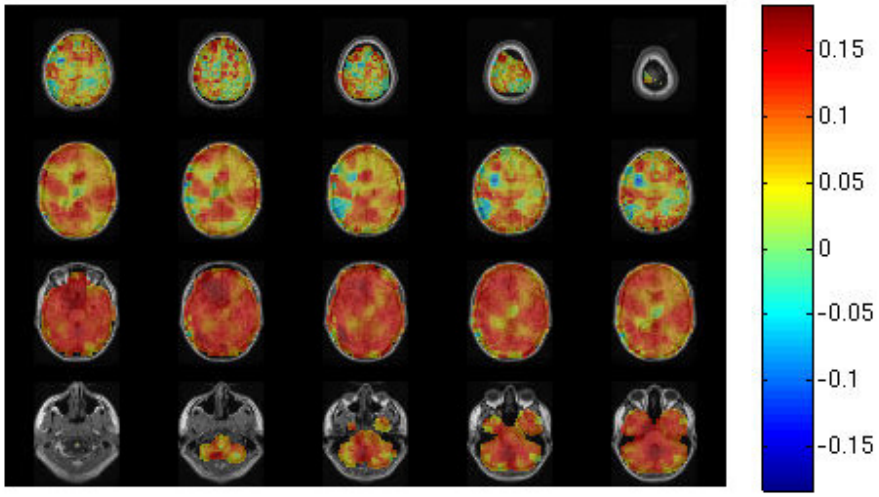

Figure 9.51: FieldTrip LCMV beamformer output for the post-stimulus time window of the tSSS-cleaned empty-room dataset (correlation limit = 0.6, κ = 60, λ = 5)

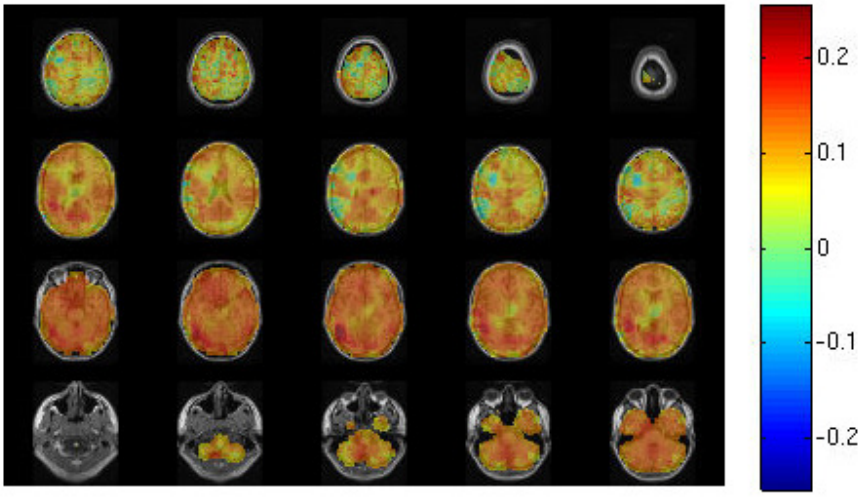

Figure 9.52: FieldTrip LCMV beamformer output for the post-stimulus time window of the tSSS-cleaned empty-room dataset (correlation limit = 0.6, κ = 60, λ = 10)

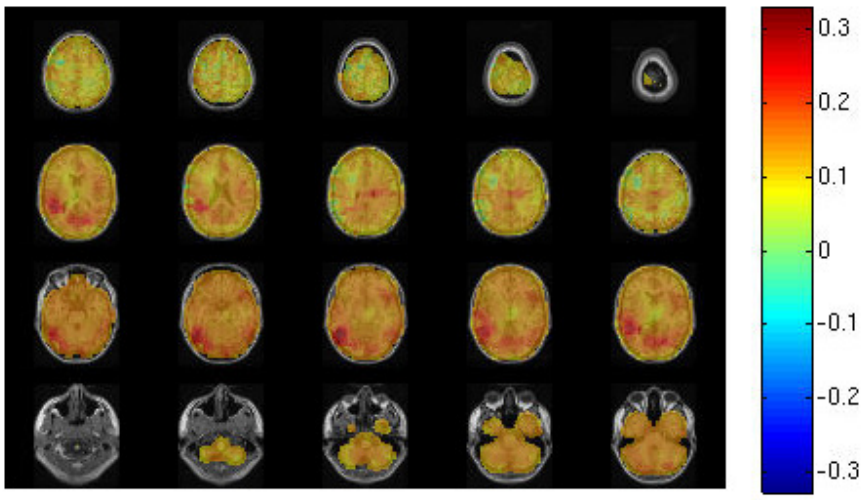

Figure 9.53: FieldTrip LCMV beamformer output for the post-stimulus time window of the tSSS-cleaned empty-room dataset (correlation limit = 0.6, κ = 60, λ = 25)

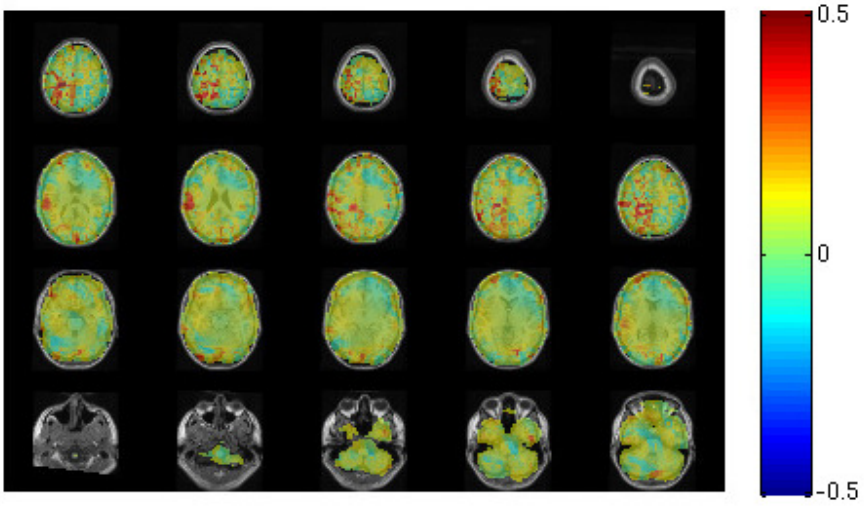

Figure 9.54: FieldTrip LCMV beamformer output for the post-stimulus time window of the tSSS-cleaned empty-room dataset, performed after removing stimulus-locked components via ICA (correlation limit = 0.6, κ = 50, λ = 0)

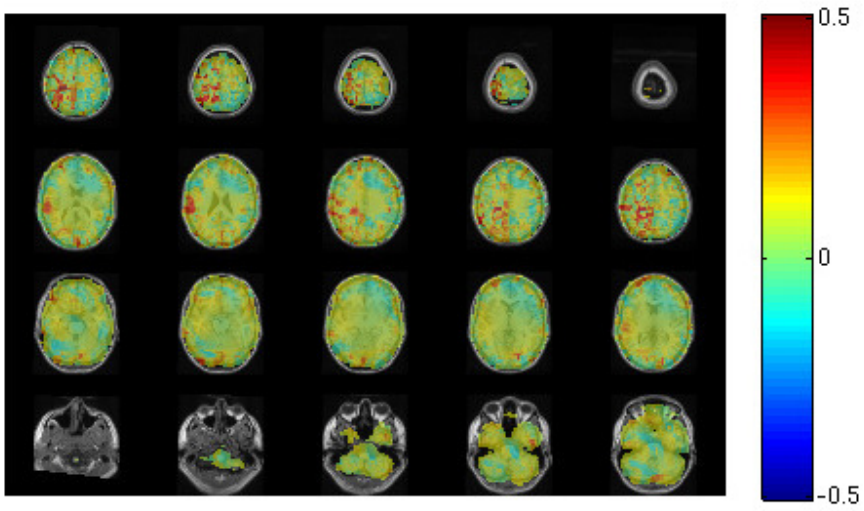

Figure 9.55: FieldTrip LCMV beamformer output for the post-stimulus time window of the tSSS-cleaned empty-room dataset, performed after removing stimulus-locked components via ICA (correlation limit = 0.6, κ = 50, λ = 5)

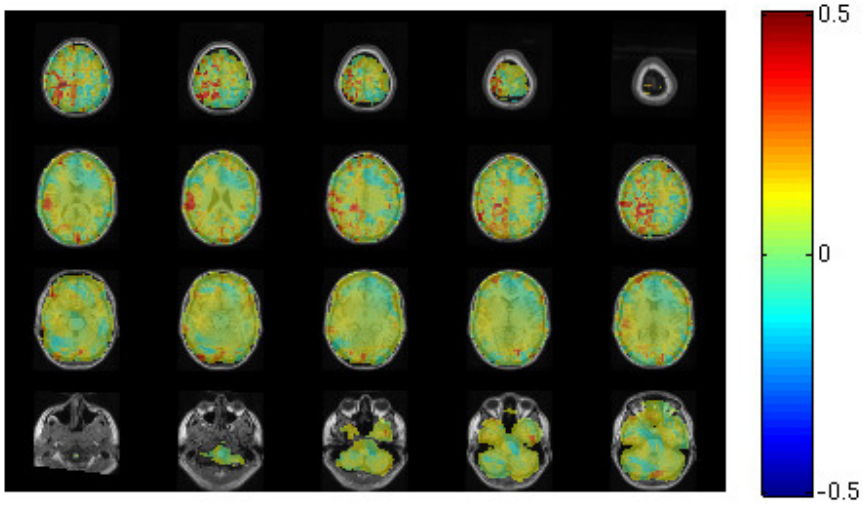

Figure 9.56: FieldTrip LCMV beamformer output for the post-stimulus time window of the tSSS-cleaned empty-room dataset, performed after removing stimulus-locked components via ICA (correlation limit = 0.6, κ = 50, λ = 10)

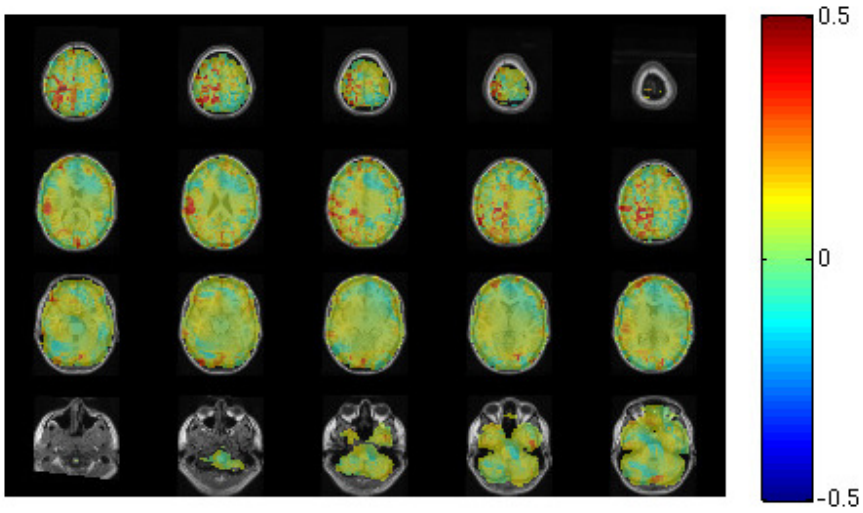

Figure 9.57: FieldTrip LCMV beamformer output for the post-stimulus time window of the tSSS-cleaned empty-room dataset, performed after removing stimulus-locked components via ICA (correlation limit = 0.6, κ = 50, λ = 25)

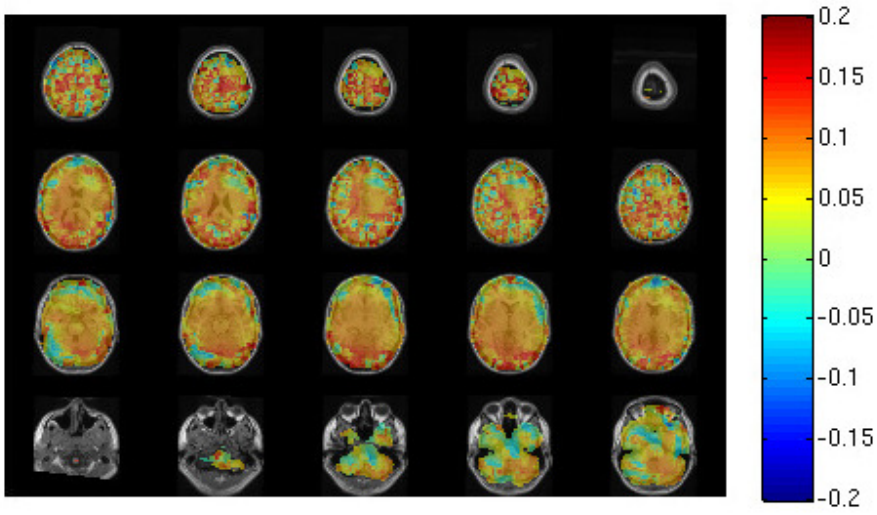

Figure 9.58: FieldTrip LCMV beamformer output for the post-stimulus time window of the tSSS-cleaned empty-room dataset, performed after removing stimulus-locked components via ICA (correlation limit = 0.6, κ = 60, λ = 0)

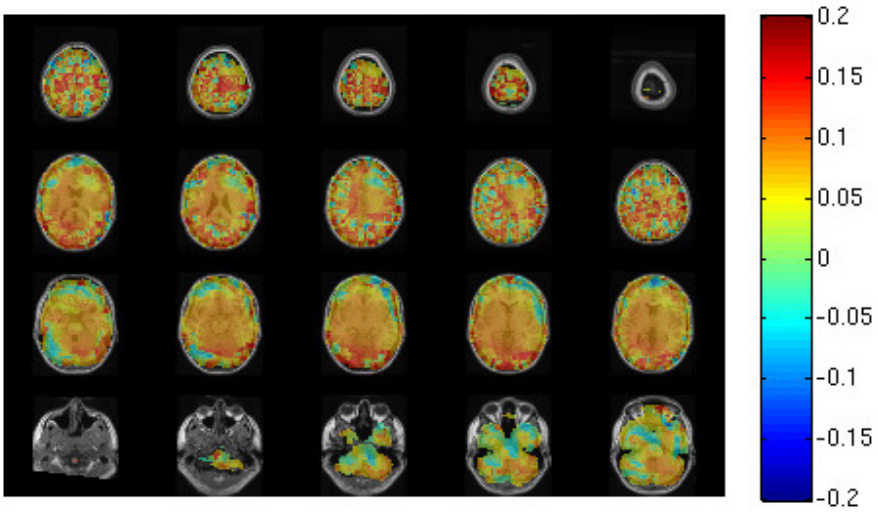

Figure 9.58: FieldTrip LCMV beamformer output for the post-stimulus time window of the tSSS-cleaned empty-room dataset, performed after removing stimulus-locked components via ICA (correlation limit = 0.6, κ = 60, λ = 5)

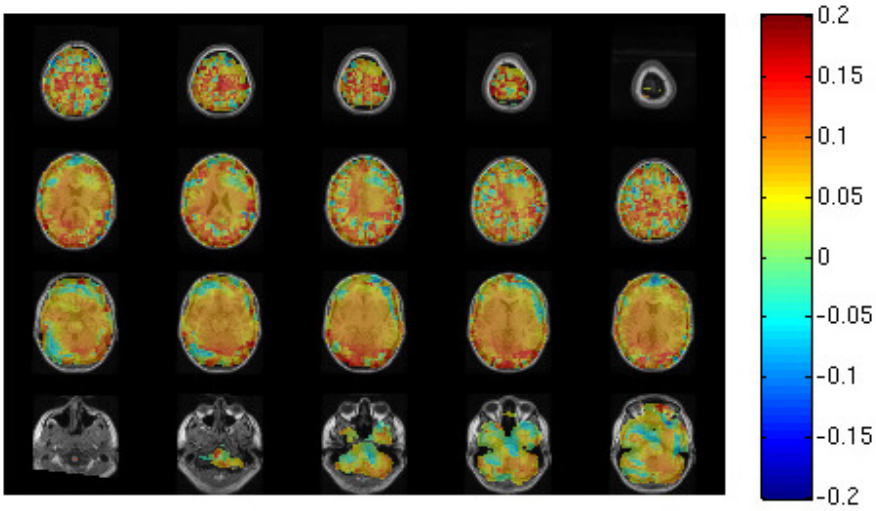

Figure 9.58: FieldTrip LCMV beamformer output for the post-stimulus time window of the tSSS-cleaned empty-room dataset, performed after removing stimulus-locked components via ICA (correlation limit = 0.6, κ = 60, λ = 10)

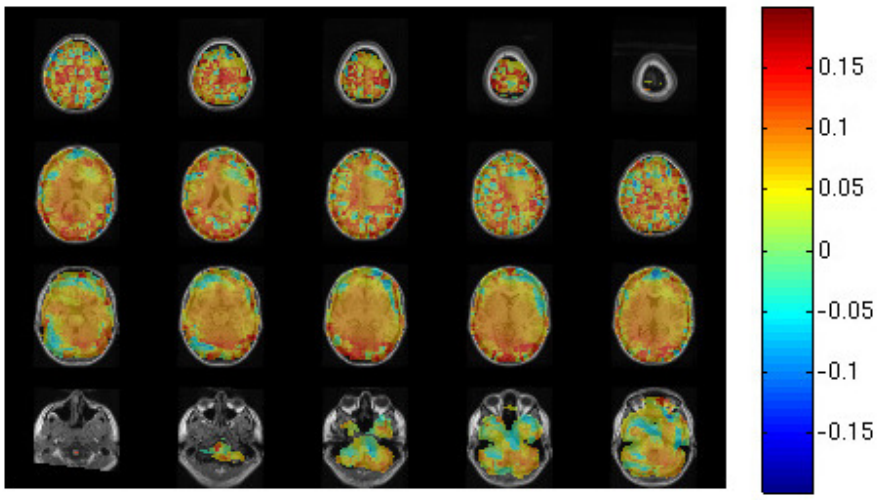

Figure 9.58: FieldTrip LCMV beamformer output for the post-stimulus time window of the tSSS-cleaned empty-room dataset, performed after removing stimulus-locked components via ICA (correlation limit = 0.6, κ = 60, λ = 25)